Improved Carbonate Reservoir Characterisation: A Case Study from the mid-Cretaceous Mishrif Reservoir in the Giant West Qurna/1 Oilfield, Southern Iraq

Ali Jameel Hanoon Al-Ali

Submitted for the degree of Doctor of Philosophy

School of Energy Geoscience Infrastructure and Society
Institute of GeoEnergy Engineering
Heriot-Watt University

May 2023

The copyright in this thesis is owned by the author. Any quotation from the thesis or use of any of the information contained in it must acknowledge this thesis as the source of the quotation or information.

Abstract

The mid-Cretaceous Mishrif carbonate reservoir in West Qurna/1 oilfield is characterized by strong heterogeneity, tidal channels, and a complicated faults system which have very strong effects on the fluid flow and can result in unrealistic forecasted behaviour of the reservoir. The central hypothesis of this thesis is that two-dimensional seismic data and well data do not delineate the reservoir channels sufficiently and their variable fairway patterns. Hence, there is a need for a high-resolution 3D seismic dataset to explore reservoir characterisation including channel geometries more accurately. This thesis focuses mainly on porosity characterisation of the Mishrif channelized reservoir. It aims to delineate the Mishrif channel fairways with their intrinsic complexity then characterize the channel fairway's reservoir properties, such as the porosity, and lithology, especially in new areas that have no well control.

The thesis project was divided into three stages. The first stage focuses on the seismic reservoir characterisation of one of the Middle East's largest complex carbonate reservoirs in the West Qurna/1 oilfield, which hosts a complex internal architecture characterized by several tidal channels whose deposits may give good reservoir properties. In the second stage, multisource data was used to establish the essential workflow elements for characterizing Mishrif tidal channel fairways. The final stage incorporates 3D seismic data as a secondary variable into the property modelling to explore a more channels distribution using a combined dataset workflow.

It was concluded that the seismic inversion interpretation demonstrates promising results, with the model-based inversion performing better than the linear programming sparse spike (LPSS). We interpreted the lithological variation in the Mishrif mA zone based on the model-based inversion, including high-energy corals, mounds, and rudist shoal facies that were not observed previously. Also, we noticed that the seismically derived porosity improved our understanding by providing the realistic distribution of the Mishrif channel's porosity. A variety of approaches has been suggested to characterizing the Mishrif carbonate tidal channels. It was observed that well data analysis and thin section micrographs provided a good understanding of Mishrif channelized facies. Also, modern channels and outcrop scales were highly valuable in acquiring information for the comparison with channel fairways detected in the Mishrif reservoir. Our study found that spectral decomposition with the colour blending of three frequency intervals provides a

better geo-body extraction of the Mishrif mB1 channelized zone than the other seismic attribute surfaces. We analysed the results of the probabilistic neural network PNN algorithm and found that the Mishrif mB1 zone is clustered into two different heterogeneity-quality lithofacies (channels and restricted lagoon facies). We incorporated seismic inversion into the 3D property model with a different weighting of the correlation coefficients in the mB1 channelized zone. Thus, we observed that the constrained model combining well log data and seismic data as a secondary variable yields better channel fairway delineation with a moderate correlation coefficient weighting, and high weighting impacted the channel distribution. The findings of this thesis can be applied in other scenarios, such as contaminant transport in groundwater resources, or CO2 storage.

Dedication

I dedicate my thesis with love and gratitude to my father, who has been a great source of motivation and inspiration to succeed in my higher education.

This thesis is also dedicated to the memory of my mother, who stayed up through the nights for my comfort and happiness, and her caring throughout my life has made me what I am.

The thesis is dedicated to my wife Samara, who stood beside me and urged me forward every step of the way, to my daughter Noran and my sons Ibrahim and Rayan.

Finally, to my beloved family (sisters and brothers).

Acknowledgments

This project would not have been possible without many people's enthusiasm, support, encouragement, and creative insight. First and foremost, I am most grateful to my supervisor, Associate Professor Karl Stephen, whose guidance, and assistance were instrumental in completing the project. This research would not have seen the light without his encouragement and advice. I can never repay him for all his valuable time, and effort. I am also extremely grateful to Professor Asghar Shams for his professional assistance and guidance concerning the production of this research.

I would like to acknowledge the financial support and professional advancement of BP Iraq, Rumaila Operating Division-Basra Oil Company for supporting my Ph.D., and UniHouse for facilitating this support.

I would like to thank Professor Adnan Aqrawi from the Equinor Company and Professor Andy Gardiner from Heriot-Watt University for being my examiners and for the constructive and valuable feedback, which helped me to improve the quality of the thesis.

I also would like to thank Schlumberger for access to PetrelTM and GeoSoftwareTM for access to Hampson-Russell Software.

A special thanks go to Ali Mohammed Hmood Al-Rudaini, Hasan Al-Ibadi and Mohamed Albreiki for their friendship, cooperation, and knowledge sharing.

Back at home, I thank my parents, who instilled in me at a very early age the virtues of knowledge and an appreciation of the world around us. I must additionally say thanks to my wife Samara, my children (Noran, Ibrahim, Rayan), my sisters and brothers, and their families for their constant moral support throughout my PhD journey in the United Kingdom.

Finally, I'll never forget my time in Edinburgh, the lovely people, the beautiful scenery, and the chance to experience all four seasons in one day.

Edinburgh, May 2023

HERIOT WATT UNIVERSITY

Inclusion of Published Works Form

Please note you are only required to complete this form if your thesis contains published works. If this is the case, please include this form within your thesis before submission.

Declaration

This thesis contains one or more multi-author published works. I hereby declare that the contributions of each author to these publications is as follows:

Citation details	Al-Ali, A., Stephen, K. D. and Shams, A., (2019). Improved Carbonate Reservoir Characterization: A Case Study from a Supergiant Field in Southern of Iraq. SPE Middle East Oil & Gas Show and Conference, held in Manama, Bahrain, 18-21 March 2019.
Ali Al-Ali	Contribution to the method development in discussion, performed data analysis, create reservoir characterization, and wrote the manuscript
Karl Stephen	Supervision and contribution to the method development in discussion
Asghar Shams	Supervision and contribution to the method development in discussion

Citation details	Al-Ali, A., Shams, A., and Stephen, K. D. (2019). Identification of Fault Systems and Characterization of Structural Model: A Case Study from the Cretaceous Reservoir in the Giant Oil Field, Southern of Iraq. SPE Europec featured at 81st EAGE Conference and Exhibition, held in London, UK, 3-6 June 2019.
Ali Al-Ali	Contribution to the method development in discussion, performed data analysis, create reservoir characterization, and wrote the manuscript
Karl Stephen	Supervision and contribution to the method development in discussion
Asghar Shams	Supervision and contribution to the method development in discussion

Citation details	Al-Ali, A., Stephen, K. and Shams, A. (2019). New Insights into the Spatial Distribution of Complex Carbonate Channels Using Geostatistical Approach: A Case Study. Fourth Petroleum Geostatistics, Extended Abstract, held in Florence, Italy, 2-6 September 2019.
Ali Al-Ali	Contribution to the method development in discussion, performed data analysis, create reservoir characterization, and wrote the manuscript
Karl Stephen	Supervision and contribution to the method development in discussion
Asghar Shams	Supervision and contribution to the method development in discussion

Citation details	Al-Ali, A., Stephen, K. and Shams, A. (2019). Characterization of Channelized Systems in a Carbonate Platform Setting: A Case Study on the Late Cretaceous Reservoir from the Supergiant Oilfield, Iraq. SPE Reservoir Characterisation and Simulation Conference and Exhibition, held in Abu Dhabi, UAE, 17-19 September 2019.
Ali Al-Ali	Contribution to the method development in discussion, performed data analysis, create reservoir characterization, and wrote the manuscript
Karl Stephen	Supervision and contribution to the method development in discussion
Asghar Shams	Supervision and contribution to the method development in discussion

Citation details	Al-Ali, A., Stephen, K. D. and Shams, A., (2020). Toward Reservoir Characterization-Comparing Inversion Methods of a Heterogeneous Carbonate Reservoir in Supergiant Onshore Field. International Petroleum Technology Conference, held in Dhahran, Saudi Arabia, 13 – 15 January 2020.
Ali Al-Ali	Contribution to the method development in discussion, performed data analysis, create reservoir characterization, and wrote the manuscript
Karl Stephen	Supervision and contribution to the method development in discussion
Asghar Shams	Supervision and contribution to the method development in discussion

Citation details	Al-Ali, A., Stephen, K. D. and Shams, A., (2020). Lithofacies Classification and Distribution for Heterogeneous Channelized System Based on Neural Network Process: Case Study from Middle East Carbonate Reservoir. SPE Virtual Norway Subsurface Conference. 2-3 November 2020.
Ali Al-Ali	Contribution to the method development in discussion, performed data analysis, create reservoir characterization, and wrote the manuscript
Karl Stephen	Supervision and contribution to the method development in discussion
Asghar Shams	Supervision and contribution to the method development in discussion

Table of Contents

Abstract ii
Acknowledgments v
Table of Contents viii
List of Publications xii
Chapter 1. Introduction 1
1.1 Overview 1
1.2 Research Objectives and Structure of the Thesis 8
Chapter 2. Background and Literature Review 11
2.1 Review of Carbonate Rocks 12
2.1.1 Carbonate Production Systems 12
2.1.2 Unique Attributes of Carbonates 12
2.1.3 Diagenesis and Porosity of Carbonate Rocks 14
2.1.4 Classification of Carbonate Rocks 15
2.1.5 Petrography of Carbonate Rocks 17
2.1.6 Sequence Stratigraphic Principles 18
2.1.7 Channelized Systems in an Inner Carbonate Platform Setting 20
2.1.8 Types of Channelized Systems 20
2.2 Review of Seismic Reservoir Characterisation 21
2.2.1 Overview of Seismic Theory 21
2.2.2 Rock Physics Model 24
2.2.3 Modelling of Acoustic Properties in Carbonate Rocks 26
2.2.4 Seismic Well Tie 27
2.2.5 Seismic Inversion Methods 31
2.2.6 Seismic Attributes Techniques 34
2.2.7 Classification of Seismic Attributes 35
2.2.8 Integrated Seismic Reservoir Characterisation Workflow 38
2.2.9 Utilizing Seismic Reservoir Characterisation for the Exploration and Development of Carbonate Reservoirs 39
2.2.10 Applications of Seismic Reservoir Characterisation in Carbonate Reservoirs 39

2.2.11 Introduction of Facies Classification 40
2.2.12 Seismic Facies Classification Techniques 42
2.2.13 Probabilistic Neural Networks (PNN) 43
2.3 Review of Integrated Reservoir Modelling Workflow 44
2.3.1 Structural Modelling 44
2.3.2 Porosity Modelling 45
2.3.3 Reservoir Modelling Using Secondary Variable 46
2.3.4 Constraining Reservoir Model Schemes 47
2.3.5 Reservoir Characterisation and Modelling Uncertainty 48
Chapter 3. Geology of the Mishrif Formation and 3D-Seismic Survey of the Giant West Qurna/1 Oilfield 49
3.1 Regional Geological Setting 50
3.1.1 Regional Paleogeography 50
3.1.2 Structural Controls 51
3.2 Geological Overview of the Studied Area 53
3.2.1 Introduction to West Qurna/1 Oilfield 54
3.2.2 Approach to Reservoir Characterisation of West Qurna/1 Oilfield 56
3.3 Comprehensive Geology Study of the mid-Cretaceous Mishrif Reservoir 59
3.3.1 Sedimentary Facies Distribution 59
3.3.2 Reservoir Zonation 61
3.3.3 Reservoir Communications and Barriers 63
3.4 Development of the Morphology of the Carbonate Tidal Channels 64
3.4.1 Distribution Regularities of The Tidal channels 65
3.4.2 Outcrop 67
3.4.4 Implications of Reservoir Architecture and Heterogeneities 71
3.5 Seismic Data Preparation and Analysis 72
3.5.1 West Qurna/1 3D Seismic Survey: Acquisition 73
3.5.2 West Qurna/1 3D Seismic Processing 77
3.5.3 Seismic to Well Calibration 80
3.5.4 West Qurna/1 3D Seismic Horizon Interpretation 83

3.5.5 Fault Systems and Structural Framework 84
3.6 Summary and Conclusion 90
Chapter 4. Mishrif Reservoir Characterisation 91
4.1 Introduction 92
4.2 Methodology 92
4.3 Rock Physics Model 94
4.4 Post-Stack Seismic Inversion 97
4.4.1 Seismic Well Tie (SWT) 97
4.4.2 Initial Model for Seismic Inversion analysis 101
4.4.3 Seismic Inversion Techniques 104
4.5 Evaluation of Geological Reservoir Characterisation Based on Seismic Inversion Results 108
4.5.1 Core-Scale Rock Types Classification 108
4.5.2 Facies Discrimination Based on the Acoustic Impedance 110
4.6 Seismically Derived Mishrif Characterisation 113
4.6.1 Porosity Estimation from Acoustic Impedance Inversion 113
4.7 Summary and Conclusion 121
Chapter 5. Multi-Dimensional Approaches to Characteristics Mishrif Carbonate Tidal Channels 122
5.1 Introduction 123
5.2 Methodology 123
5.3 Sedimentary Characteristics of Mishrif Tidal Channels 124
5.3.1 Sequence Stratigraphic of the Mishrif Channel Fairways 125
5.3.2 Petrographic and Petrophyicsal Characteristics 127
5.3.3 Modern Analogue of Carbonate Tidal Channels 130
5.3.4 Carbonate Channelized Outcrops 131
5.4 Seismic Attributes Expression: Identification of Channel Geometries 132
5.4.1 Combination of Surface Attributes 132
5.4.2 Frequency Spectral Decomposition Techniques 134
5.5 Seismic Reservoir Characterisation: Mishrif Tidal Channel Fairways 137
5.5.1 Interpretation of Seismic Inversion Results 137

5.5.2 Capturing Channel Geometries Based on Seismically Derived Porosity.....139
5.5.3 Facies Classification Framework of Mishrif Channel Fairways 144
5.6 Summary and Conclusion 147
Chapter 6. Constraining Property Model of Mishrif Channelized Fairways Using 3D Seismic Data.....149
6.1 Introduction.....150
6.2 Methodology, Data.....150
6.3 Seismic Inversion 154
6.4 Analysing the Relationship Between Primary and Secondary Variables 155
6.5 Structural Modelling 157
6.5.1 Mishrif Top Horizons 157
6.5.2 Fault Modelling 158
6.5.3 Reservoir Zonation 160
6.5.4 Layering.....162
6.6 Porosity Modelling.....163
6.7 Rescaling Seismic Inversion into 3D Model Framework 168
6.8 Integration of Seismic Data into 3D Property Modelling and Models Comparison 169
6.8.1 Porosity Models Using Different Geostatistical Approaches.....170
6.8.2 Porosity Models Using Different Reflection Coefficients (RC) 177
6.9 Discussion 178
6.10 Summary and Conclusion 180
Chapter 7. Conclusion and Recommendations 181
7.1 Conclusion.....181
7.2 Recommendations.....183
Appendix.....184
References.....187

List of Publications

This thesis contains excerpts from the following papers:

Al-Ali, A., Stephen, K. D. and Shams, A., (2019a). Improved Carbonate Reservoir Characterization: A Case Study from a Supergiant Field in Southern of Iraq. *SPE Middle East Oil & Gas Show and Conference,* held in Manama, Bahrain, 18-21 March 2019.

Al-Ali, A., Shams, A., and Stephen, K. D. (2019b). Identification of Fault Systems and Characterization of Structural Model: A Case Study from the Cretaceous Reservoir in the Giant Oil Field, Southern of Iraq. *SPE Europec featured at 81st EAGE Conference and Exhibition,* held in London, UK, 3-6 June 2019.

Al-Ali, A., Stephen, K. and Shams, A. (2019c). New Insights into the Spatial Distribution of Complex Carbonate Channels Using Geostatistical Approach: A Case Study. *Fourth Petroleum Geostatistics, Extended Abstract,* held in Florence, Italy, 2-6 September 2019.

Al-Ali, A., Stephen, K. and Shams, A. (2019d). Characterization of Channelized Systems in a Carbonate Platform Setting: A Case Study on the Late Cretaceous Reservoir from the Supergiant Oilfield, Iraq. *SPE Reservoir Characterisation and Simulation Conference and Exhibition,* held in Abu Dhabi, UAE, 17-19 September 2019.

Al-Ali, A., Stephen, K. D. and Shams, A., (2020a). Toward Reservoir Characterization-Comparing Inversion Methods of a Heterogeneous Carbonate Reservoir in Supergiant Onshore Field. *International Petroleum Technology Conference,* held in Dhahran, Saudi Arabia, 13 – 15 January 2020.

Al-Ali, A., Stephen, K. D. and Shams, A., (2020b). Lithofacies Classification and Distribution for Heterogeneous Channelized System Based on Neural Network Process: Case Study from Middle East Carbonate Reservoir. *SPE Virtual Norway Subsurface Conference.* 2-3 November 2020.

Chapter 1. Introduction

1.1 Overview

Despite continuous and much-needed efforts to reduce the world's reliance on fossil fuels and replace them by alternative green energy sources, oil and gas production plays a significant role in the global economy. An IEA (International Energy Agency) 2022 report states that in the Organisation for Economic Co-operation and Development (OECD) regions, rising gasoline prices and a deteriorating economic climate are slowly beginning to restrain the increase in oil demand. In contrast, demand outside the OECD countries dramatically recovered in May 2022, driven by China, as it emerged from Covid lockdowns, and the Middle East as increased demand for electricity drove up consumption (Figure 1.1a). Thus, oil-producing will continue to increase somewhat until 2030, even if all states pledged to lower greenhouse gas emissions and stick to their scheduled goals (Figure 1.1b). However, keeping these promises as a whole and on schedule is not guaranteed. Net zero emissions by 2050, the third IEA scenario, is a normative scenario that would need enormous investment and is thus not practical.

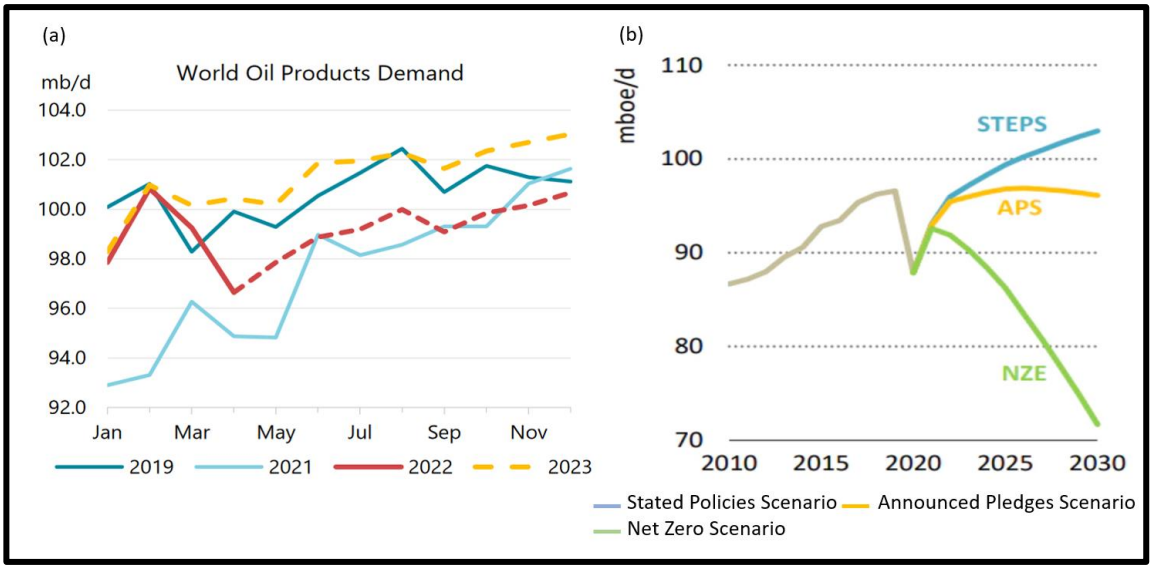

Figure 1.1. (a) Predicts oil demand by 2023. (b) World oil products demand until 2030. Taken from the International Energy Agency (2021) and (2022).

Additional petroleum industry investments, including exploration, reservoir management of existing fields, and new technologies, are required to boost oil recovery. Also, increasing the efficiency of upstream and downstream performance and reducing expenses are necessary to meet the world's oil production needs. Conventional crude oil and gas condensates are projected to contribute significantly to the supply of hydrocarbons. According to the OPEC Annual Statistical Bulletin, the Middle East is the top oil producer in the world, contributing 32% of global oil production (2021). Given that it contributes 20% of the world's gas production, it is also regarded as the second-largest gas producer. The Middle East has 62 percent of the world's conventional crude oil reserves (Figure 1.2), with 70 percent being found in carbonate reservoirs (Montaron, 2008).

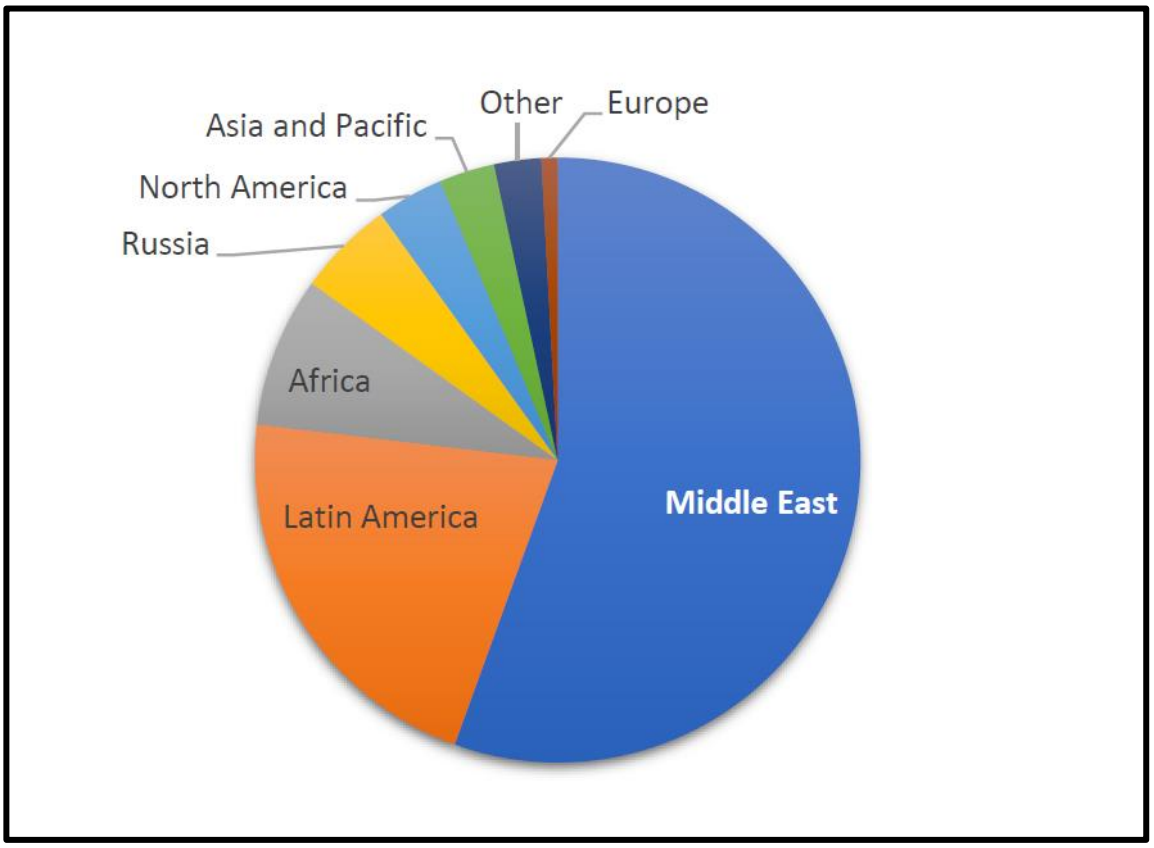

Figure 1.2. Global reserves of proven crude oil, by region, in 2020. the OPEC Annual Statistical Bulletin (2021).

Carbonate reservoirs are important to understand because they hold approximately 60% of the world's petroleum reserves and 40% of the world's gas reserves (Figure 1.3) (Garland *et al.*, 2012). Additionally, it accounts for almost 70% of the Middle East's

petroleum and 90% of its gas. Carbonate deposits occur naturally in current tropical marine settings and ancient sediments, and form important hydrocarbon reservoir rocks (Ahr, 2008). However, carbonate reservoirs are still enigmatic in geological and petrophysical characteristics and much different from siliciclastic reservoirs and so need a focused understanding and better knowledge to model and characterize them successfully (Burchette, 2012). This includes a detailed description of the porosity distribution, permeability, fluid saturation, lithology of reservoir rock (lithofacies), and the nature of fractures. More details about carbonate rocks and the Dunham classification will be explained in the Chapter 2.

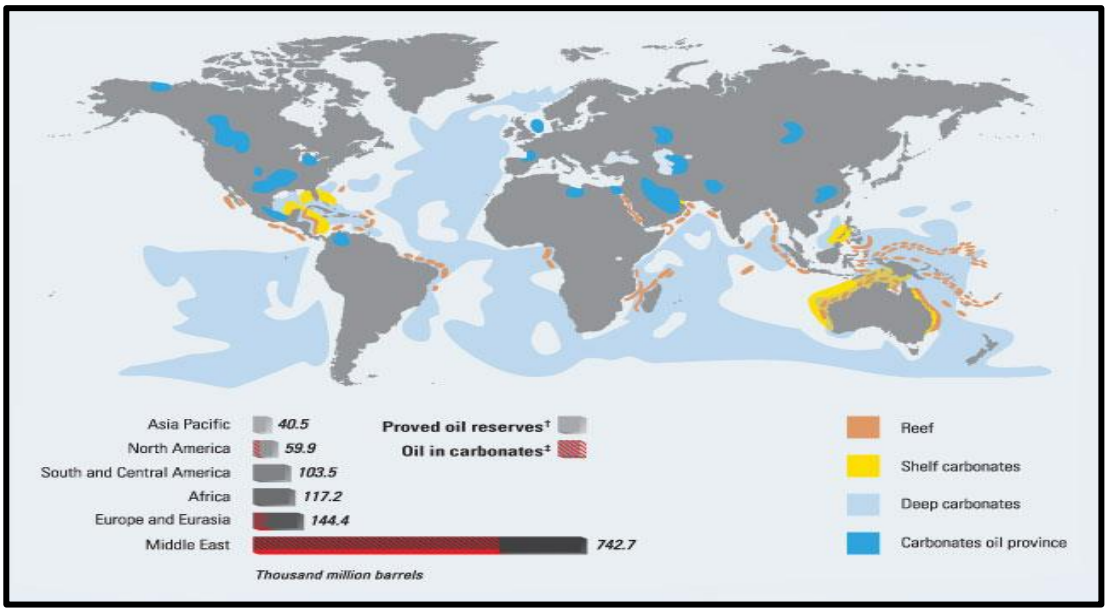

Figure 1.3. World distribution of carbonate reservoirs (Ahr *et al.*, 2005).

Because of many diagenetic overprints, and tectonics (Burchette, 2012; Ringrose and Bentley, 2016) that can occur during various burial and uplift periods throughout geological history, the petrophysical characteristics of carbonates differ dramatically from those of modern sediments. Carbonate features can be improved or degraded during diagenetic. Garland *et al.* (2012) state that fractures and diagenesis processes played a vital role in creating the architecture of pore systems and storage space, which may be increasing productivity. Carbonate reservoirs often contain multi-scale geological heterogeneities (fractures, karst features, and faults) that can provide very high permeability in carbonate rocks, but their surrounding rock matrix could display a low permeability (Liu and Wang, 2017) (Figure 1.4). Therefore, carbonate reservoirs are

geologically heterogeneous and consist of facies variation from low energy (muddy) to high energy (grainy) according to Dunham's classification: grainstones, packstones, wackestones, and mudstones based on the amount of mud and grains in the rock, as shown in the outcrop section (Figure 1.5).

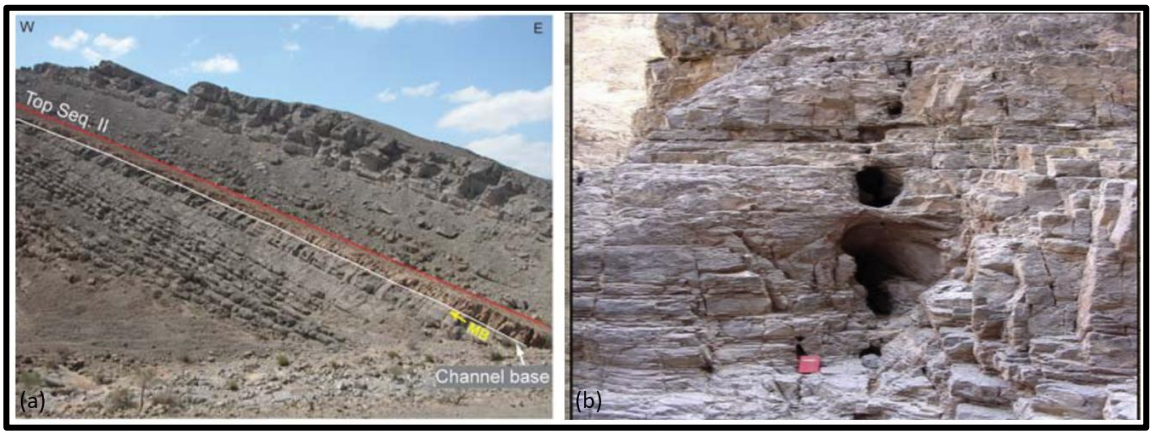

Figure 1.4. Carbonate heterogeneities. (a) Outcrop view of the bioclastic channel cropping out in the NW of the Jabal Madmar (Madmar 6 wadi) just below the top of Sequence II. (b) A strike-slip fault tip area in the Yijianfang outcrop, with caves, vugs, fractures in the fault zone, and the natural fracture system (after Grélaud *et al.*, 2010; Lu *et al.*, 2017).

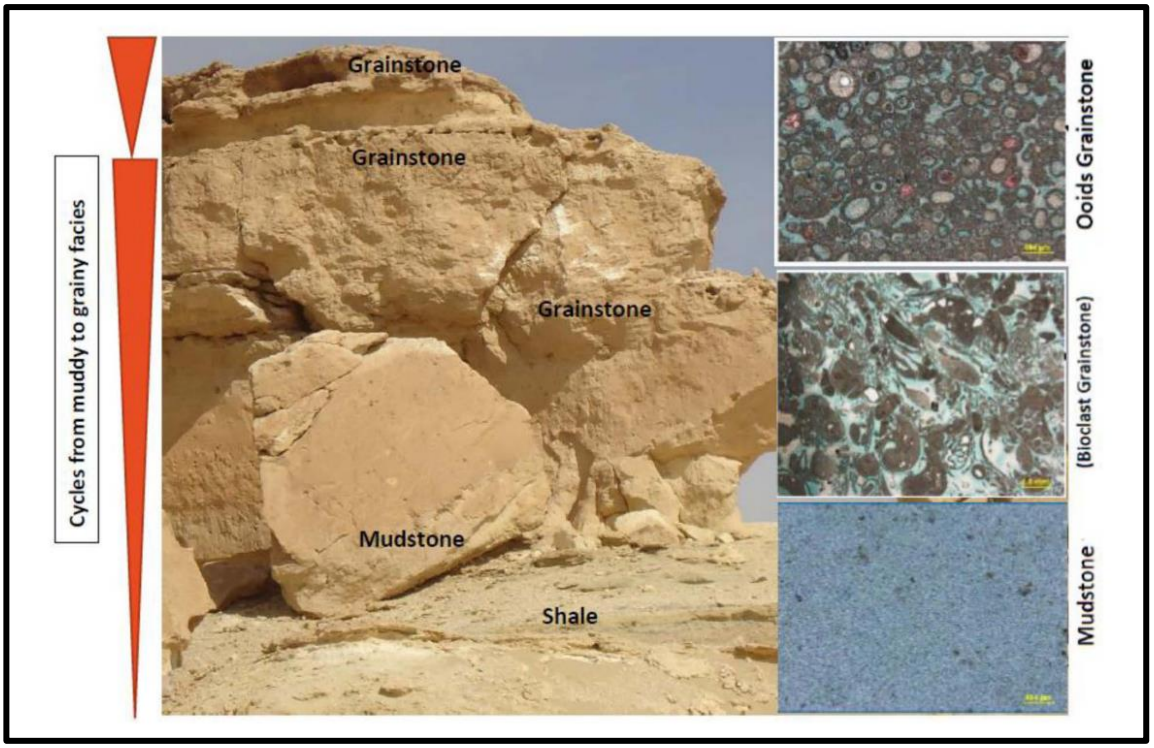

Figure 1.5. The vertical outcrop section shows an overall shallowing upward succession from mudstone to grainstone facies (Dam Formation, early Miocene) Eastern Arabian Platform, Saudi Arabia (Elhaj *et al.*, 2019).

Reservoir characterisation is critical throughout the life of any oil and gas development. Despite this, reservoir characterisation efforts are frequently hampered by a lack of data. As a result, extracting as much value as possible from all data in the asset is critical. Porosity, permeability, transmissibility, geometry, saturations, pressures, and rock-fluid interactions are all important during reservoir characterisation (Chopra *et al.,* 1990; Wong, 2020).

Reservoir characterisation is challenging in the case of carbonate reservoirs due to the complexity of carbonate depositional environments. Carbonate reservoirs' elastic properties (velocity, density, acoustic impedance) are also strongly related to diagenetic processes and mineralogical composition. Thus, Carbonate reservoirs pose a significant difficulty in establishing full-field development plans throughout the field life due to the uncertainty in the petrophysical properties. Understanding carbonate platforms and depositional processes have been enhanced due to the improved seismic data quality in recent years. Herein, 3D seismic comes into play through the inventive use of seismic attribute combinations, extraction of geomorphological data, and novel quantitative methodologies. In other words, flow units, barriers, and related carbonate depositional and diagenetic facies can now be mapped using 3D data due to seismic acquisition's extensive coverage (typically the entire field), providing a unique view of how these facies interactions have altered through time in response to tectonic, oceanographic, and climatic forcing (Hendry *et al.,* 2021).

We can gain additional insights into the producing fields by combining well log and core data with seismic characteristics. Cross-well seismic can supplement this strategy, especially where overburden effects make vertical imaging difficult (Hendry *et al.,* 2021). Tidal channel fairways, fracture networks, palaeokarst cave systems, and gas chimneys can be recognized and interpreted from 3D seismic attributes, allowing well placements to target the best prospective reservoir properties and avoid crucial drilling dangers (Zeng *et al.,* 2011). This contribution should be considered with geological knowledge of carbonate systems since seismic interpretation is merely the initial stage in understanding the potential for carbonate reservoirs in the subsurface (Agar and Geiger 2015). Thus, for accurate and trustworthy reservoir characterisation, it is crucial to understand how they are deposited and altered and how they generate distinctive geometries with different rock characteristics.

In the context of using an integrated workflow to quantify seismic reservoir characterisation, seismically derived porosity modelling and facies classification schemes constitute a key concept that needs to be included (Zare *et al.,* 2020). The characterisation process includes the analysis of reflection configuration, amplitude, magnitude, frequency, and continuity in carbonate seismic facies. Similar processes have grown to be accepted practice. Today, a more deterministic and iterative workflow that is geologically conditioned and reduces uncertainty allows for a more accurate inter-well volume and reservoir modelling prediction (Hendry *et al.,* 2021). These approaches include the inversion of seismic data, relationships between rock typing and rock physics, and seismic resolution of depositional geometries (Liu and Wang 2017).

Russell *et al.,* (2002) pointed out the geostatistics approach and multiattribute prediction for integrating seismic and well-log data to estimate the porosity model in the Blackfoot field of central Alberta. The new procedure demonstrated an excellent correlation between porosity and the inverted acoustic impedance and outlined the channel geometries much more clearly than the original seismic volume. Yose *et al.,* (2006) illustrated how 3D seismic data are used to differentiate platform facies and flow units and populate them into a sequence stratigraphic framework for reservoir model construction, through a combination of volume types and integrated techniques. The integrated reservoir characterization approach is preferable to seismic attributes because it offers different scenarios to address lateral-sweep interpretation, which cannot be done with the well log or seismic volume. Reservoir characterisation studies could suggest the 'best' interpretation approach that enhances the reservoir properties' detectability and calculates oil-in-place estimations and the dynamic behaviour of the reservoir model.

Challenges of Reservoir Characterisation in the West Qurna/1 Oilfield

The West Qurna/1 field was discovered in 1973 and has been in production since 1999; however, it was intermittent because of the previous wars. From the onset of production until 2010, the field was under primary depletion and, initially, field development did not include water flooding, which caused a problem of reservoir pressure decline and the closure of several wells. The field is estimated to hold approximately 30 to 40 billion barrels of recoverable reserves (Finlayson *et al.,* 2012).

West Qurna/1 oilfield has a high level of heterogeneity, and this was observed through the existence of numerous pore types and laboratory observations of core porosity and permeability. The mid-Cretaceous Mishrif reservoir is a key oil-bearing interval and accounts for more than half of the oilfield, it is also one of the most producing oil and gas reserves. It comprises thick shallow-marine rudstones, grainstones, and packstones/wackstones, bounded by non-reservoir calcareous mudstones. The best reservoir quality is grainstones. The depth of the Mishrif formation is approximately 2500 meters, with a thickness of approximately 250 meters, deposited on a low-angle carbonate ramp (Stoneley, 1990; Yose *et al.*, 2012). The Mishrif Reservoir displays varying quality and is highly heterogeneous due to depositional cycles and the sequence stratigraphic framework. The pore types of the Mishrif facies are characterized by a multimodal porosity from high values of 30% grading into lower values of 5 to 10% (Figure 1.6). The hydrocarbon-bearing interval is called mB2 and is relatively homogenous, especially the upper part (a,b). However, the lower unit of this zone with the mC zone represents the greater volume of the low-permeability microporous reservoir. For that reason, large permeability contrast can be observed in the Mishrif from high permeability grainstones to low permeability microporosity (1000-10 mD) (Davies *et al.*, 2015). However, the extent of lateral and vertical heterogeneity in the field is uncertain due to the limited number of cored wells. This complicates reservoir characterisation and fluid-flow prediction because tight and highly permeable zones might be confined or spread out laterally.

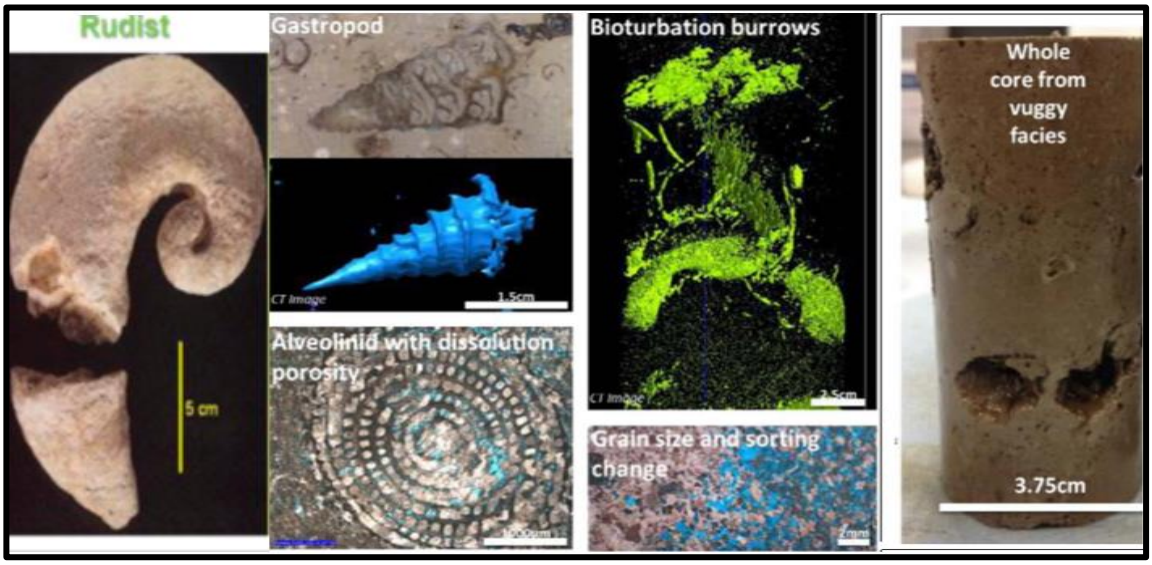

Figure 1.6. Mishrif facies heterogeneity from core data (rudist, gastropod, alveolinid with dissolution porosity, bioturbation burrows, and vuggy) causes multimodal porosity and larger contrast permeability (Mahmood *et al.*, 2017).

Additionally, the upper mid-Cretaceous Mishrif reservoir developed a kind of geobody that be similar to rivers, which is termed a tidal channel (Figure 1.7). Tidal channels highly affect the mB1 zone, causing strong heterogeneity of the facies and petrophysical properties. Traditionally, tidal channels are represented as irregular patterns but are complex 3D structures containing various geometry and facies. Therefore, it is important to decipher the complexity of the carbonate tidal channels architecture with integrated multisource data and compare it with modern analogue and outcrop data. More details about the reservoir properties of mB1 tidal channels will be provided in Chapters 4 and 5.

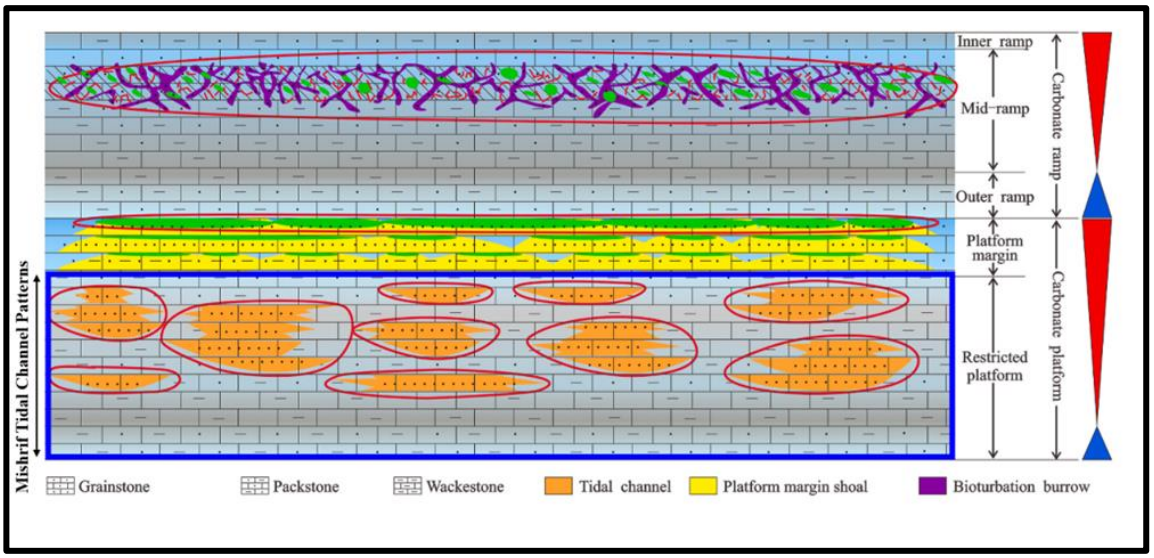

Figure 1.7. Schematic diagram of the vertical stacking distribution in the Mishrif mB1 tidal channels, identified based well log and core data (Liu *et al.*, 2021).

1.2 Research Objectives and Structure of the Thesis

This Ph.D. thesis aims to implement, test, and apply multiple workflows to compare and contrast how 3D seismic data influence reservoir characterisation in a giant carbonate reservoir with a complex fault and channelized transition zone. Instead of basing a model on a single base case and just expressing the main uncertainties through a restricted sensitivity assessment, multi-deterministic procedures allow us to build a large variety of potential geological situations (Ringrose and Bentley, 2021). Here, the specific goals are following to characterize the carbonate channelized reservoir for reservoir development and to answer the following questions:

• How can the available data be analysed to reveal the complexity and the heterogeneity of the Mishrif reservoir characterisation and explore how seismic data can increase the reliability of reservoir characteristics; this objective is covered in Chapters 3 and 4.

• How to demonstrate that jointly analysing multiple approaches can be applied effectively to predict mB1 reservoir zone characteristics by applying inversion methods, probabilistic neural network (PNN), and different geostatistical methods; this objective is presented in Chapters 5 and 6.

• What is the 3D seismic dataset's overall significance in reservoir management and field development?

To the best of my knowledge, it is the first time such a study, combining well data, core data, outcrops, and high-resolution 3D seismic data, has been applied to a real giant carbonate channelized field for improved reservoir characterisation through different approaches while considering key operational constraints and geological uncertainties.

This thesis contains seven chapters. The following is a summary of each chapter:

Chapter 1 is the current chapter. It introduces a brief overview of carbonate reservoirs, highlights the importance of reservoir characterisation and its applications in these reservoirs, and explains the importance of integrated workflow. The research objectives are then described in detail.

Chapter 2 provides a comprehensive review and background of carbonate rocks and their various rock typing as well as different classification methods of carbonate rock porosity. This chapter also reviews the seismic reservoir characterisation workflows and their associated uncertainties. In addition, the chapter presents an overview of channelized systems in carbonate reservoirs and discusses how tidal channels can be charactered and integrated into a reservoir characterisation workflow. Finally, a review of integrated reservoir modelling workflows is discussed as well as how to constrain property models using seismic reservoir characterisation.

Chapter 3 presents a regional geological setting and geological overview of the West Qurna/1 oilfield. Also, it covers the reviews of the mid-Cretaceous Mishrif reservoir and

the development of the morphology of the Mishrif tidal channels. Additionally, the chapter investigates and defines the fault systems and structural model of the Mishrif reservoir, and this section is based on Al-Ali *et al.*, (2019b).

Chapter 4 discusses how a seismic reservoir characterisation workflow that combines multiple source data (geological and geophysical) is used to characterize the Mishrif reservoir in the West Qurna/1 oilfield. In particular, the focus is on both acoustic impedance and seismically derived porosity models. This chapter is based on Al-Ali *et al.*, (2019a) and Al-Ali *et al.*, (2020a)

Chapter 5 presents a multi-dimensional workflow to characterize Mishrif tidal channel fairways through the sedimentary characteristics, seismic attributes expression, and seismic reservoir characterisation by generating seismically derived properties. This workflow defines the distribution of tidal channels using seismic data, well logs, and core data, taking into account variations in channel dimensions and petrophysical properties (i.e., length, orientation, porosity, and facies classification). This chapter is based on Al-Ali *et al.*, (2019c), Al-Ali *et al.*, (2019d), and Al-Ali *et al.*, (2020b).

Chapter 6 builds on the knowledge of Chapters 3 to 5 and investigates how different the constraining geological model of Mishrif mB1 channelized zone is using a secondary variable (3D acoustic impedance (AI) volume). The comparison of 3D porosity models will be introduced at the chapter's end.

Chapter 7 summarizes the key results and conclusions from the preceding chapters. The recommendations for further study in this area are then given.

Chapter 2. Background and Literature Review

This chapter introduces the definitions of carbonate rocks, their classification, and the channelized system in an inner carbonate platform setting. The next part looks at the seismic reservoir characterisation. Finally, a review of the integrated reservoir modelling workflow is discussed.

2.1 Review of Carbonate Rocks

2.1.1 Carbonate Production Systems

Geologically, carbonates are sedimentary rocks formed in warm, shallow marine locations and are generally of biogenetic origin. As its name implies, carbonate rock mostly includes calcium carbonate (CaCO3), which comprises marine creature fragments, coral, or algae. Carbonate heterogeneity is typically due to the variation and complexity of a range of processes (depositional, diagenetic and the structural) (Ghafoori *et al.*, 2009; Ling *et al.*, 2014). However, the severe change in carbonate rocks mainly occurred through deposition control and diagenesis processes (chemical reaction) such as cementation, chemical leaching, karstification, and dolomitization (Figure 2.1). These processes cause modification of the original characteristics of carbonate rocks, such as multimodal porosity and diversity of permeability (Mahmood *et al.*, 2017).

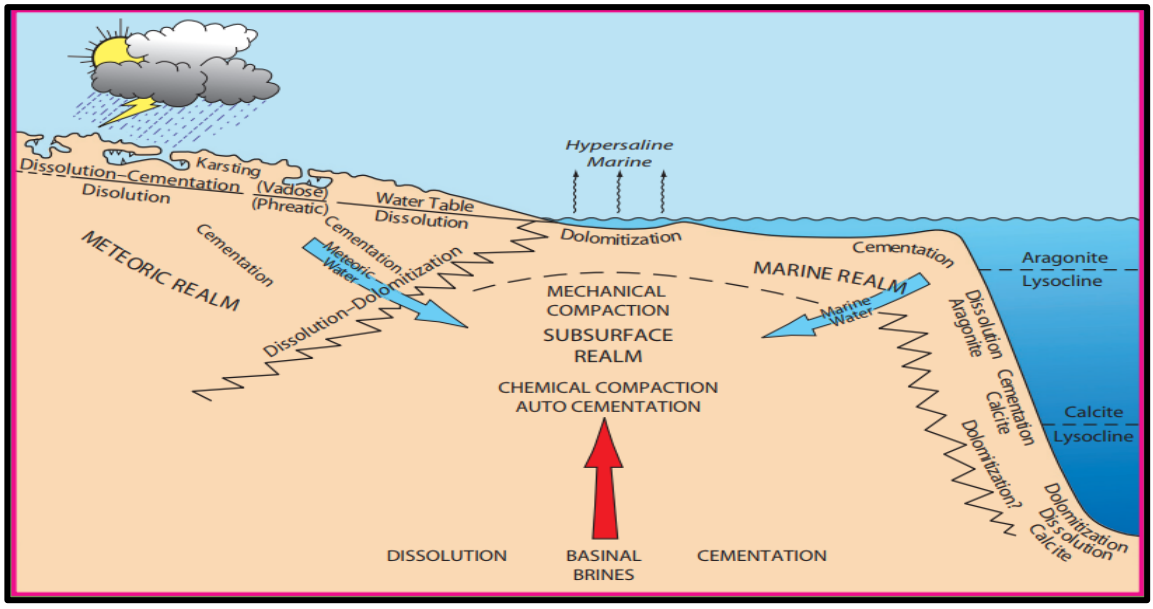

Figure 2.1. Schematic diagram showing the modification process in the carbonate rocks in three environments (meteoric, marine, and subsurface) (Moore and Wade, 2013).

2.1.2 Unique Attributes of Carbonates

Carbonates have distinct characteristics that set them apart from siliciclastics and necessitate different research methodologies. Carbonate rocks, unlike terrigenous sediments, are created from elements found near or on the site of the sediment's ultimate

deposit, the carbonate factory. Biological, chemical, and detrital activities contribute to forming carbonates within the depositional basin (Ahr, 2008); their mineralogy, grain types and textures all reflect the local environment. In contrast, the mineralogy of siliciclastic sediments is strongly influenced by the parent rock type, and the weathering and transport history. The grain size and texture of clastic sediments also reflects the transport processes. All contrasts between carbonate and terrigenous sediments and rocks are seen in Table 1.

Reservoir Characteristic	Carbonates	Terrigenous Sandstones
Amount of depositional porosity	40 to 70%	25 to 40%
Amount of ultimate porosity	A small fraction of original porosity, commonly 5 to 15%	Half or more of primary porosity, commonly 15 to 30%
Type of primary porosity	It can be interparticle, intraparticle, intercrystalline, moldic, vuggy, cavernous, fenestral, or "constructed void."	Almost exclusively interparticle
Type of ultimate porosity	Highly variable owing to different origins or pore types	Almost exclusively primary interparticle
Typical pore size	Diameter and throat size may not be related to depositional texture	Diameter and throat sizes related to depositional texture
Typical pore shape	Varies from strongly related to particle shape to totally unrelated	Dependent on particle shape; typically, a "negative" of particles
Uniformity of pore size and shape distribution	Variable from fairly uniform to extremely heterogeneous – even within a body made up of a single rock type	It may be relatively uniform in homogenous sand bodies
Influence of diagenesis	Major – can create, obliterate, or modify porosity; cementation and solution important	Minor – usually reduction by compaction or cementation
Influence of fracturing	Major importance in reservoir properties if present	Not a major importance in reservoir properties
Visual estimation of porosity and permeability	Semi-quantitative estimates may be easy or impossible; instrumental measurements commonly required	Semi-quantitative estimates may be relatively easy
Adequacy of core analysis for reservoir evaluation	Core plugs are commonly inadequate; may require whole core analyses (~4 inches by 1-foot segments) for large pore sizes	Core plugs of 1-inch diameter may be adequate to determine matrix porosity
Porosity-permeability relationships	Highly variable; may be independent of particle texture	Relatively consistent; may be dependent on particle texture
Reliability of log characteristics as indicators of depositional facies (electrofacies mapping)	Not reliable because logs cannot generally detect differences in carbonate grain types or textures	The standard practice that may provide reliable proxies for depositional facies

Table 1. A Comparison of carbonate rocks and terrigenous sandstone reservoir characteristics (Ahr, 2008).

2.1.3 Diagenesis and Porosity of Carbonate Rocks

Because of many diagenetic overprints that can occur during various burial and uplift periods throughout geological history, the petrophysical characteristics of carbonates differ dramatically from those of modern sediments. Carbonates' petrophysical characteristics can be improved or degraded during diagenesis. Garland *et al.*, (2012) state that the processes of fractures and diagenesis played a vital role in creating the architecture of pore systems and storage space, increasing productivity. Fractures and faults can provide very high permeability in carbonate rocks, but the surrounding rock matrix could display a low permeability (Liu and Wang, 2017). Initially, carbonate sediments may display high porosity values during deposition. However, this decreases due to alteration and burial processes down to the depth of the reservoirs. There are many classifications of porosity in carbonate rocks. We will review the classification by Choquette and Pray (1970).

Choquette and Pray (1970)

The porosity systems of carbonates can be divided into three main categories, according to Choquette and Pray (1970) (Figure 2.2). Fabric selective pore systems relate to the sediment texture, due to the original depositional environment or diagenesis. The second group includes fractures, channels, and vugs not connected to the original strata, which are considered 'not-fabric-selective' porosity in their categorization. The third type could be fabric selective or not and can be induced by several processes, including those caused by animals and plants, including boring and burrowing. Geologists and sedimentologists frequently use Choquett and Pray's (1970) approach for determining carbonate porosity types because it gives a complete sedimentological description. These porosity types significantly influence volumetrics, permeability, flow behaviour, production rates, and reserve estimations; they must be thoroughly assessed using all available geological and geophysical data.

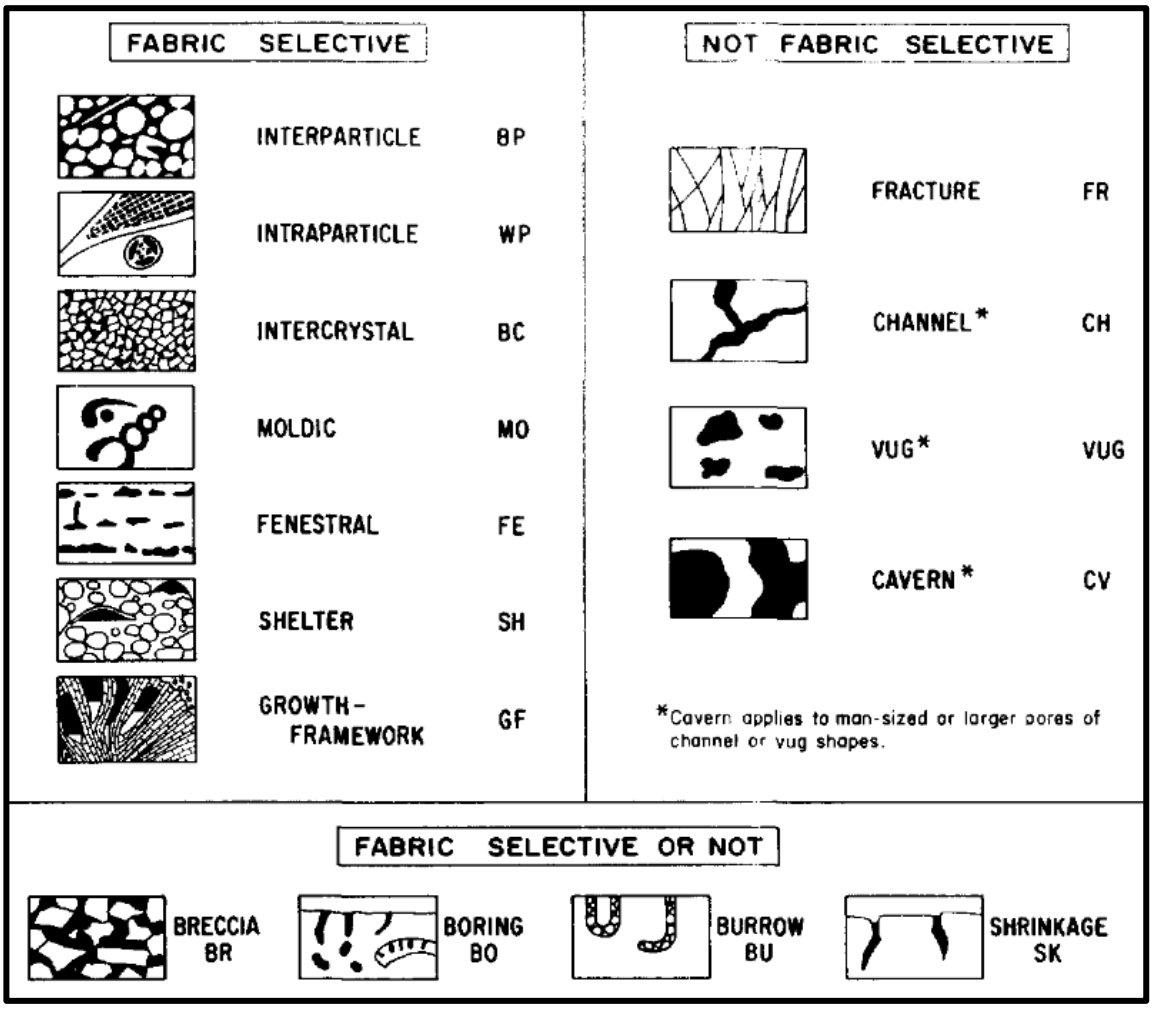

Figure 2.2. Choquette and Pray's criteria are used to classify carbonate porosity. Fabric-selective (on the left), non-fabric-selective (on the right), and variably fabric-selective (below), (Choquette and Pray 1970).

2.1.4 Classification of Carbonate Rocks

The descriptions acquired using microscopes or hand lenses are used to classify carbonate rocks in practice. Dunham (1959, 1962) is one of the most often used categories to classify carbonate rocks. It classified limestones primarily based on proportions of matrix and primary component grains, and the method of grain support.

Dunham (1962)

Dunham developed a classification system in 1962 to codify the classification of carbonate rocks based on their depositional textures. This was accomplished by splitting limestones into the four textural characteristics listed below:

1. The existence or absence of carbonate mud.

2. The proportion of grains.

3. The method of grain support (grain-supported v. matrix-supported).

4. The existence or absence of indications of binding (framestone, baffling, etc) during deposition.

Dunham's classification is straightforward and sufficient for geologists to utilize. Grainstones, packstones, wackestones, and mudstones are the four primary names used for sand-grade carbonates, based on the amount of mud and grains in the rock (Figure 2.3).

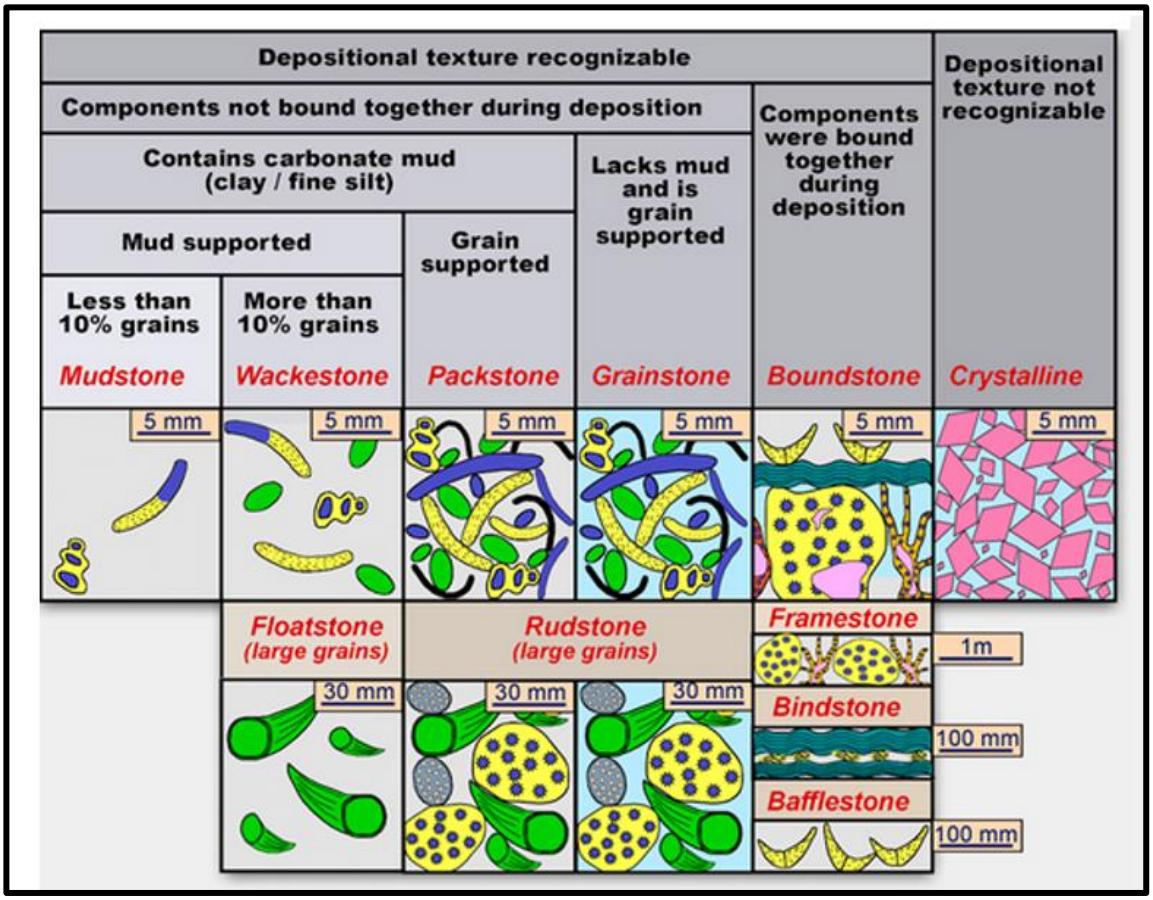

Figure 2.3. Dunham's classification approach for carbonate rocks is according to the depositional texture, the pale buff colour is a fine-grained carbonate matrix and the blue is porosity (Dunham, 1962; Perras and Diederichs 2011).

2.1.5 Petrography of Carbonate Rocks

Carbonate petrography is a difficult subject. Carbonate is produced by various species, which necessitates learning to distinguish a wide range of shell morphologies and wall structures. The shifting assemblages of organisms exacerbate the difficulty of recognizing skeletal grains throughout time, and the randomness of thin sections cuts through complicated shell morphologies. Furthermore, because many initial carbonate grains are made up of unstable minerals (particularly aragonite and high-Mg calcite), diagenetic modification in carbonate rocks is prevalent (Scholle and Ulmer-Scholle, 2003). The diversity of inorganic and biogenic carbonate mineralogy across time makes predicting diagenetic alteration patterns challenging. Therefore, carbonate rocks have a far wider variety of petrophysical characteristics than siliciclastic rocks, owing to pore system heterogeneity, such as distinct porosity classes, including secondary porosity, with variable pore throat diameters. Figure 2.4 illustrates various thin section of carbonate morphologies, textures, and bioclastic components with distinct morphologies and textures, which aid the experienced geologist in determining depositional settings and diagenetic processes.

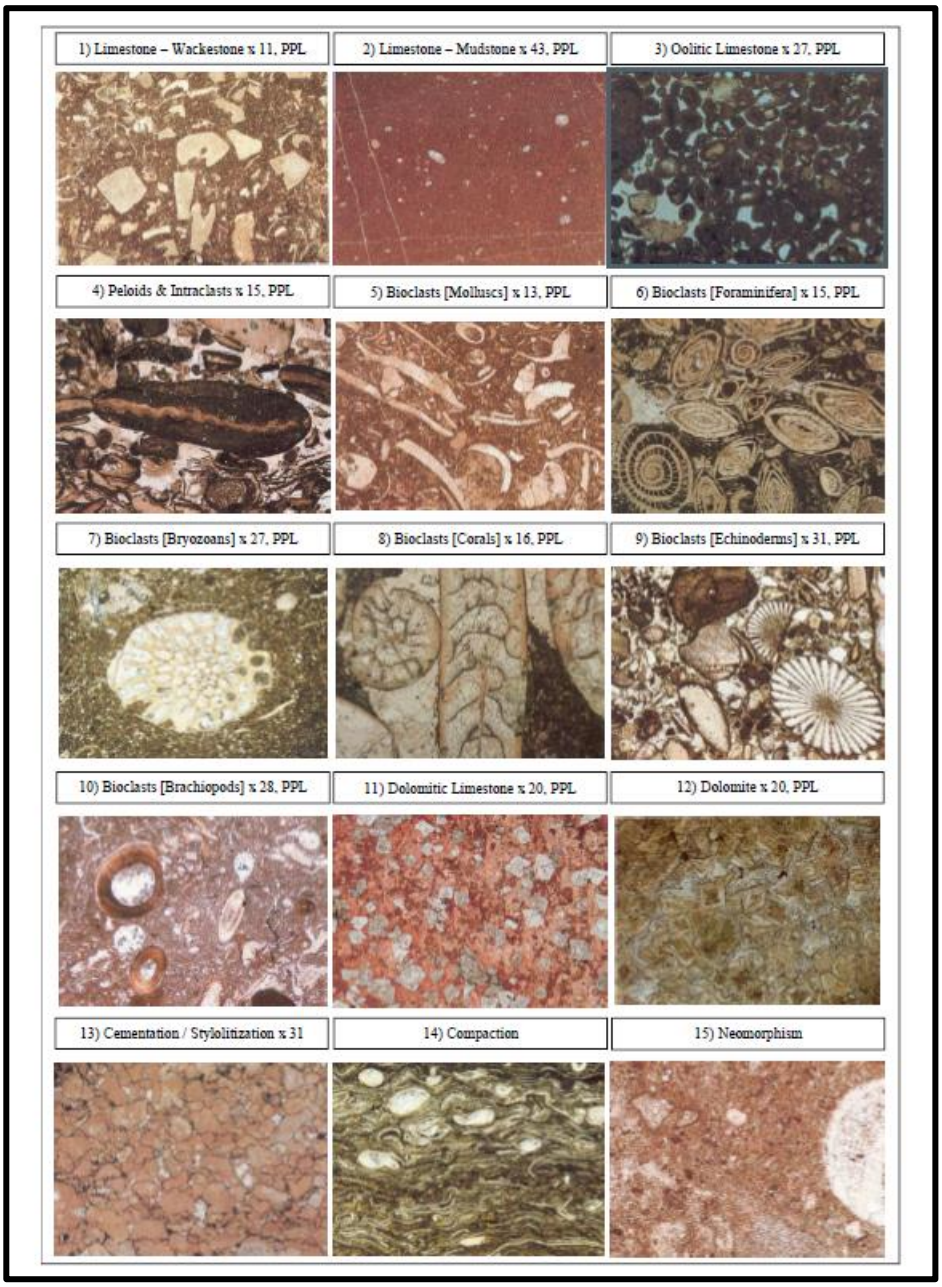

Figure 2.4. Thin sections of multiple carbonate morphologies, textures, and fossiliferous material (Adams *et al.*, 1984; Costa Gomes, 2022).

2.1.6 Sequence Stratigraphic Principles

Sequence stratigraphy is generally defined as the study of stratified rocks through geological history, genetically related strata bounded by surfaces of erosion or nondeposition (Posamentier *et al.*, 1988). An unconformity (the sequence boundary) is a surface separating younger from older strata along which there is evidence of subaerial exposure with a significant hiatus. The deposition of carbonate facies is highly affected by changes in relative sea level (RSL) (Tucker, 1985; Tucker and Wright 1990). Thus,

new carbonate geometries, such as prograding clinoforms, rudist buildups, tidal channels, and incisions, can be reproduced. Understanding the stratigraphic modelling that reveals the distribution of original reservoir properties, including the porosity and lithology, is important. Changes in sea level impact the depositional environment for carbonate sediments. In practice, stratigraphic architectures can usually be divided into three systems tracts: highstand systems tracts HST, lowstand systems tracts LST, and transgressive systems tracts TST (Handford and Loucks, 1993). At highstands of sea level, sediments migrated towards landward and formed high systems tracts. The depositional successions formed at low sea level stands and moved the deposition toward the basin is lowstand systems tracts (Figure 2.5). Those deposited during relative sea level rise are transgressive systems tracts. Unlike siliciclastic rocks, carbonate deposition is driven by biogenetic activities, for instance, sunlight, temperature, and salinity. These conditions play a vital role in constraining most carbonate deposition by flooding shallow marine platforms. It can be observed that the deposition of carbonates is mainly formed by the highstand systems tract. Moreover, through lowstand systems tract, carbonate sediments could be exposed to waters such as acidic rains that change them chemically (for example, karst and dissolution). This heterogeneity can eventually influence reservoir quality regarding the pore system and the deposition of carbonate facies.

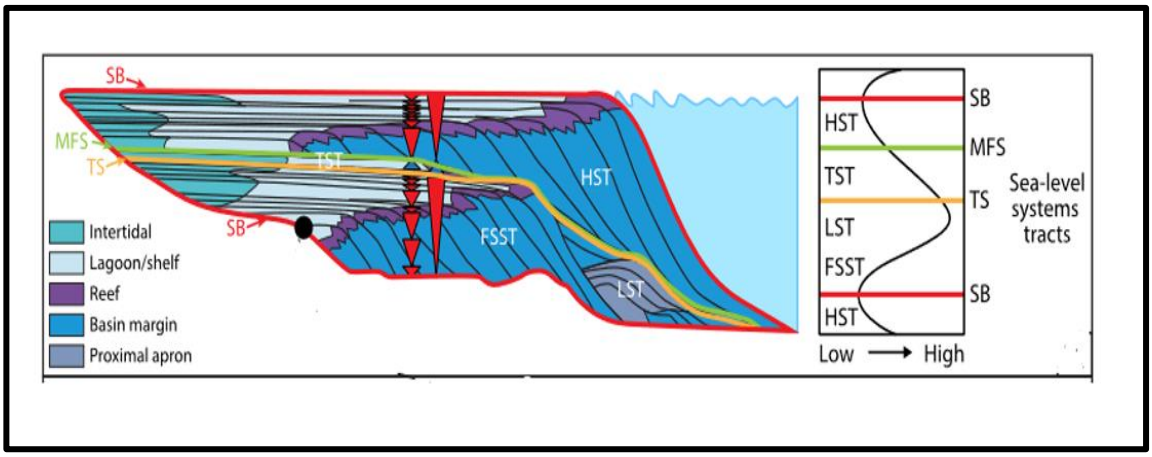

Figure 2.5. An illustration of the sequence stratigraphic model of carbonate depositional system showing sequence boundary (SB), maximum flooding surface (MFS), transgressive surface (TS), highstand system tract (HST), lowstand system tract (LST), transgressive system tract (TST), and falling stage system tract (FSST) (Borgomano *et al.*, 2020).

2.1.7 Channelized Systems in an Inner Carbonate Platform Setting

Grélaud *et al.*, 2010 stated that channelized systems are formed in an inner carbonate platform during the intervals of flooding or a significant drop in relative sea-level in the Cenomanian to Turonian of the Late Cretaceous. The interior of carbonate platform systems is often a relatively flat and shallow-water region. The depositional system in this environment is characterized by the aggradation of highly continuous and low-energy muddy lagoon facies. Within the carbonate platform, the formation and filling of intrashelf basins result in complicated geometries (Yose *et al.*, 2006). These structures cause significant heterogeneities at the regional and reservoir scales, which might significantly influence stratigraphic correlations and the occurrence of higher-quality reservoirs.

2.1.8 Types of Channelized Systems

There are two types of channelized systems: tidal channels, and incisions (Grélaud *et al.*, 2010). Generally, tidal channels are shallower than incisions; however, in some cases, they can extend to depths similar to the incisions (see figure below). Tidal channels are mostly related to the depositional systems that occur through flooding cycles of the inner platform. On the other hand, incisions are consistent with erosion systems during falls in relative sea level at the top of the sub-aerial exposed platform. The changes in morphology between incisions and channels are relatively modest. The major distinction between incisions and channels is the stratigraphic setting in which they form, as shown in Figure 2.6, summarizing the characteristics of both incision and channel erosion features.

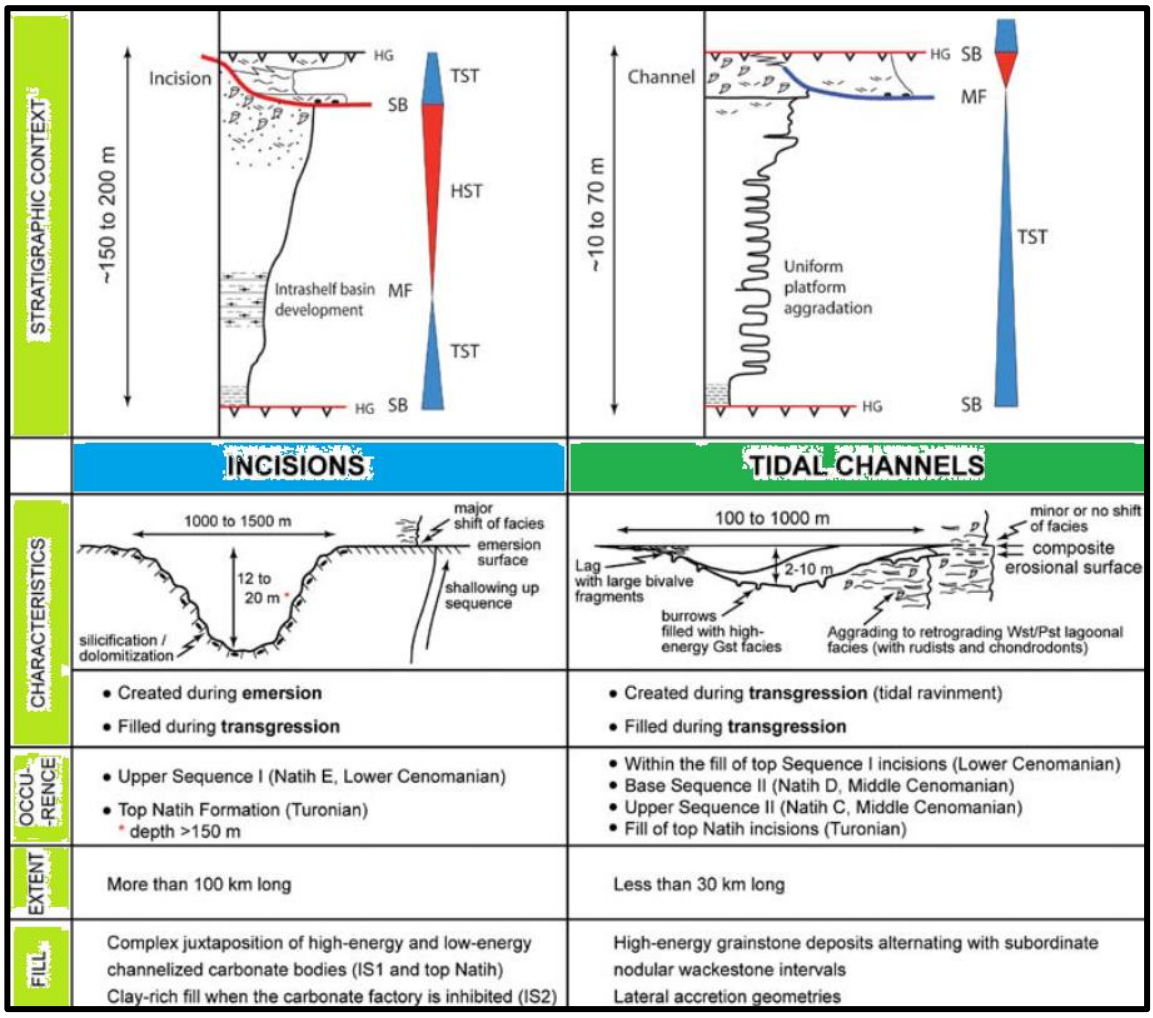

Figure 2.6. Schematic outlining the distinctions between the two channelized systems constructed on the Natih carbonate platform. Incision vs. channel terminology (Modified from Grélaud *et al.*, 2006).

2.2 Review of Seismic Reservoir Characterisation

2.2.1 Overview of Seismic Theory

At its most fundamental level, the seismic image is simply an expression of the amplitude of a seismic wave dependent on measuring the travel time and recording the variations in seismic amplitude and transit time which will be captured in the seismic rock physics model in terms of the wave velocity. The amplitude anomalies caused by abrupt vertical changes in the subsurface's seismic contrasts (density and velocity). Seismic waves travel through the ground due to the seismic soucouese generated for survey purposes which propagate a short tracing wave termed a "pulse." The propagation of seismic waves from a source point on the ground can be reflected or refracted by subsurface acoustic boundaries. The wave propagation velocity depends on the medium's density and elastic

modulus. There are two main types of seismic waves in the rock volume: compressional waves (P-wave) and shear waves (S-wave) and their respective velocities (P-wave velocity Vp, S-wave velocity Vs) (Telford *et al.*, 1990). Compressional or primary waves are the most important type of seismic wave propagation for survey purposes. The following equation explains their velocity of propagation (Vp) in terms of the medium's elastic moduli and density:

$$\mathrm{Vp} = \sqrt{\frac{k + \frac{4}{3}\mu}{p}} \qquad (1)$$

Where:

k = bulk modulus

μ = shear strength

ρ = density

The shear or secondary wave can be equally important in carbonates. The calculation of S-wave velocity is simply the root of shear strength divided by density:

$$\mathrm{Vs} = \sqrt{\frac{\mu}{p}} \qquad (2)$$

Several factors play important roles in determining seismic velocities, such as porosity and grain size. The relationship between porosity and grain size is scattered because of other interrelated factors such as grain shape, packing, and mineralogy. Hamilton and Bachman (1982) state that "the sound velocity increases with increasing mean grain size and decreasing amount of clay-sized material." Consequently, grain size indicates the velocity of sound. Further, other factors affecting seismic velocity include pressure, temperature, and rigidity.

Figure 2.7 illustrates the application of forward modelling (convolution model). It is possible to calculate the acoustic impedance of each layer in the earth model at wells using logs of the P-wave velocity, S-wave velocity, and bulk density. When seismic waves travel through two materials with different acoustic impedance, they will be partitioned at the acoustic boundary into reflected and transmitted. Acoustic impedance (I_p) is the product of the density (ρ) and velocity (V_P) of seismic wave propagation in the medium:

$$I_p = \rho V_P \qquad (3)$$

A seismic wave passing from medium 1 to medium 2, which is a thick elastic medium, the reflection coefficient (R) is given by:

$$R = \frac{\rho 2 Vp2 - \rho 1 Vp1}{\rho 2 Vp2 + \rho 1 Vp1} \qquad (4)$$

Where:

$\rho_1 V_{p1}$ = acoustic impedance of medium 1

$\rho_2 V_{p2}$ = acoustic impedance of medium 2

A layer interface's normal incidence reflectivity, R, is determined by the impedance contrast between the layers on either side. Then, the seismic amplitude of a wave that passes across the boundary can be calculated by multiplying the transmission coefficient and Wavelet. This, according to Yilmaz (2001), is the 1D convolutional model in its most basic form:

$$s(t) = w(t) \otimes R(t) + \epsilon(t) \qquad (5)$$

Where:

$s(t)$ the seismic trace

$w(t)$ the seismic Wavelet

$R(t)$ the reflectivity

$\epsilon(t)$ the random noise and

$\otimes$ the convolution operator

Convolutional forward modelling generates synthetic traces by combining a sequence of reflectivity coefficients with a seismic pulse represented by a wavelet. The issue is that there is frequently no appropriate model for the earth or the seismic source wavelet. Surface seismic data may be accessed and utilized to estimate layer thickness and impedance or velocity.

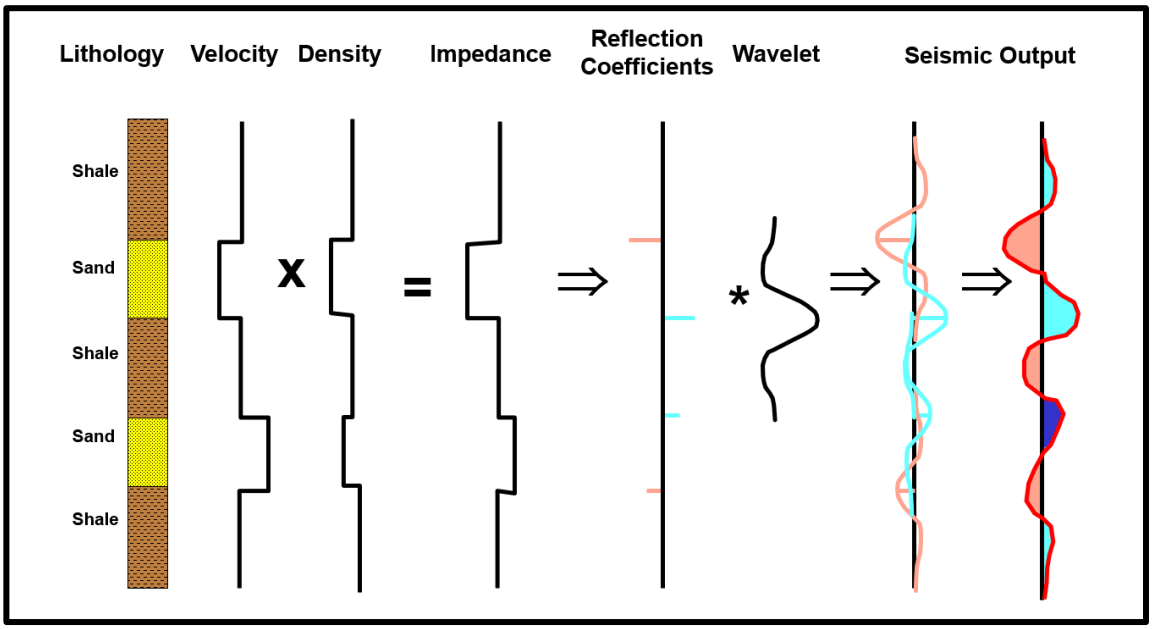

Figure 2.7. A Schematic depicts the basic steps of the convolutional forward modelling and the seismic response by multiplying the velocity and the density to get the impedance, then calculating the reflection coefficient at each significant rock boundary to convolve with the wavelet to get a modelled seismic trace.

2.2.2 Rock Physics Model

The rock physics model (RPM) is part of any seismic reservoir characterisation workflow. It links the reservoir properties (porosity, lithology, and water saturation) and the acoustic properties of the reservoir rock (velocity, bulk density, and acoustic impedance) (Figure 2.8). Sonic or P-wave/S-wave velocities could be applied to indicate reservoir properties such as the changes in lithology or fluid (Avseth *et al.*, 2010b).

The technique has been successfully used to estimate pore types as the main seismically derived feature to characterize reservoir quality (see Wagner *et al.*, 2012, Gavotti *et al.*, 2013, Mahgoub *et al.*, 2017). Also, it has been used quantitatively as the primary input of the static geological modelling, which is used to allocate the drilling locations for new wells and estimate oil reserves. The rock physics model should continuously be assessed and understood before a seismic inversion is undertaken (Sams *et al.*, 2017). It is critical to examine and correlate the data observed from the log and other well data, such as porosity (Ø), sonic (velocity), and density, and how these relate to facies parameters. Also, the velocity and density data could be utilized to characterize the field more accurately through the seismic well-tie.

Empirical models and effective medium theory are widely used in oil and gas exploration and production. Rock physics models can be derived in a variety of ways. It is represented by cross-plotting of anticipated elastic characteristics for litho-facies classes that revealing a more precise separation of classes. After the elastic properties at well sites have been analysed, seismic inversion spreads elastic values away from the wells. Some researchers have directly created empirical correlations using well data or core data to predict rock stress sensitivity. For example, Ødegaard and Avseth (2003) proposed an approach to analysing fluid and mineral volume variations over a cross plot of acoustic impedance versus Vp/Vs ratio. Also, Russell (2015) presented a new approach for linking rock physics to the seismic reservoir characterisation process (more details will be given in section 2.2.8).

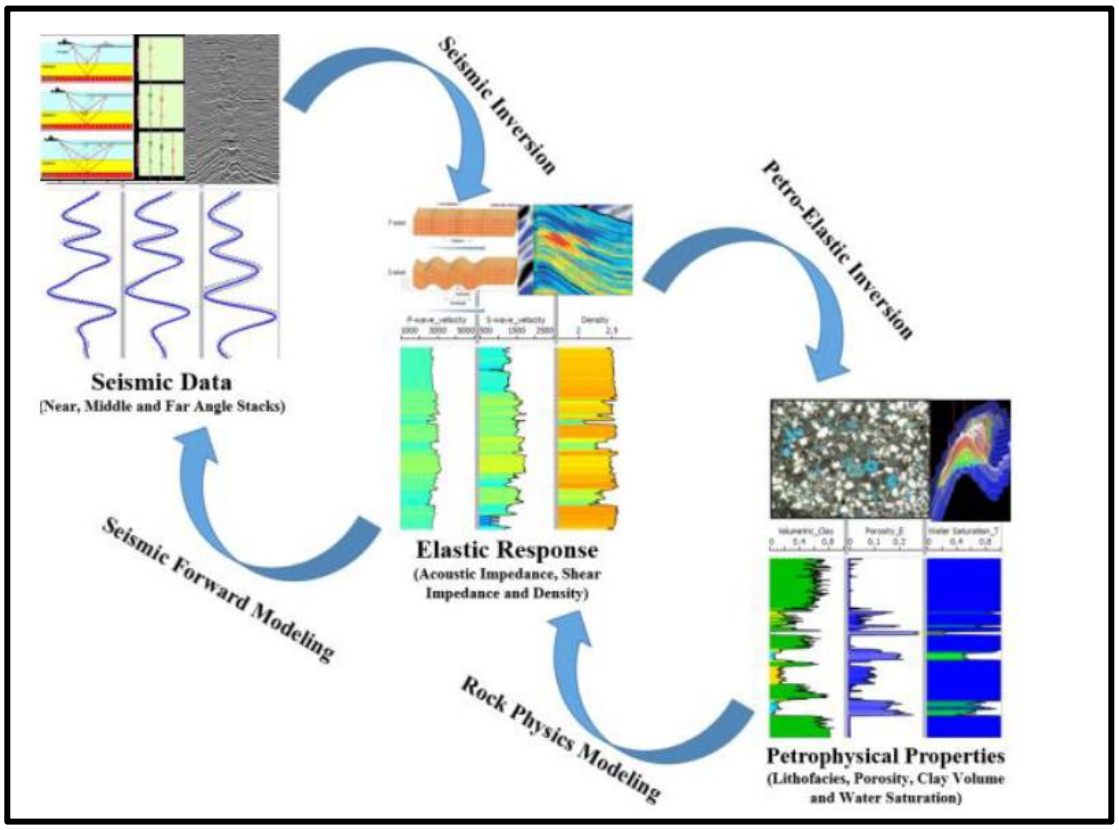

Figure 2.8. Detailed steps of rock physics modelling (RPM) are used to transform reservoir properties into elastic ones and explain the relationship between the seismic data, seismic inversion, and petrophysical characteristics (Babasafari *et al.*, 2018).

2.2.3 Modelling of Acoustic Properties in Carbonate Rocks

The rock physics model is quite challenging in carbonate rocks because the pore networks are more complicated than those in clastic rocks. Carbonate rocks are characterised by a range of pore types, including moldic, vuggy, interparticle, and intraparticle. Clastic rocks mostly feature intergranular pores. A large part of the evolution of such a pore system is frequently impacted by diagenesis. According to recent experimental findings, pore type can alter P-wave velocity by up to 40% for a given porosity (Xu and Payne 2009). It is essential to create a rock physics model that can handle various pore types to define carbonate reservoir rocks accurately. Each type of pore has a pore aspect ratio (the ratio of the short axis to the long axis). The concept is easily expandable to accommodate more than three pore types if necessary. However, the three-pore-type model is frequently enough (Figure 2.9).

Several schemes exist in the literature for modelling acoustic properties. Gassmann's (1951) hypothesis is well-recognized in petrophysics, mainly acoustic modelling. A theory of porous sandstone production (in the shape of a sphere), which is supposed to be homogeneous, and elastic waves, is developed in this work. The Gassmann hypothesis posits that the pore space is linked and that the pore fluid may freely move throughout the rock volume fast enough to equilibrate the seismically generated pore pressure during the seismic period, however, it may not apply to many carbonates (Rossebø *et al.*, 2005). Different materials are examined for acoustic wave propagation in dry and completely saturated liquid or gas conditions. The mathematical formula for the model that is proposed in this work to estimate wave velocities from confining pressure is provided below (Elhaj *et al.*, 2019):

$$V_p = A_p * P^{B_P} \qquad (6)$$

$$V_s = A_s * P^{B_S} \qquad (7)$$

Where:

V_p: compressional velocity

V_s: shear velocity

A & B: constant empirical factors

P: confining pressure

Due to the intricate pore structure, the link between porosity and velocity is highly scattered and unpredictable. These are known as scattering theories and include the first-

order scattering model of Kuster and Toksöz (KT) (1974), self-consistent approximations (SC) of Berryman (1980), and differential effective-medium (DEM) models proposed by Berge *et al.*, (1992). Forward modelling is used to compute the effective acoustic characteristics given the qualities of the solid medium, fluid medium properties, and pore space information. Zhan *et al.*, 2012 described a novel computational rock physics technique for understanding and predicting carbonate rocks' geophysical (elastic and electrical) response from the Middle East.

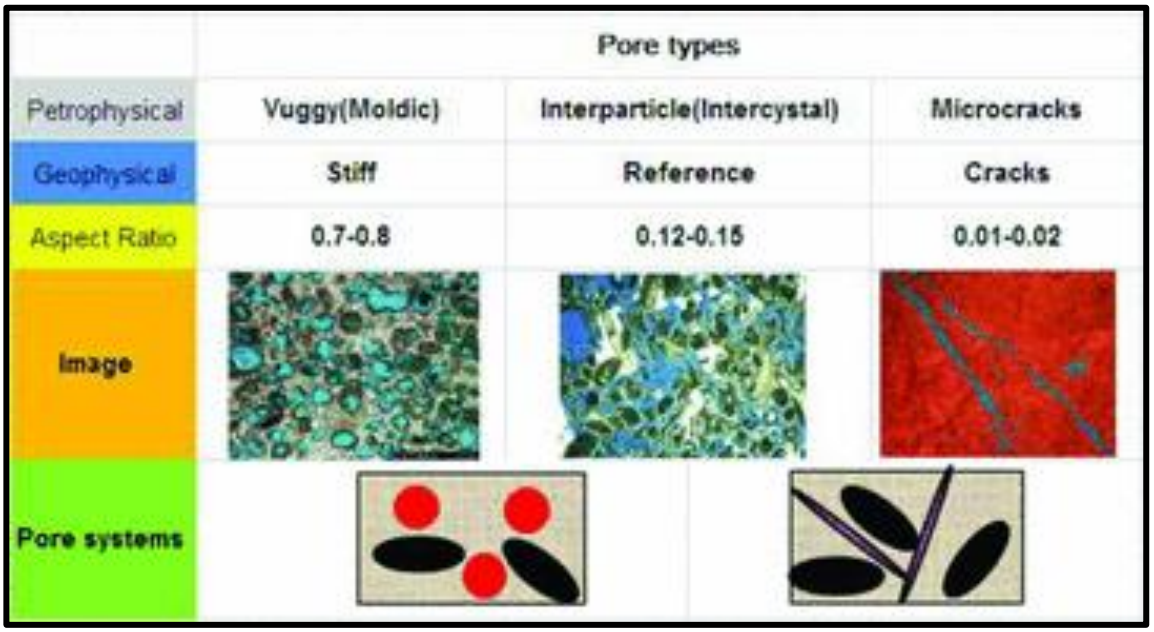

Figure 2.9. Pore-type classification in carbonate rocks and how to represent them in the rock physics model. A detailed description of the geophysical pore systems is as follows: a higher aspect ratio represents round stiff pores (vuggy or moldic pores), an intermediate aspect ratio represents reference pores (interparticle porosity), and a low aspect ratio indicates crack-like pores (Zhao *et al.*, 2013).

2.2.4 Seismic Well Tie

A crucial step in tying seismic data to the geological property is the well log to the seismic trace. The seismic well tie enables the relation of geological features (formation tops, location of a fault) with peaks or troughs on the seismic line that runs through or near the well location. While well logs are kept in the depth domain, seismic data is typically examined in the time domain. Hence, a precise seismic well tie is necessary for seismic inversion and reservoir characterisation. Seismic well ties typically follow a four-step process, which has been outlined by several authors (White and Simm, 2003; Wu *et al.*,

2022). The process involves: (1) calculating a reflectivity series using the velocity log and density log, (2) estimating a suitable wavelet, (3) creating a synthetic seismogram by convolution, and (4) comparing the synthetic and actual seismograms.

2.2.4.1 Calculating a Reflectivity Series

As mentioned in section 2.2.1, a reflection coefficient is calculated from the sonic and density logs (see Equation 2). The well log top of the reservoir might be measured in feet or meters, but the seismic data is measured in two-way transit time, which can be either in milliseconds or seconds (Figure 2.10). The velocity affects the time-depth relationship between seismic and well-log data. It is challenging to create an accurate velocity model since the velocity is nonlinear and varies with depth. As a result, check shots are typically employed to transform well data from the depth domain to the time domain. Zero offset vertical seismic profiles (VSPs) or check shots are frequently sampled to calibrate the integrated sonic. For a more precise time-depth relationship, sonic log calibration inserts extra samples between the check shot location (Martínez *et al.*, 2021).

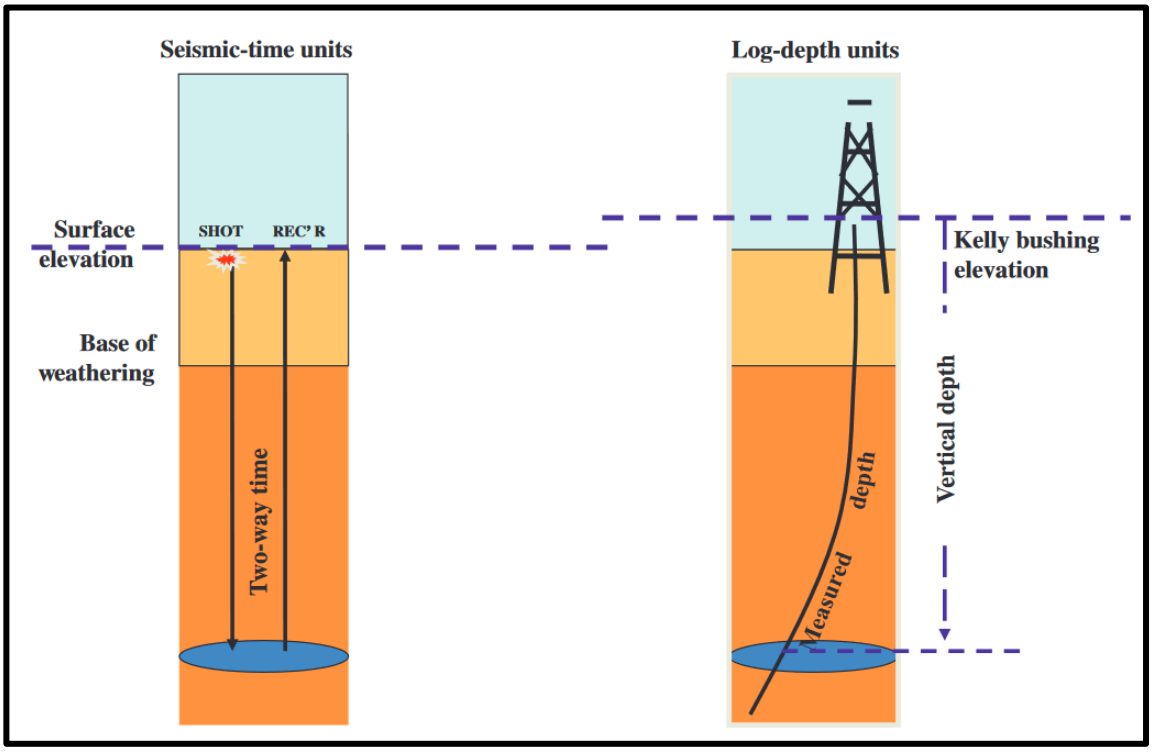

Figure 2.10. The comparison between the 3D seismic survey and the well-measurement vertical seismic profile (VSP) survey (Martínez *et al.*, 2021).

2.2.4.2 Estimating the Wavelet

Wavelet is created using the standard seismic well tie procedure, spectral smoothing over a specific frequency, and averaging over various seismic traces. The wavelet to use for the well tie can be selected or established in various ways. An analytical approach or statistical analysis can be used to identify the wavelet (Martínez *et al.*, 2021). Analytical techniques through analytics could determine the wavelet's form (minimal phase or zero phases) and the central frequency of the wavelet. Another approach is constructing a wavelet, using seismic statistics to identify the wavelet by statistical methods. It may provide a window around the seismic data and let the computer extract the wavelet structures using statistics. However, if good quality well data are available, a practical and quantitative method of extracting the wavelet is by a least-squares matching methodology in which the wavelet is directly computed from the seismic data (White and Simm, 2003). Perfect wavelets like the ricker can be utilized as the input signal, but they are likely to provide less accurate results and correlate less with actual seismic data.

2.2.4.3 Synthetic Seismogram

Sonic and density logs are combined to create an acoustic impedance (AI) log, which defines the reflection coefficients at subsurface boundaries and is used to create a reflectivity series. Then, the reflectivity series is convolved with a wavelet to produce a synthetic seismogram (Figure 2.11) (see Equation 4). In order to have a good well tie, the peak or trough from the synthetic seismogram should match the corresponding peak or trough in the seismic trace.

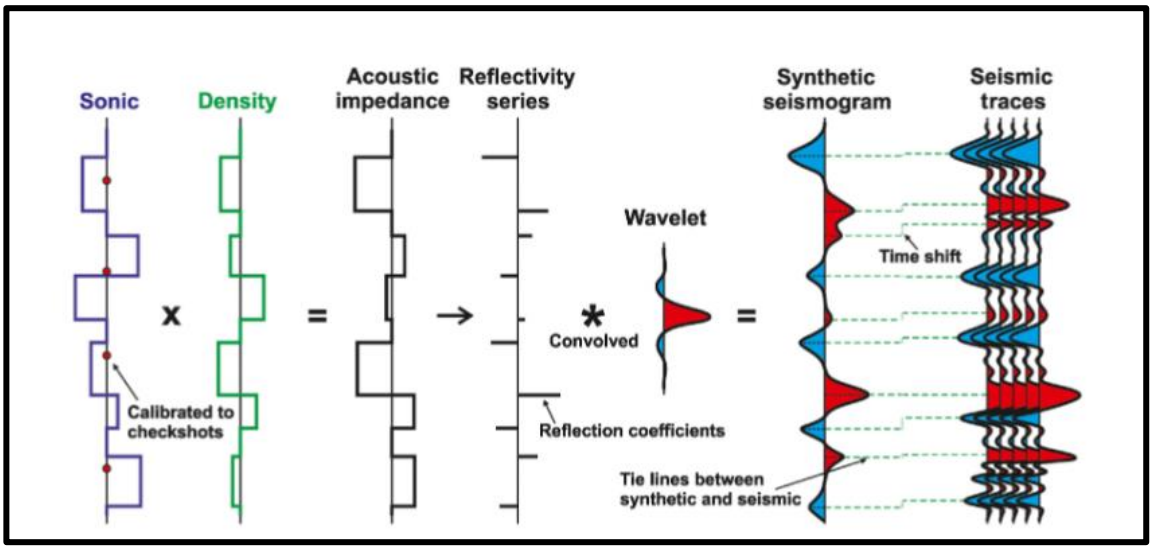

Figure 2.11. Workflow for generating a synthetic seismogram, the seismogram is then compared to the real seismic traces (Cox *et al.*, 2020).

2.2.4.4 Matching the Synthetic and Seismic Traces

As the quality and properties of the data frequently change over time, the well tie is normally conducted during a constrained time window rather than the whole depth extent of the well logs. White and Simm, 2003 stated that the synthetic trace derived from well logs could be shifted, stretched, and squeezed during the seismic well tie process to match the seismic traces near the well location. All these steps are shown in Figure 2.12.

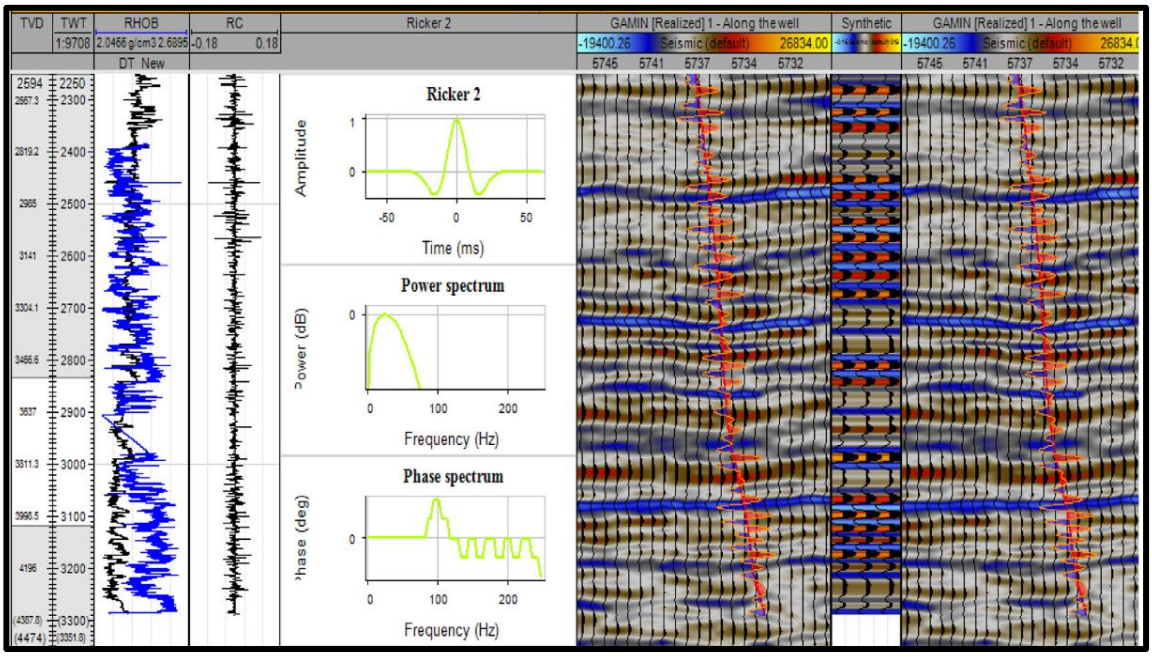

Figure 2.12. Comparison of the synthetic seismic traces (using the analytic technique) derived from the same well logs with actual seismic traces (Martínez *et al.*, 2021).

2.2.5 Seismic Inversion Methods

On a layer-by-layer basis, seismic attributes do not provide sufficient information regarding reservoir features. Thus, seismic inversion is a process commonly used in reservoir characterisation. The main objective of this technique is to convert seismic amplitude from interface properties to measurable rock properties (Simm and Bacon, 2014). It is an integration tool that uses seismic and well log data to characterize the spatial distribution of acoustic layering, (i.e. acoustic impedance) for subsurface rocks. The outputs of the inverted data can be helpful and more interpretable than the conventional seismic amplitude in providing rock properties such as porosity, lithology, sequence stratigraphy, and pore fluid (Hampson *et al.*, 2001; Naeem *et al.*, 2015). Consequently, seismic inversion delivers lithologic properties rather than just an interface property such as seismic amplitude and has been used since the 1980s (Li and Zhao, 2014). Seismic inversion can be classified into two main types, post-stack, and pre-stack (Figure 2.13).

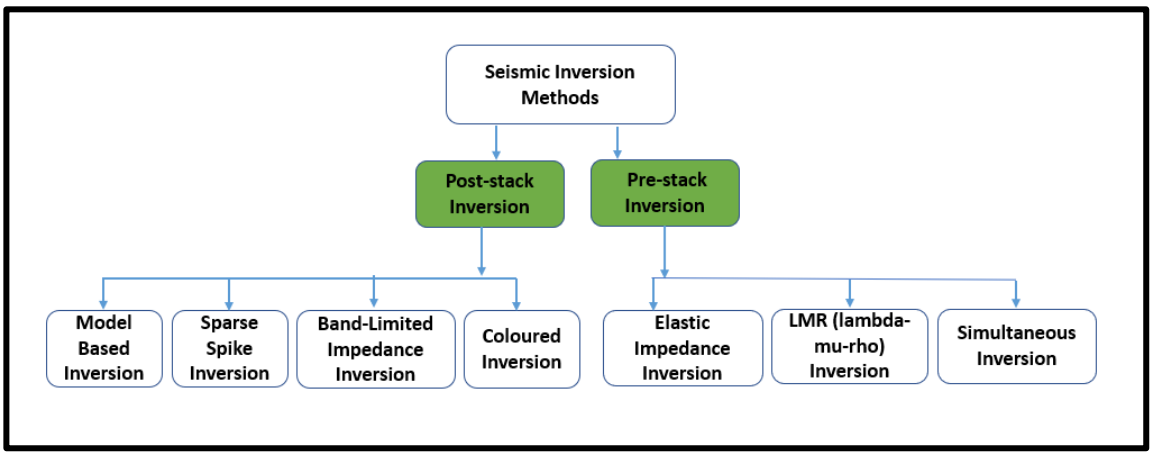

Figure 2.13 Seismic inversion methods.

A generalized workflow for integrating seismic data and well-log data during seismic inversion is shown in Figure 2.14. The input data of the seismic inversion are compressional wave (P-wave) and density logs with post-stack seismic amplitude. Various methods are used with post-stack seismic inversion, for instance, model-based, bandlimited, and sparse-spike inversion techniques (Russell and Hampson, 1991). Whatever methodology is used, an inversion algorithm is required for implementation, and there are two significant difficulties to consider when computing seismic inversion.

Firstly, the frequency in seismic data is often confined in the region of 10 Hz to 80 Hz (bandlimited), so it lacks the original low and high-frequency data that well-log data possesses. Secondly, the impedance model solution obtained from seismic inversion is non-unique. It is critical to recover as many missing frequencies as possible during inversion, and because log data contains frequencies higher and lower than seismic data, it is used to restrict the inversion.

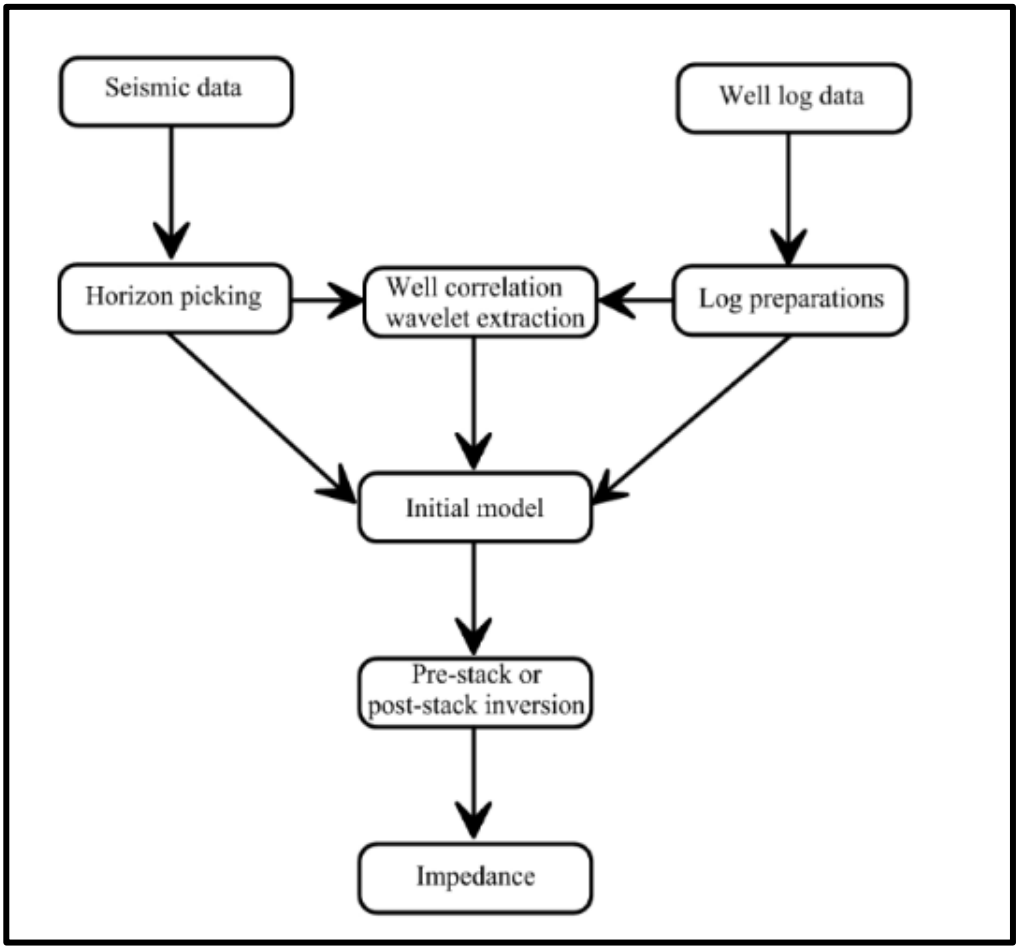

Figure 2.14. Seismic inversion workflow for integrating seismic and well log data (Maurya and Singh, 2018).

2.2.5.1 Seismic Inversion Theory

The objective of the seismic inversion method is to create the actual reflectivity or Reflectivity Coefficient (RC) from the observed seismic trace. However, since the seismic trace is bandlimited by the seismic wavelet, Lindseth (1979) proposed to recover the low-frequency component is to generate an impedance model from well log, applying

a high-cut filter to this model to produce a low-frequency trend, and then adding back the trend to final inverted log (Figure 2.15). Seismic inversion is undertaking a convolutional model for a noise-free seismic trace, which can be shown below:

$$s(t) = r(t)*w(t) \qquad (8)$$

s(t) is the observed seismic trace, *r(t)* is the actual reflectivity, *w(t)* is the seismic wavelet, and * denotes convolution.

Seismic inversion can be classified in several ways based on the input of seismic traces (post-stack, angle-stacks, or gathers) and the number of output property solutions (single or multiple). Thus, output properties can broadly be divided either as seismic rock properties (e.g., Acoustic Impedance (AI), Elastic Impedance (EI), Extended Elastic Impedance (EEI), Compressional-wave Velocity (V_p), Shear- wave Velocity (V_s), V_p/V_s Ratio) or petrophysical properties such as porosity, Net-to-Gross, the volume of Shale (V_{sh}). A more general and complete description of the process can be found in Hampson *et al.*, (2001). The following sections provide a brief overview of both techniques which were used in this research to estimate the acoustic impedance of the main reservoir in inter well-region.

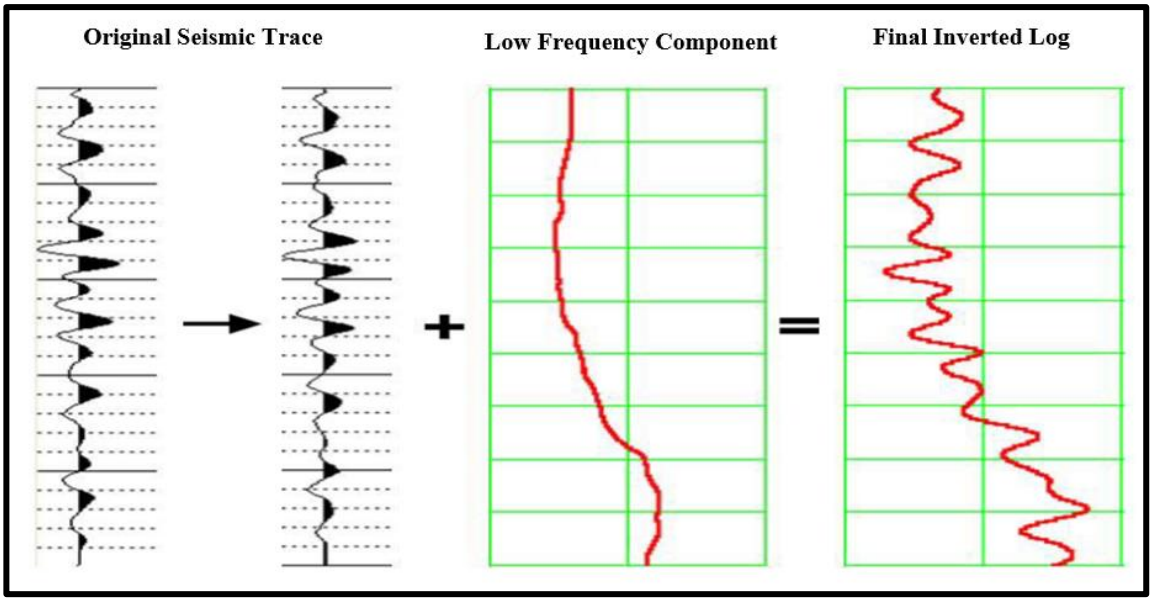

Figure 2.15. An illustration of the production of the final inverted log that is used in the seismic inversion technique to recover the low-frequency component. Left to right, the original seismic trace and then adding a low-frequency component to produce the inverted log (Russell, 2004).

2.2.5.2 Model-Based Inversion

The approach is based on guessing the reflectivity coefficients and comparing synthetic traces to the seismic trace (Maurya and Singh, 2018). The convolutional model calculates the synthetic trace as a convolution of the Wavelet and reflectivity. Since this results in missing low-frequency content, this vital component can be recovered using log data, using the method developed by Lindseth (1979). The differences between the synthetic and real traces are calculated and minimized by successive updates of reflectivity.

2.2.5.3 Linear Programming Sparse Spike (LPSS)

This inversion was initially suggested by Oldenburg *et al.,* (1983) and then improved by Li (2001). The inversion of the seismic trace is carried out under the sparseness assumptions of the reflectivity series. Linear programming is used to create the estimation of the sparse reflectivity from the seismic data (Maurya and Singh, 2018); it could be written as below:

$$S = L_m + N \qquad (9)$$

S is the actual seismic data, *(L)* is the linear that connected the model to actual seismic, *(m)* model parameters, *and (N)* is noise (Russell, 2004). As the bandlimited seismic Wavelet often means that the low and high-frequency components of the seismic spectrum are missing, we use the frequency domain constraints to gain them.

2.2.6 Seismic Attributes Techniques

Seismic attributes are derived from the original seismic data through statistical processing to emphasize specific geological, physical, or quantitative measurements of reservoir properties. They look at the form or other characteristics of one or more seismic traces and how they correlate with time (Aminzadeh and Dasgupta, 2013). Since the 1970s, seismic attribute analysis has progressed. Instantaneous amplitude was employed as the direct indication of oil and gas. Scientists identified a huge number of seismic attributes in the 1980s. These attributes were mathematically well-defined and had well-defined implications in other areas (Li and Zhao, 2014). 3-D continuous attributes were widely

employed in the late 1980s, with the emergence of multidimensional attributes such as dip and azimuth since these attributes had obvious and explicit geological meanings. Further, seismic attributes are often used to convey information about a seismic waveform's shape, location, and amplitude (Koson *et al.*, 2014). The following section discusses in more detail the classification of the seismic attributes.

2.2.7 Classification of Seismic Attributes

Geophysicists have put forth much effort toward the classification of seismic attributes. Today, over 50 distinct attributes measured from seismic waves are utilized to understand sequence stratigraphy, structure, and reservoir quality (Chopra and Marfurt, 2005). In actual applications, there are a lot of accessible seismic attributes, and suitable categorization helps understand and exploit seismic features. Seismic attributes can be classified into geometric and physical attributes (Li and Zhao, 2014). Geometric attributes or seismic reflection configurations are employed for seismic stratigraphy, sequence stratigraphy, and structural interpretation, such as the travel time, seismic event reflection intensity, and lateral continuity. The second group (physical attributes) are used mainly for lithology and reservoir characteristics. Several categorization methods for seismic properties are based on various factors. Table 2 summarises some of the most regularly utilized seismic characteristics. The following section will review and introduce some seismic attributes used in this research to understand the seismic attribute application at the basic stage.

Geological Characteristics	Bright spots, dark spots, sand bodies	Petroliferous property	Sequence	Faults and cracks
Seismic Attributes	Instantaneous amplitude, reflection intensity, the maximum value of the peak amplitude	Instantaneous phase, instantaneous frequency, reflection intensity, power spectrum	Instantaneous frequency, decibel-based reflection intensity	The first, second, third spectral peak frequencies, limited frequency bandwidth energy, KLPC1 average correlation, correlated kurtosis

Table 2. A classification scheme for seismic attributes and associated geological characteristics is used in seismic interpretation (Li and Zhao, 2014).

2.2.7.1 Variance Attribute

The variance attribute is an edge detection approach for estimating the seismic signal's localized variance. It is calculated in three dimensions and depicts trace-to-trace variability over sample intervals. High-variance coefficients come from a discontinuity in the seismic horizon, whereas low-variance coefficients emerge from continuous seismic horizons (Li and Zhao, 2014). As a result, it may detect discontinuities in seismic data related to faulting or stratigraphy. The variance attribute has been used to aid in imaging channels and faults on both horizon slices and vertical seismic profiles. It also highlights large fault zones, fractures, unconformities, and major sequence boundaries. Hence, variance volumes considerably improve the capability to image structural incoherence and stratigraphic deposition on time and horizon slices (Almasgari *et al.*, 2020).

2.2.7.2 (RMS) Amplitude

The RMS amplitude attribute is calculated by taking the square root of the sum of the squared amplitudes and dividing it by the number of samples utilized. It is calculated in a sliding tapered window of N samples as the square root of the sum of all the trace values (x) squared, where (w) and (n) are the window values as presented in Equation 9 (Koson *et al.,* 2014).

$$x_{rms} = \sqrt{\frac{1}{N}} \sum_{n-1}^{N} w_n x_n^2 \qquad (10)$$

The RMS amplitude is a useful feature for highlighting variations in amplitude strength in horizontal and vertical dimensions. It is used in the same manner as reflection strength to identify bright spots and amplitude abnormalities in seismic data. In contrast to reflection strength, resolution can be set by adjusting the window length; more oversized windows offer smoother amplitude estimates, which is occasionally advantageous. Additionally, this attribute can be used as an indicator for facies variations, channel bodies, compaction effects, and unconformities (Almasgari *et al.,* 2020).

2.2.7.3 Frequency Spectral Decomposition

These attributes provided us with crucial information on the lithology, stratigraphic channels, and geologic characteristics for a very long period (Chopra and Marfurt, 2007). A seismic signal's time-frequency breakdown, also known as spectral decomposition, describes the time-dependent frequency response of underground reservoirs and rocks (Othman *et al.,* 2016). The seismic signal is dissected via spectral decomposition into its frequencies. Castagna *et al.,* (2003) used matching pursuit decomposition to identify low-frequency shadows underlying hydrocarbon reserves for instantaneous spectrum analysis. For seismic interpretation, spectral decomposition has proven to be a reliable method. It is used to map the thickness of the temporal bed and identify stratigraphic traps (Partyka *et al.,* 1999). Through mathematical techniques like a discrete Fourier transform (DFT), continuous wavelet transform (CWT), and other techniques, spectral decomposition converts seismic data into the frequency domain (Othman *et al.,* 2018). According to Hardy *et al.,* (2003), the average frequency characteristic obtained from sine bend fitting strongly correlates with the amount of shale in a particular area. The modified outputs

include tuning cubes and a variety of discrete standard frequency cubes. More details about the application of the frequency spectral decomposition method will be in Chapter 5.

2.2.8 Integrated Seismic Reservoir Characterisation Workflow

Seismic reservoir characterisation, also known as reservoir geophysics, has been growing as a field in petroleum exploration and is widely applied in oil and gas exploration, production, and development. The seismic reservoir characterisation process integrates vertical high-resolution data (wells) or core data with lateral survey data (seismic). The main objective is to characterize and model the spatial distribution of the petrophysical properties and lithofacies across the field area. These models play a vital role in developing the wells and optimizing the oilfield performance more reliably. In addition, integrating data from multiple sources and geology and geophysics disciplines is essential for a better understanding of the reservoir properties (Walls *et al.*, 2004).

The reservoir geophysics workflow processes use both deterministic and statistical approaches. Russell (2015) explained the main steps of reservoir geophysics in his study. The start point of the seismic reservoir characterisation is the two primary sources of the data (well log and seismic) as input data (Figure 2.16). In order to do proper rock physics and synthetic modelling, the well data should ideally comprise P-wave velocity (V_p), S-wave velocity (Vs), and density. Before tying the zero-offset synthetic seismogram to the stacked seismic data, a wavelet must first be extracted from the seismic data for the following phase, synthetic seismic modelling. The post or pre-stack seismic data may then be compared to post or pre-stack synthetics developed after that.

Following that, the data available for the project will help determine the primary target. Full pre-stack inversion can be used if pre-stack data with offset or angle information is available, producing P-impedance, S-impedance, and density (from which additional elastic volumes such as Vp/ Vs ratio, Poisson's ratio, Young's modulus, lambda-mu, lambda-rho, Vp and Vs can be formed. On the other hand, if only post-stack data is available, post-stack inversion yields P-impedance (the sum of density and P-wave velocity). The outcome of the reservoir geophysics workflow will be utilized to predict various petrophysical properties in the inter-well region based on geostatistical methods such as linear regression or probabilistic neural network methods (PNN).

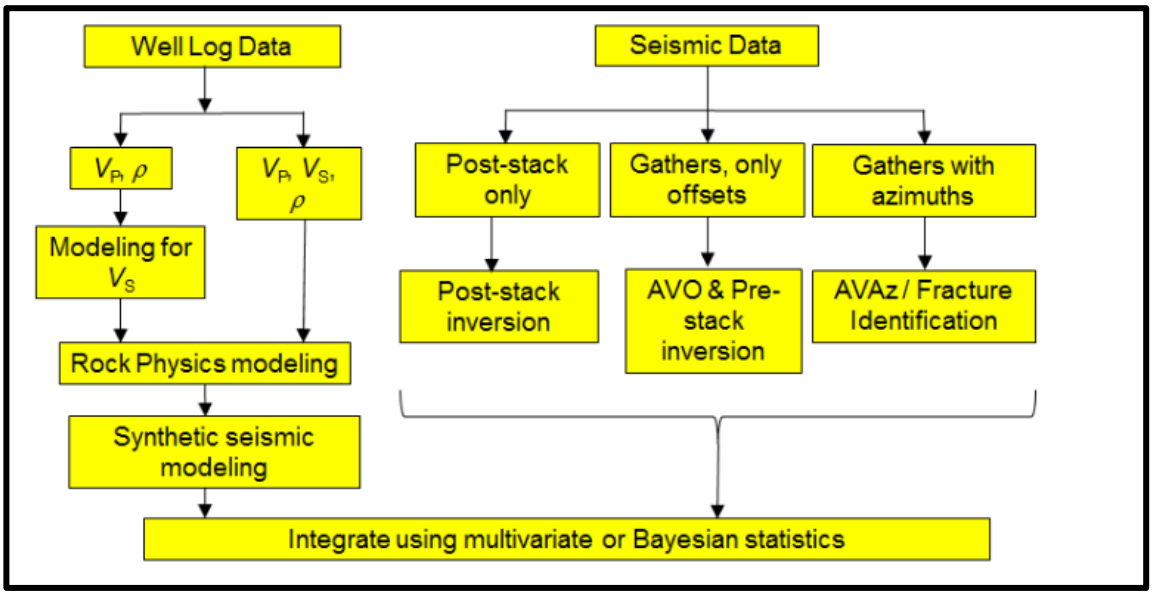

Figure 2.16. Integrated seismic reservoir characterisation workflow (Russell, 2015).

2.2.9 Utilizing Seismic Reservoir Characterisation for the Exploration and Development of Carbonate Reservoirs

Seismic reservoir characterisation is a complex project in the case of carbonate rock due to the complexity of carbonates. Also, carbonate reservoirs' elastic properties (velocity, density, acoustic impedance) are strongly related to diagenetic processes and mineralogical composition. Understanding of carbonate platforms and processes has been improved because of improved seismic data quality in the last years, inventive use of seismic attribute combinations, extraction of geomorphological data, and novel quantitative methodologies (Liu and Wang 2017). In other words, flow units, barriers, and related carbonate depositional and diagenetic facies can now be mapped using 3D data, providing a unique view of how these facies' interactions have altered through time in response to tectonic, oceanic, and climatic pressures. By combining dynamic data with seismic properties, drill log and core data, and seismic characteristics, producing fields can gain additional insights. Cross-well seismic can supplement this strategy, especially where overburden effects make vertical imaging difficult (Hendry *et al.*, 2021).

2.2.10 Applications of Seismic Reservoir Characterisation in Carbonate Reservoirs

The characterisation process includes the analysis of reflection configuration, amplitude magnitude, frequency, and continuity in carbonate seismic facies. Similar processes have

grown to be an accepted practice. Today, a more deterministic and iterative workflow that is geologically conditioned and reduces uncertainty allows for a more accurate inter-well volume and reservoir modelling prediction. These approaches include the inversion of seismic data, relationships between rock typing and rock physics, and seismic resolution of depositional geometries.

Russell *et al.,* (2002) pointed out the approach of geostatistics and multi-attribute prediction for integrating seismic and well-log data and illustrated this new procedure with a case study. In their approach, a case study involved the prediction of porosity in the Blackfoot field of central Alberta. Russell *et al.,* (2002) demonstrated an excellent correlation between porosity and the inverted acoustic impedance volume and provided a better match to the observed well logs, as well as outlined the channel sand much more clearly than on the original seismic volume. Yose *et al.,* (2006) illustrated how 3D seismic data is used to differentiate platform facies and flow units and populate them into a sequence stratigraphic framework for reservoir model construction through a combination of volume types and integrated techniques. This approach is preferable to seismic attributes because it offers different scenarios to address lateral-sweep interpretation, which cannot be done with the well log or seismic volume.

2.2.11 Introduction of Facies Classification

The analysis and classification methods can be applied based on several datasets (different scales) such as geological information (core samples) or well control data and seismic attributes to characterize the 3D reservoir model. Thus, the term facies definition refers mainly to the facies analysis from geological data; seismic lithofacies indicates the classification and spatial distribution of facies obtained from seismic scale, and electro-facies (log-facies profile) from petrophysical logs at the well. Facies classification is different based on the datasets; hence the recognition of facies in a seismic dataset is less precise than facies acquired from log data or geological information due to the limited resolution and signal-to-noise ratio. Moreover, the number of facies distributions from seismic data is often lower than initial facies (Grana *et al.,* 2017).

Statistical classification approaches can be used to assess facies modelling based on well-log data because they could identify multiple characteristics concurrently (Grana *et al.,* 2016). Initially, one of the main steps to characterize 3D reservoir models is the facies

model along the well section. The most common well log data in facies modelling are gamma-ray (GR), resistivity, and spontaneous potential (SP), or they could be from other volumetric fractions (such as porosity). The primary lithology, depositional system, and one or multiple facies can be identified based on the log-facies classifier. Additional information from cores or outcrops could add valuable information to the facies from well log scale, yet cores are not available for all wells. The facies recognition can be extended to the whole reservoir model by incorporating regional geologic data, core analysis, and depositional system model. The accuracy of facies identification based on well data is very high at the wellbore position. It could be challenged if the facies extension goes further away from the well control in fields with a few wells and significant heterogeneity of the reservoirs.

From the seismic exploration side, lithofacies is described as stratigraphic units with specified reflection characteristics and seismic properties (velocity and density). Consequently, the discrimination of the seismic facies is complementary to other methods of facies classification. Previously, seismic facies recognition was carried out by hand. However, this approach includes a time consumption and is not appropriate for large seismic data volumes. There is one approach to estimating a vast amount of data and predicting facies characteristics through computer and automatic seismic facies classification techniques (Marroquín, 2014; Song *et al.*, 2016). In recent years, as a result of the increased number of seismic attributes and seismic inversion, the task of seismic facies recognition has been extended in the modelling of reservoir properties. Typically, facies classification includes data at different scales: core samples and thin sections, and well log data (Grana *et al.*, 2016). This will provide more understanding of the lateral facies estimation by matching facies obtained from well data with seismic attribute models. Integration of lithofacies with the physical features of rocks can increase the ability to use seismic interpretation to predict reservoir description. Also, facies classification based on well data plays a vital role in calibrating statistical populations to constrain seismic reservoir characterisation (Avseth *et al.*, 2010a).

The classification and delineation of rock facies is an effective procedure for characterizing reservoir properties and extracting more features than reservoir structure (Liu *et al.*, 2017). Therefore, it is one of the initial steps to construct or update a reservoir model and delineate the heterogeneity (John *et al.*, 2008). The facies patterns are typically recognized through analysing electro-facies and core data. However, such techniques

pose challenges and limitations due to the sparseness and limited distribution of the well. Also, the provided information is restricted to the vertical reservoir description and does not entirely provide reservoir characterisation (de Matos *et al.,* 2007). This will lead to a partial knowledge of the spatial distribution of the facies between the wells, and many fields lack well control, particularly at the onset of the exportation phase. The characterisation of the reservoir model requires a combination of various datasets to delineate a more descriptive and reliable geological feature (Johann *et al.,* 2001). Therefore, integration of seismic facies classification and other data will effectively characterize vertical and lateral heterogeneity in the reservoirs. The result of the seismic facies identification is predominantly a single map or volume that leads to the prediction of the variations in the porosity, lithology, and fluid saturation (Marroquín, 2014; Song *et al.,* 2017).

2.2.12 Seismic Facies Classification Techniques

There are two major techniques of seismic facies classification: unsupervised and supervised. The main difference between these two techniques is added prior information (such as geological and well information). If this is available, the classification is supervised (Barnes, 2001). On the other hand, without using prior information, the classification is unsupervised (Marroquín, 2014). The latter is of prime use for oil exploration in new areas with few or no wells explored, while the former is most valuable in the developing of oilfields, where the information acquired at the wellbores may be appropriately distributed to the areas between the wells (Saggaf *et al.,* 2003). The approach classified seismic attributes into a finite number of facies classes (also called clusters) through the distribution of the shape of seismic waveforms (Marroquín *et al.,* 2009). As for the supervised method, the classification and training of facies clusters are first applied based on well log and seismic data around the wells, such as probabilistic neural network (PNN). Secondly, the classification results are used in seismic data after the training to classify the facies in inter-well regions. These classes are similar in their geological features and vary from other facies (John *et al.,* 2008; Saggaf *et al.,* 2003). Based on the variation of the structure, seismic traces can be classified into many attributes: curvature, coherence, and that sensitivity to the rock and fluid properties such as seismic inversion and amplitude versus offset (AVO) (Roy and Marfurt, 2011). The outcome usually estimates lithofacies or petrophysical properties (porosity and fluid saturation) (Figure 2.17).

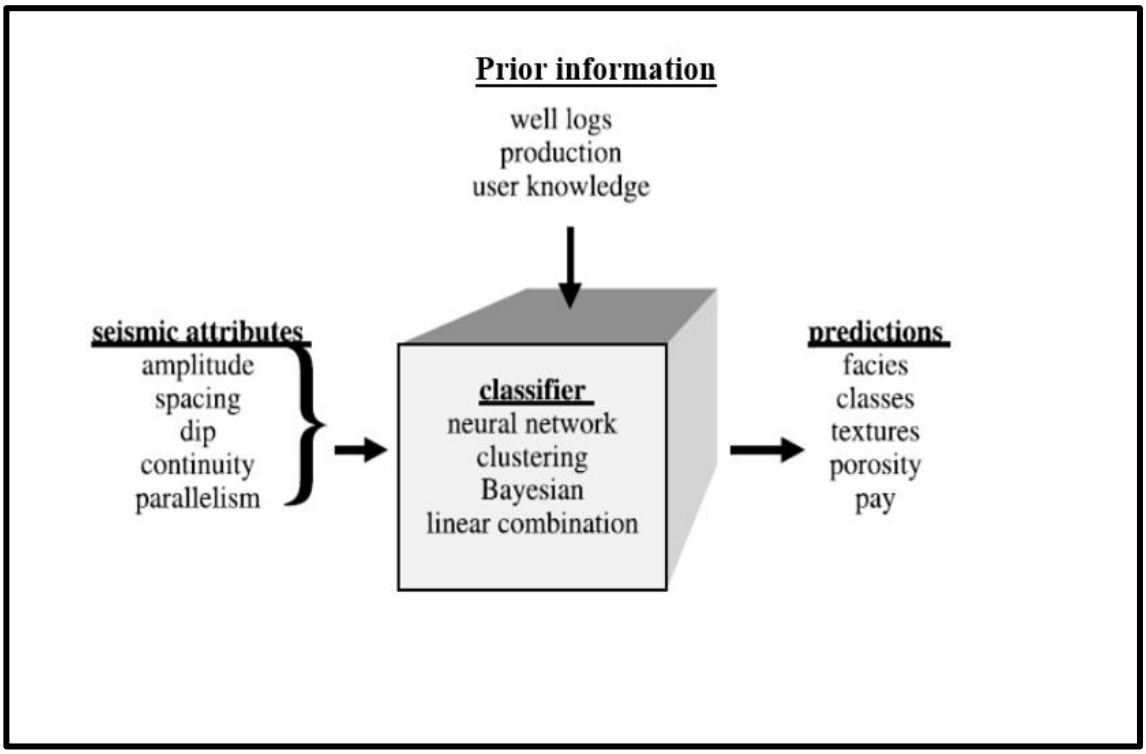

Figure 2.17. Schematic illustration of seismic pattern recognition (multi-attribute analysis). A set of attributes are fed into a black-box algorithm, which could contain a neural network. The black box classifies the input data at each data point. The output is typically a prediction of seismic facies or a physical property such as porosity (Barnes, 2001).

2.2.13 Probabilistic Neural Networks (PNN)

The probabilistic neural network (PNN) is a mathematical algorithm using neural network architecture for its implementation (Figure 2.18) (Hampson *et al.* 2001). The PNN can be used either for mapping or classification of properties such as porosity and lithology. The probabilistic method uses a set of one or more parameter measurements, called independent variables, to estimate the value of a single dependent variable. This algorithm is similar to the Kriging theory, which adopts each new output value and can be set up as a linear combination of the training data. However, the most crucial feature of PNN is the capability of the classification to learn from massive data and improve its implication through learning. The algorithm analyses various seismic attributes estimated directly from the seismic data plus the external attributes generated indirectly, such as acoustic impedance inversion, and then selects the best attributes to cross-plot with the predicated well log (Maurya and Singh, 2018). This technique aims to find an operator to predict well logs from seismic data, mainly seismic attributes that are defined as any

mathematical transform of the seismic trace. It is used with seismic inversion as a constraint to obtain a seismically derived property.

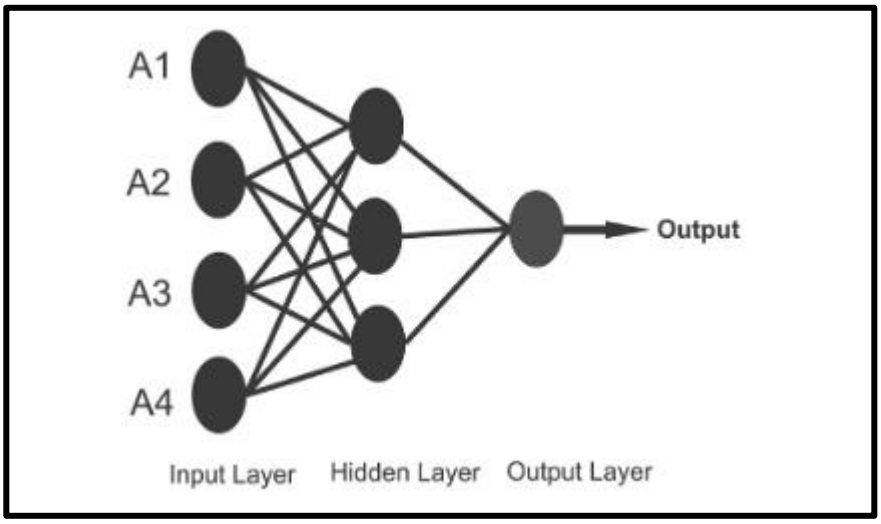

Figure 2.18. Neural network architecture consists of one input layer, one hidden layer, and one input layer (Hampson *et al.*, 2001).

2.3 Review of Integrated Reservoir Modelling Workflow

The 3D modelling approach has become popular in viewing and evaluating the environment and is extensively utilized in various industries. Integrating good quality static and dynamic data makes it crucial to use geological modelling to comprehend the subsurface data quantitatively in terms of structure, sedimentological facies, and petrophysical characteristics (Li *et al.*, 2019). The workflow of gas and oil exploration and production benefits significantly from geological modelling. Several crucial steps are included in the geological modelling workflow to create a three-dimensional reservoir model. The steps of the modelling process are as follows: (e.g., Yan-lin *et al.*, 2011).

2.3.1 Structural Modelling

It is common to practice building 3D structural and fault models using a combination of structural inputs (seismic interpretation data and well logs) and stratigraphic inputs (to define internal layering), enabling a "Modelling While Interpreting" methodology to build

models as needed (Ringrose and Bentley, 2016). A geological structural framework for all reservoir models is created by extracting the major geological surfaces from seismic and well data. The framework is then given the finite-difference flow grid, with little freedom for grid distortion to suit the actual reservoir design (Bentley and Ringrose, 2017). The structural model is the initial step in creating the three-dimensional grid, depicting the reservoir design's depth and size. The building of the structural model is subdivided into multiple components, including fault modelling, building and refining the horizon model, and structural gridding.

2.3.2 Porosity Modelling

One of the fundamental petrophysical features of reservoirs is porosity, which offers essential storage for hydrocarbons. A critical step in the geological modelling workflow is determining a reservoir's porosity distribution. Both deterministic and stochastic algorithms can be used to model porosity. The method used to populate the porosity values and distribute them across the 3D model, however, can provide a variety of outcomes since the porosity distribution dictates the reservoir model's pore volume, which affects STOIIP estimates. Additionally, after the porosity model is built, other petrophysical parameters, such as fluid saturation and permeability, can be modelled based on their correlation with porosity. Porosity can be modelled using a variety of geostatistical methods. A 2D map or 3D model conditioned to well porosity data may be created using these methods. Facies models, seismic data, and spatial trends in porosity can all be used to condition the porosity model. Geostatistical estimation methods for porosity modelling include the following (Pyrcz and Deutsch, 2014; Ma and Zhang, 2019).

• **Kriging:** A technique of deterministic estimating. Reasonability mainly determines the use of the kriging technique for the assumption of stationarity. The variogram and the input data are used to calculate the values between the input data points deterministically.

• **Sequential Gaussian Simulation (SGS):** A stochastic approach used in the spatial domain is called Sequential Gaussian Simulation (SGS). The technique can maintain input data distributions, trends, and variograms.

• **Gaussian random function simulation (GRFS):** When honoring input statistical characteristics like mean, variance, and variogram, a Gaussian random function

simulation (GRFS) is faster and more reliable than a sequential Gaussian simulation because it is non-sequential, allowing for parallelization (Daly *et al.*, 2010).

Porosity models are frequently built via stochastic simulation (e.g. Williams and Aqrawi, 2006). In Figure 2.19, the same input data was used to build both the stochastic and deterministic porosity models. In contrast to Kriging, Gaussian Random Function Simulation (GRFS) seeks to retain the heterogeneity of the modelled attribute and the data histogram will be approximated in a simulated model (Figure 2.19b) The Kriging algorithm has the drawback of having a smoothing effect that leads to a reduction of the overall heterogeneity (Figure 2.19a). Stochastic algorithms, in contrast, add a random seed to the input data.

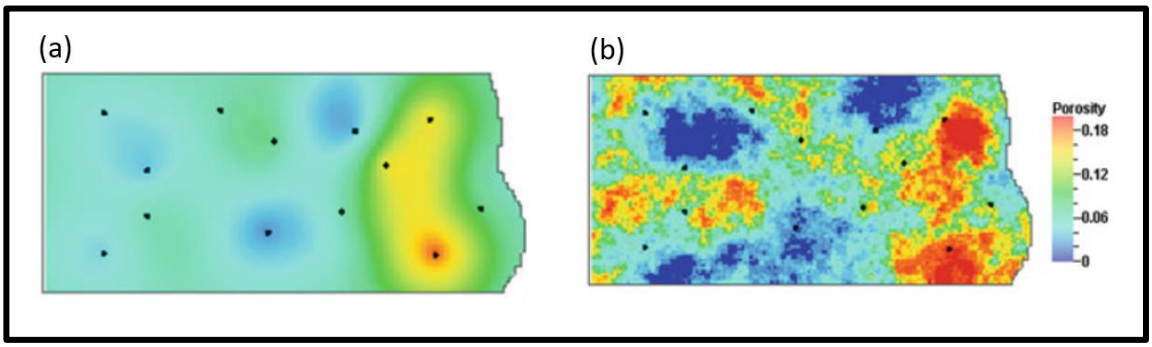

Figure 2.19. (a) Using Kriging, a deterministic porosity model was created, (b) Gaussian Random Function Simulation (GRFS) was used to create a stochastic porosity model (Ma and Zhang, 2019).

2.3.3 Reservoir Modelling Using Secondary Variable

Sizeable mature oilfields, in this case producing from a complex carbonate reservoir, exhibit significant vertical and lateral heterogeneities due to the characteristics of the sedimentary facies at the time of its formation and the impact of numerous subsequent phases of channelized depositional or diagenetic, fracturing (Budkina *et al.*, 2014). Also, in the broad study area with sparse wells, there were often various ways to interpret the data during the exploration stage. The prominent trend was bound by probability throughout the modelling phase, and the entire region's sedimentary pattern was then examined. In contrast, the development stage has higher requirements for crosswell prediction accuracy due to the smaller study area and many wells. Furthermore, most definitive studies of the 3D property model of petroleum reservoirs exclusively used well

data as their foundation. As a result, there are a variety of complex dynamic field behaviours that can be challenging to predict. Hence, a secondary variable is utilized to constrain the property modelling to increase the accuracy of the models (Yong *et al.*, 2014). These behaviours include substantial saturation variation in the long transition zone, localized dual porosity or permeability flow, early water breakthrough, strong water-cut, and uneven/non-uniform pressure support.

Property modelling using a secondary variable has been improved by various contemporary methods, including kriging with a varying mean (VMK) and collocated co-kriging. These methods are two geostatistical techniques that can incorporate a secondary variable. These approaches can be used to model the reservoir properties using deterministic or stochastic simulation. A secondary constraining variable is frequently produced using geological trends, acoustic impedance (AI), seismically derived porosity, or extracted trends from facies probabilities. The trend must reflect the local mean of the porosity when employing the kriging with varying mean. This limitation does not apply to collocated co-kriging since it uses a technique to scale the weights based on covariance, independent of the absolute values of the second variable (Ma and Zhang, 2019).

2.3.4 Constraining Reservoir Model Schemes

The new software and computer advancements enable the generation of many surfaces and seismic volume attributes and are integrated with geostatistical methods. Based on existing seismic reflection data, seismic inversion techniques can estimate the subsurface's acoustic or elastic spatial distributions, which will be used in 3D property modelling through resampling and rescaling acoustic impedance. One of the examples of such a conditioning 3D reservoir property was presented by Melville and Guruswamy (2002), who proposed a simple method that used 3D seismic data (acoustic impedance AI) with well log data and a simulation model of a giant carbonate reservoir. Another integrated approach is using seismic inversion for reservoir characterisation (Budkina *et al.*, 2014; Yong *et al.*, 2014) and building two crucial geo-model properties: porosity and facies modelling.

Different constraining reservoir modelling approaches, such as Xinghe *et al.*, (2008) used the depositional facies and genetic evolution as the constraint using well data and seismic

data to optimize the model of microfacies. In other workflow schemes, some researchers have focused on better modelling reservoir rock types by integrating seismic-derived porosity into 3D rock-type constrained property modelling (Bahar *et al.,* 2004). Zachariassen *et al.,* (2006) developed a multiscale workflow by incorporating 3D and 4D elastic inversion data as input to an iterative model work process to generate a sand probability cube used to condition the geological model of the fluvial reservoir. Likewise, Azevedo *et al.,* (2017) presented an integration of geostatistics and rock physics to generate elastic volumes (wave impedance bodies) that are then employed as secondary variables to infer the property modelling of the reservoir (e.g., porosity, facies).

2.3.5 Reservoir Characterisation and Modelling Uncertainty

The property model is susceptible to several forms of uncertainty because of a number of variables, including intrinsic errors in the geological data, such as various geological heterogeneities or heterogeneities in petrophysical properties, and data bias due to over/under-sampling. Structure, stratigraphy, depositional facies, lithofacies, pore networks, and fluids at different heterogeneity scales frequently affect subsurface formation diversity. Uncertainty in reservoir characterisation exists in many disciplines, such as seismic processing, interpretation, time-to-depth conversion, petrophysical analysis, fluid contact determination, spatial distributions of reservoir properties, fault transmissibility, and pressure/volume/temperature measurements (Ma and Zhang, 2019).

Uncertainties in the 3D models created at each stage of the hierarchical workflow can exist and be measured. There are many ways to handle and manage reservoir characterisation and modelling uncertainty, such as multiple reservoir characterisation workflow or multiple stochastic approaches. Considering various deterministic scenarios is an alternative workflow that tries to reduce the influence of bias in reservoir characterisation and explore a more realistic range of geological uncertainty. Multiple stochastic methods provide a lot of probabilistic models using geostatistical simulations (Coburn *et al.,* 2006). An ensemble of geological models, produced by altering one or more parameters of the base case model, is created using various stochastic techniques.

Chapter 3. Geology of the Mishrif Formation and 3D-Seismic Survey of the Giant West Qurna/1 Oilfield[1]

This chapter begins with an overview of the regional geological setting description. The second section of this chapter provides a geological summary of the study area and the Mishrif reservoir, a giant carbonate reservoir in the Middle East. Following that, a section is devoted to defining a conceptual geological model of the Mishrif reservoir based on well logs correlation and core data. Afterward, the morphology of Mishrif carbonate tidal channels is analysed. Finally, a high-resolution 3D seismic survey of West Qurna/1 is described for reservoir characterisation and highlights the most significant uncertainties associated with seismic data.

[1] This chapter contains material from "Al-Ali, A., Shams, A., and Stephen, K. D. (2019b). Identification of Fault Systems and Characterization of Structural Model: A Case Study from the Cretaceous Reservoir in the Giant Oil Field, Southern of Iraq. *SPE Europec featured at 81st EAGE Conference and Exhibition,* held in London, UK, 3-6 June 2019".

3.1 Regional Geological Setting

3.1.1 Regional Paleogeography

During the Paleozoic and early Mesozoic periods, the Arabian Plate suffered significant shifts in orientation and paleolatitude location (Cantrell *et al.*, 2020.) The plate migrated northward throughout this period, from a tropical low southern latitude setting in the early Triassic to a tropical low northern latitude setting by the Cretaceous (Konert *et al.*, 2001). Southern Iraq was around 5° north of the paleo-equator by the late Cretaceous period (Figure 3.1). Although tectonic activity was limited throughout the Triassic, crustal-scale warping increased during the Late Jurassic and Cretaceous periods, resulting in an elevation in western Iraq and subsidence in eastern Arabia, forming the Gotnia and proto-Mesopotamian Basins (Grabowski, 2014). The eastern Arabian Plate's depositional record demonstrates the interaction between eustasy and tectonics during most of the Cretaceous period, with tectonics becoming more prominent during the early Turonian. These basins with a greater depth were bordered by shallow-marine carbonate sediments that prograde into the basins from all sides and were filled with fine-grained organic-rich sediments.

The Mesopotamian Basin is positioned on the northwestern corner of the Arabian Plate. It is a foreland basin that extends eastward into the folded zone and western into the Arabian stable shelf's Salman zone. Tectonic activity in southern Iraq persisted through the late Cretaceous and into the Tertiary, resulting in the construction of a range of compressional structures. During this period, the closure of the Neo-Tethys and thrust emplacement of the Hawasina and Semail nappes in the Oman Mountains led to a sizeable erosional unconformity in the Middle Turonian (Sharland *et al.*, 2001). Also, at the top of the sequence, conglomerates, early cement, bored limestones, and brackish lithologies with fresh-water algae suggest that the Mishrif carbonate platform has been eroded and exposed (Al-Siddiki, 1978). Over the whole of the Arabian Plate, the Mishrif-Khasib break represents the upper boundary of the middle Cretaceous Wasia Group. It was caused by a combination of tectonic uplift and a worldwide eustatic sea-level decline through the Mid-Turonian (Mahdi *et al.*, 2013).

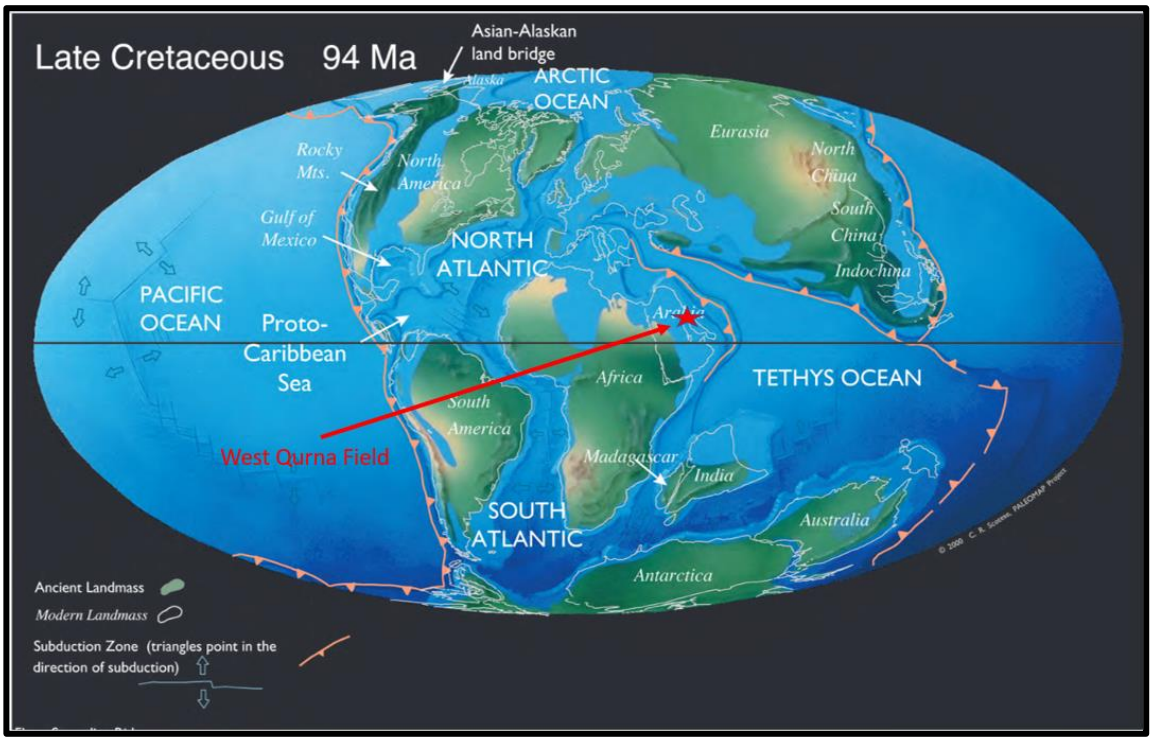

Figure 3.1. Late Cretaceous paleogeography (94 Ma) (Scotese, 2001).

3.1.2 Structural Controls

The main structural elements of the Iraq region are presented and described by Jassim and Goff (2006), shown in Figure 3.2. According to the deformation degree, three tectonic zones can be identified: Mesopotamia Basin Zone, Zagros Folded Zone, and the Arabian Stable Shelf Zone. The Mesopotamian Basin is oriented roughly northwest of the Zagros Thrust Zone (Aqrawi *et al.*, 1998), which was geologically generated due to the collision of Eurasian and Arabian platforms. Mesopotamian Basin Zone was divided into three tectonic subzones: Tigris, Euphrates, and Zubair (Jassim and Buday, 2006; Mahdi *et al.*, 2013). Many field structures in southern Iraq are the product of salt diapirism, as evidenced by negative gravity residuals beneath major supergiant oilfield structures, including Zubair, Rumaila, and Nahr Umr (Mahdi *et al.*, 2013).

The mechanism of the structural setting of the West Qurna field was indeterminate, especially in the absence of 3-D seismic data. However, Buday and Jassim (1987); presented a comprehensive insight into trending faults and lineaments that indicated the considerable structural complexity in Iraq in general and the Mesopotamian Basin in particular (including the West Qurna Field). A series of major faults control the tectonic setting of the Iraqi basement from northwest to southeast (Najd Fault System), from

northeast to southwest (Transversal Fault System), and from north to south (Nabitah Fault System) (Figure 3.3). These fault systems were created during Late Precambrian, with re-activation repeatedly occurring (Beydoun, 1991). The most interesting is that the Nabitah Fault System is very prominent in the South and West of Iraq. The tectonic elements (including the main anticline trends of the oilfields) and these extensional fault systems were re-reactivated, and the growth of the faulting during and after the Late Cretaceous (Christian, 1997). The depositional thinning and the key feature (unconformity surfaces) were observed over some of the north-south trendings of the region, south of Iraq (main oilfields) and Kuwait.

Figure 3.2. Tectonic structure elements (Mesopotamia Basin Zone, Zagros Folded Zone, and Arabian Stable Shelf Zone), also show the three tectonic subzones of the Mesopotamian Basin Zone (Tigris, Euphrates and Zubair) The West Qurna oilfield is located within the Zubair Subzone (Buday and Jassim 1987).

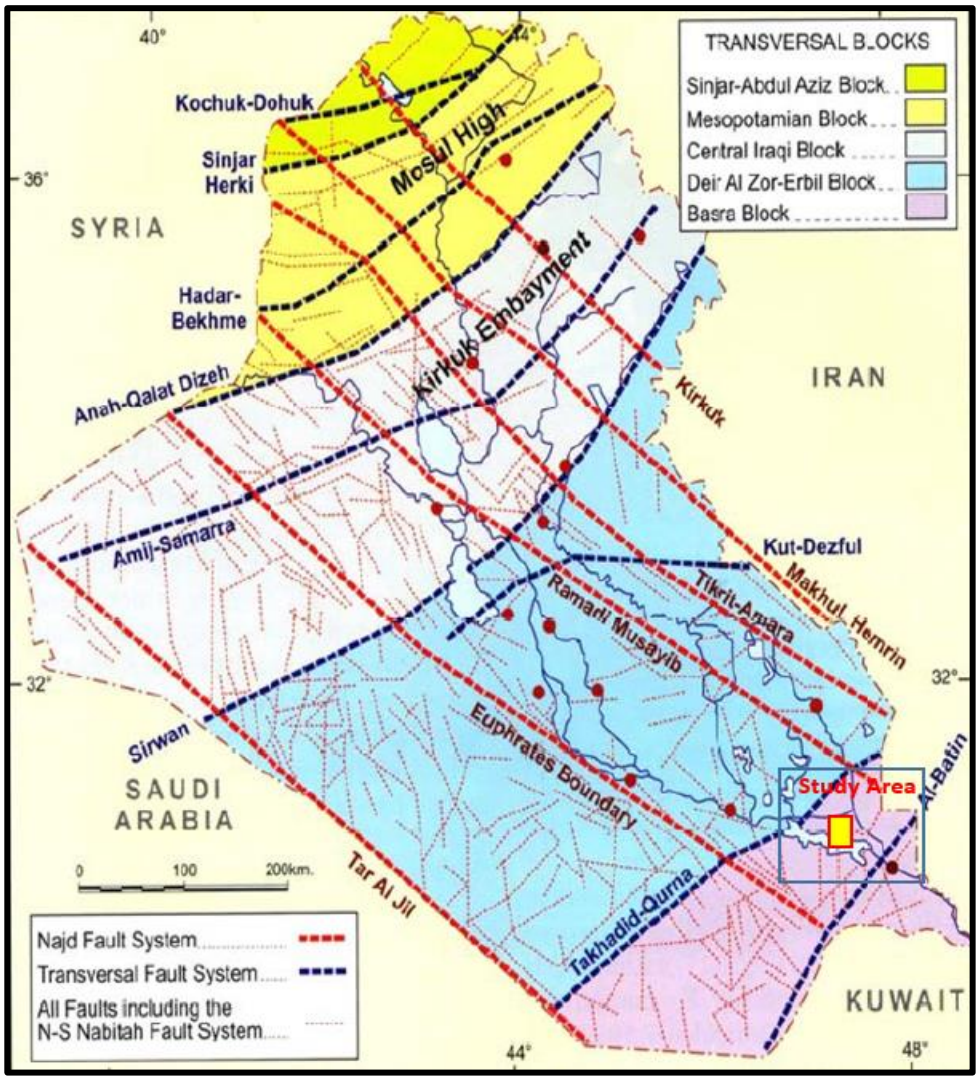

Figure 3.3. Tectonic map of Iraq, showing three central fault systems inferred from the gravity map: Najd Fault System, Transversal Fault System, and Nabitah Fault System (Jassim and Buday 2006). Note the study area in the SE of this map.

3.2 Geological Overview of the Studied Area

Cretaceous Middle East reservoirs are located widely, and they can geographically lie within a broad but sharply defined geographical band (a series of foreland basins), which extend from North Oman to Southeast Turkey (Ehrenberg *et al.*, 2008). It can be identified that the main supergiant oilfields in the Middle East lie between two tectonic regions: Zagros Fold Belt and the Arabian Platform (Figure 3.4). Carbonate rocks are primarily located in the Mesozoic and Cenozoic eras in the Middle East. This type of carbonate reservoir is entirely different from other regions due to the strong diagenesic processes in these periods (Li *et al.*, 2018). Therefore, the pore systems are mostly fractures and vugs. Many researchers have studied Middle East-Cretaceous reservoirs and focusing on the

reservoir quality. They revealed that the Middle East Cretaceous formations included 50% of the recoverable oil and 13% of the recoverable gas from the global (Ehrenberg *et al.*, 2008).

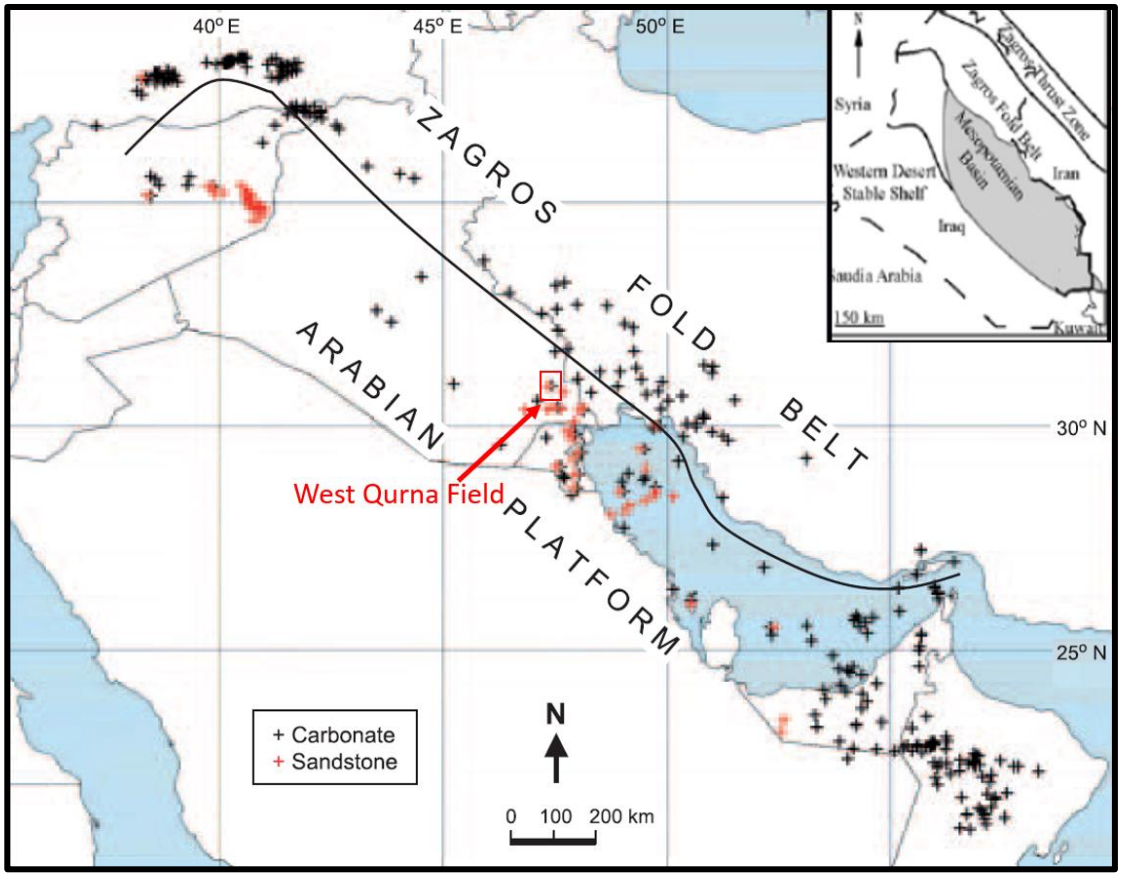

Figure 3.4. Regional structural map and distribution of the Middle East Cretaceous reservoirs located between Zagros Fold Belt and Arabian Platform, including Mesopotamian Basin and West Qurna oilfields (modified, after Ehrenberg *et al.*, 2008).

3.2.1 Introduction to West Qurna/1 Oilfield

In the Mesopotamian Basin, oilfields hold roughly two-thirds of the proven oil reserves of Iraq (Aqrawi *et al.*, 2010). The West Qurna oilfield is one of the Iraqi supergiant fields in the Basra Province, famous for its giant oilfields 50 km Northwest of Basra City and extends almost 29 km long and 17 km wide (Figure 3.5). The field is located in the Southern Mesopotamian Basin, adjacent to the eastern edge of the Arabian plate, within the Zubair Subzone. It is structurally a part of a large anticlinorium towards the north and represents the northern extension of the supergiant Rumaila field. Accordingly, West Qurna and Rumaila (north and south) anticlines create a greater anticlinorium of three

oilfields and hold about 110 billion barrels of oil in place (Mahdi and Aqrawi, 2018; Armitage *et al.*, 2018). The current production is about 600,000 barrels per day, and the target product is up to one million barrels per day when the development plan will complete for the next 20 years. Initially, the field was one oil block; in 2009, after the first oil licensing round, it was geographically divided into West Qurna Phase/1 (operated by ExxonMobil) and West Qurna Phase/2 (operated by Lukoil). Exxon Mobil is the principal contractor of West Qurna/1 with 32% interest, PetroChina with 32% interest, Itochu Corp with 19.6% interest, Petamina with 10% interest, and Iraqi Oil Exploration Company with 5% interest. Its reservoir rocks are mainly of the Cretaceous period, with many oil-bearing formations: Mishrif, Zubair, Yamama, and Mauddud. However, the giant Mishrif Cretaceous reservoir is the main reservoir and currently provides the most production rate.

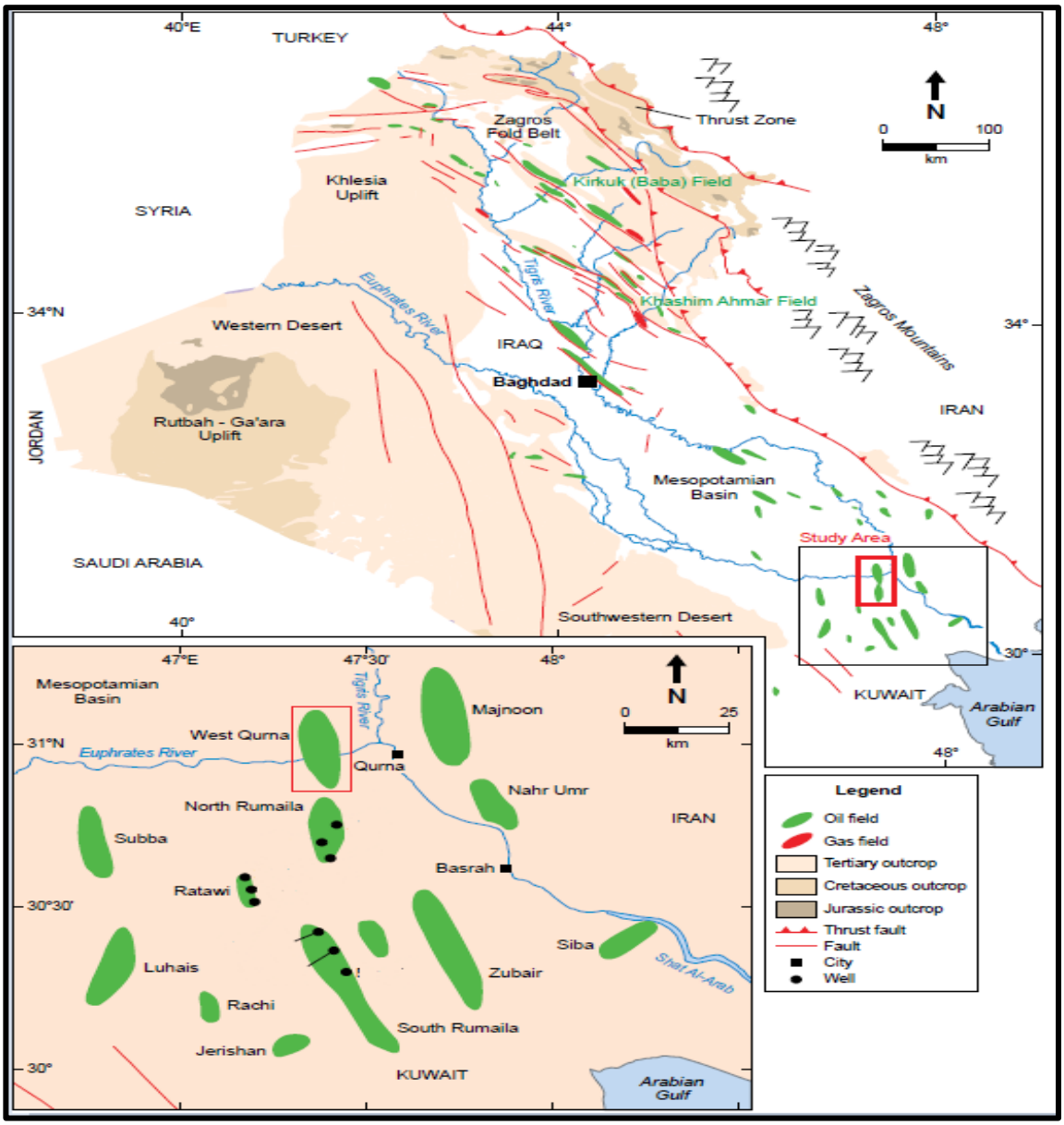

Figure 3.5. The location map of West Qurna/1 Oilfield and nearby Iraqi oil-gas fields (modified after Al-Ameri *et al.*, 2009).

3.2.2 Approach to Reservoir Characterisation of West Qurna/1 Oilfield

Before commencing seismic reservoir characterisation, it is necessary to understand the conceptual depositional environment and diagenetic history of the complex Mishrif reservoir in the West Qurna/1 oilfield. The Cenomanian-Early Turonian Mishrif Formation in the South Mesopotamian Basin represents a world-class reservoir and the most prolific hydrocarbon reservoir in many supergiant oilfields, for instance, West Qurna/1, West Qurna/2 Rumaila, Zubair, Majnoon and Halfaya. It is defined as a thick sequence of carbonate rock and makes up 30% of the oil reserves in Iraq. Aqrawi *et al.*

(1998), Sadooni (2005), Al-Ameri *et al.* (2009) and Aqrawi *et al.*, (2010) described the depositional evolution and stratigraphic model of the Mishrif Formation. The depositional environment was subjected to tectonics and eustatic sea-level changes resulting in carbonate sequence variation (Mahdi *et al.*, 2013). Shelf margins displayed the best environment to accumulate rudist biostromes in this period. Accordingly, the rudist lithosomes in the Mesopotamian Basin formed the most hydrocarbon reservoirs.

The strata in the Arabian Plate, including Iraq, are grouped into 11 Megasequences (AP1 to AP11) stratigraphically (Sharland *et al.*, 2004) (Figure 3.6). The main oil reservoirs are the Cretaceous formations in the West Qurna/1 oilfield, which includes the bulk of AP8 (Late Tithonian-Early Turonian) and the entire AP9 (Late Turonian-Danian). The Mishrif, Rumaila, Mauddud, Zubair, and Yamama are all found in Megasequence AP8. The reservoirs of the Said, Tanuma and Khasib are found in AP9. The Cretaceous stratigraphy of this basin is divided into six super-sequences (I-VI) or named second-order sequences (Aqrawi *et al.*, 2010). These successions are separated by intervals of maximum flooding surfaces (MFS) due to the relative sea-level changes (transgressive and regressive cycles) and regional tectonic movements (Mahdi and Aqrawi, 2014; Vogel and Follows, 2016).

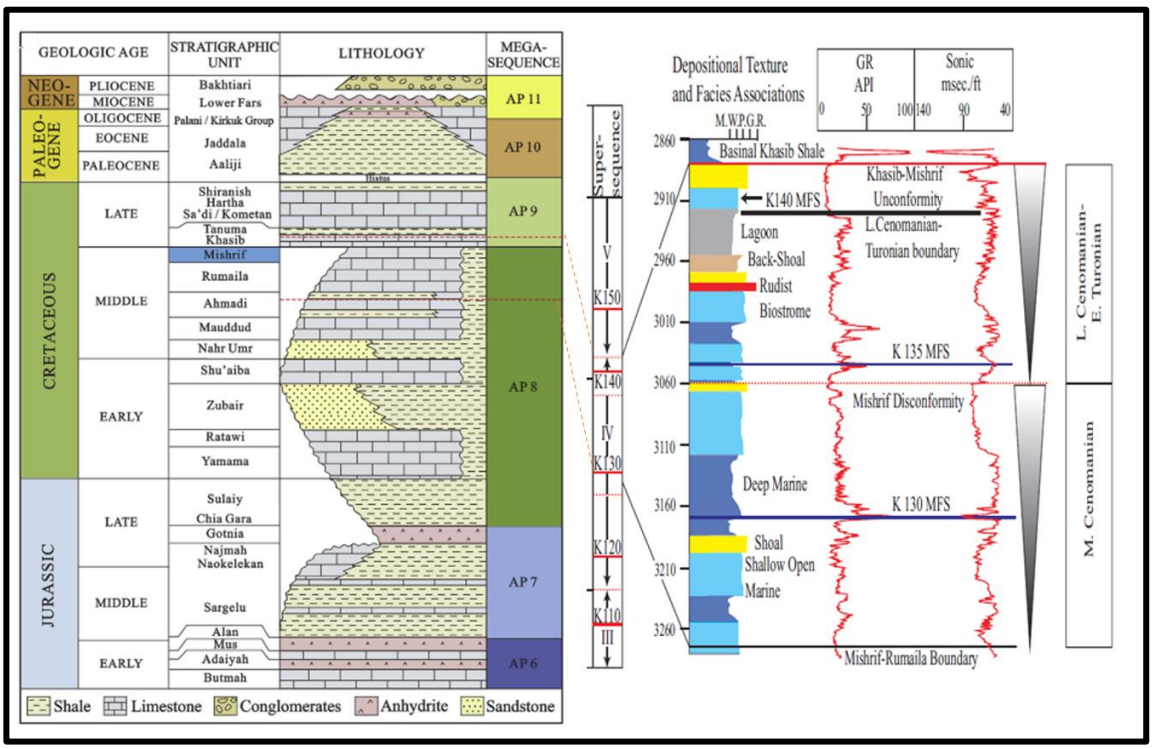

Figure 3.6. Generalized stratigraphic column in Iraq (the strata divided into 11 Megasequences (AP1 to AP11) and the Mishrif stratigraphic succession with lithostratigraphic facies (Mahdi and Aqrawi, 2014; Liu *et al.*, 2018).

The Mishrif Formation is classified as the fourth super-sequence (IV) in Megasequence AP8; it is the uppermost part of this succession and is covered by the Khasib Formation with a wide unconformity surface between them (Figure 3.7). The lower boundary of the Mishrif Formation gradually contacts the Rumaila Formation and cannot be recognized these two formations, such as in the West Quena/1 oilfield (Aqrawi *et al.,* 2010). According to Aqrawi *et al.* (1998), the Mishrif Formation was divided into lower and upper sequences or third-order sequences. This classification is based on recognizing regional unconformity surfaces, which separate these sequences and the facies evolution. However, at the West Qurna/1 oilfield, Yose *et al.,* (2012) pointed out that the Mishrif contained three sequences (third-order) that extend from the Lower Cenomanian to the Early to Middle Turonian (a period of about 5-7 million years (Ma)). These sequences are from oldest to youngest: Sequence 1, Sequence 2, and Sequence 3 separated by unconformity surfaces by including the Ahmadi and Rumaila formations too.

Every one of these sequences was exposed to transgressive and regressive cycles. The first sequence partly includes the Ahmadi Formation, separated from Mishrif by a maximum flood surface (MFS). Between SQ1 and SQ2 is sequence boundary SB1 which is not identified in some regions, and SB2 is an unconformity surface separating SQ2 from SQ3. The second sequence boundary (SB2) can be seen clearly on well loge data and cores by leaching of vugs. This boundary (SB2) capped SQ2 and represents a major exposure surface that forms a tight "caprock II" interval after deposition. Similarly, the top of Mishrif carbonate is underlain by another exposure surface (SB3) or "caprock I." This boundary (SB3) corresponds to Arabian Plate wide unconformity and represents a Mishrif-Khasib regional disconformity surface (Aqrawi *et al.,* 2010; Mahdi *et al.,* 2014).

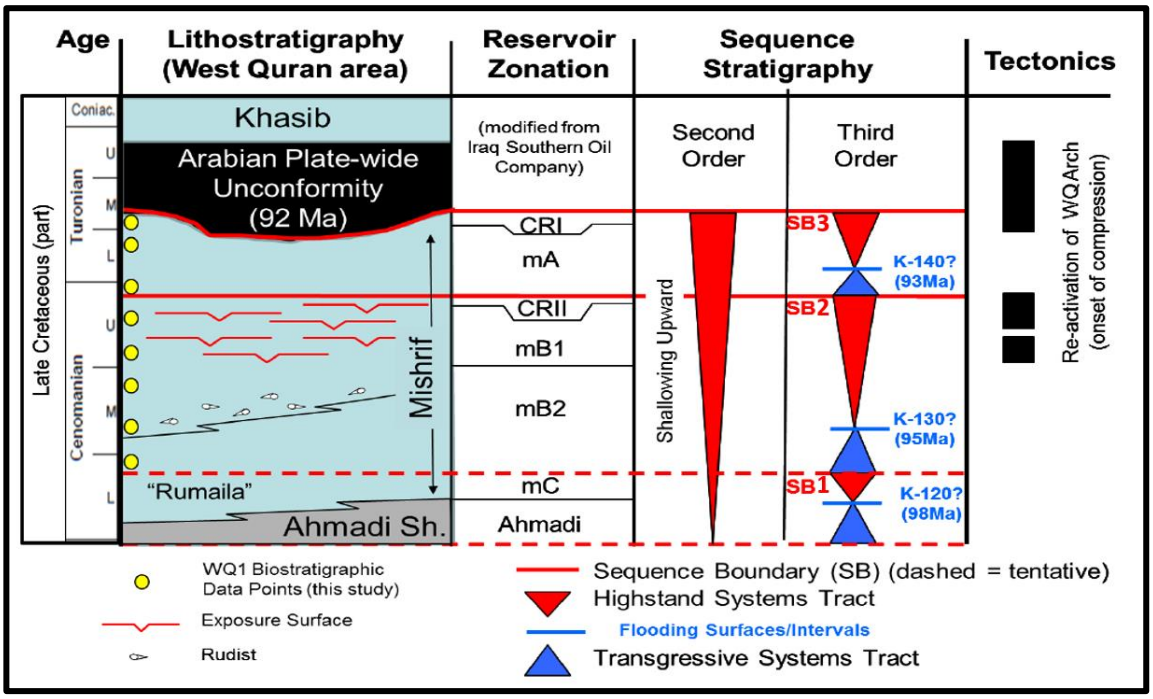

Figure 3.7. Chronostratigraphy of Mishrif Formation in West Qurna/1 Oilfield and reservoir zonation (Basra Oil Company, 2013).

3.3 Comprehensive Geology Study of the mid-Cretaceous Mishrif Reservoir

3.3.1 Sedimentary Facies Distribution

Numerous authors have comprehensively discussed the depositional model of the Mishrif Formation in the Mesopotamian Basin (e.g., Aqrawi *et al.*, 2010; Awadeesian *et al.*, 2014; Al-Khafaji, 2014). Mahdi and colleagues constructed a regional facies framework and stratigraphic framework for the Mishrif Formation (Mahdi et *al.*, 2013; Mahdi and Aqrawi, 2014). Mishrif depositional model was categorized under these two types of carbonate platforms: reef-rimmed shelf and carbonate ramp. Mahdi *et al.*, (2013); Mahdi and Aqrawi, (2014) described the Mishrif carbonate model as a reef-rimmed carbonate platform in the Mesopotamian Basin with facies found in the Mishrif Formation corresponding to the rimmed platform. However, Miraglia *et al.*, (2015) mentioned the deposition of Mishrif carbonates in a well-developed ramp system. The paleo-depositional model ranges from shallow open-marine to lagoon deposits. This depositional model can classify Mishrif facies into four main groups: shallow open-marine facies, shoal facies, rudist biostrome facies, and lagoonal facies (Mahdi *et al.*, 2013). All these types of facies can be seen in Figure 3.8.

1-Shallow Open-Marine Facies: This type includes thick limestone units involved in bioclastic packstones and wackestone. These facies change upward to more grain and rudist-rich sediments.

2-Rudist-Bearing Facies: These facies represent the principle lithofacies of Mishrif Formation in reservoir quality. It is predominately an accumulation of rudist biostromes (limestone detrital) within grainstones, and packstones occur along an exterior shelf margin of the basin without developing a continuous rim (Miraglia *et al.,* 2015). Aqrawi *et al.,* (2010) pointed out that rudist facies extend from the Hamrin region, in the north, to the south of Iraq.

3-Shoal Facies: These are well-developed, and one of the most important reservoirs mainly included grainstones and packstones, namely platform margin shoal (Wang *et al.,* 2016; Zhong *et al.,* 2018). These facies are considered to be deposited with an increase in energy above the fair-weather wave base (FWWB). It contains little carbonate mud, hence gamma-ray logs identify just small deflections, and porosity logs show high porosity intervals. The grain shoal facies reservoir is well developed there, known as one of the most important reservoirs in the Persian Gulf Basin and even in the Middle East. (Zhong *et al.,* 2018).

4-Lagoon Facies: They are deposited in a restricted environment and subtidal shoals channels within platform carbonate. The successions of the lagoon include thin beds of peloidal limestone and may contain shoal and rudist. Log data indicate a high gamma-ray and low porosity comparison with shoal facies in these facies.

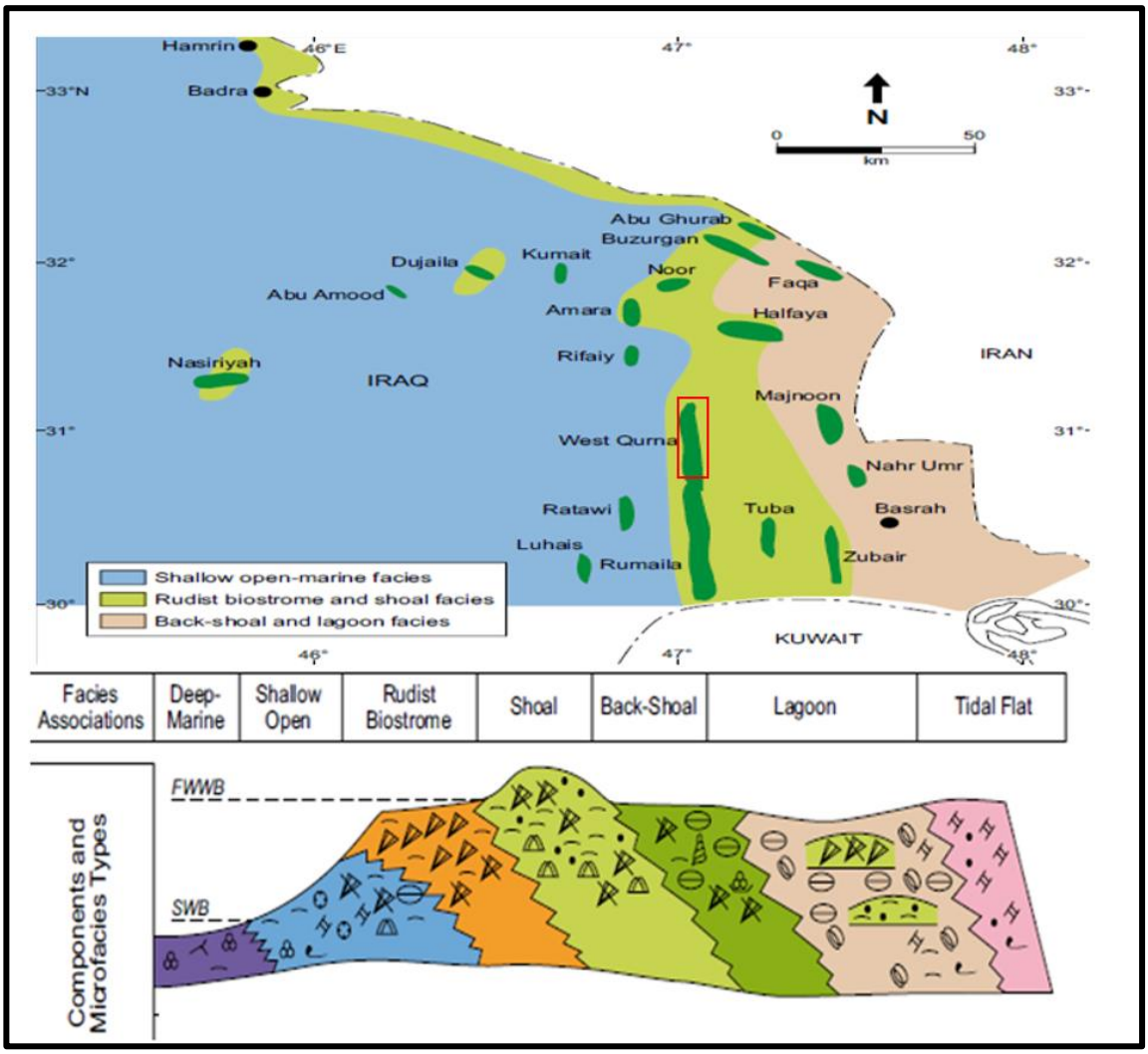

Figure 3.8. Regional paleogeographic map and Mishrif facies distribution in the south of Iraq (Mahdi *et al.*, 2013).

3.3.2 Reservoir Zonation

According to the difference between depositional facies and the sequence stratigraphic, reservoir zonation can be divided into these members (from top to bottom as shown in the Figure 3.8) CRI, mA, CRII, mB1, mB2, and mC. A brief description of the Mishrif reservoir zonation (Figure 3.9), follows:

1- Cap-rock Intervals (CRI and CRII)

They are non-reservoir facies and cemented zones at sequence boundaries. These intervals at the top of the upper sequence represents a major regional exposure. They formed in limited platform facies and a portion of open platform facies, resulting in poor

connectivity with the ocean basin, calm and weak hydrodynamic energy, and several lagoons. CRI represents top Mishrif unconformity.

2- mA Zone

This zone is divided into three layers mA (a), mA (b), and mA (c), with a total thickness of almost 40 m (Figure 17) deposited in different environments including shoals (lower part) and lagoon (upper part). It mainly consisted of microporous subtidal foram-peloidal ramp facies, contained in some regions sponge/coral mounds, and bioclastic shoals facies reflect a good reservoir quality. Consequently, this zone displays a high heterogeneity in lithofacies and porosity.

3- mB1 Zone

This consists of restricted lagoonal facies (milliolids) and subtidal grainstone channels or shoals deposited in the inner ramp domain with a maximum thickness of about 50m. This zone displays a wide range of porosity and permeability fluctuation due to the impact of the depositional environment (subaerial exposure) (Miraglia *et al.,* 2015). Therefore, it mainly shows the reservoir's low-quality facies with porosity value (8%) and permeability (0.4 md). However, some intervals have sweet spots and good-quality facies, particularly grainstone channels or shoals. mB1 tidal channel is formed in the mud supported by peritidal carbonates and filled by high-porosity grainstones, identified in many outcrops. Grélaud *et al.,* (2010) mentioned that these channelized systems are formed in an inner carbonate platform during transgressive systems tracts. More details and the full geological descriptions of this zone can be found in Chapter 5.

4- mB2 Zone

The petrophysical properties are high porosity (more than 30 %) and high permeability (above 1000 mD), the thickness of (80-90m) with a net-pay thickness of almost 50 m. Mahdi *et al.,* (2013); Mahmood *et al.,* (2017) mentioned that rudist-bearing facies characterized the best quality reservoir and main hydrocarbon-bearing deposit (rudist shoal system). According to the reservoir zonation, these prolific hydrocarbon facies are called mB2 and, especially in the upper part (a and b), are relatively homogeneous and demonstrate high flow rates. However, the lower part of mB2 (c,d,e) layers was deposited in a shallow open-marine environment and represented high porosity, but low permeability because of the small sizes of pore throats. This interval could be produced in some regions (skeletal shoals) (Yose *et al.,* 2015).

5- mC Zone

This represents the base of the Mishrif reservoir (thickness ranging 20-30m) and includes a subtidal foram-peloidal ramp deposited in the outer ramp. The mC zone shows a high porosity with low permeability (microporous); the upper part could provide better quality than the lower mC in some field regions (Yose *et al.*, 2012). It can be seen that the great volume of the low-permeability microporous reservoir is located in the lower Mishrif (mC and lower mB2 zones).

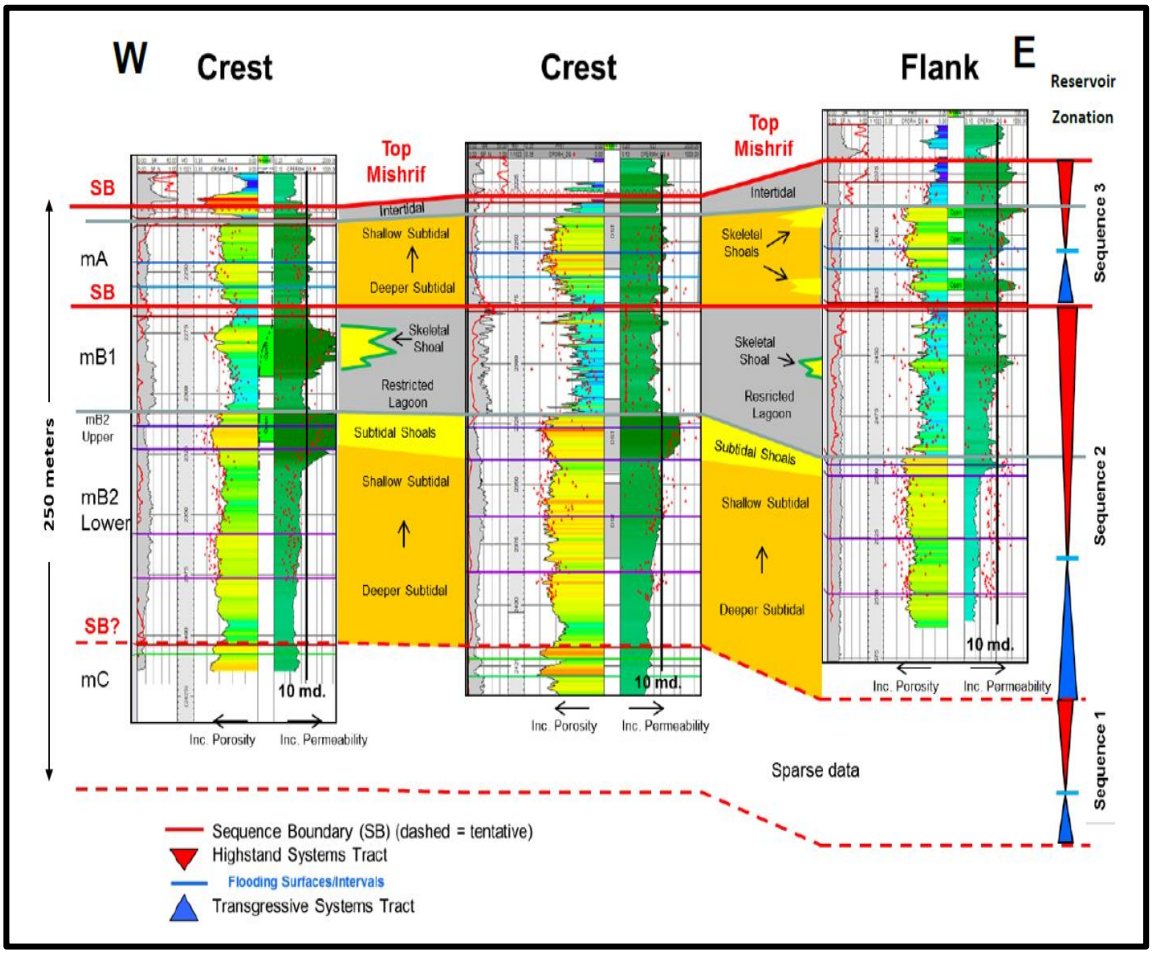

Figure 3.9. Mishrif reservoir zonation is based on well-logs and core sections from crest to west and east flanks, highlighting generalized depositional trends within Sequences 1-3 (Basra Oil Company, 2013).

3.3.3 Reservoir Communications and Barriers

Studies on faults and barriers focus on their definition, classification, genesis, distribution pattern, and effect on oilfield development. The multiple faults and stratigraphic barriers in the West Qurna/1 oilfield impact lateral and vertical flow and are the main reservoir uncertainty. Determination and modelling of these faults are crucial to evaluating and

understanding the flow of oil and water, defining the structure away from well control, and understanding the evolution of the West Qurna arch over geologic time.

The high resolution of the West Qurna/1 3D seismic data aids the identification of faults, particularly large faults. The study of Mishrif interval faulting indicates a significant number of faults striking north-south along the western edge of the anticline. In combination with seismic attributes volumes, the seismic interpretation delivers a valuable structural framework to be used for building a better geological model. More details about the identification of fault systems based on 3D seismic data will be discussed later in this chapter.

As mentioned in the previous section, the stratigraphic barriers in the Mishrif reservoir were mainly distributed in CRI and CRII (non-reservoir zones). These barriers have been viewed as carbonate, dominated by wackstone and mudstone with good continuity across the field. The lateral extent and thickness variation was measured for each barrier based on core sections and well logs. The CRI interval is the most significant barrier as a cemented zone at the sequence boundary at the top Mishrif reservoir between Khasib and Mishrif Formations. The thickness of the CRI interval has been verified on average between 3-10 m across West Qurna/1 Field. Another barrier interval (CRII) is a laterally continuous flow barrier across the field area and separates the mA zone from the mB1 zone, with a thickness average between 0-5 m.

3.4 Development of the Morphology of the Carbonate Tidal Channels

Despite the abundance of important carbonate reservoirs, geological and seismic evidence for carbonate channelized systems is previously unreported in the literature. The connectivity of channelized reservoirs is massively dependent on the geological circumstances and has always been done through reservoir characterisation. In the inner carbonate platform, channelized systems play an important role in reservoir architecture and heterogeneity, thus could be constituted the best productive reservoir facies (Javaux and Chenot, 2014).

3.4.1 Distribution Regularities of the Tidal Channels

Tidal channels in an inner carbonate platform setting were explained previously in Chapter 2 (section 2.1.7 and section 2.1.8). The tidal channel fairways in an inner carbonate platform setting are controlled by depositional processes which formed during phases of flooding. The origin of channelized bodies determines their distribution regularities and presence in vertical successions and lateral expansion. The distribution regularities of the channelized systems are summarised based on the distribution features in the lateral and vertical directions. This could aid in the identification and prediction of similar tidal channel fairways. Channel fairways could be vertically or laterally compartmentalized due to periods of sea-level change (stratigraphic factors) accompanying changes in depositional systems (Larue and Hovadik, 2006). Vertical compartmentalization can happen in a variety of ways. Several forms of connectedness may be defined between the channels or other depositional features. Individual constituents of a reservoir are connected via geobody or sand body connection (Figure 3.10a). Geobodies are channel-sized or larger potential flow units that are defined by linked and disconnected channel deposits. Accordingly, reservoir connectivity can be classified into several stacking patterns, such as amalgamated channel deposits. Also, increasing the width of the channel deposits compared to thickness at a particular net: gross ratio will boost connectivity, as shown in Figure 3.10b. When separate channel bodies fail to intersect, lateral compartmentalization of channelized deposits ensues. Laterally disconnected channel deposits may be caused by slow migration or by the more sudden movement of the channels to another position in the depositional system, known as avulsion. Figure 3.11c shows an example of channels being severed by an avulsion event.

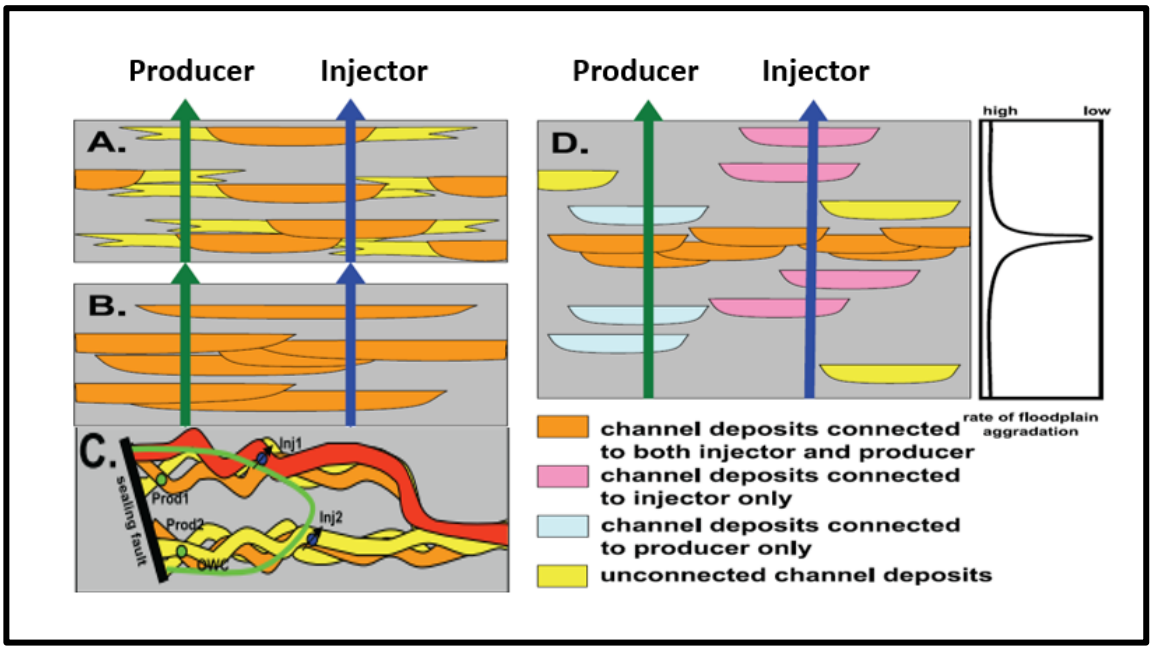

Figure 3.10. Illustration diagram displaying vertical compartments and different stacking patterns of channelized systems. (a) Lateral geo-body facies can increase channel width. (b) High width/thickness ratio channels. (c) Lateral compartments in a channelized reservoir by avulsion. (d) Lateral channel shifting causes lateral channel amalgamation and the creation of complexes with higher width/thickness ratios due to times of low floodplain aggradation (Larue and Hovadik, 2006).

In the case of the Mishrif reservoir, carbonate tidal channels are mainly found in the lagoonal environment of the highstand system tract. Because of the vertical accretion and diversion, the Mishrif mB1 tidal channel fairways have a sizeable cumulative depth and lateral dispersion range. Figure 3.11 is useful for considering the concept of vertical compartments, with four examples of different stacking patterns of the mB1 channel fairways in the West Qurna/1 field. The channel mainly extends from to E to W with banded distribution, nearly perpendicular to the paleoshore line. The channel geometry is 1-2 km in width and has a cumulative thickness of up to 40 meters, depending on the migration of the tidal channels. The above is confirmed by interpreting the West Qurna/1 3D seismic data; more details of the channelized reservoir characterisation can be found in Chapter 5.

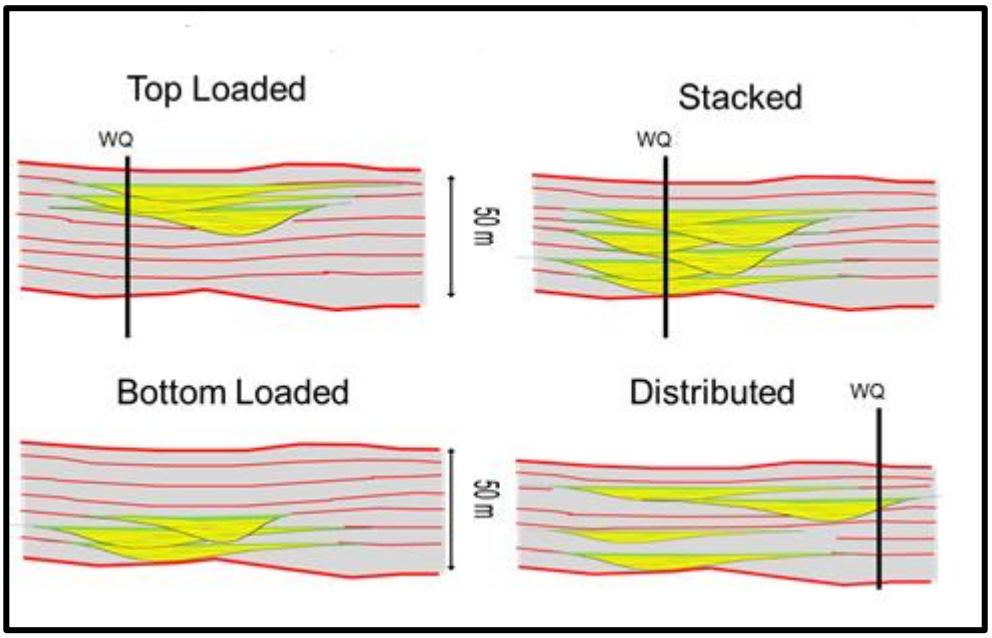

Figure 3.11. Mishrif mB1 tidal channel stacking patterns (top-loaded, stacked, bottom-loaded, and distributed).

3.4.2 Outcrop

It is critical to use reservoir analogues from similar depositional environments to guarantee that the interpretations of seismic data, reservoir characterisation, and internal configuration of reservoir geometry are geologically realistic. As a result, references to the outcrops and analogue of carbonate tidal channels were presented. The outcrops from northwest of the Jabal Madmar, Northern of Oman, based on the work of Grélaud *et al.*, 2010, depict the vertical property distribution of facies in tidal channels. The modern-day analogue, located in Abu Dhabi, United Arab Emirates, will give further information on the lateral extent of the tidal channels and the influence of winds and tides on the distribution of their petrophysical properties. Knowing how these analogues are characterized could aid in determining reservoir characteristics based on 3D seismic and well data of the giant West Qurna/1 oilfield.

I) Jabal Madmar, Sultanate of Oman

The mountains of Oman provide a variety of outcrops that can be utilized as carbonate analogues in the region (Grélaud *et al.*, 2010). The carbonate outcrops cover a wide variety of ages and structural contexts. Carbonates range in age from Permo-Triassic to early Cenozoic, with depositional environment ranging from interior and platform top

settings to deep marine carbonate. The carbonate exposures studied here are part of the Lower Cretaceous Upper Thamama Group carbonates, which were deposited on a huge shallow carbonate platform, and the Upper Cretaceous to Lower Cenozoic, which were tectonically and eustatically controlled.

Grélaud *et al.*, 2010, published a paper on a channelized systems in an inner carbonate platform setting in the Natih Formation, Late Cretaceous, Oman. According to their study, the sequence records a shift from argillaceous to carbonate sedimentation in an increasingly open inner platform setting in a transgressive context. A bioclastic channel develops in the top section of this strata at the Jabal Madmar outcrop position (Figures 3.12 and 3.13). This channel is around 750 meters wide and has a maximum depth of about 10 meters. The commencement of the erosion surface on the western border of the channel begins a few decimetres below the hardground and cuts through the whole series, down to peritidal cycles in the upper section of Sequence I. (Sequence I-7). The cross-section is asymmetric, with the western margin being steeper than the eastern border. Because this is merely a 2D exposure, no orientation can be identified.

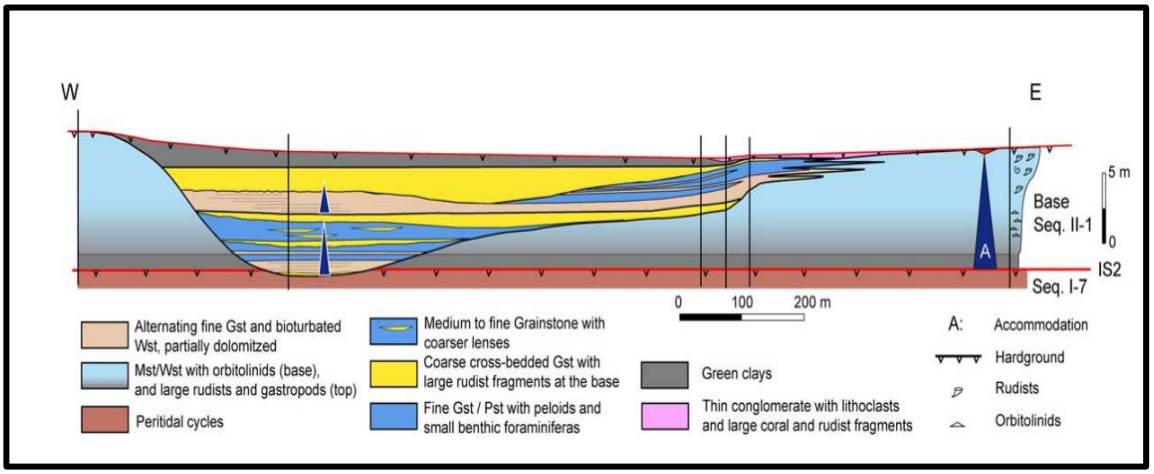

Figure 3.12. Outcrop correlation transect demonstrating the geometry and fill succession of a tidal channel cropping out on the southern edge of the Jabal Madamr.

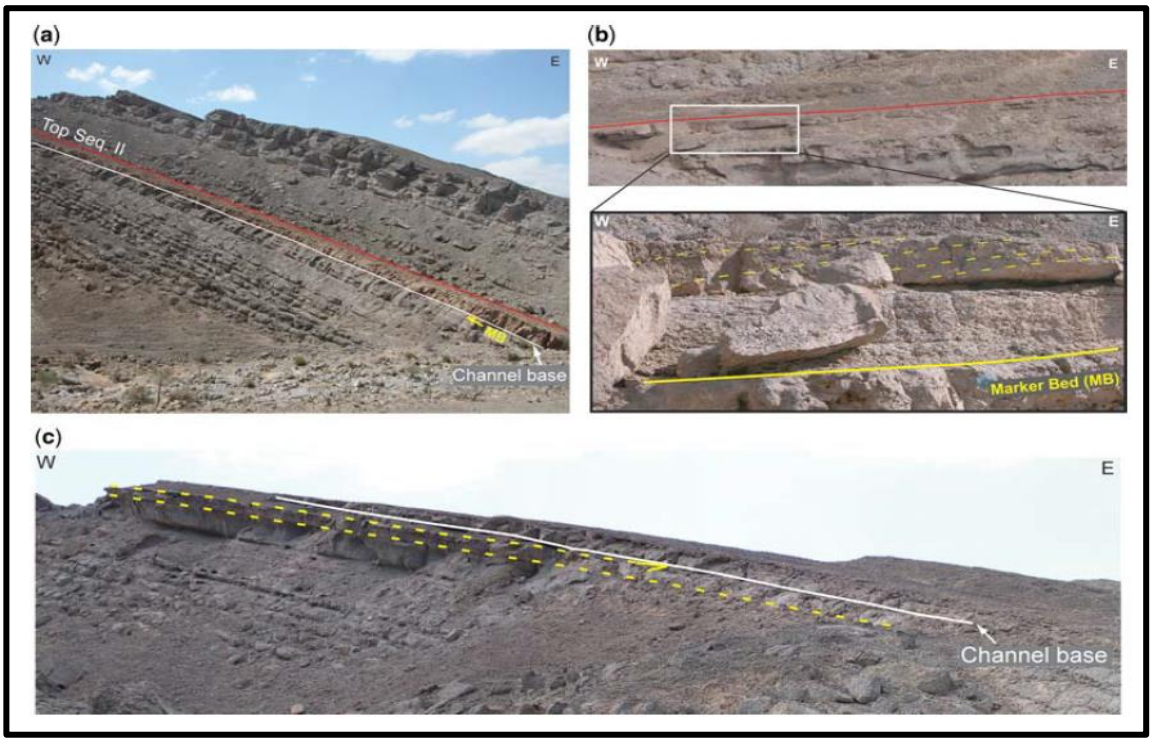

Figure 3.13. Outcrop view of the tidal channel (a) Cropping out in the northwest of the Jabal Madmar (Madmar 6 wadi) (b) The eastern margin of the channel shows laterally accreting geometries (yellow dashed lines) (c) The channels western edge, where the underlying strata have been eroded (Grélaud *et al.*, 2010).

II) Coastal System of Abu Dhabi UAE, Arabian Gulf

In addition to outcrops, modern tidal channels of the Arabian Gulf have served as an important analogue for interpreting and understanding ancient channelized systems. Carbonate tidal flats have also been discovered in the current Holocene period. Many tidal flats and coral banks can be seen in the coastal system of the Arabian Gulf. The shamal (Northwest trending wind) blows onshore in this region, causing water currents and waves to produce different depositional environment zones. However, the intensity of the waves fluctuates throughout the coast due to the Qatar peninsula's shielding effect, which produces a more protective environment to the west along this coast (Davis and Dalrymple, 2012). Various islands and peninsulas distinguish the complicated coastline of Abu Dhabi Island.

This coastline has a low-angle ramp geometry and consists of a network of subtidal carbonate-dominated depositional shoals, reefs, tidal channels, sheltered intertidal lagoons, and supratidal sabkhas stretching several hundred kilometers along strike and up to 15 kilometers wide, tapering to the northeast (Davis and Dalrymple, 2012). The surface

sediment can be tracked over the lower tidal channels to the high supratidal into the neighbouring sabkha south of Al Qanatir Island on the northward-facing bank to the Khor Al Bazam west of Al Dhabaiya Peninsula. Surface characteristics include carbonate mud to tidal channels covered locally by indurated carbonate crusts, followed by unique cyanobacterial mat surfaces that transition laterally into a thin polygonally mud cracks (Figure 3.14). These surface sediment composition and morphology differences reflected the tidal flat and surrounding sabkha terrain and their relationship to the tidal range (Alsharhan and Kendall, 2003).

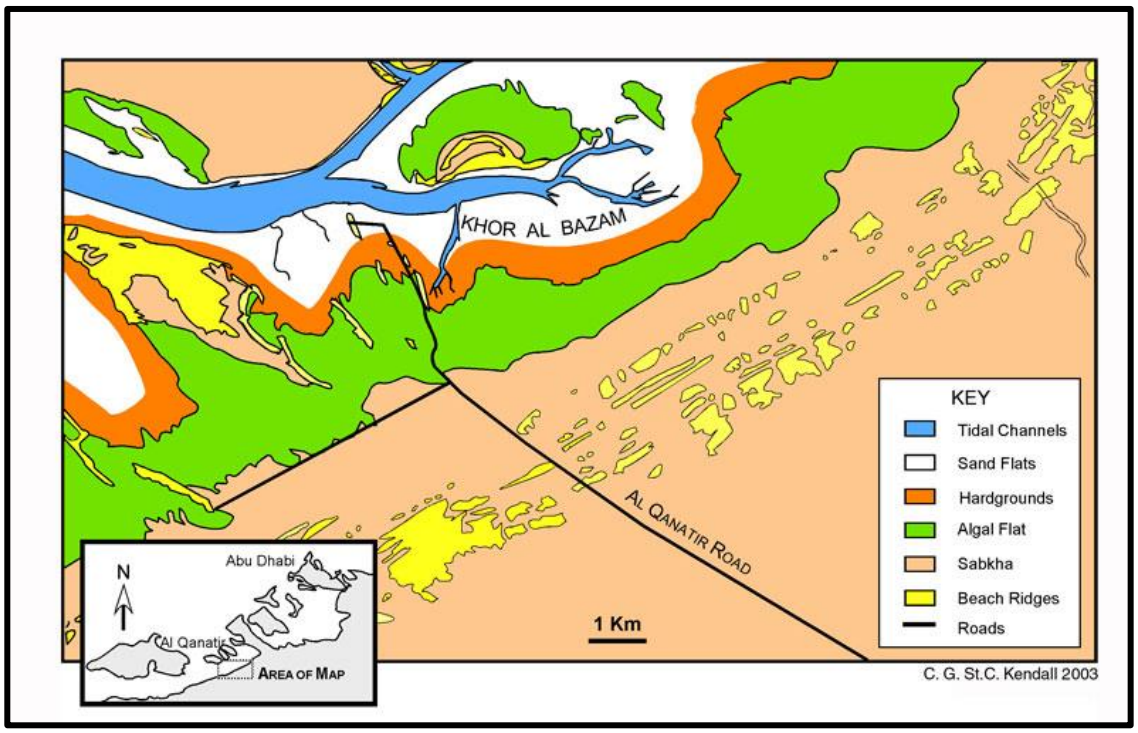

Figure 3.14. The map of the coastal depositional zones illustrates various depositional environments on the southwest Khor al Bazam south of Al Qanatir Island, Abu Dhabi, UAE (Alsharhan and Kendall, 2003).

Large tidal channels generally associated with tidal deltas connect the open sea with the lagoons behind the seaward islands. The major axis of these channels is oriented roughly perpendicular to the coast. The tides and onshore northern winds regularly remodel the tidal channels of the modern Abu Dhabi coast, accumulating on ebb deltas. These tidal channels can be extended up to 28 kilometers, 1-6 kilometers in width, and a depth between 2-13 meters. Between Abu Dhabi Island and Halat al Bahrani, the major channels are better defined, narrower, and deeper, reaching a maximum depth of 13.4 meters. It can be seen that the geomorphic observations of the modern-day tidal channels are similar

characters to the Mishrif tidal channels, which are interpreted based on the 3D seismic data of the West Qurna/1 oilfield (Figure 3.15) (more details in Chapter 5).

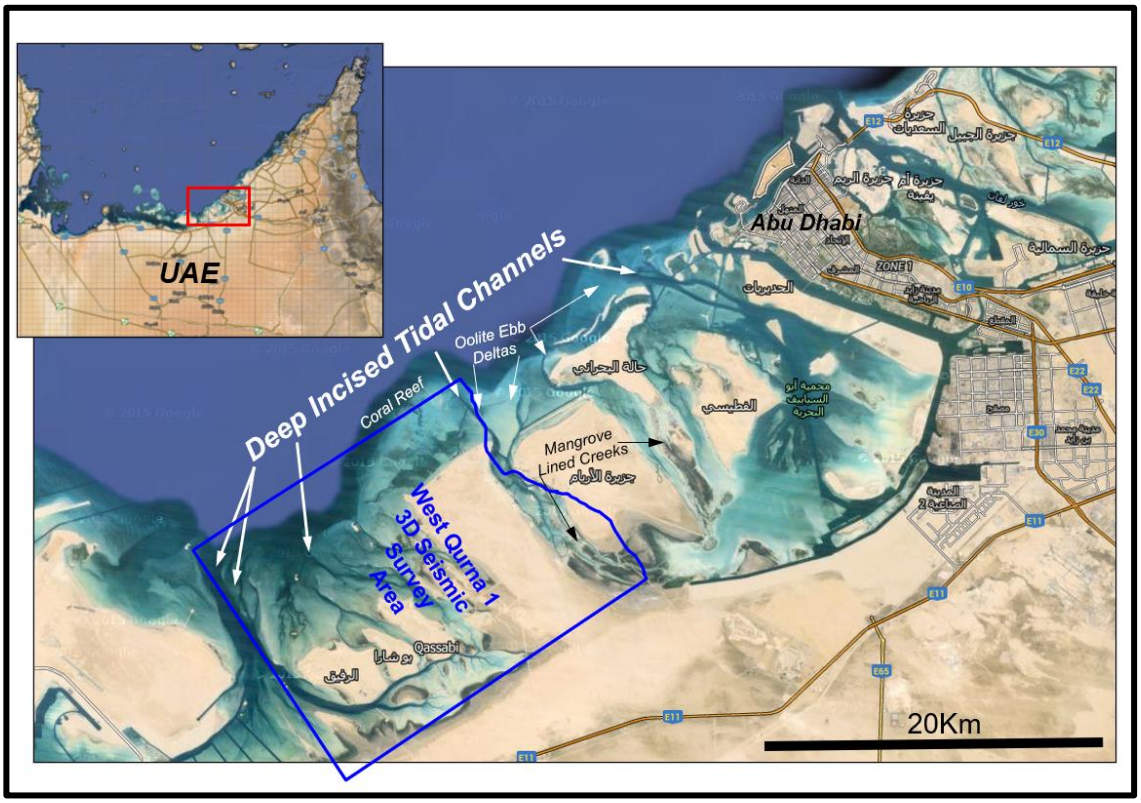

Figure 3.15. An aerial photograph of modern-day subtidal channels near Abu Dhabi, Arabian/Persian Gulf, and also a simplified map showing the size of the West Qurna/1 3D seismic survey area indicated how these modern incised tidal channels have a similar scale to the Mishrif tidal channels (Google satellite earth map).

3.4.4 Implications of Reservoir Architecture and Heterogeneities

In carbonate reservoir characterisation, the main difficulty faced is the identification of channel connectivity due to the complexity of pore systems across different facies and processes (Ghafoori *et al.*, 2009; Ling *et al.*, 2014). The presence of channel geobodies introduces complexity and is a challenge because reservoir modelling should have a reliable connection with geological features such as the channels' shapes and facies (Hashemi *et al.*, 2014). When they are filled with non-reservoir facies like mud, they may cause the reservoir to compartmentalize. Alternatively, if the channels are filled with reservoir facies and exist in non-reservoir stratigraphic intervals, they could form isolated reservoir units. On the other hand, when filled or partially filled with high-permeability reservoir facies, they can also generate permeability conduits (Figure 3.16).

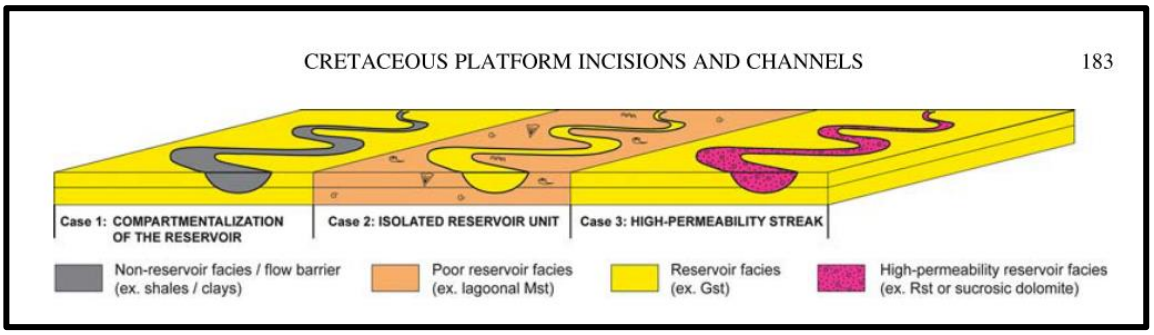

Figure 3.16. Carbonate tidal channels meandering and incisions in the Cretaceous Platform with different reservoir and non-reservoir facies (Grélaud *et al.*, 2010).

In terms of the channelized carbonate systems of the Mishrif reservoir in the Iraqi oilfield, tidal channels were widely developed on the Arabian Plate during the sea-level changes with high energy process (Cretaceous period). They are deposited in a restricted environment with subaerial exposure (lagoonal facies). This is mainly a result of the depositional systems formed through the fluctuations of relative sea-level change and the flooding of the inner platform (Grélaud *et al.*, 2010). Nevertheless, some regions have sweet spots and good quality facies, particularly grainstone and tidal channels within platform carbonate. An example of similar channels of the Mishrif is the Savark reservoir in Iran (Dong and Zhao, 2013) and the Natih reservoir in Oman. The characterisation of these complex tidal channels can be identified using seismic techniques such as the generation of acoustic impedance inversion or porosity model derived from high-resolution 3-D seismic data. More detail about the Mishrif tidal channel fairways will be provided in Chapter 5.

3.5 Seismic Data Preparation and Analysis

High-resolution seismic data allows visual inspection of the reservoir properties and quantitative interpretation to improve the reservoir model. The West Quena/1 3D seismic survey aims to define the structures away from well control and fault determination (orientation, length, depth, and type of faulting). This is critical to understanding the fluid flow of both oil and injected water in terms of distribution and movement. Also, this survey was designed to identify areas with acoustic property changes to better understand reservoir heterogeneity regarding porosity distribution, facies classification, and fluid flow behavior, and ultimately optimize the largest producing reservoir.

Noise affects seismic datasets, masking the genuine seismic signals from providing a realistic interpretation. Noise in seismic data can be caused by various things, including geology, reflection strength, processing, acquisition approaches, velocity model, and frequency content (van Gestel, 2015). This depends on the quality of the obtained seismic and seismic processing procedures to decrease noise and maximize the signal-to-noise ratio. The following sections will explain acquisition and processing, comparison of seismic signals to synthetic traces, and extraction of seismic attributes of the structural model.

3.5.1 West Qurna/1 3D Seismic Survey: Acquisition

The structure of West Quran heterogeneous reservoirs remained problematic and subject to many uncertainties and controversial ideas. The first full-field 3D seismic survey was recently acquired in the West Qurna/1 Field area, for reservoir characterisation for both discovered developed and discovered undeveloped reservoirs. Also, it was to support the development plan and assessing the main producing reservoirs. The survey area was planned to be 500 km^2, bordering the Third river in the south and the Euphrates River in the north; the final survey was 461 km^2 due to the exclusion of Al-Medina town (almost 41 km^2) in the north (Figure 3.17). Western Geco was given a contract to acquire the data in the fourth quarter of 2012 and the third quarter of 2013.

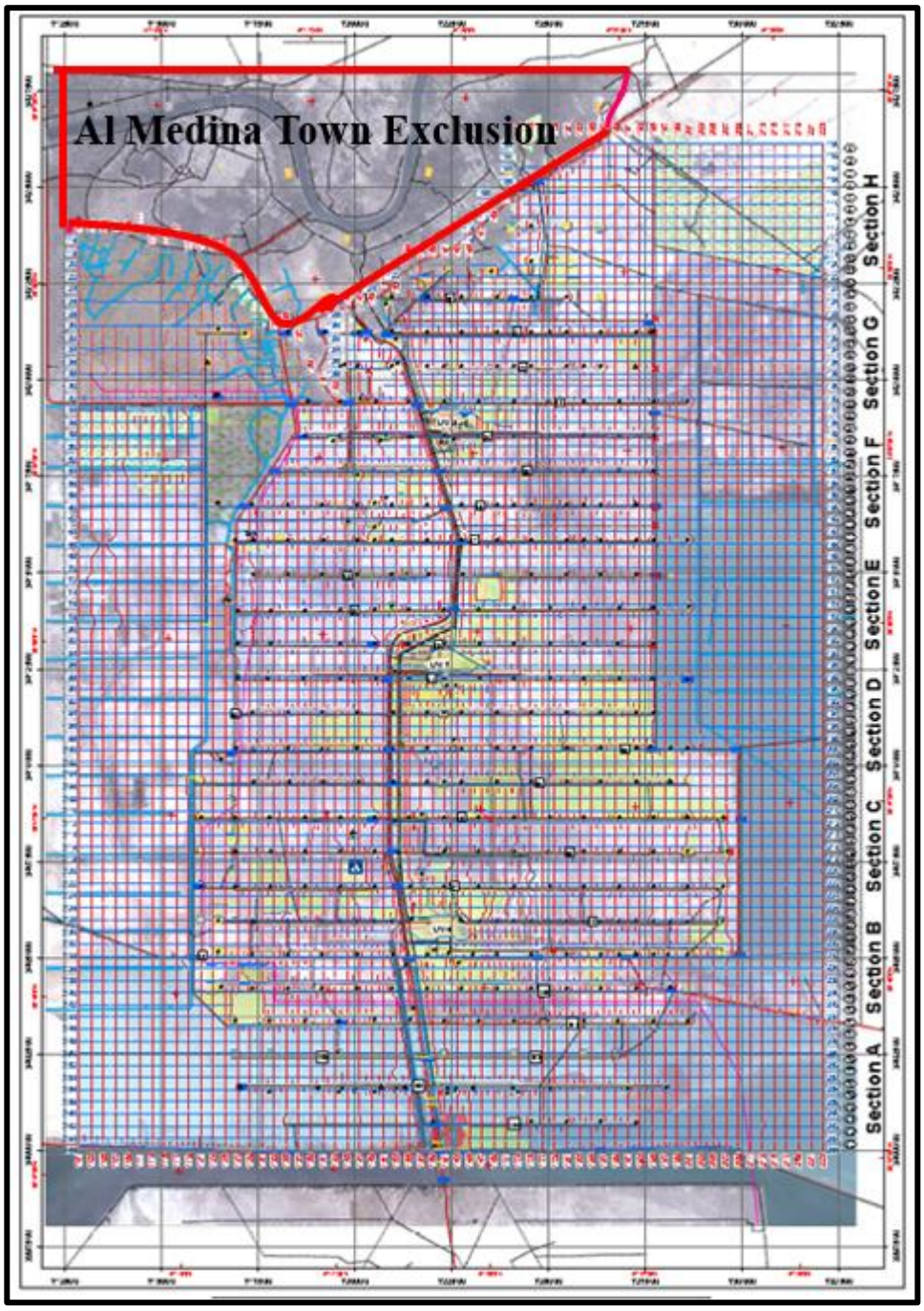

Figure 3.17. The geometry of the seismic source locations (red lines) and geophones locations (blue lines) in the West Qurna/1 3D seismic survey (Basra Oil Company, 2014).

The survey was acquired over the West Qurna/1 oilfield and had a very high resolution. The survey began in the south and finished off in the north, with dynamite as the source of seismic waves. The total good shots are 43213, and the actual number of the holes with re-drills is 47754. All the acquisition parameters are listed in Table 3.1. Before the survey was carried out, there was a test program of the source parameters. The recording showed sensible clarity for reflecting energy returning from deep subsurface reflectors, illuminating far offsets with 2 kg of dynamite and a depth of 15 m compared with 2kg

with 10 m, as shown in Figure 3.18. Although, there were many varied technical challenges, such as working in the marsh and dry areas, acquisition difficulties in an active production zone, and simultaneous operations with construction projects. However, this led to the full coverage fold map that can be calculated using 17.5m x 17.5m in common depth point (CDP) bins (Figure 3.19). The West Qurna/1 seismic survey is considered the best available and the highest quality onshore seismic in the Middle East fields.

Table 3.1: Acquisition parameters summary of the West Qurna/1 seismic survey.

Year of Acquisition	2012-2013
Original Survey Area (km^2)	500
Final Survey Area (km^2)	461
Receiver Line Interval (m)	315
Receiver Group Interval (m)	35
Source Line Interval (m)	315
Source Point Interval (m)	35
Number of Recevier Line per Shot	26
Number of Live Stations per Shot	342
Maximum Live Channels per Shot	8892
Acquisition Bin Size (m)	17.5 x 17.5
Weight per shot (kg)	2
Depth of Hole (m)	15

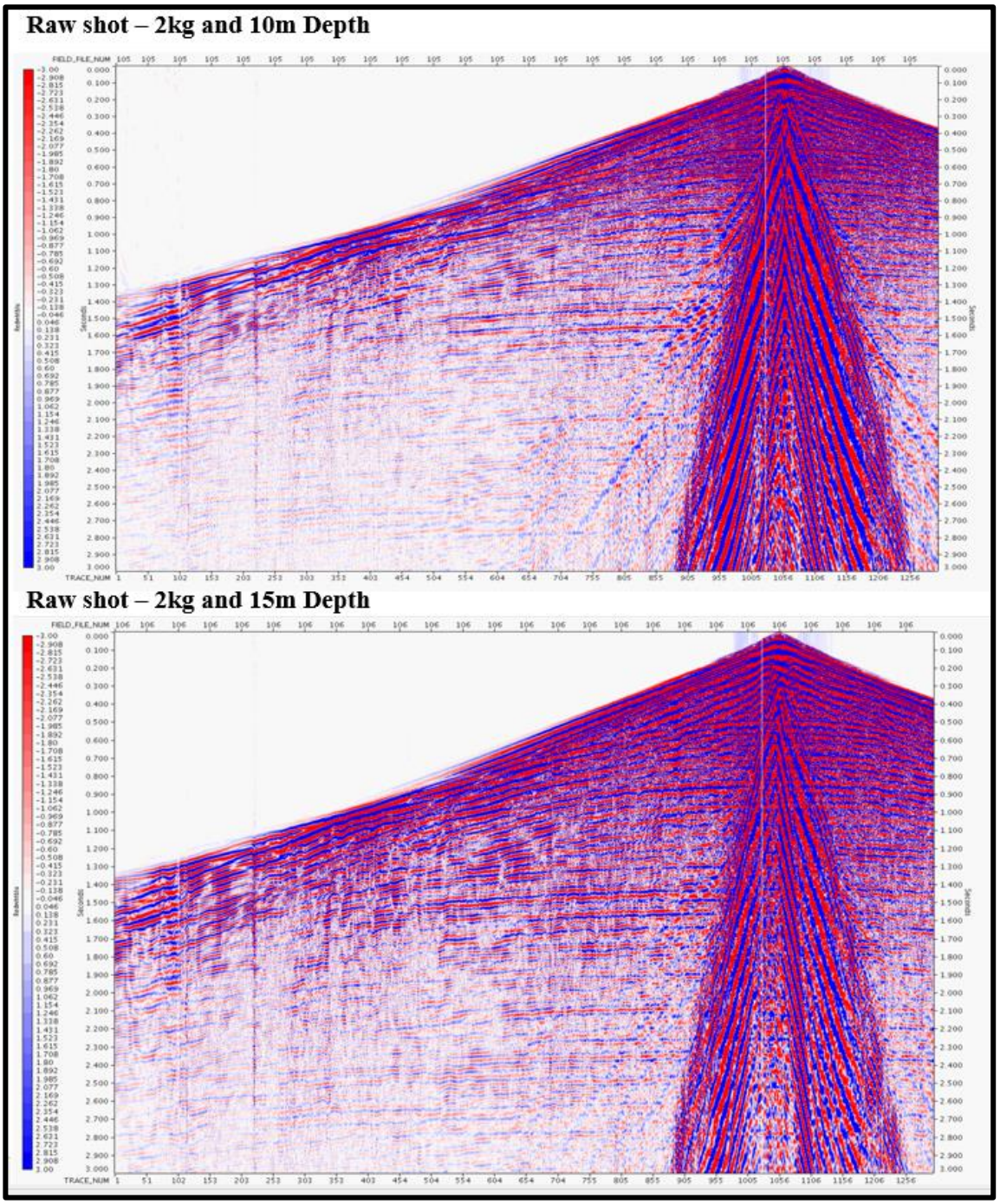

Figure 3.18. Comparison of the raw shot recording to the different drilling depths of the holes (seismic shots) (Basra Oil Company, 2014).

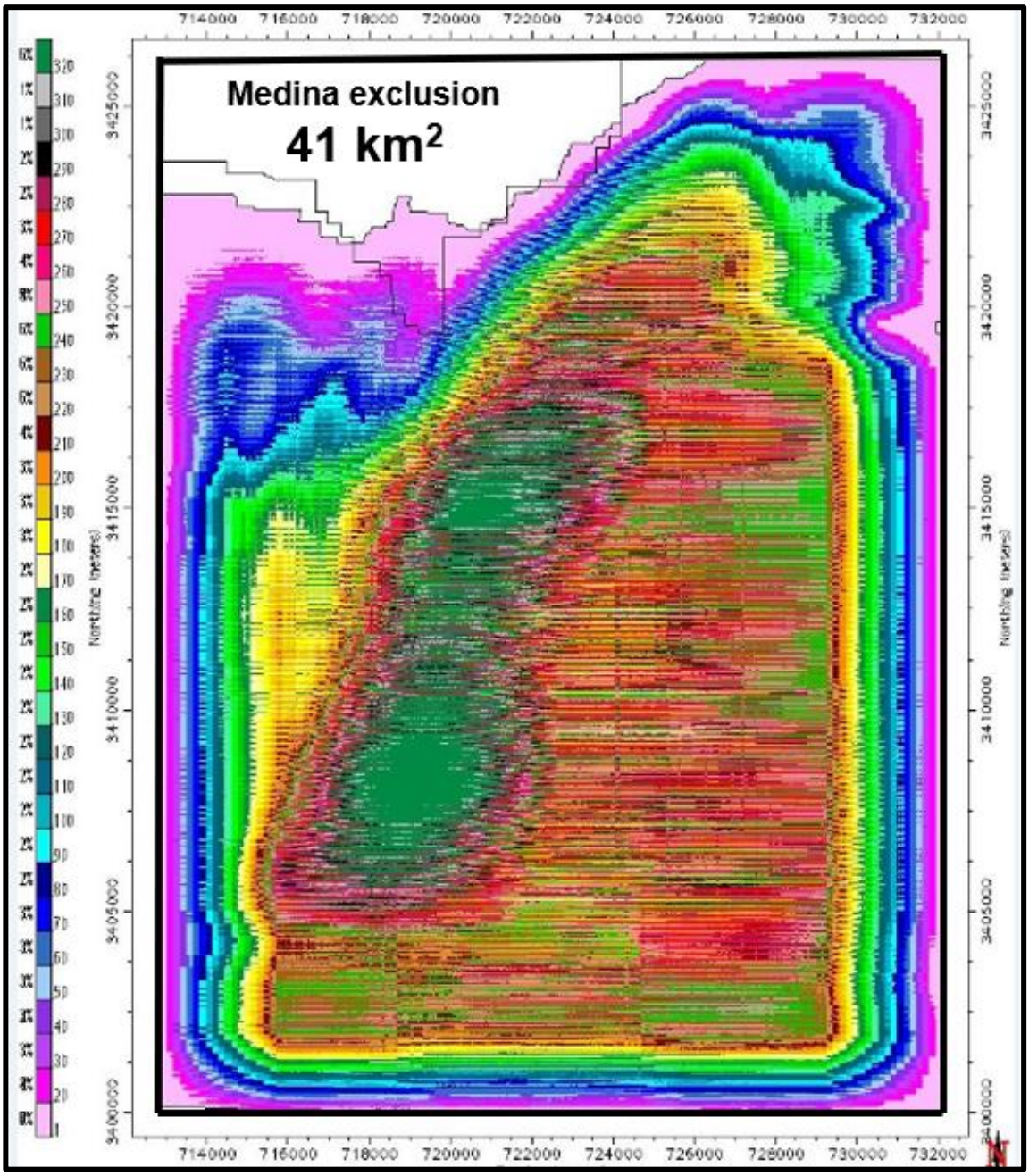

Figure 3.19. Final full fold offset map of West Qurna/1 3D seismic survey (Basra Oil Company, 2014).

3.5.2 West Qurna/1 3D Seismic Processing

Interpreting land seismic data has always been extremely difficult due to interbed multiples, especially in basins in the Middle East where impedance differences may be fairly strong and arise at various depths in the subsurface (Ourabah *et al.*, 2015). Seismic processing starts in different steps, and there was preliminary processing in the field location. The Kirchhoff Pre-stack time migration (PSTM) possessing flow was carried out on 3D seismic data, and the first volume was submitted in 2014. Surface-related

multiple attenuations are a routine process; inter-bed multiple attenuations are still a challenge due to poor velocity discrimination between primaries and multiples.

The previous de-multiple (multiple removing) effort of Westen Geco in 2014 was carried out on pre-interpolation data and focused on improving the image at the Mishrif reservoir. As part of the Western Geco seismic contract, the West Qurna study team received a final West Qurna/1 seismic volume in 2017 after removing interbed multiples from Zubair, Yamama, and deeper reservoirs. By comparing the two seismic volumes (2014 and 2017) (Figures 3.20), the results show an improvement in seismic image quality of the primary target level (Mishrif) and the horizons of shallow reservoirs. In addition, it enhanced fault interpretation and fracture prediction for static and dynamic model conditioning and development scenarios. Figure 3.21 shows an improvement in the Jurassic reservoirs (Zubair and Yamam), and there were more definitions of the Hercynian unconformity that could be used in the future exploration program. These horizons respectively define the base of the West Qurna/1 reservoirs in the time domain used in the analysis to the window (well tie) the seismic data in the vertical direction and guide the analysis in the horizontal direction. Ultimately, this will enhance the WQ-1 3D seismic interpretation for a better understanding of reservoir connectivity and petrophysical property prediction.

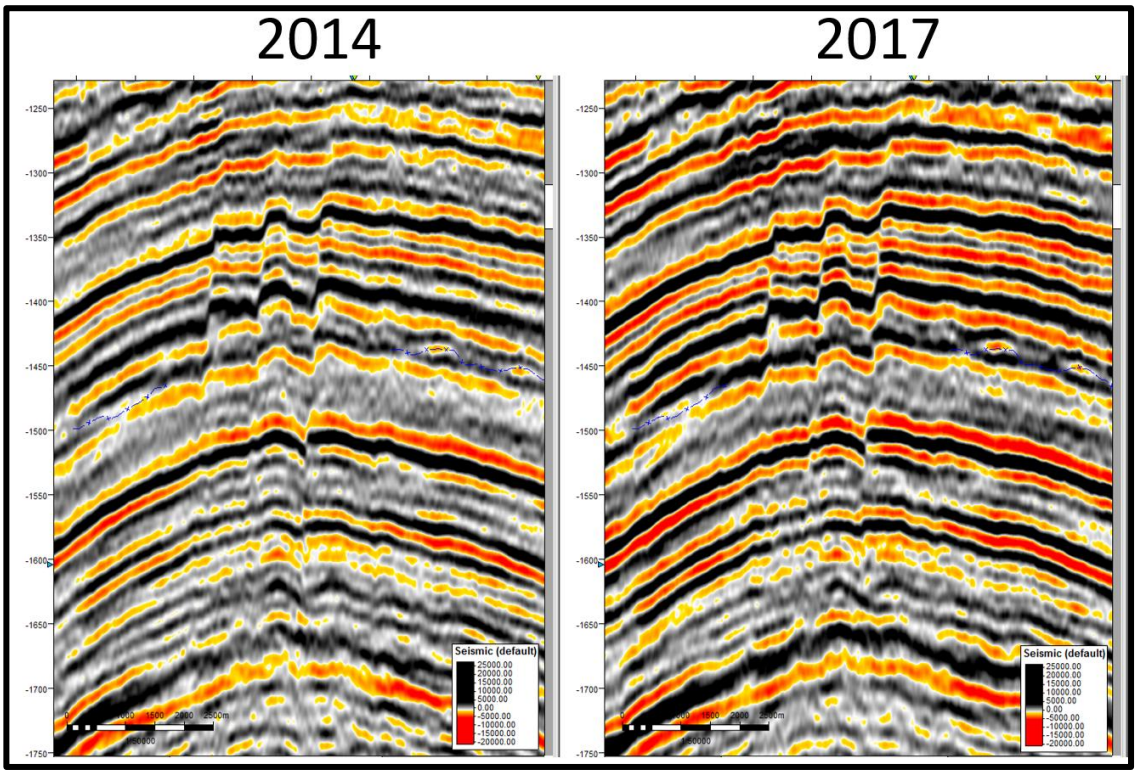

Figure 3.20. Comparison of West Qurna/1 3D seismic volumes (2014 and 2017) in Mishrif reservoir intervals, with seismic volume (2017) enhanced horizons (more bright) and faults interpretation after removing more interbed multiple energy (Basra Oil Company, 2017).

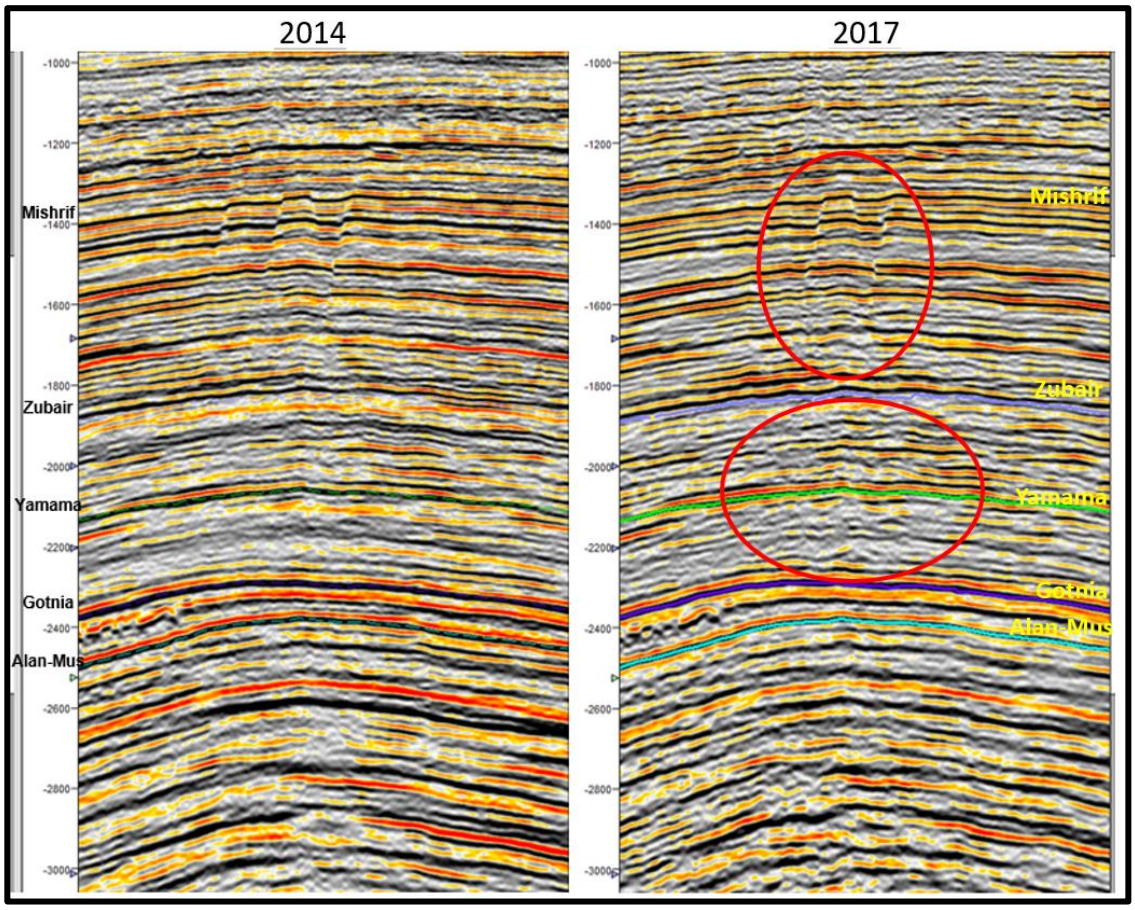

Figure 3.21. West Qurna/1 3D seismic volumes (time domain), the red ellipses indicate the improvements in seismic interpretation (faults and Hercynian unconformity) based on the seismic volume (2017) in targets reservoirs (Zubair and Yamama) compared to the first seismic volume (2014) (Basra Oil Company, 2017).

3.5.3 Seismic to Well Calibration

Before using the seismic data for interpretation, the survey volumes must be calibrated with well data due to the poor reflectors common in reservoirs, making it challenging to match synthetic and seismic traces. Another purpose for matching the synthetic and seismic overburden traces is to connect the seismic horizons to the well-tops. This facilitates the correlation of seismic occurrences in the study region (reservoir interval). Synthetic seismograms were generated for vertical seismic profiles (VSP) wells WQ1-Y64, Y66, Y68, Y93, Z02, Z09, and Z38 and can be divided into the north and south VSP wells (Figures 3.22 and 3.23), representing high-density measurements from each VSP survey. The synthetic seismogram is calculated throughout the log section until it reaches the area of interest. Hence, VSP wells were selected to test if there are velocity differences between the crest and flank, differences between the east flank and west flank, and

differences between the northern and southern portions of the field. Surprisingly there were very few changes between the east, crest, and west, but significant changes were observed between the north and south velocities. This is supported by the seismic imaging velocities.

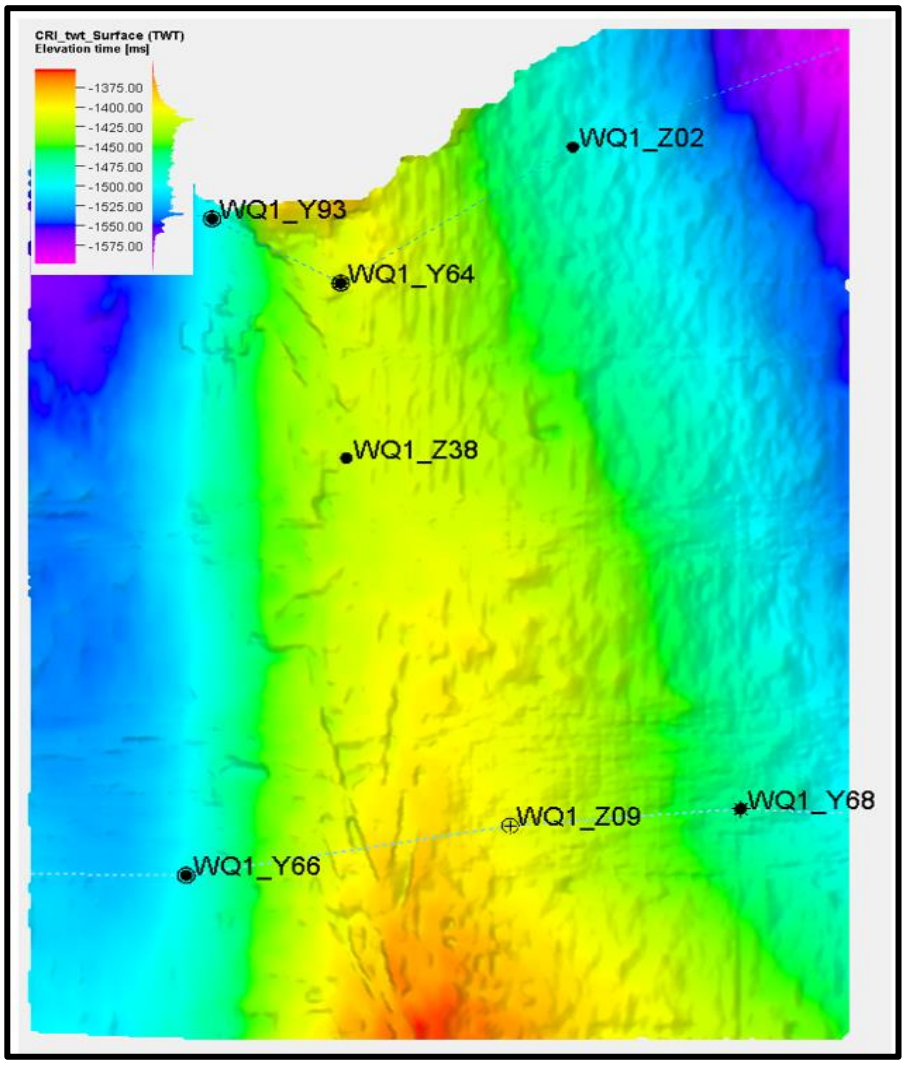

Figure 3.22. The time structure map of the Top Mishrif Reservoir (CRI) illustrates the North (WQ1_Y93, WQ1_Y64, WQ1_Z02) and South (WQ1_Y66, WQ1_Z09, WQ1_Y68) vertical seismic profile (VSP) well distribution.

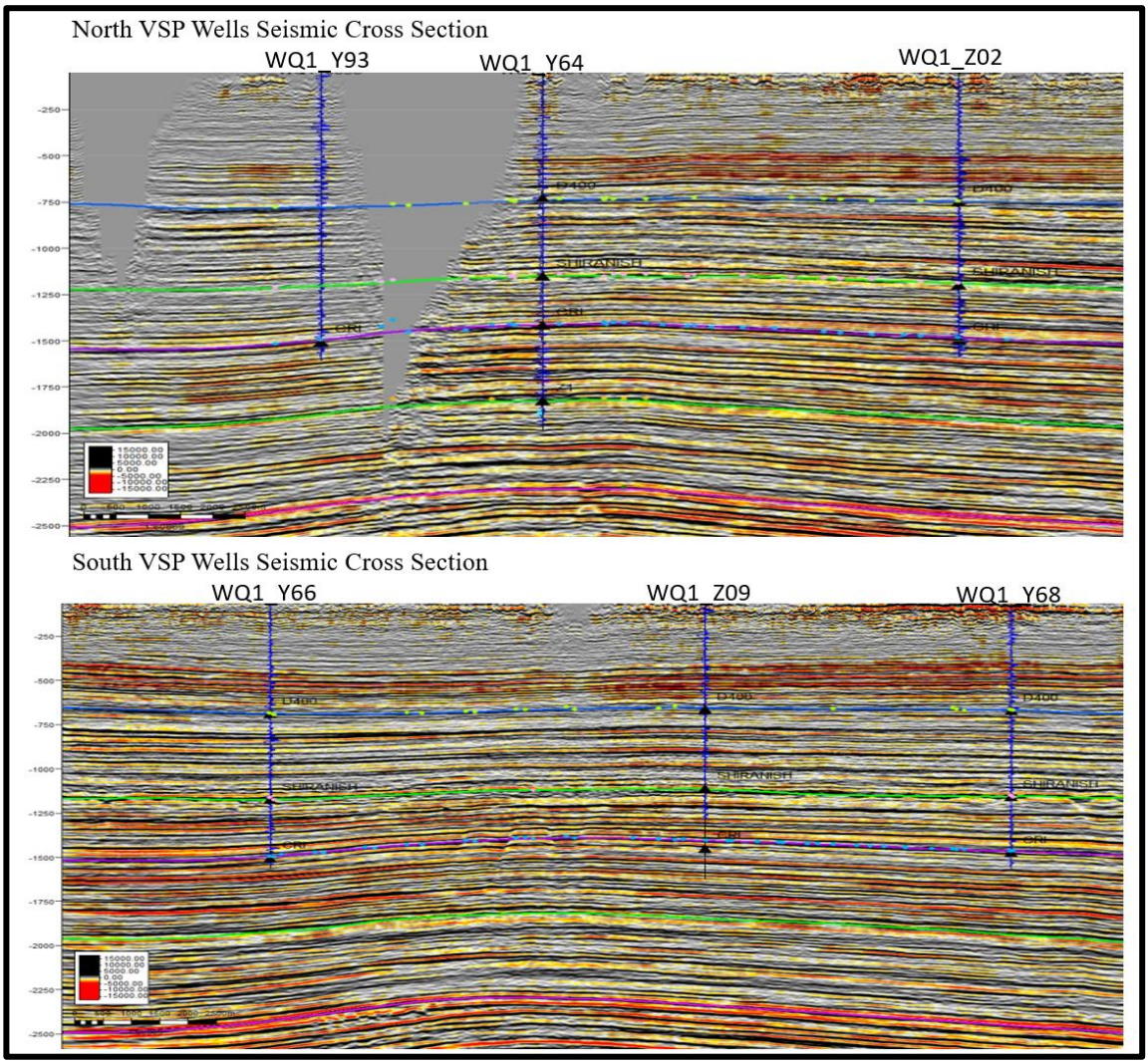

Figure 3.23. North and South VSP wells seismic cross-sections in the time domain.

The main task of the West Qurna/1 seismic to well calibration process is to match a synthetic seismogram peak to a seismic trace peak or a synthetic seismogram trough to a seismic trace trough, as shown in Figure 3.24; stretching and squeezing the synthetic is not recommended since it alters the time-depth connection provided by the calibrated check shots. However, using a continuous shift to match the synthetic with the seismic is widely accepted.

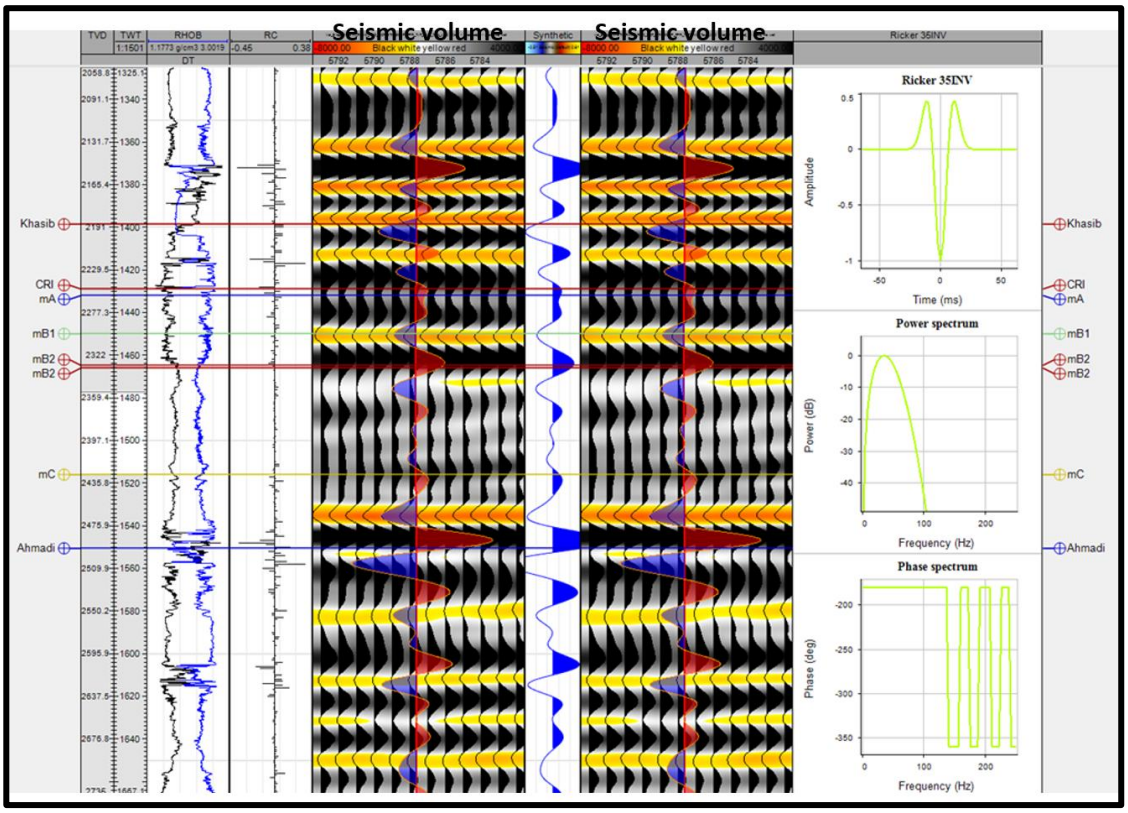

Figure 3.24. Integrated seismic well tie of Well Z38. Track 1: Measured depth. Track 2: Two-way travel time. Track 3: Density and sonic logs. Track 4: Reflection coefficient. Track 5: Seismic trace at zero-phase. Track 6: Synthetic seismogram. Track 7: Seismic trace at zero-phase. Track 8: A zero-phase analytical wavelet (reverse polarity) constructed with a frequency of 35 Hz. The horizontal lines across the tracks label the top of each Mishrif zones (from logs).

3.5.4 West Qurna/1 3D Seismic Horizon Interpretation

Initially, the interpretation was made in the time domain. 17 Horizons (from shallow to deep formations) were interpreted using seismic well-ties, gridded in the time domain, then converted into the depth domain using the well-based velocity model. This model was also used to help the infield processing team in the seismic velocity picking and was determined to be close to the velocities observed. Horizon and fault interpretation must be transferred into the depth domain to generate a 3D model for volumetric analysis (Figure 3.25). The well-based velocity model was created for the time-to-depth conversion of the horizons and faults. Based on the interpretation of horizons in both the time and depth seismic cubes, interval velocities between surfaces were calculated and adjusted to well tops.

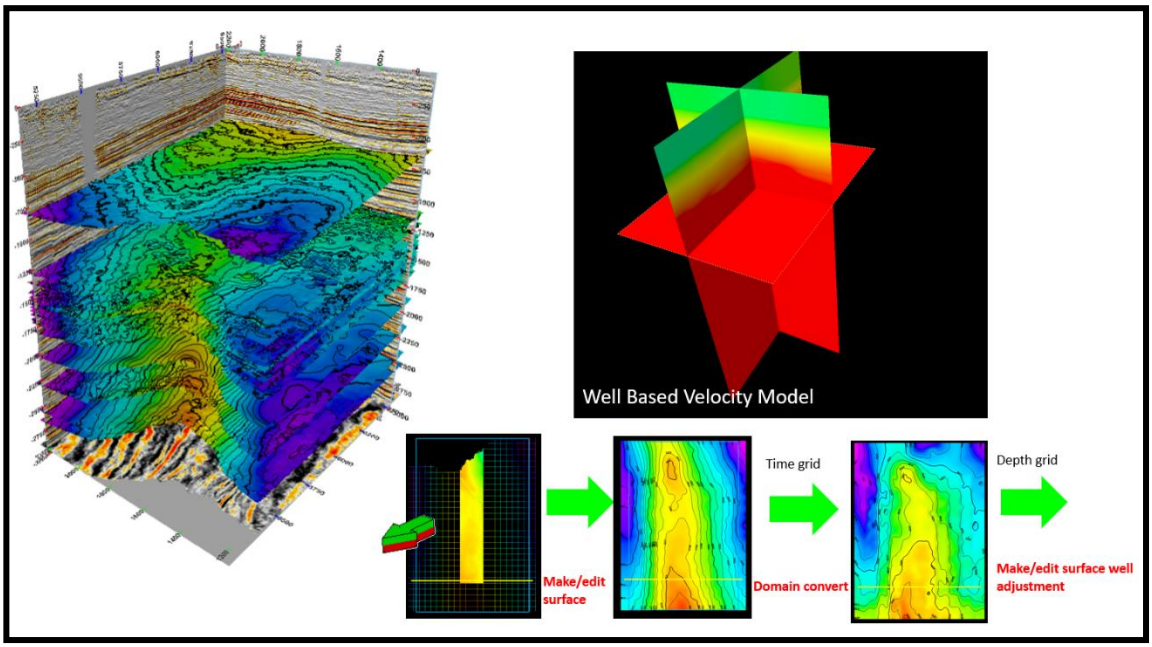

Figure 3.25. Illustration showing the steps for the West Qurna/1 seismic horizon interpretation in the time domain and then converting these horizons into depth domain using the well-based velocity model.

3.5.5 Fault Systems and Structural Framework

Seismic data are used to obtain structural and stratigraphic information for West Qurna/1 reservoirs. High-resolution West Qurna/1 3D seismic data show a high level of information on the architecture and structural settings. The structural modelling of the fault zones in the Mishrif reservoir is based on the integrated use of seismic technologies and approaches. The first step included intensive seismic interpretation and building structure maps. Then, seismic attribute cubes are also carried out to provide an overview of the 3-D network of the Mishrif fault systems as part of the structural analysis. A three-dimensional model of the fault network was constructed in the next step. The main outcome gained from the last step was to highlight the seismo-structural framework of the Mishrif reservoir. The significant steps of the Mishrif structural model are explained and discussed in the following subsections.

3.5.5.1 Fault Array and Seismic Attribute Analysis

The use of well data can help identify the estimation of fault zone thickness and properties. Based on the well log correlation, it can be observed that the fault offset of the Mishrif reservoir is almost 30 m through the well correlation of the top Mishrif reservoir.

(Figure 3.26). However, analyses of log data alone cannot reveal the effect of lateral variations and cannot discover if the fault structure consists of one significant or several smaller-scale faults. Consequently, it is better to gather precise information on structural reservoir properties by integrating seismic data, well-log correlation, and core data. The interpretation of faulted Mishrif reservoir display on different vertical seismic cross-sections and time slices were chosen at different depths. A complex faulting pattern is observed in the reservoirs, including an array of steep fault zones vertically segmented that define a broad pattern of faults trending northwest and northeast (Figure 3.27). The analysis of faulting styles indicates en-echelon faults, which refer to wrenching stresses (strike-slip tectonics) and extensional faults (normal). These faults exist mainly between the Hartha formation and extend to the Ahmadi formation, with just a few faults extending down into the upper Nahr-Umr formation (Figure 3.28). The fault throw is extended from 8 meters (minimum seismic resolution) to 40 meters. As illustrated in Figure 3.29, the time slice sections show large-scale structural characteristics of the Late Creatures faults have been mentioned previously as one of the major faults and discussed by (Jassim and Buday 2006), displaying an en-echelon to discontinuous faults at Mishrif reservoir intervals.

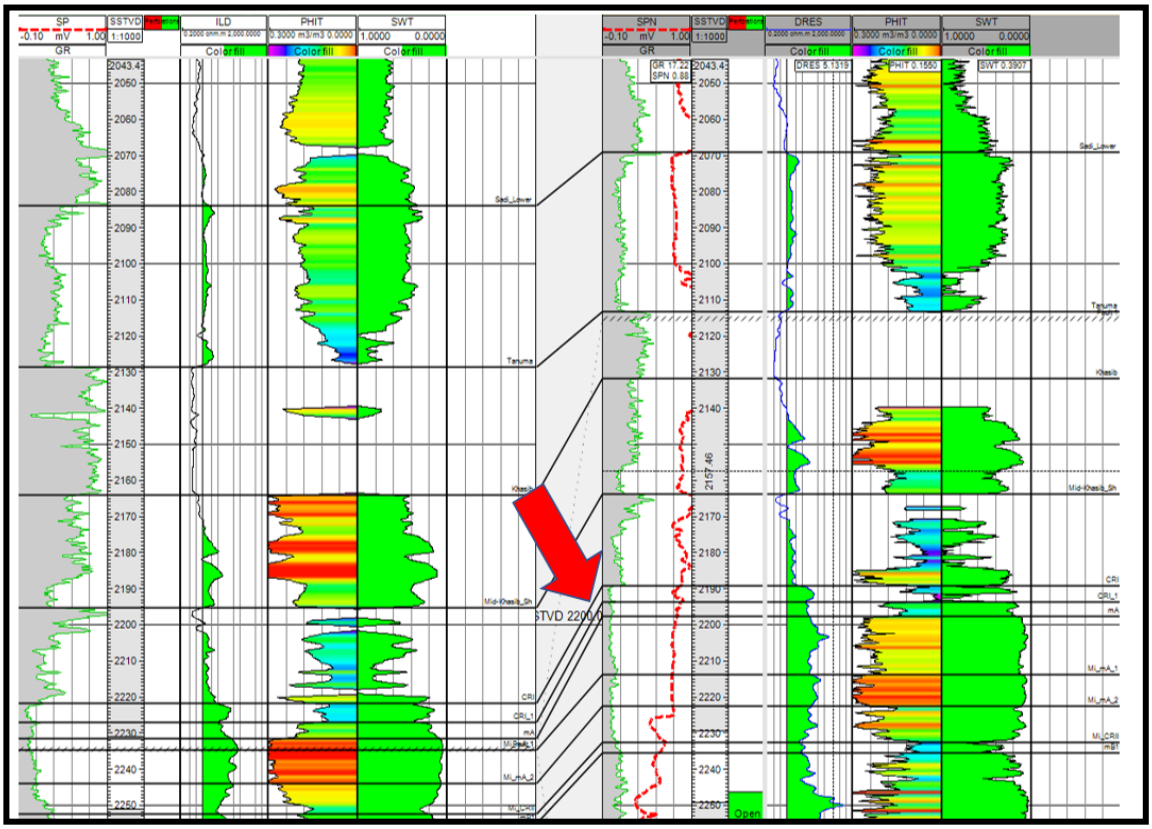

Figure 3.26. A fault distance location (30 m) in the top of the Mishrif reservoir between two wells based on the manual well-to-well correlation which was implemented to identify fault displacement.

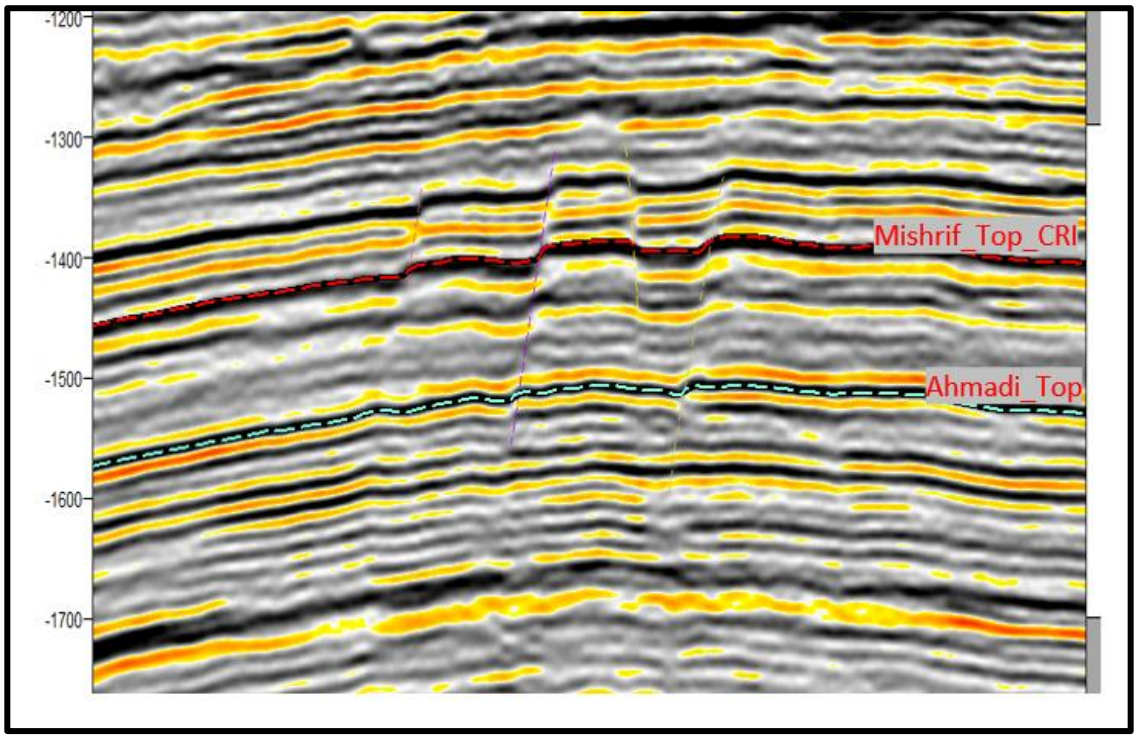

Figure 3.27. A composite seismic section illustrating the complex style of Cretaceous fault intervals in time domain shows the extension in the Mishrif interval.

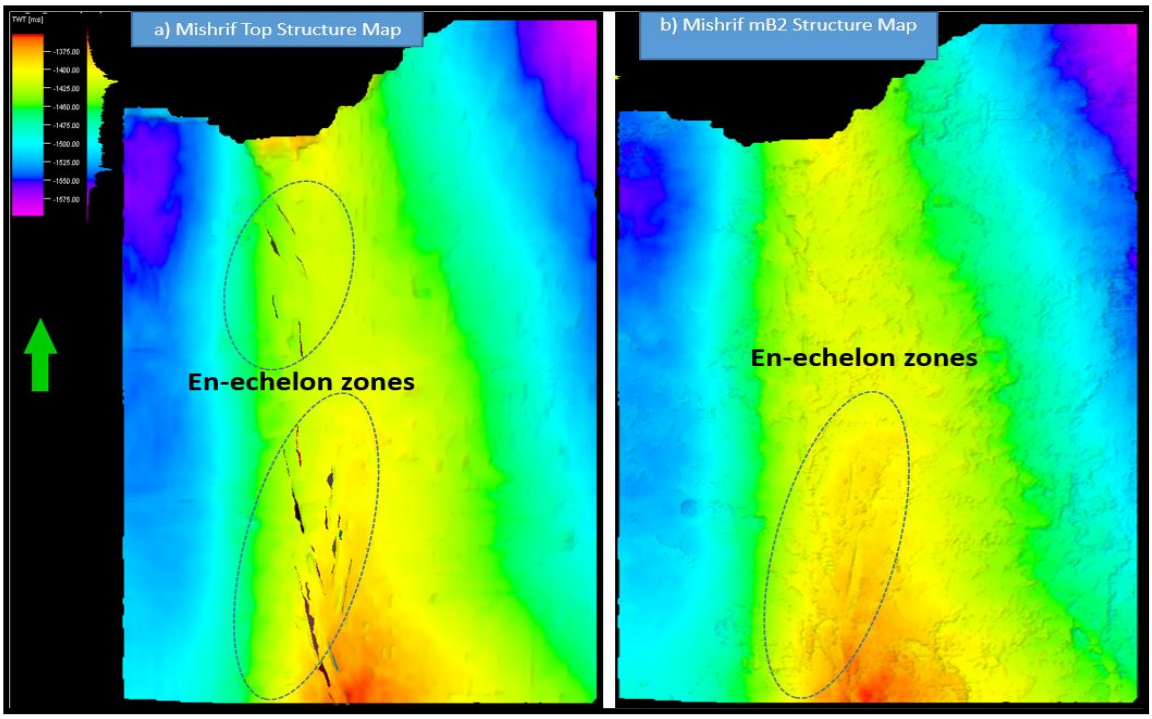

Figure 3.28. Time structure maps of Mishrif intervals showing the trending lineaments of en-echelon fault zones to a) the top of the Mishrif and b) Mishrif mB2 surface, derived from interpretation of 3-D seismic data of the West Qurna/1 field.

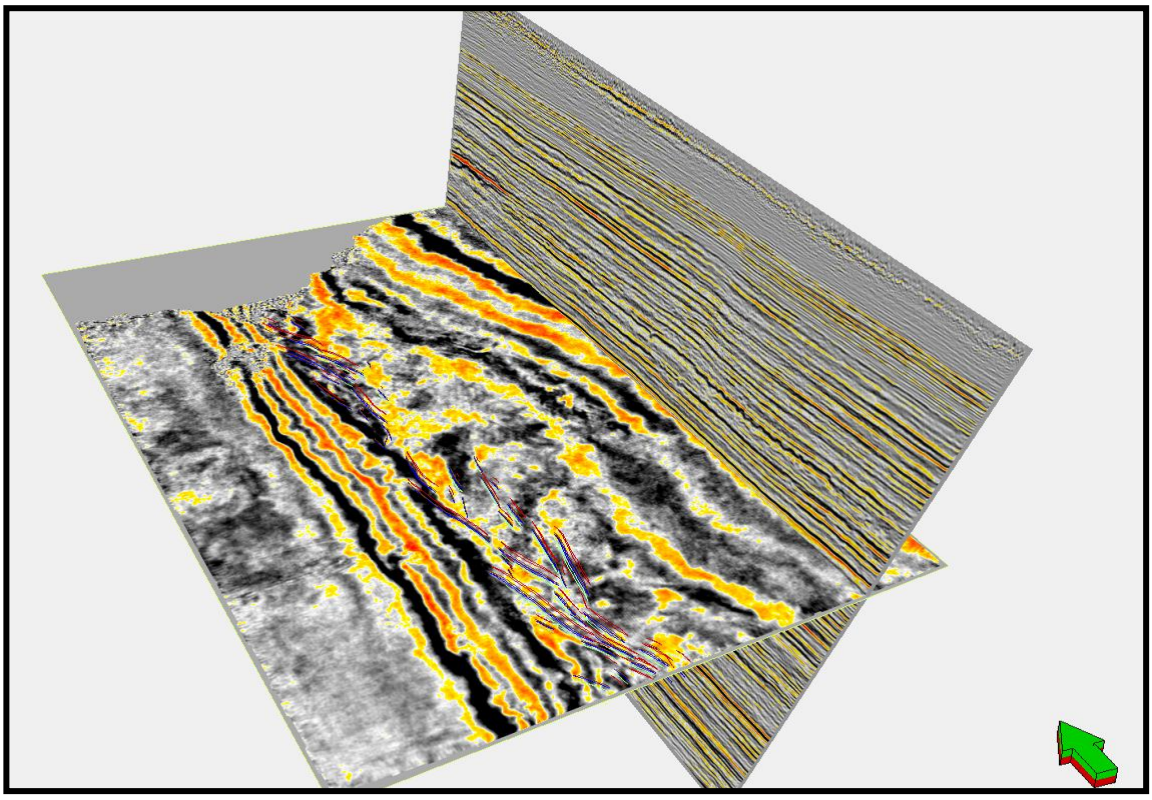

Figure 3.29. The seismic time slice section displayed the interpretation of an En-echelon Mishrif faults from north to the south.

Seismic attributes can be obtained from amplitude, velocity, and frequency to image the structure in time or depth and characterize the reflections' amplitudes. Further, it helps to extract information that could be subtle in traditional seismic amplitude interpretation. Consequently, seismic attributes such as variance at different levels revealed the structural setting from 3D high-resolution West Qurna/1 seismic data. This seismic attribute volume (Figure 3.30) indicates the local changes in waveform shape and shows a system of dominantly northwest and northeast-trending faults that extend to the lower Cretaceous reservoirs.

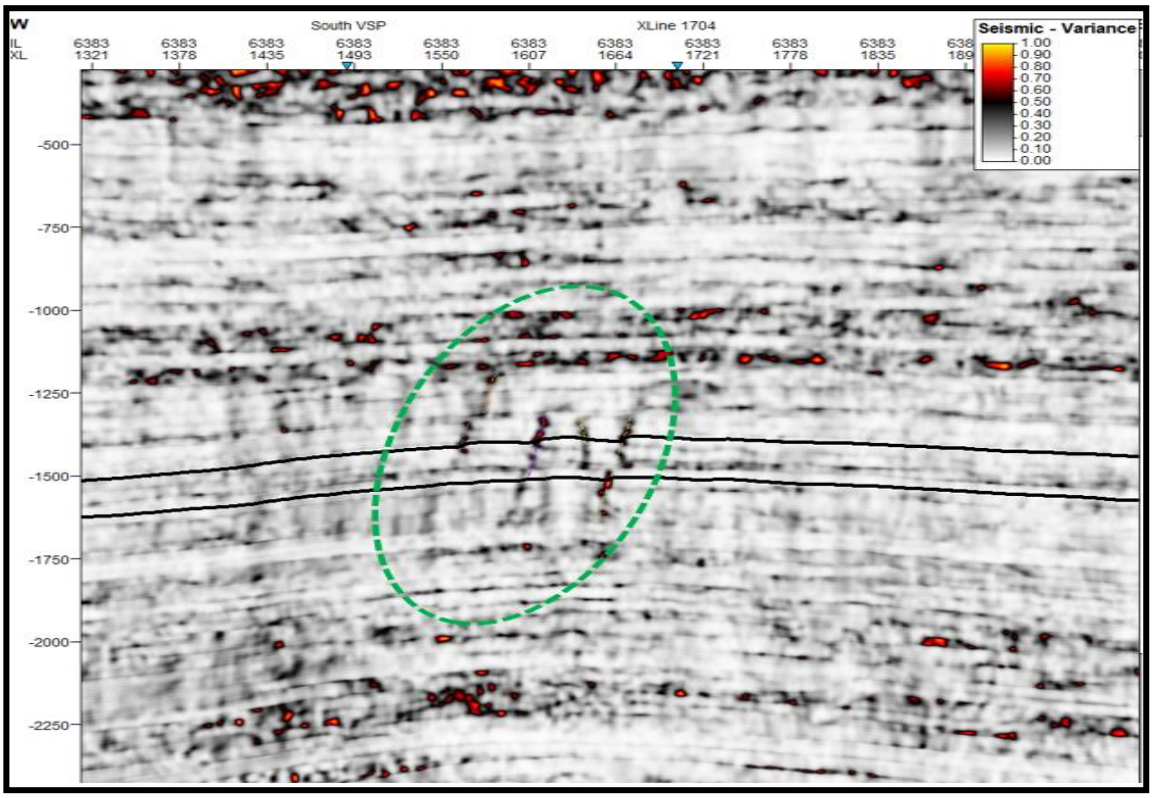

Figure 3.30. The seismic section from the 3-D variance cube shows the fault interpretation in the Cretaceous reservoirs (including the Mishrif interval).

3.5.5.2 Structural Framework of the Mishrif Fault Systems

A 3D fault framework has been generated for the field. A total of more than 50 major faults with significant displacement and 17 horizons were built through the faults model. Based on a seismic interpretation of fault geometry and seismic attribute analysis, it can be seen that these faults are consistent with a regional fault setting described across the Iraq region (Jassim and Buday, 2006; Jassim and Goff, 2007). Accordingly, modelling of the major fault zones in the Cretaceous Mishrif reservoir has been established and identified. The seismic structural framework illustrated in Figures 3.31 and 3.32 provides a clear image and better understanding of the Mishrif structure setting. Therefore, it will explain the porosity and permeability anomalies that were previously mapped from wellbore data. Also, a good understanding of fault distribution is critical to reducing the reservoir model's uncertainty and might be applicable in similar carbonate geological settings.

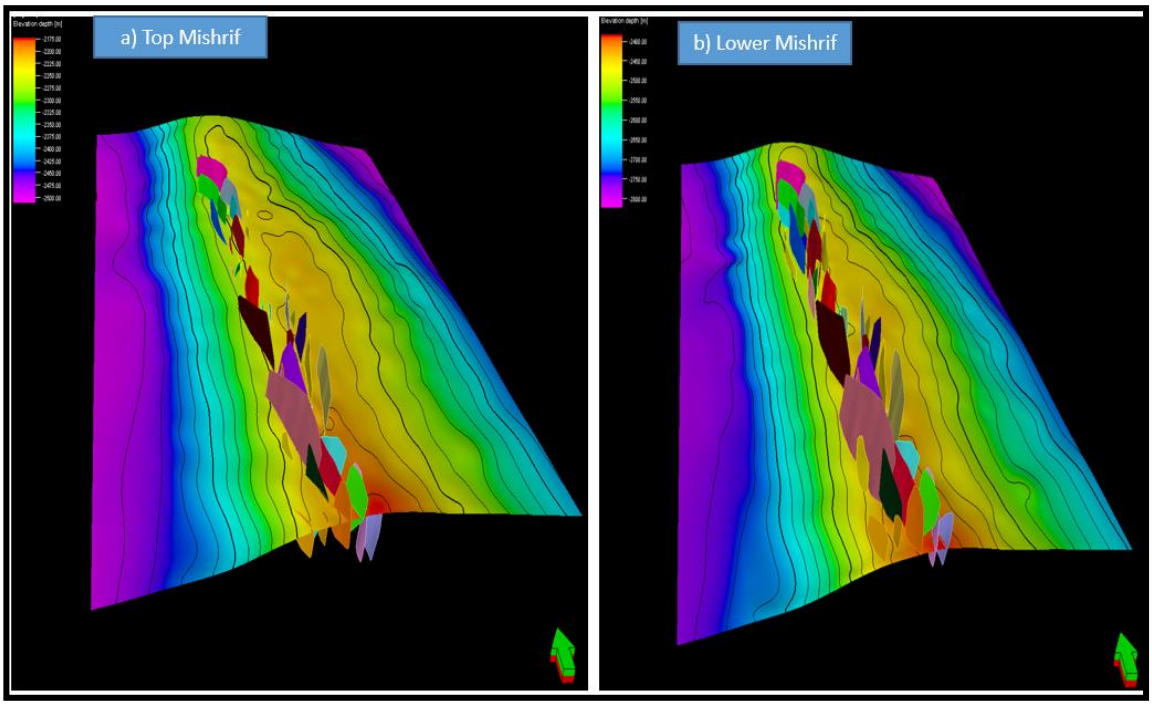

Figure 3.31. Depth structure maps illustrate en-echelon faults and their extensions at the top Mishrif (a) and the lower Mishrif (b) horizons used within this study as mapped within the 3-D seismic volume.

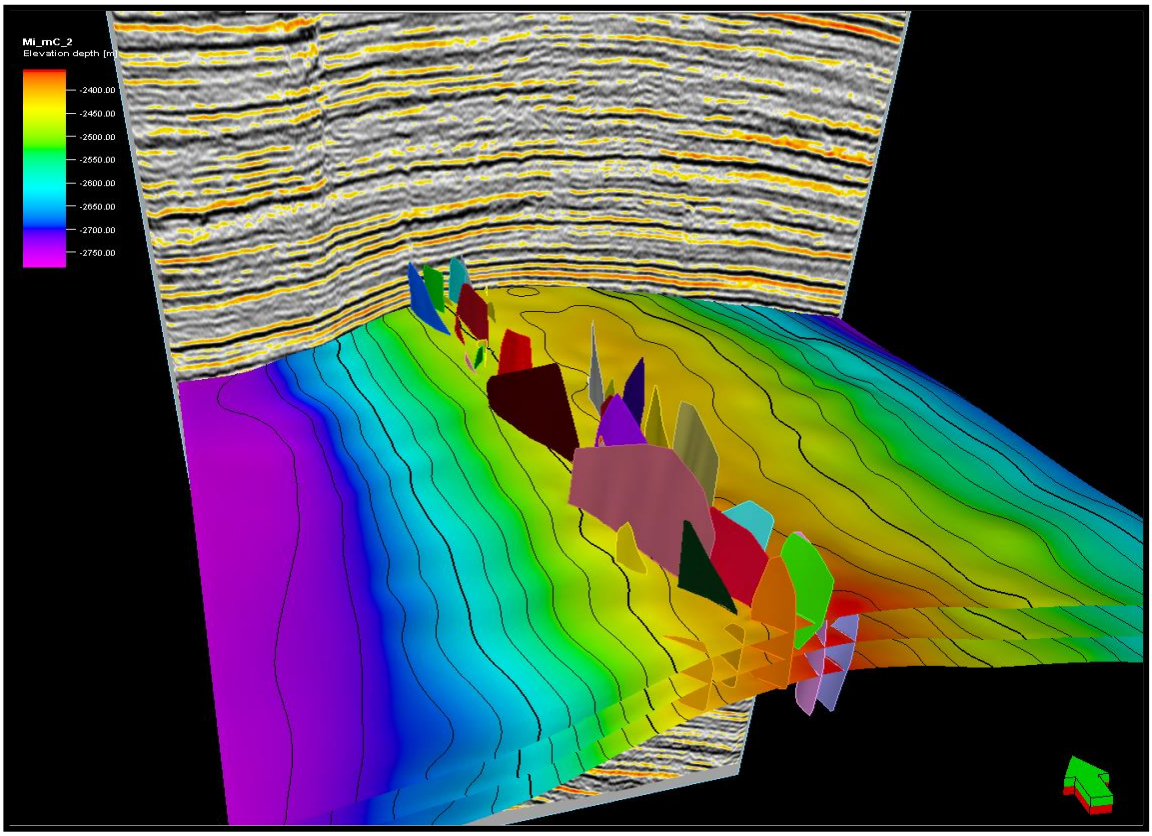

Figure 3.32. 3D visualization of the structural framework of the Mishrif faulted reservoir (fault network and the main horizon) highlights the reservoir's fault distribution.

3.6 Summary and Conclusion

This chapter has presented a geological overview of the West Qurna/1 oilfield to construct an accurate reservoir characterisation of the Mishrif channelized reservoir. First, an initial understanding of the regional geological, geological overview, and the West Qurna/1 Field sequence stratigraphy was presented. Next, the conceptual geological model for the mid-Cretaceous Mishrif reservoir was developed by analysing sedimentary facies distribution through the impact of variation in relative sea-level and reservoir characteristics to identify high permeability zones. Based on the reservoir zonation, it can be seen that depositional facies and the sequence stratigraphic are utilized as an indicator of the presence of high flow units thief zone such as the upper part of Mishrif mB2 and Mishrif mB1 channel zones since the flooding surfaces occur at the top of each Mishrif genetic zones. Thus, the Mishrif mB1 channelized zone was introduced into the reservoir characterisation to ensure conformance of the distribution to the internal architecture of tidal channels within the reservoir. Subsequently, a conceptual diagenesis model and the morphology of Mishrif tidal channels were established. Then, based on the analysis of fault systems and seismic attribute volumes, a new insight of structural modelling for the faulted Mishrif reservoir was introduced. Mishrif faults system is complex and far from a simple and non-faulted reservoir. In the vertical seismic profile and seismic attributes analysis, most fault systems show an en-echelon system, the most common type in the reservoirs. The faults system is characterized by a throw range between (10-40) meters with a structure trending northwest and northeast. Despite an important benefit of this interpretation to evaluate reservoir connectivity, the representativeness of sealing or non-sealing fault systems is uncertain due to unavailable measured data. Thus, combined with seismic attribute volumes, the seismic interpretation provided a valuable structural framework that described the Mishrif faults system as complex and far from a simple and non-faulted reservoir.

Chapter 4. Mishrif Reservoir Characterisation[2]

This chapter focuses on the characteristics of the Mishrif reservoir based on the seismic and well-log data. A reservoir characterisation workflow was employed to characterize the Mishrif reservoir based on the rock physics model and it also includes all the necessary steps for implementing seismic inversion. The integrated reservoir characterisation workflow and constraints are established and, finally, the porosity model based on seismic inversion is modelled and analysed in this chapter.

[2] This chapter contains material from "Al-Ali, A., Stephen, K. D. and Shams, A., (2019a). Improved Carbonate Reservoir Characterization: A Case Study from a Supergiant Field in Southern of Iraq. *SPE Middle East Oil & Gas Show and Conference*, held in Manama, Bahrain, 18-21 March 2019".

4.1 Introduction

Carbonate reservoirs require a modern, high-resolution 3D/4D seismic dataset to identify and characterize architectural heterogeneities with intrinsic complexity. Identifying the pore system and the spatial distribution of lithology are keys to constructing the reservoir model, which can help with decision-making in developing and managing the most prolific reservoir in the field. In this chapter, seismic reservoir characterisation is applied by integrating seismic inversion results, well-log data, a rock physics model, and core data analysis. The objectives are to characterize the porosity distribution and carbonate facies in the Mishrif reservoir. The workflow used for this study is similar to that applied in 3D feasibility studies. It enables modelling porosity and lithology as a distribution in 3D space between the wells. The outcomes of this chapter will also be used in the forthcoming chapters to characterize the channelized carbonate reservoir.

4.2 Methodology

The characterisation of a reservoir requires a combination of various datasets to identify prominent geological features. Integrating seismic data and other data will effectively characterize the reservoir's vertical and lateral heterogeneity. For the West Qurna/1 field, a high-resolution 3-D seismic volume was used to obtain stratigraphic and structural information for reservoir characterisation. Hampson-Russell software suite has been used for seismic reservoir characterisation. 19 well logs were selected in the survey area; in addition, the availability of five main horizons and the faults of the Mishrif reservoir were previously interpreted in the 3D seismic volume, as shown in chapter 3. Initially, quality control of the data (seismic and wellbore data) is critical to conducting quantitative seismic analysis. The suite of wells covers the entire field and is considered an excellent input to carry out acoustic impedance inversion and porosity characterisation.

The workflow for seismic reservoir characterisation of West Qurna/1 field mainly includes four major components, namely:

a) The rock physics model is the first step in the workflow through the vertical porosity distribution evaluation based on well-log data and its relationship with elastic properties.

b) Post-stack seismic inversion is the second step, where the well log data and seismic data are then imported into a commercial seismic reservoir characterisation software.

c) Facies discrimination is delineated and analysed based on core data and acoustic impedance.

d) Finally, post-stack seismic inversion techniques are used as input data for Mishrif reservoir characterisation by deriving the porosity model based on 3D seismic data. The porosity model is generated based on linear regression analysis over the entire West Qurna/1 field. The spatial distribution of the porosity is validated carefully using core data. The steps of the methodology workflow are summarized in Figure 4.1.

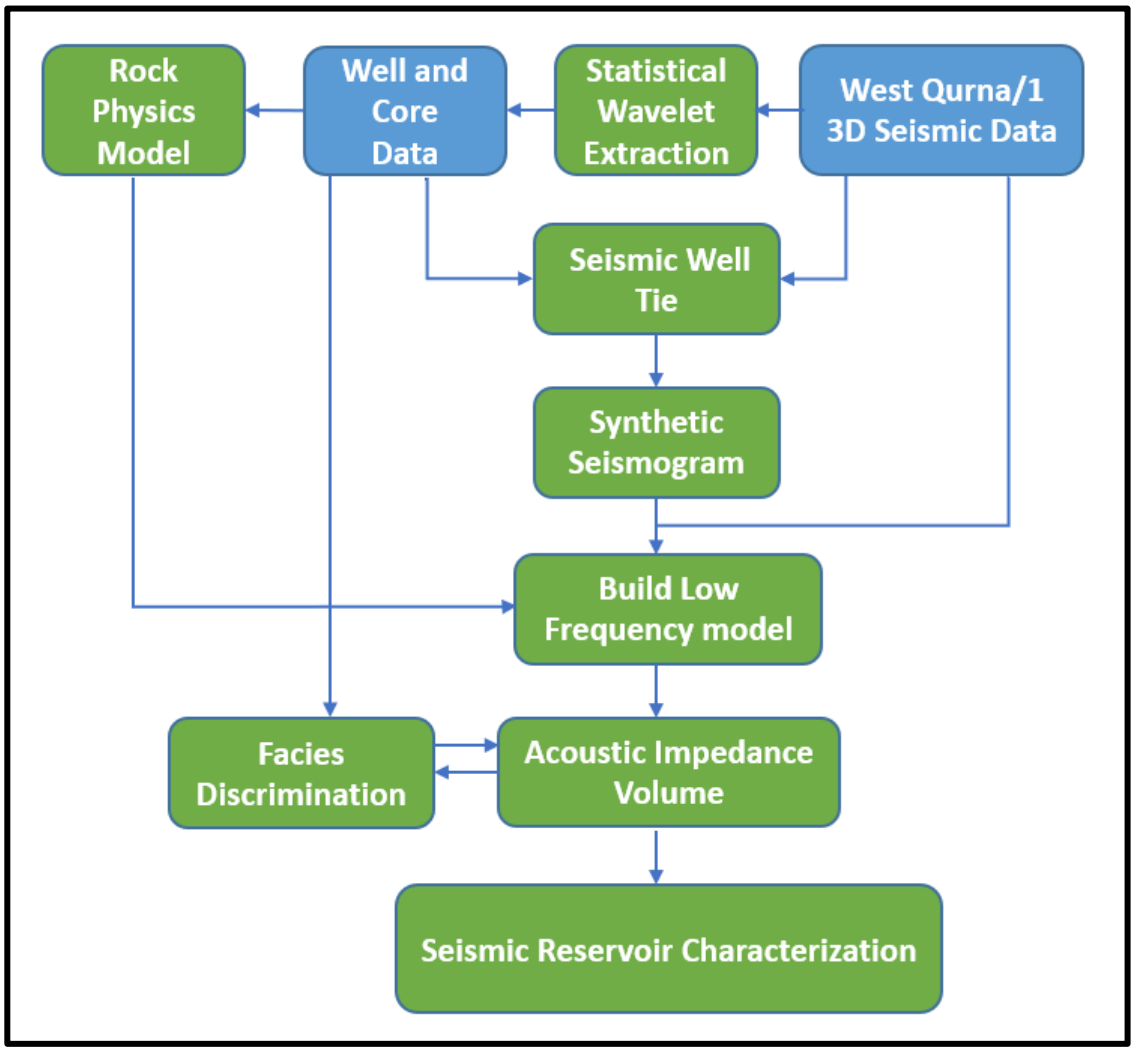

Figure 4.1. Schematic overview showing the reservoir characterisation workflow methodology for generating seismic inversion and porosity model for West Qurna/1 oilfield. The blue rectangles display input data, and the green rectangles represent the seismic reservoir characterisation process of the Mishrif reservoir.

4.3 Rock Physics Model

Before initiating the seismic inversion workflow, it is vital to perform a rock physics analysis to confirm that elastic properties are associated with reservoir properties and compare with porosity derived from 3D seismic inversion at well locations (Promrak *et al.*, 2018). According to Eberli *et al.* (2003), the porous medium of the carbonate rocks is the primary constraint of the elastic property variation (seismic velocity). Thus, based on rock physics analysis and the relationship between porosity and elastic properties in the carbonate reservoirs, the base for estimating petrophysical properties can be created from seismic-derived impedance in the Mishrif reservoir.

Compressional wave sonic data was acquired from wells in the West Qurna/1 field and covered almost all studied areas. The results demonstrate a good relationship (correlation factor of more than 90%) between the porosity and the P-wave velocity in the target reservoir (Figure 4.2). The analysis demonstrates a negative trend, meaning porosity declines with the increase of the P-wave velocity. However, the velocity variation displays a wide scatter between 300-500 m/s due to the distribution of overburden anomalies and the pore features (shape and size) (Karimpouli *et al.*, 2013; Kumar and Han, 2005). Based on rock physics model analysis that rounded pores make the velocity faster, and microcracks make it slower, the porosity of typical rocks can be classified into two broad categories, rounded pores, and cracks (Xu and Payne, 2009). The velocity in the rounded pores (vuggy, moldic) is faster than in cracks (Figure 4.3).

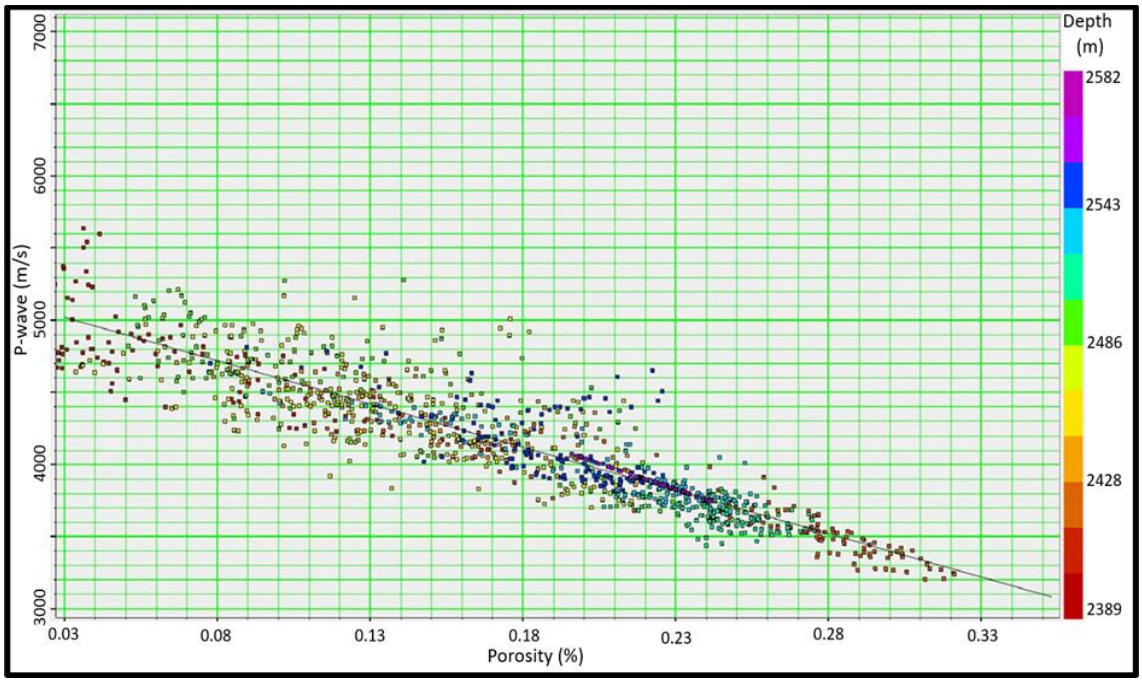

Figure 4.2. Rock physics analysis demonstrates a clear linear relationship between porosity

and P-wave velocity in the Mishrif reservoir (the colours of the data points indicate depth).

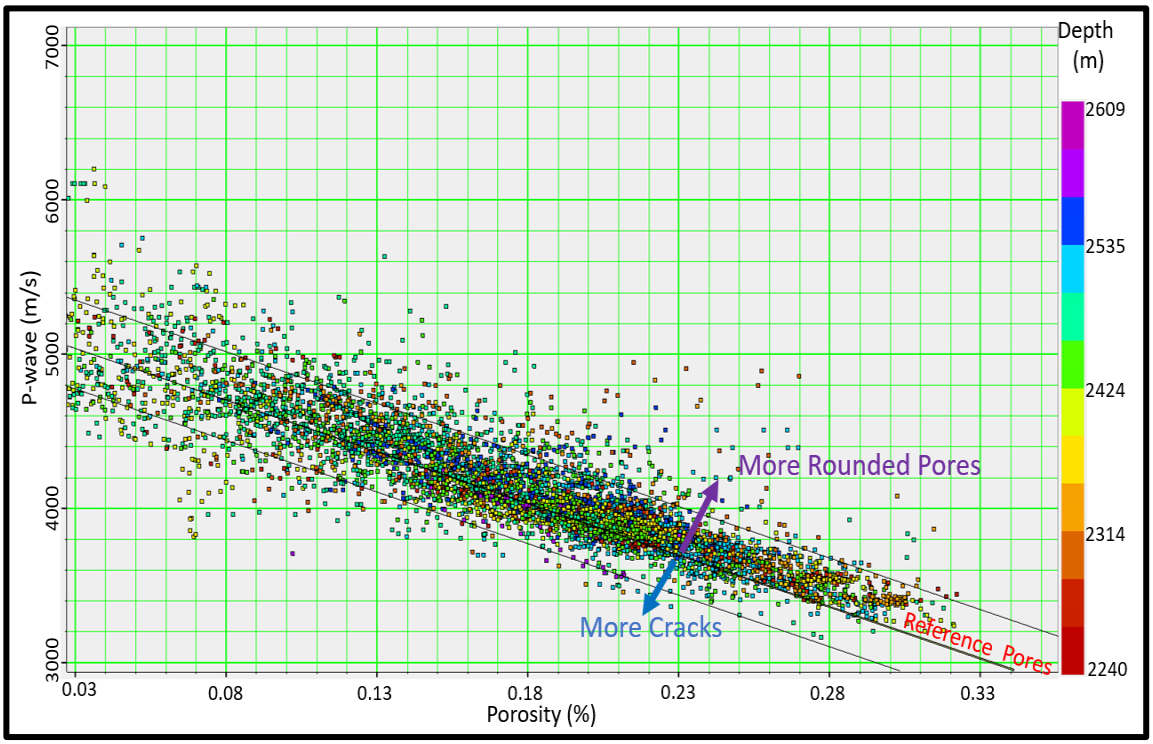

Figure 4.3. The cross plot of porosity versus P-wave velocity from the analyzed well data of the Mishrif reservoir shows the variation and lower velocity in cracks than rounded pores (the colours of the data points indicate depth).

Furthermore, log data (acoustic impedance and P-wave velocity) were analysed to recognize and separate the reservoir from non-reservoir carbonate facies in the Mishrif reservoir (Figure 4.4). This analysis illustrates that elastic property variation can separate each carbonate facies type based on the relationship between acoustic impedance and porosity. Thus, it will be reasonable to classify pore types from seismic inversion products. Another cross-plot was created between acoustic impedance and porosity measurements in the wells of the study area (Figure 4.5). The results demonstrate a well-defined narrow trend and good correlation. It suggests good evidence that inverted elastic properties from post-stack seismic inversion could be used to estimate petrophysical properties such as porosity in the following research steps.

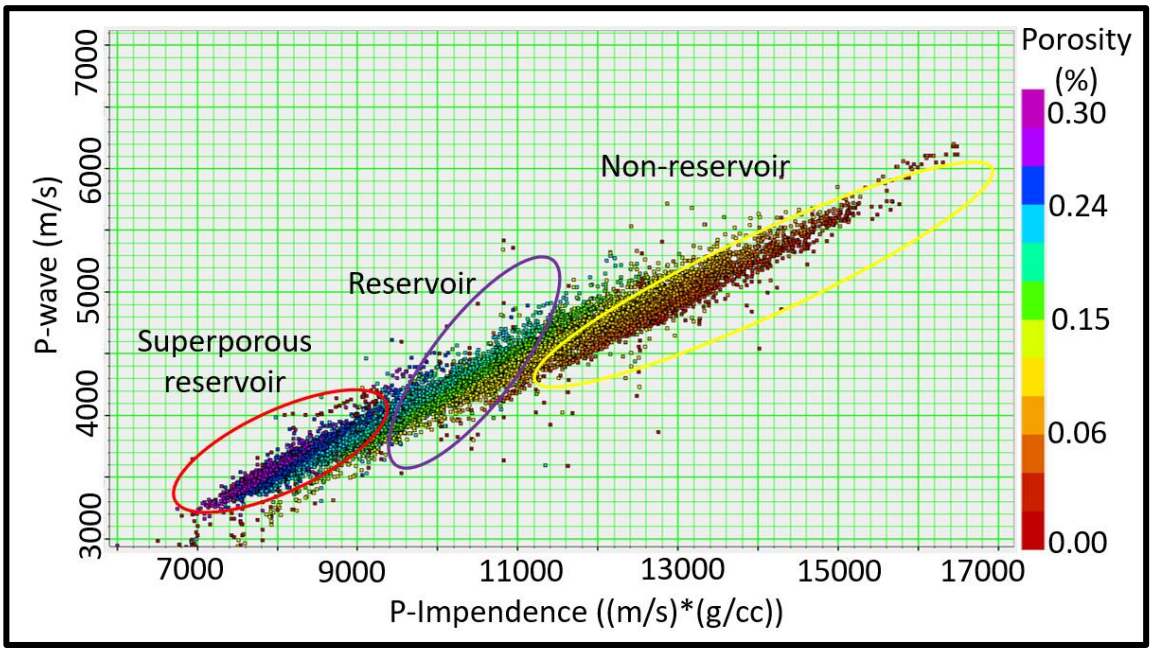

Figure 4.4. Cross plot of P-Impedance versus P-wave velocity, colour-coded by porosity exhibiting a good distribution of the Mishrif facies within elastic property domain.

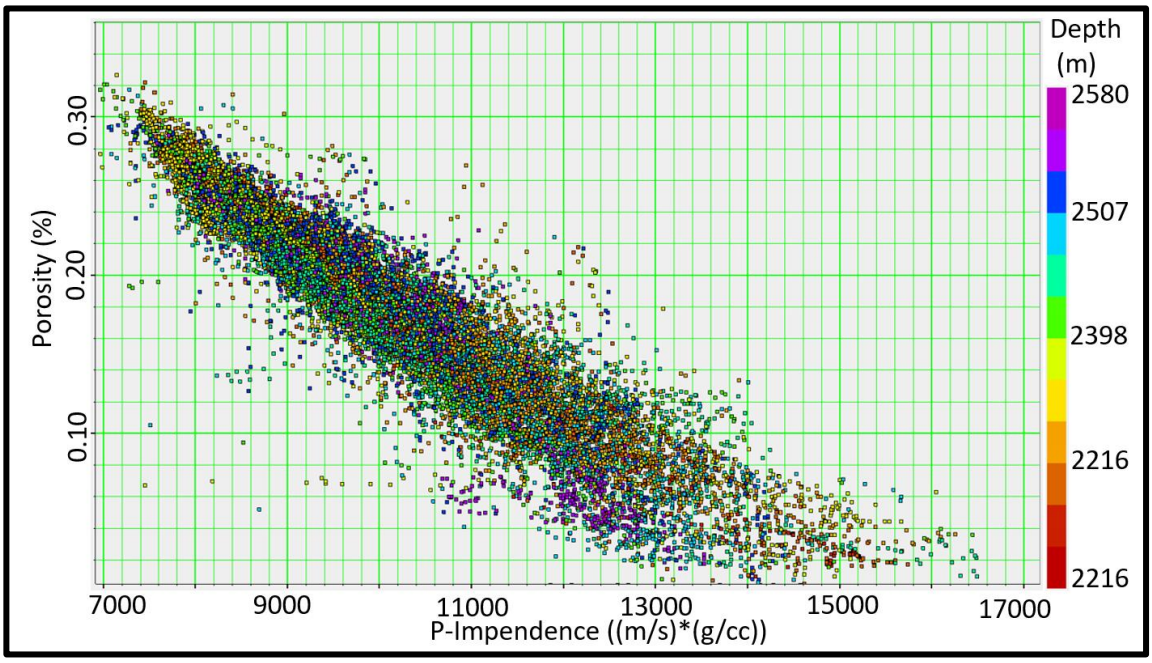

Figure 4.5. Rock physics template analysis between P-Impedance and porosity from the well log data of the study area, the variation in the porosity distribution due to the heterogeneity of the reservoir (the colours of the data points indicate depth).

4.4 Post-Stack Seismic Inversion

The seismic inversion is used to estimate the elastic properties of rocks, such as, in simpler cases, acoustic impedance or relative impedance. As described in the literature review chapter, different options exist for seismic inversion. We will use the model-based inversion and linear programming sparse spike inversion (LPSS) inversions applied on West Qurna/1 seismic volume for an area of about 500 km^2 (Figure 4.6).

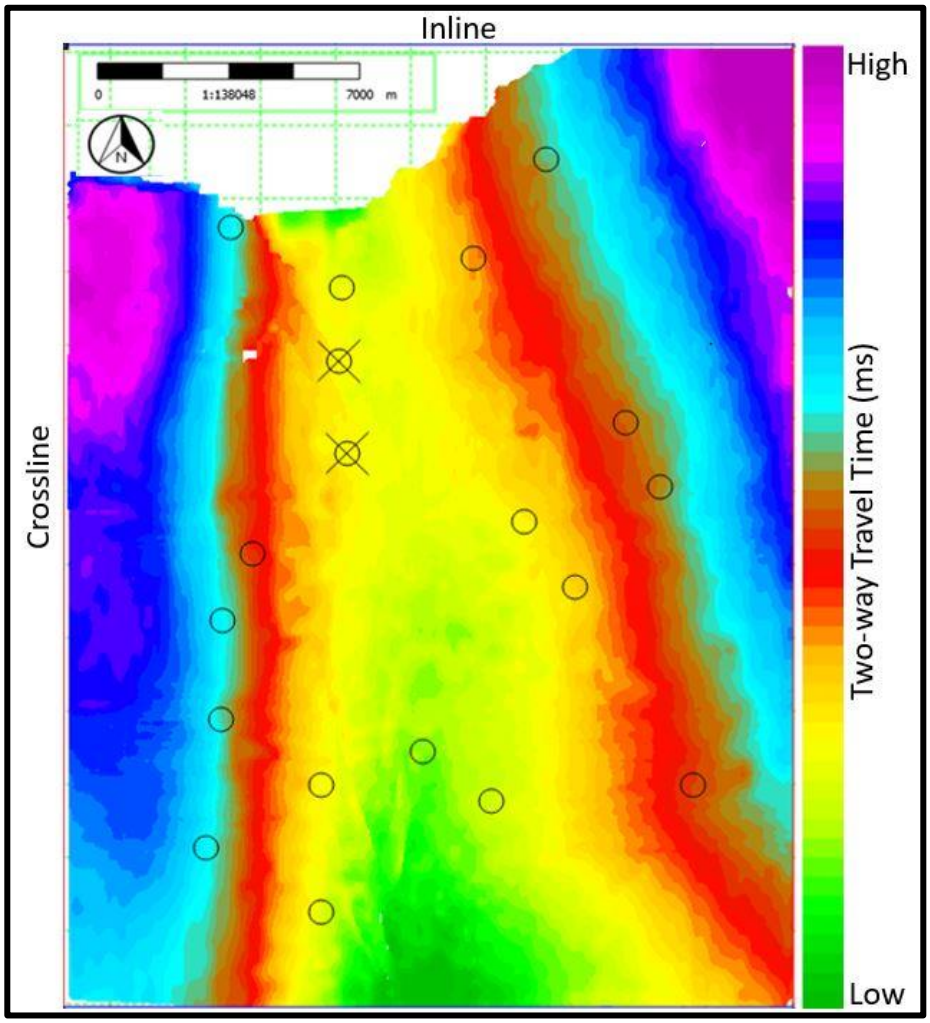

Figure 4.6. Time structure map of the top-Mishrif horizon (CRI) indicating well log locations used in the post-stack seismic inversion.

4.4.1 Seismic Well Tie (SWT)

A good seismic reservoir characterisation requires a real seismic-to-well relationship. The 3D seismic inversion procedure starts with tying the seismic data with the well's data, in

which seismic events are linked to the well log events. These reflectors and events should be matched before moving to the next inversion level. There are significant steps in the seismic well tie workflow (de Macedo *et al.*, 2017):

(1) The sonic and density logs should be edited.
(2) Calibrate time-depth relationships.
(3) Convolve the reflectivity series with an extracted wavelet to generate a synthetic seismogram.
(4) Compare an actual seismic amplitude with an output of the convolution.

Step 1: A quality check of data is performed before moving on to the seismic well tie steps, especially in the case of well logs. Before well logs can be utilized in reservoir characterisation, they should be edited, normalized, and repaired, and prevent noise or spikes in the produced reflectivity series. There may be occasional spikes and null values in both the sonic and density curves, which should be dealt with. Spikes can be removed from well logs in various ways: manually modifying the area surrounding the spiky portion of the log, removing indefinite data using filters, and replacing sections of a set of logs with one or more blocks. Anomaly spikes can be removed using this technique.

Step 2: The calibration of the sonic log is one of the initial steps of the SWT; for example, see Figure 4.7. Sonic calibration is used to reconcile seismic timings from a check-shot survey with integrated sonic log times at any depth in the well. Calibration of sonic data is frequently necessary since generating a synthetic seismogram from a sonic log is a transformation process that can introduce seismic travel time errors due to cycle skipping, or a washed-out zone effect are present in the sonic log. In comparison, a check-shot survey examines a significantly greater cylindrical volume of reservoir rock than the sonic log. Furthermore, due to dispersion effects, sonic velocities are higher than check-shot velocities; the sonic signal has a higher frequency (about 20 to 25 kHz) than the seismic source (≈ 50 Hz) (Yadav *et al.*, 2004; Asheibi, 2018).

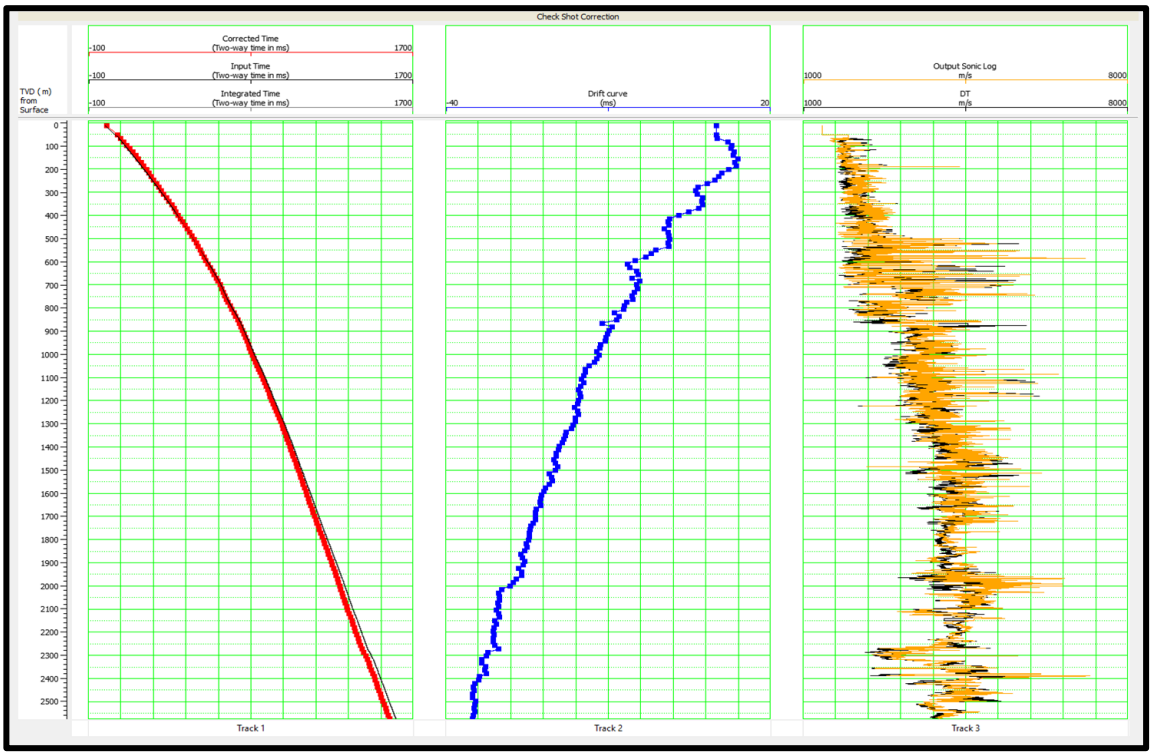

Figure 4.7. Check shot correction (depth-time relationship) at WQ1_Z02 well. Track 1: corrected check shot depth-time (red) and original input time (black); Track 2: a drift curve fitted to the data to measure the discrepancy between the time-depth curve and the check shot data; Track 3: corrected sonic log (yellow) and original input sonic log (black); TWT: Two-way travel time, TVD: True vertical depth.

Step 3: The success of the seismic inversion depends on the accurate estimation of the wavelet. The form of the wavelet can significantly impact the inversion findings and, as a result, the reservoir characterisation. Different approaches for estimating the seismic wavelet are used in seismic inversion (Appendix contains additional information about another approach to estimating the seismic wavelet). The analytical technique was used to derive the wavelet and finally applied an analytical zero-phase Ricker in synthetic seismograms. Many synthetic seismogram makers used Ricker wavelets. The functions of these wavelets can be approximated using an analytical formula, namely a product of a polynomial series and a Gaussian waveform, the notion that a 'Ricker wavelet' is a readily specifiable and computable function that can be used to simulate a wavelet propagating in the actual world (Hosken, 1988). It is popular method for 35 years in the industry to create Ricker wavelets with a single frequency or period and assume that everyone understands it. The advantages of these wavelets are that they are easy to design and computationally efficient. When the seismic reflection data are zero phase, the seismic resolution is improved, and interpretation is simplified. Two parameters, the

shape and frequency, define the wavelet. At a wiggle event, the zero phases indicate that the underlying wavelet is symmetric, with a center peak or trough (depending on the event polarity) (El-Behiry *et al.*, 2020). Figure 4.8 depicts a correct zero-phase wavelet that generates the best synthetic seismogram. A zero-phase analytical wavelet (reverse polarity) is constructed with a frequency of 35 Hz after sonic and density log conditioning to make up the reflectivity log.

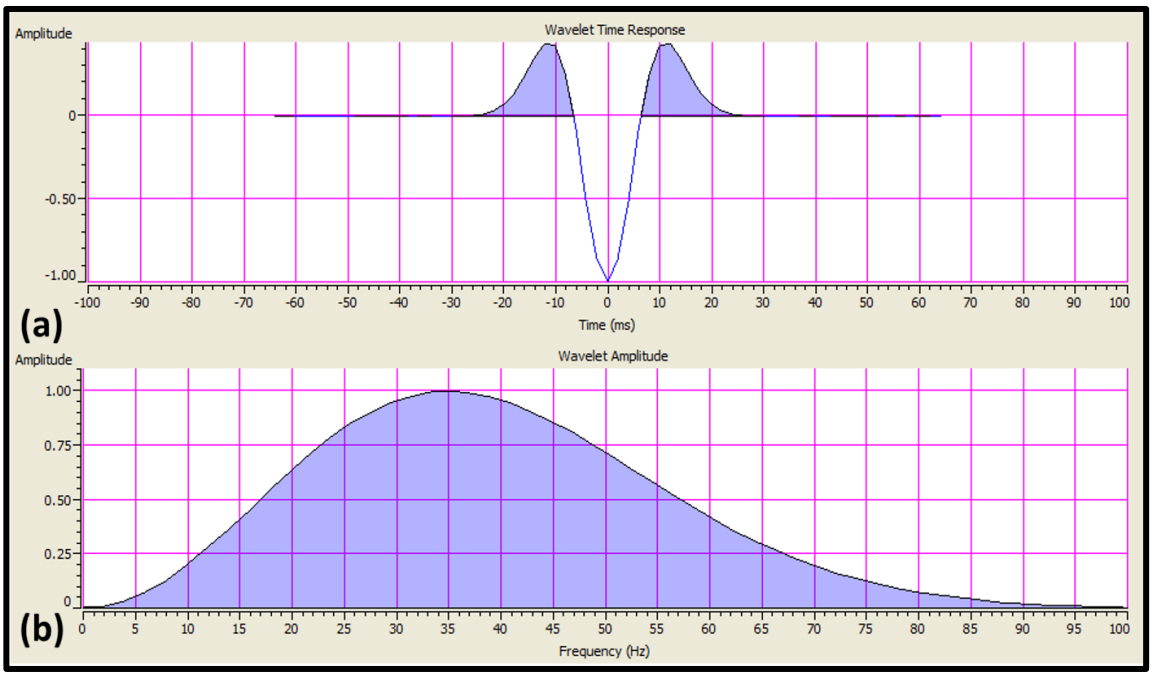

Figure 4.8. Zero-phase analytical Ricker wavelet used for a seismic well tie for the synthetic seismogram, with a maximum frequency of around 35 Hz (reverse polarity). (a) time, and (b) frequency response.

Step 4: When a seismic well tie is inadequate, it is difficult to provide any recommendations for fixing it other than the general one of going back to apply quality control to the seismic and calibrated log data (White and Simm, 2003). It is also critical that the seismic data represent the genuine stratigraphy and rock characteristics as closely as possible. The seismic well tie was generated for seven wells with sonic and check shot data (WQ1_Y64, WQ1_Y66, WQ1_Y68, WQ1_Y93, WQ1_Z02, WQ1_Z09, WQ1_Z38). A synthetic seismogram was created by convolving the Ricker zero-phase wavelet with a reflectivity coefficient to obtain the seismic traces. The calibrated sonic log velocities were multiplied by calibrated density logs to generate acoustic impedance logs, and then the acoustic impedance was turned into reflectivity. After implementing the specified synthetic trace time shift, it can be observed that there

is a good correlation between the synthetic seismogram and sampled 3D seismic volume at WQ1_Y93 well and recognized the main stratigraphic horizons of the Mishrif reservoir, as shown in Figure 4.9.

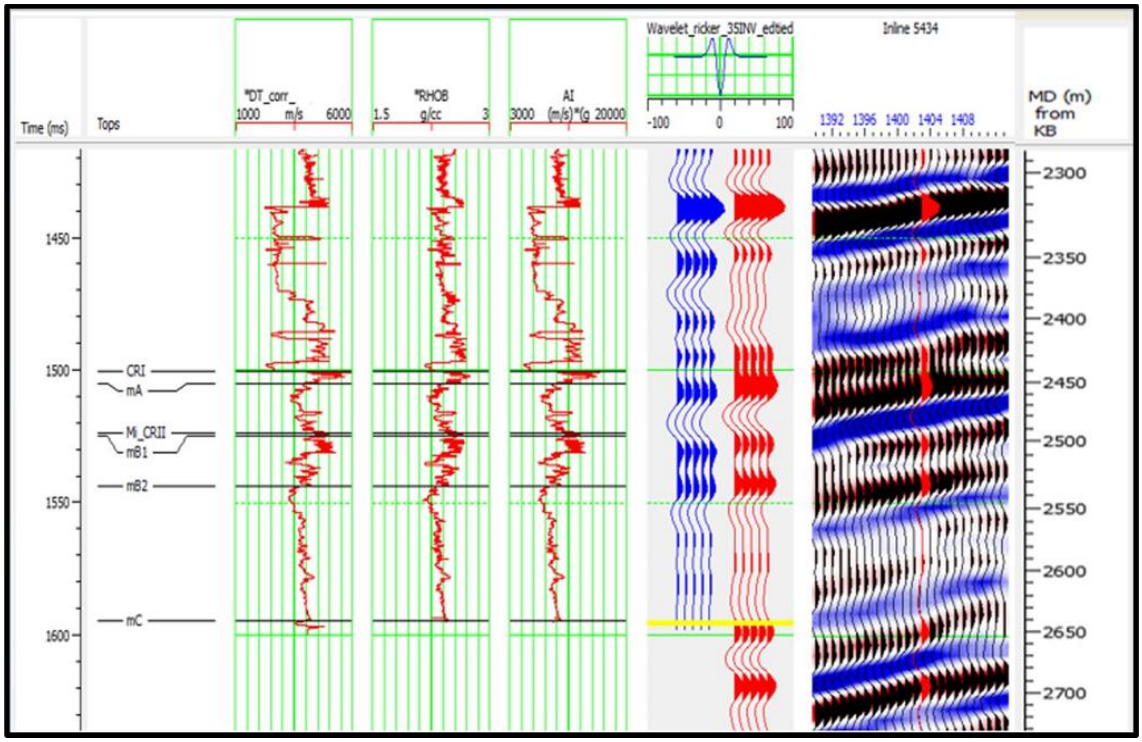

Figure 4.9. Well to seismic tie of the seismic data to synthetic data computed from sonic and density logs of the target reservoir (blue: synthetic seismic from well log (WQ1_Y93), red: average of seismic traces).

4.4.2 Initial Model for Seismic Inversion Analysis

In order to determine fundamental elastic properties, an initial (low frequency) model was produced to populate the elastic property gaps not recorded by seismic data. The model was built from an acoustic impedance log and seismic data. Extrapolating low-pass filtered well logs (sonic and density), rock physics trends, and other information throughout the study area create a 3D distribution of elastic characteristics, which can be used to create the initial model. It is the key input into the inversion analysis, derived from interpolation between well control. Before creating the low-frequency model, several factors had to be defined. These factors included the presentation of horizons in the model, the inclusion of wells, the selection of calculated impedance logs used to create the model and trace filtering choices. The Ricker wavelet was employed for all of the inversion approaches.

Inversion analysis was carried out on selected well locations to test a range of inversion parameters. The procedure includes inverted synthetics at each wellbore location to compare the actual elastic properties (velocity and density). Quality control of adopted parameters was applied using two inverted acoustic impedance models; model-based and linear programming sparse-spike. The inversion analysis was carried out for a particular time window (1200-1700 milliseconds) covering the upper and lower of the Mishrif interval and employed throughout the seismic data inversion (Figure 4.10). Statistically, the investigation findings indicated a high-quality inversion and a high correlation coefficient of 99% presented with almost the same results of both techniques. According to Veeken *et al.*, (2009), there is an error with the seismic data, well-tie, or well data if the correlation coefficient is less than 70%.

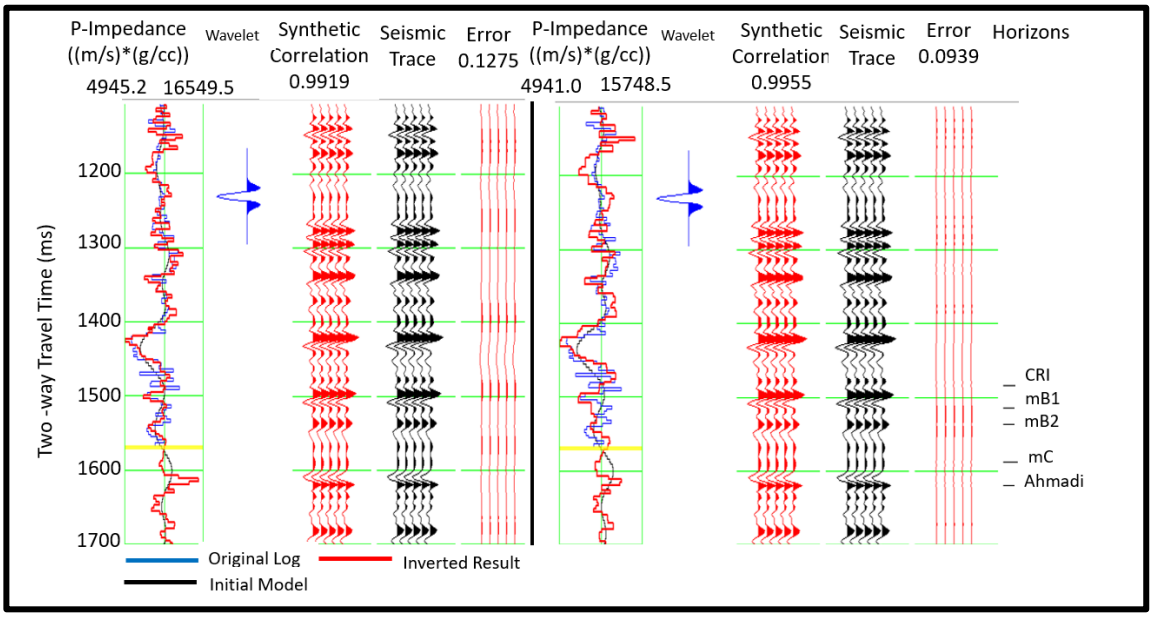

Figure 4.10. Post-stack seismic inversion analysis to compare two approaches, Model-Based (left) and Linear Programming Sparse-Spike (right), the plot shows a reasonable matching between the inverted (red line) and computed acoustic (blue line) impedance. The black curve indicates the low-frequency impedance extracted from the observed impedance logs. The red and black seismic traces are the synthetic and actual seismic data at WQ1_Z02.

A detailed comparison of the model-based inversion and LPSS inversion is shown in Figure 4.11, cross plots of the actual acoustic impedance from the well log data with inverted acoustic impedance. These plots show that the distribution of data points is very close to the best-fitted line for both inversions; hence, both techniques create acoustic impedance with high accuracy. The fact that the predicted and original acoustic

impedance logs in the model-based and linear programming sparse spike techniques have a high correlation (more than 98 %) demonstrates that seismic amplitudes are trustworthy for estimating inter-well impedance (Figure 4.11). This study used both techniques to invert post-stack seismic volume into impedance volume and compare the results. The model-based inversion was undertaken on a seismic volume covering almost 500 km^2 to build a low-frequency model (LFM), as illustrated in Figure 4.12.

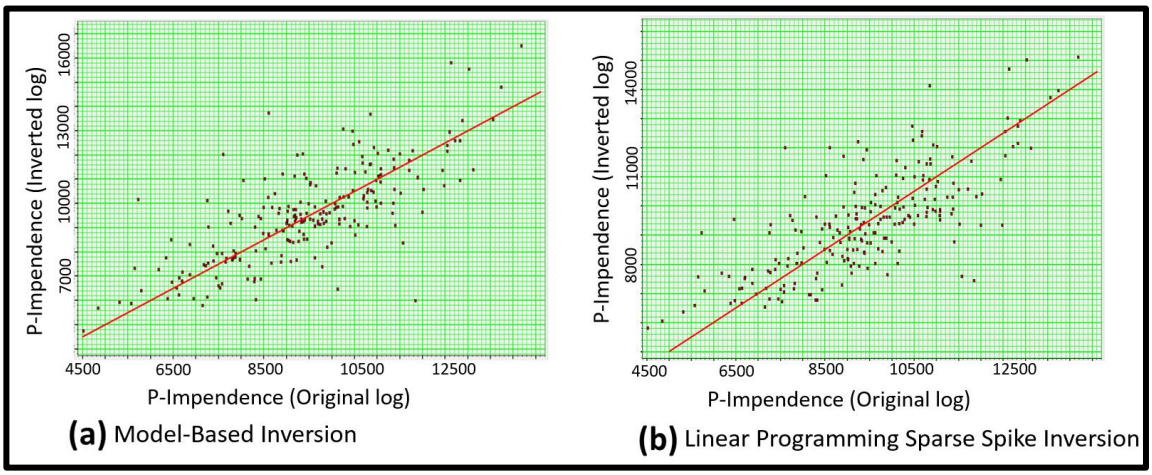

Figure 4.11. Cross-plots between actual acoustic impedance (x-axis) and inverted acoustic impedance (y-axis) both have a high correlation (more than 98 %) a) Model-Based inversion and b) Linear programming sparse spike inversion at WQ1_Z09.

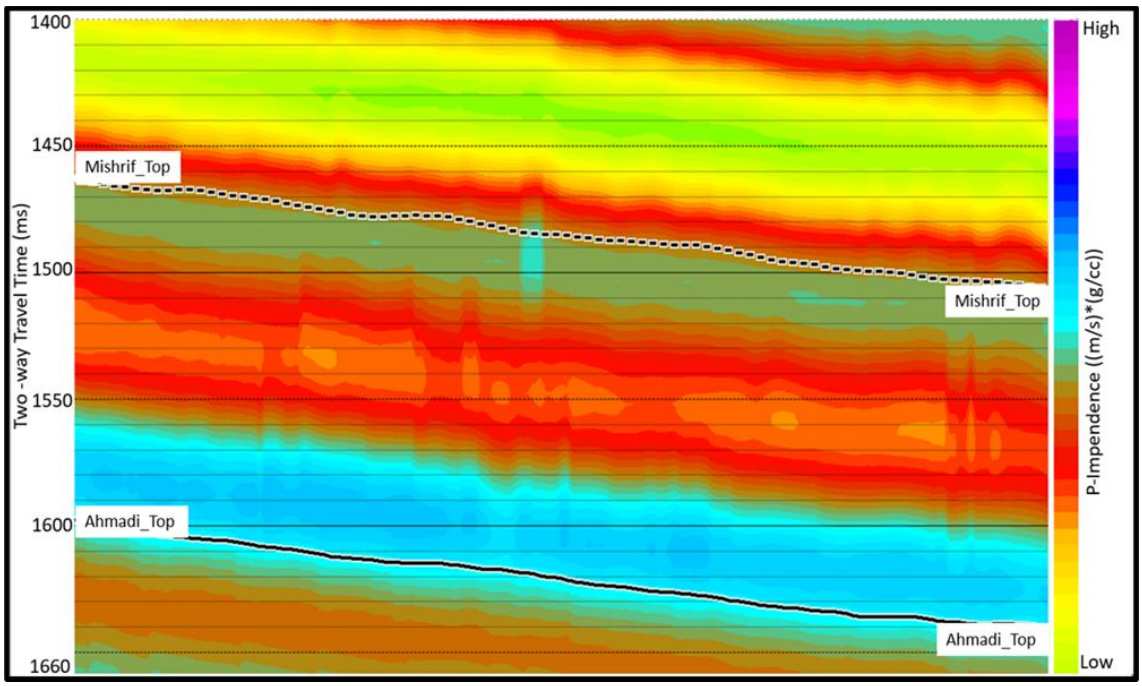

Figure 4.12. A cross-section of the low-frequency model in the Mishrif interval (between Mishrif_Top and Ahmadi_Top) along Inline 5328.

4.4.3 Seismic Inversion Techniques

4.4.3.1 Model-Based Inversion

The inversion models are based on assumptions of the reservoir architecture characteristics, such as blocky impedance layers. The model-based inversion workflow is the same as the general workflow presented in the previous section; the required inputs in the case of this inversion are only the seismic volume and the well logs. The composite seismic traces are extracted near well locations, and a model-based inversion technique is applied to these traces to optimize parameters and compare inversion results with actual AI from the well log. The inverted AI matches the actual AI from the well log data with a high correlation coefficient of 98%, indicating that the results could be used for qualitative and quantitative interpretation (Figure 4.13). This inversion was also explained in more detail in section 2.2.4 of Chapter 2.

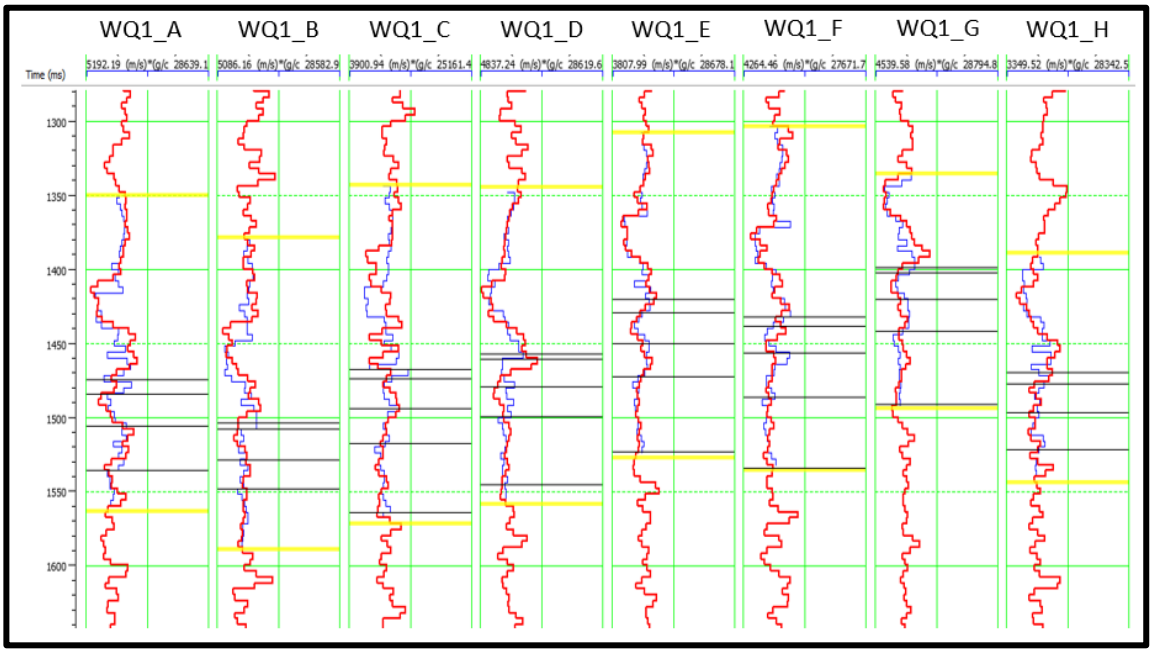

Figure 4.13. Model-Based inversion (red) and the measured acoustic impedance from logs (blue) for eight wells illustrate that the final inversion findings and the measured data from wells are similar.

A final 3D seismic inversion model was generated, indicating a reasonable tie with input wells. Also, the inverted acoustic impedance shows the compaction effect due to the rock stiffness and density increase with depth (Figure 4.14). The best way to validate post-stack seismic inversion results is to compare computed acoustic impedance at well log

location using blind well data to find any discrepancies. Generally, the results were carefully controlled for quality between computed acoustic impedance and acoustic impedance volumes. Figure 4.15 demonstrates a good match along inverted acoustic impedance volume at WQ1_X70. The thicker zones are categorized by low impedance signature, and thin zones are relatively characterized by high value, such as the top zone of the Mishrif, called CRI.

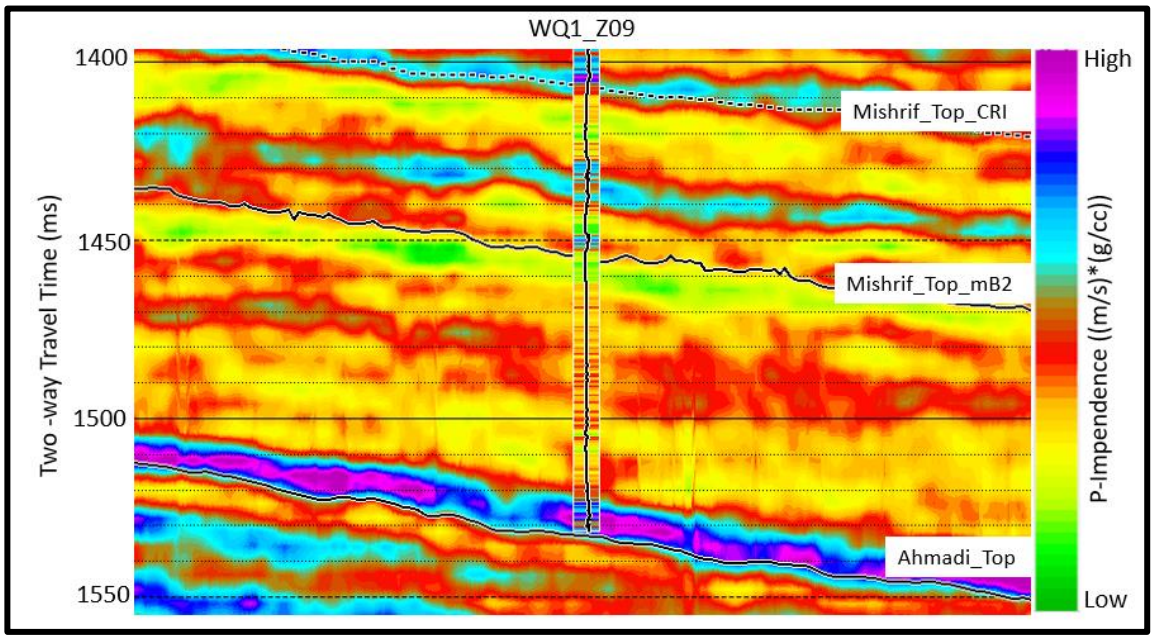

Figure 4.14. Acoustic impedance volume -Inline 6330 with the overlaid impedance trace in the well log-driven impedance (WQ1_Z09), lateral and vertical changes of the Mishrif reservoir are clear. Horizons shown here are Mishrif_Top_CRI, Mishrif _Top_mB2, and Ahmadi_Top.

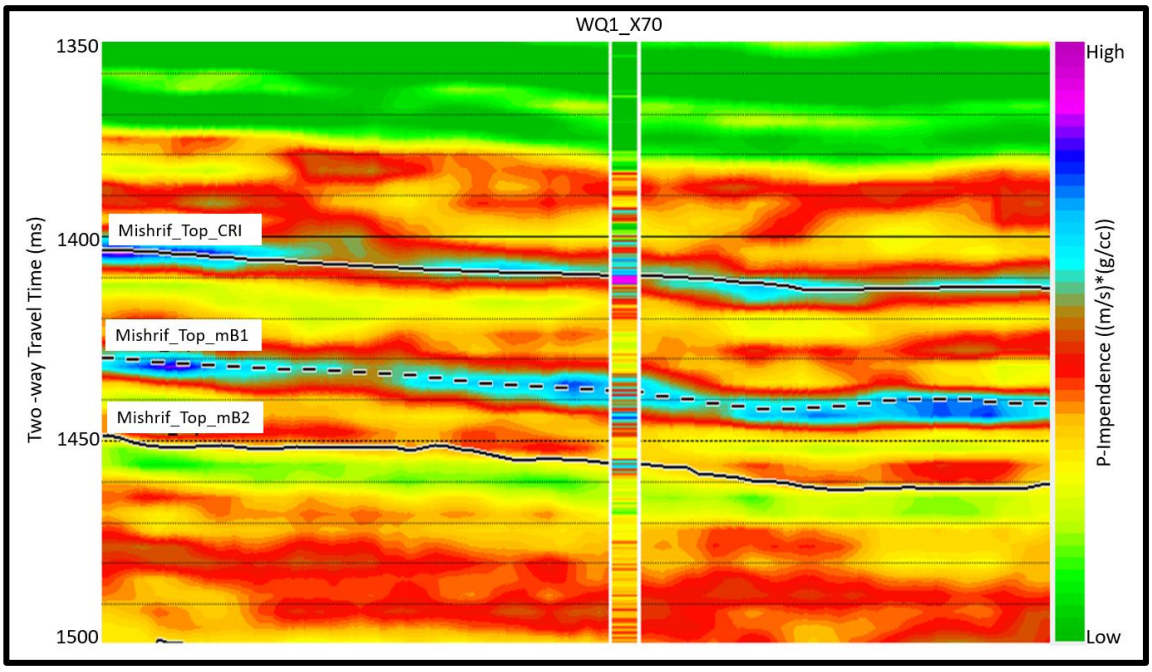

Figure 4.15. Inline (6355) from model-based inversion impedance volume and inserted computed acoustic impedance log at WQ1_X70 well.

4.4.3.2 Linear Programming Sparse Spike Inversion (LPSS)

A linear programming sparse spike inversion has been applied to the seismic volume used to achieve the comparison goal. Figure 4.16 shows that the match between inversion and well-log data for acoustic impedance is good (correlation coefficient of 95%). The acoustic properties are the direct output of the inversion, and their distributions are more consistent with expectations of the reservoir properties. The LPSS inversion was also explained in more detail in Chapter 2.

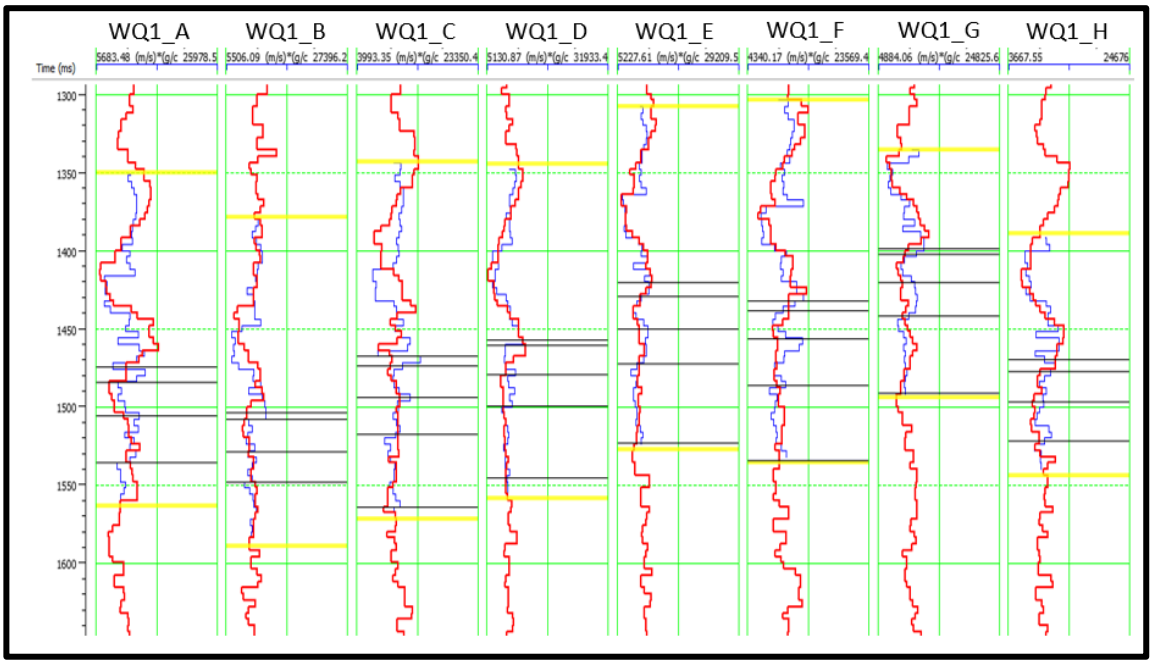

Figure 4.16. Linear programming sparse spike inversion (red) and the measured acoustic impedance from logs (blue) for eight wells.

When the two inverted models are compared in Figures 4.17 and 4.18, the acoustic impedance of the model-based inversion showed a higher impedance contrast and lithological variation of the Mishrif zones compared to those derived from the linear programming sparse inversion (a more detailed description will be later). Both techniques estimated the AI values ranging from low to high within 1420 - 1550 ms of the Mishrif reservoir zones. The acoustic property of the model-based inversion (Figure 4.17) has sharp interfaces with high acoustic impedance at the top and lower Mishrif boundaries, indicating different reservoir facies. The variation of acoustic impedance is due to the limestone layers with thin lime mudstone at the top of the Mishrif reservoir (CRI) and the shaly Ahmadi formation at the lower part of the Mishrif reservoir. Also, the resulting impedance from model-based inversion distinguishes upper and lower Mishrif reservoir characteristics more clearly than linear programming sparse spike inversion (Figure 4.18). The model-based inversion findings appear more geologically plausible (more continuous and blocky features) with fine details, simplifying the definitions of the lithological and petrophysical properties. A greater acoustic contrast in the Mishrif zones and the lower of the Mishrif (Ahmadi top) can be seen. This is because the model-based inversion can produce excellent findings even with limited well control and low seismic quality.

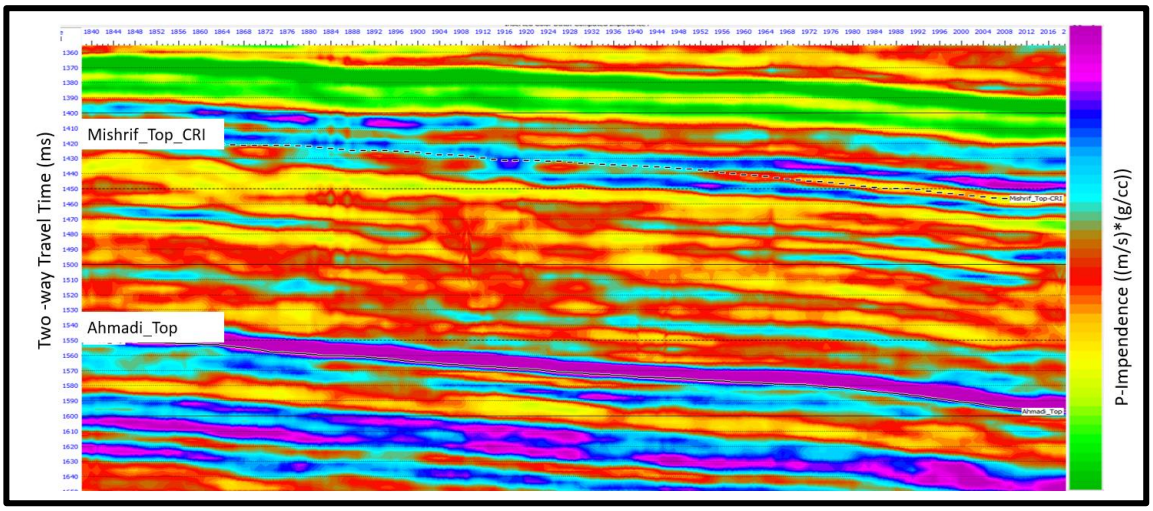

Figure 4.17. Inverted AI using the Model-Based inversion displays the Mishrif_Top and Ahmadi_Top horizons, better continuity is visible along the lower part of the Mishrif formation, and the purple colour shows the high acoustic interval (non-reservoir) in the lower of Mishrif .

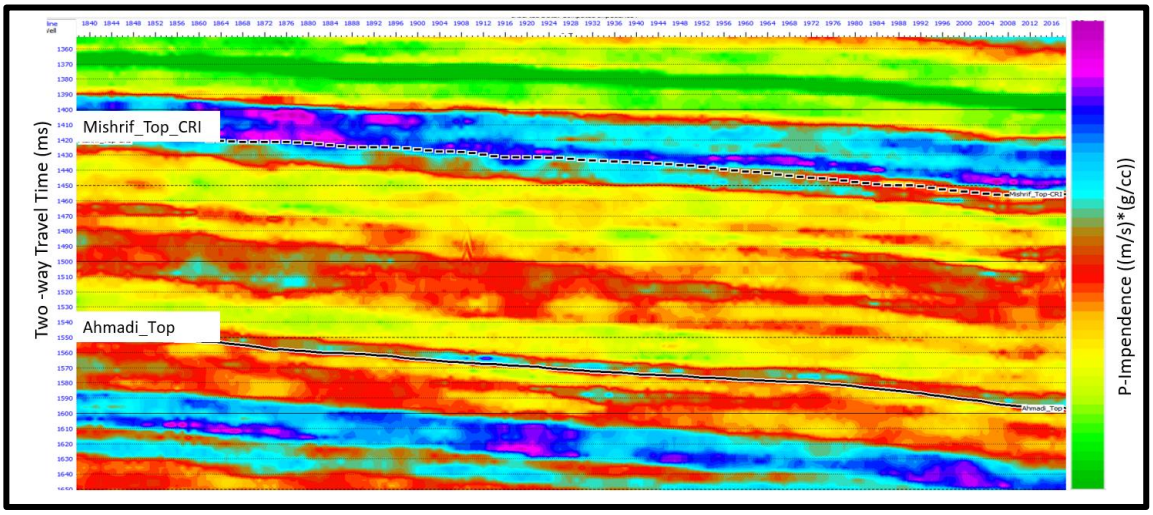

Figure 4.18. Using linear programming sparse spike inversion, inverted AI displays the Mishrif_Top_CRI and Ahmadi_ Top horizons.

4.5 Evaluation of Geological Reservoir Characterisation Based on Seismic Inversion Results

4.5.1 Core-Scale Rock Type Classification

Based on the core description and observations from thin sections, there are three main reservoir rock type groups representing the existence of three different facies. An illustration scheme of key facies types is provided below in Figure 4.19 (Basra Oil Company, 2013), showing the detailed descriptions:

1-High Porosity, High Permeability rock types: Reservoir flow units correspond to skeletal-dominated grainstone-rudstone facies. Dominant pore types include interparticle and moldic. Pore throat sizes average around 4-5 microns in RRT-3. Extreme permeability (high 100s to 1000s of millidarcies) characteristic of RRT-4 is developed in rocks with well-connected interparticle and moldic pores and, in some cases, with touching vugs. The highest reservoir quality is generally associated with rudist-dominated facies, consistent with regional observations (Aqrawi *et al.,* 1988; Sadooni, 2005).

2-Moderate to High Porosity, Low Permeability rock types (high storage, low flow potential): These types correspond to the facies with packstone-wackestone textures and are dominated by microporosity. Microporosity develops through fine-scale of micritic limestones and is common in many Cretaceous Middle East carbonate reservoirs (e.g. Hollis, 2011). Microporosity reflects a high porosity (18-28%), but the permeability is low (0.1-10 md) due to small pore and pore throat sizes. Porosity and permeability are slightly lower in rock type 2 than rock type 1 due mainly to differences in the microporosity fabric; crystal morphology in RRT-1 is mainly subhedral (rounded crystals), while RRT-2 is more fitted fabric with lower porosity and permeability.

3-Low porosity, Low permeability rock type (flow barriers and baffles): This group was developed around sequence boundaries in lagoonal and peritidal facies in the late highstand of sequence 2 (mB1 zone). Low reservoir quality in these rock types is attributed to cementation associated with exposure surfaces. It comprises restricted lagoonal facies in the mB1 (late highstand of sequence 2) and forms discontinuous barriers and baffles to flow.

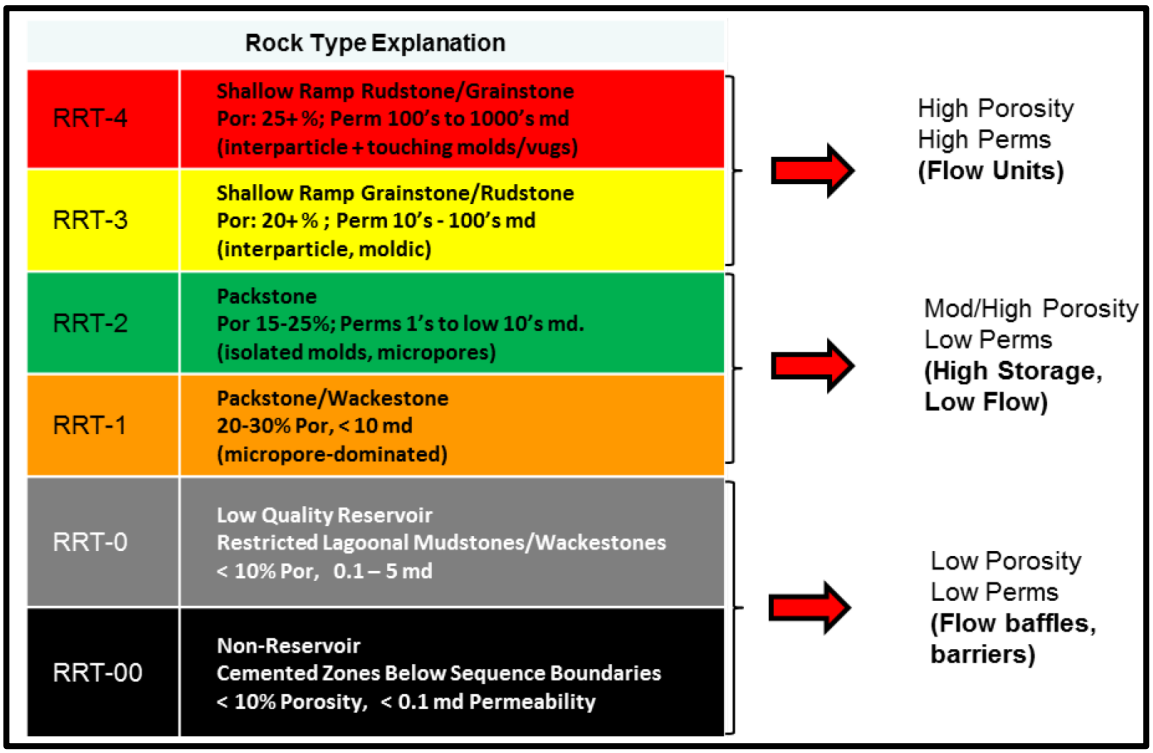

Figure 4.19. Summary of reservoir rock types, including (texture, pore types, porosity-permeability range, and flow properties) (Basra Oil Company, 2013).

4.5.2 Facies Discrimination Based on the Acoustic Impedance

The Mishrif reservoir can be characterized and classified based on acoustic impedance in a complementary study. First, based on the well log-core and a thin section analysis, Mishrif zones are mostly low gamma-ray values and good-quality facies, reflecting good reservoir quality, as shown in Figure 4.20. However, there are high gamma-ray and low-quality facies in some intervals of these zones.

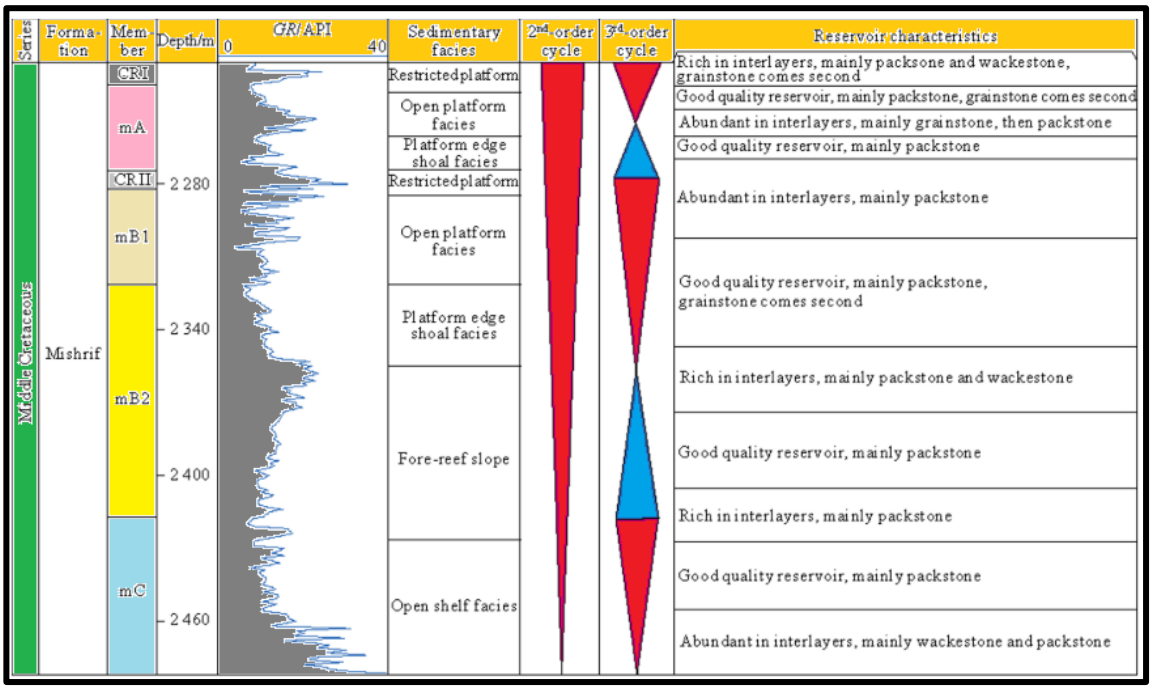

Figure 4.20. Well log and core analysis of the Mishrif reservoir highlights the depositional environment and main facies associations (Ya *et al.*, 2016).

Consequently, the Mishrif reservoir was categorized into three main clusters based on acoustic impedance: low (AI <7800), medium (8000 < AI < 10800), and high (AI>11000) (Table1). Accordingly, the high acoustic impedance facies represent non-reservoir and low-quality facies at the top of the Mishrif reservoir (Caprock intervals-CRI) and mB1 zone. This could be due to detrital clay contents and restricted lagoonal facies in the mB1 zone, forming discontinuous barriers and baffles to flow (Figures 4.21a and b). However, the mB1 zone shows low AI value facies (sweet spots and good quality) in some regions due to subtidal grainstone channels or shoals deposited in the inner ramp domain (Liu *et al.*, 2016). The second cluster demonstrates a medium acoustic impedance (lower mB2 zone); this corresponds to facies with packstone/wackestone textures dominated by microporosity which developed through fine-scale recrystallization of the rock (Figure 4.21c). The last cluster (3) is characterized by a low acoustic impedance value (upper of mB2 and mA-a zones) with the highest reservoir quality facies. It is generally associated with skeletal-dominated grainstone/rudstone (Figure 4.21d). The correlation of low acoustic impedance with rudist grainstone and reef facies can be explained by the lower velocity of connected molds of the grains compared to the cemented facies in lagoonal regions in the field. Consequently, acoustic impedance inversion is a valuable tool in reservoir characterisation to classify the Mishrif reservoir lithology in the West Qurna/1 oilfield.

Table 1. Reservoir characterisation of Mishrif facies in differentiated groups based on acoustic impedance (AI) and core analysis data.

Mishrif Reservoir Facies	Acoustic Impedance (AI.)	Porosity (PHIE)	Description
High-AI facies	**AI >11000**	**PHIE<10**	Non-reservoir (flow barriers, baffles) facies are developed around sequence boundaries and in lagoonal and peritidal facies
Medium-AI facies	**8000 < AI<10800**	**15<PHIE <25**	Microporous subtidal foram-peloidal ramp deposited in outer ramp
Low-AI facies	**AI <7800**	**PHIE>25**	Rudist-bearing and sponge coral mounds (skeletal shoals) facies characterized the best quality reservoir and main buildups (rudist shoal system).

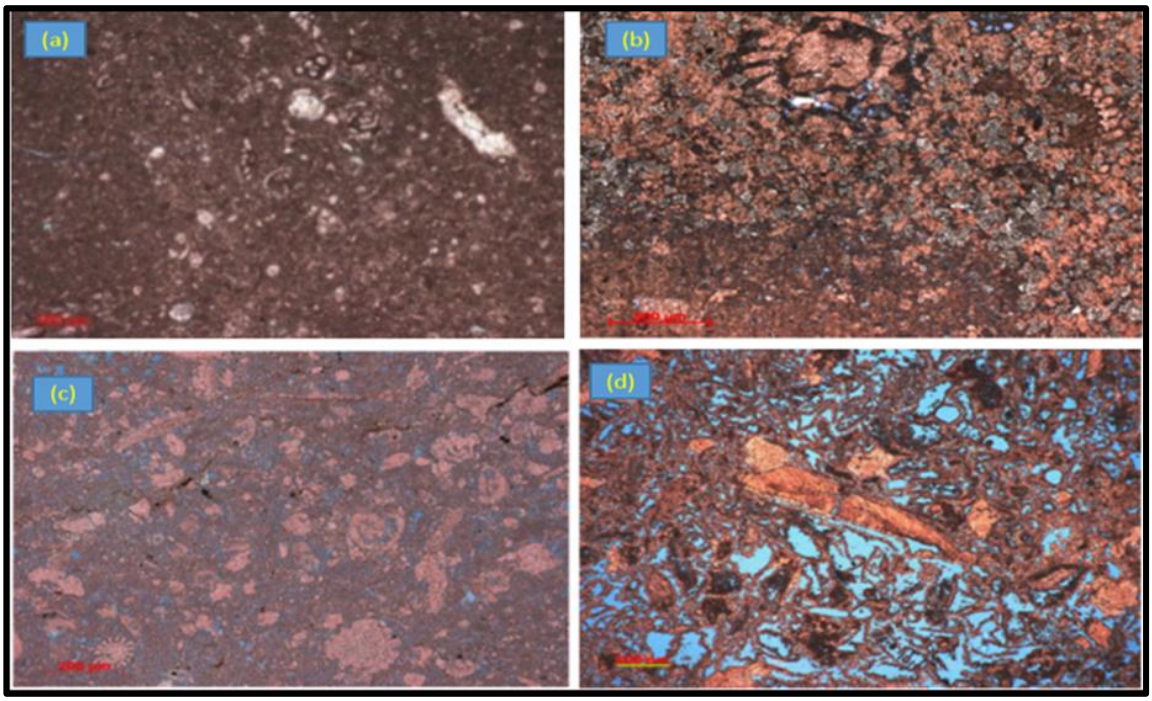

Figure 4.21. Petrographic analysis of the Mishrif reservoir facies clustering from core data (WQ1_X68). a) Non-reservoir facies. b) Low-quality reservoir facies. c) Moderate quality (microporosity facies) at the depth 2394.50. d) High-quality reservoir facies at the depth 2442.0 (Basra Oil Company, 2013).

4.6 Seismically Derived Mishrif Characterisation

The previous section compares acoustic impedance (AI) and core analysis data. Accordingly, the inversion results with petrographic analysis obtained the relationship between low acoustic impedance and high porosity zones and are very clear in the Mishrif interval. This section will focus on the crucial quantitative interpretation of reservoir characterisation based on seismic data. The porosity model is generated to classify the facies and the complex carbonate reservoir distribution based on linear regression analysis over the entire West Qurna/1 oilfield.

4.6.1 Porosity Estimation from Acoustic Impedance Inversion

As mentioned previously, the relationship between acoustic impedance and porosity in carbonate reservoirs is well known (e.g., Williams and Aqrawi, 2006) and was very obvious in the Mishrif carbonate reservoir. It formulates the basis of characterisation of the reservoir properties from the seismic-derived impedance. The seismically-derived porosity model was generated using a statistical linear regression approach (Hampson *et*

al., 2001; Pramanik *et al.*, 2004). A step-wise rock physics analysis was used first to determine the best linear relationship between the porosity and P-impedance logs from available Mishrif wellbore data and then used for the final reservoir quantitative interpretation of porosity characterisation. For instance, WQ1-Y74 demonstrated a distinct linear regression with a high correlation coefficient ($R^2 = 0.96$) even with the scattering of the data which is due to the heterogeneity of the reservoir and the variation in the porosity distribution. In this analysis, a regression formula for the porosity (PHIT) versus the Acoustic Impedance (AI) was derived (Figure 4.22):

$$PHIT = 0.545 - 0.000037 * AI$$

Thus, we can successfully predict the porosity model using acoustic impedance, then the resulting porosity distribution in 3D was generated.

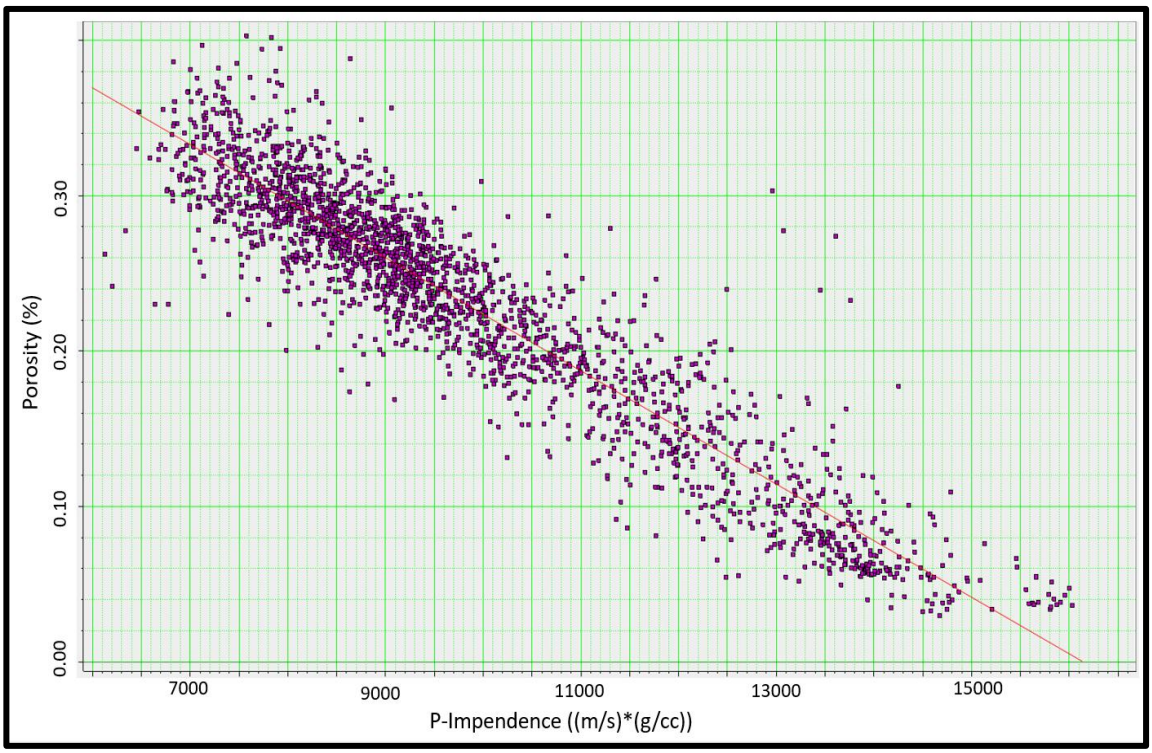

Figure 4.22. Cross-plot to generate a regression formula between P-Impedance and porosity in the Mishrif reservoir showed a high correlation ($R^2 = 0.96$) in well WQ1-Y74.

The analysis shows a high correlation coefficient, indicating the algorithm's excellent performance. The predicted porosity correlates with actual porosities measured from logs and demonstrated a reasonable match of the porosity between the seismic-derived (red) and well-based (blue) (Figure 4.23). Estimated porosity results are generally promising.

However, some Mishrif intervals were inconsistent due to the error of the predicted porosity. The error analysis for the estimated porosity and original logs are shown in the figure as a deviation. This difference could be due to many reasons, such as the multiple seismic reflections, time-depth relationship, and log quality.

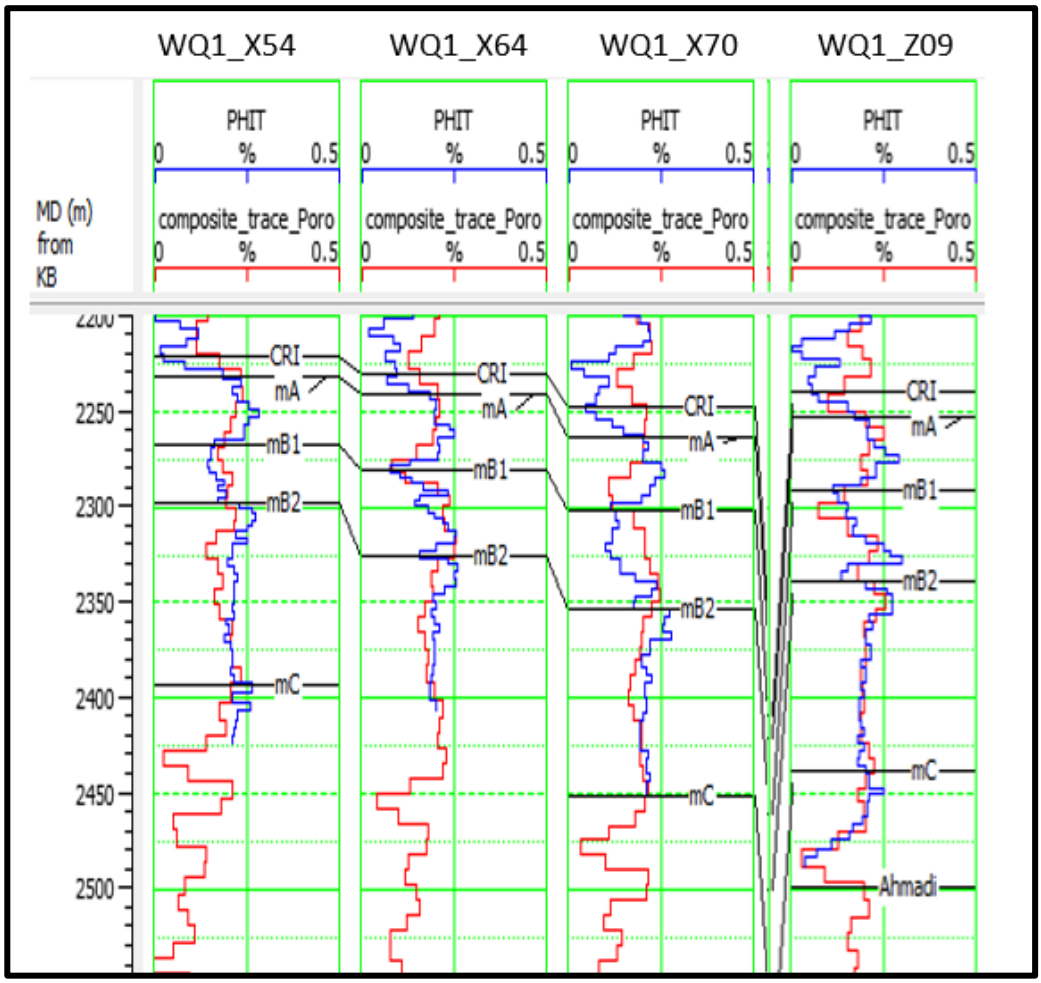

Figure 4.23. Comparison of the porosity between the seismic-derived (red) and well-based (blue) in the West Qurna/1 oilfield wells.

The spatial distribution of the porosity model was cautiously assessed with blind wells in the adjacent area. Interestingly, the porosity model indicated that high porosity zones are congruent with the low acoustic impedance value of the Mishrif reservoir. For instance, the upper mB2 zone (dark green colour) is highly porous (more than 25%) and consistent with low acoustic impedance value and vice versa observed in CRI and mB1 zones (Figure 4.24). The porosity distribution of the mA zone reflects the vertical and lateral changes in the depositional facies trends and their geometries related to changes in accommodation during relative sea-level cycles (Mahdi and Aqrawi, 2018). There is a

good correlation between the core-based well cross-section (Figure 4.20) and the seismic-based porosity of the mA zone (Figure 4.24).

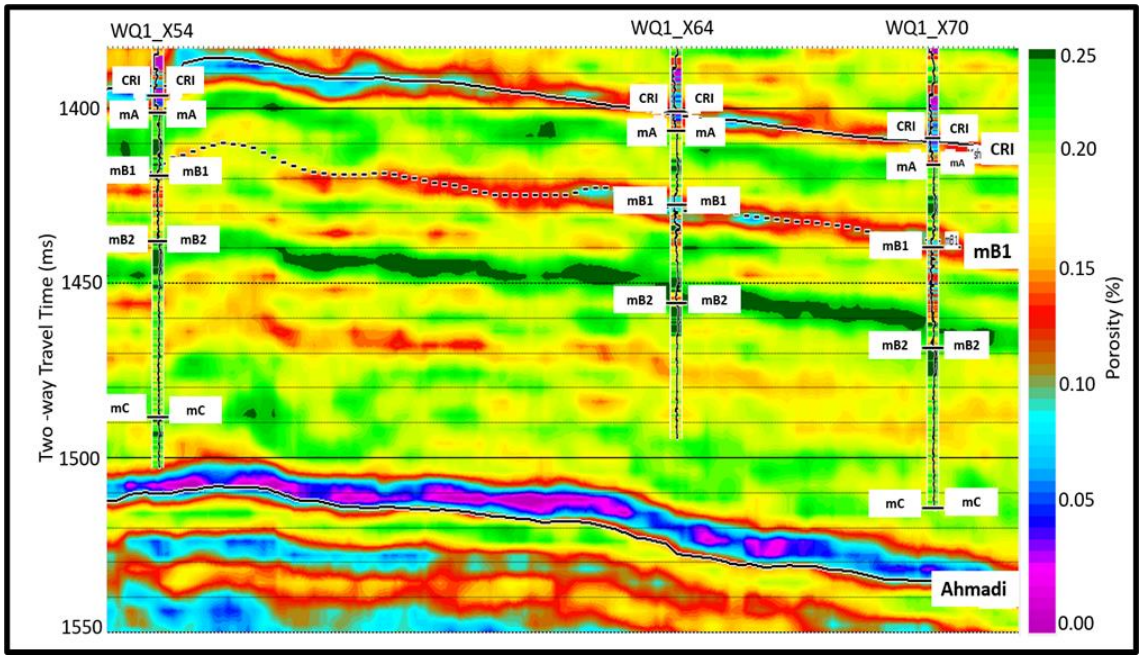

Figure 4.24. Estimated Porosity model of Mishrif reservoir using a linear regression approach and porosity logs inserted at the well locations.

Grainstone facies are best developed in the upper mA zone, mainly accumulating as coral-sponge mounds and shoals. The results showed a concentration of high porosity values in the centre and north of the field area. This can be seen vertically through several wells and formed higher permeability flow units. Consequently, the seismically-derived porosity model results show a higher quality at three well locations (WQ1_A17, WQ1_B15, WQ1_B59), where a thicker and higher quality mA zone may have a better chance of developing high permeable layers (Figure 4.25).

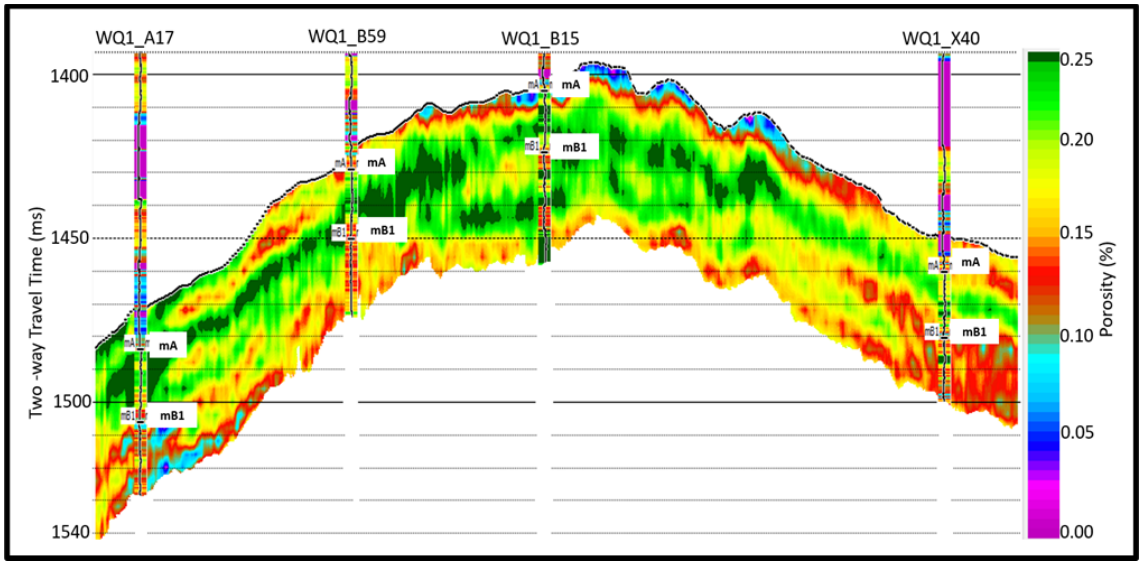

Figure 4.25. The arbitrary line of the Mishrif porosity model shows high porosity distribution, particularly for the reservoir interval between the top of mA to the top of mB1.

However, as mentioned earlier, the mA zone shows a different porosity quality in some regions due to the packstone and wackestone textures. These are dominated by micro-porosity developed through recrystallization of the calcite and are very common in many Cretaceous Middle East carbonate reservoirs (de Periere *et al.*, 2017). This can be seen towards the east side of the field (Figure 4.26).

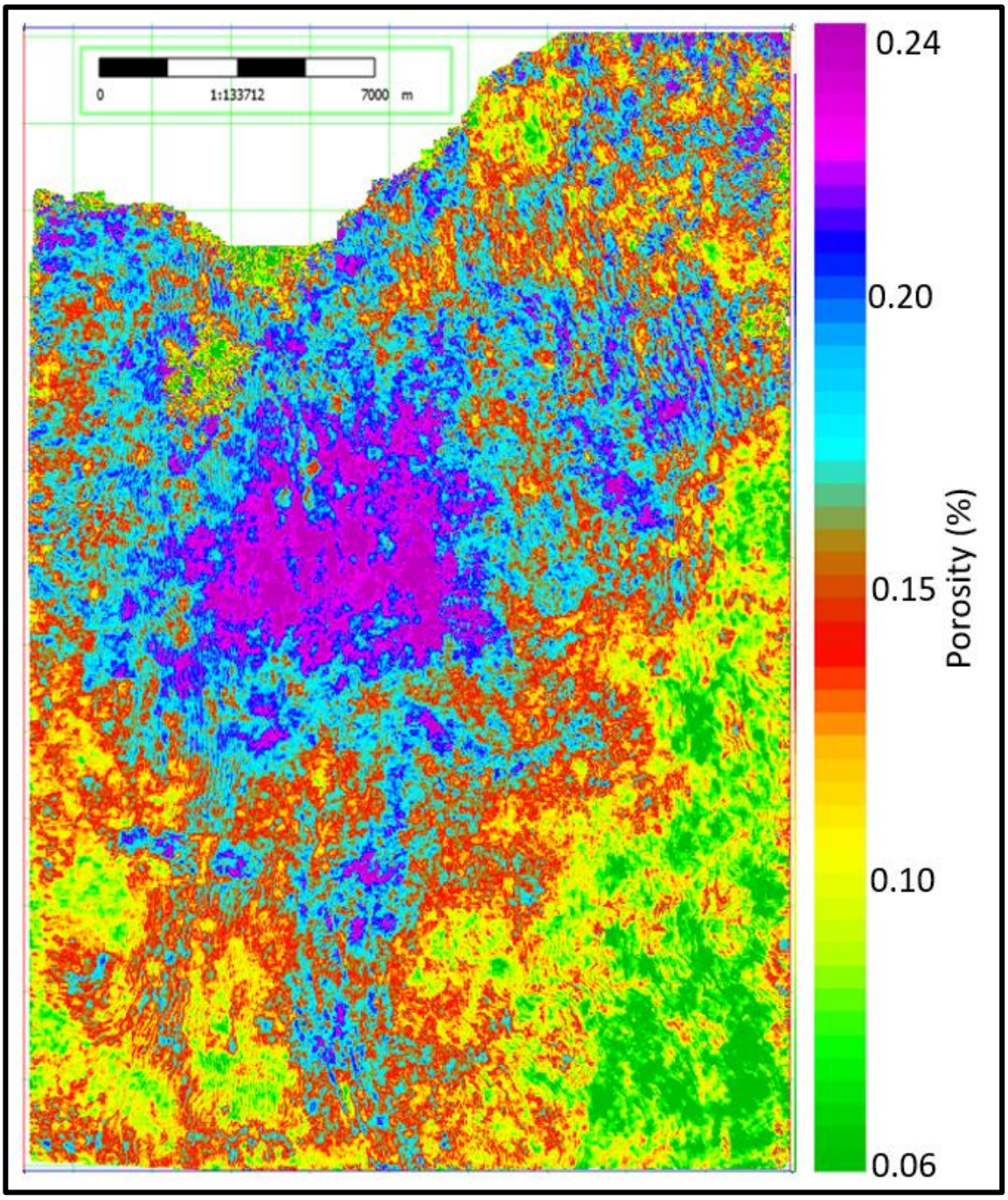

Figure 4.26. The seismically derived porosity model shows scattered distributions within the mA zone, indicating the lateral change in deposition facies (Coral-sponge mounds and shoals).

Based on representative horizon slices through AI volume, the mA-acoustic impedance slice from model-based inversion (Figure 4.27a) highly corresponds to the estimated porosity results of mA zone (Figure 4.27b). This is because the grainstone facies within the mA is the best developed in the upper mA layer, which is mainly an accumulation of coral-sponge mounds and shoals.

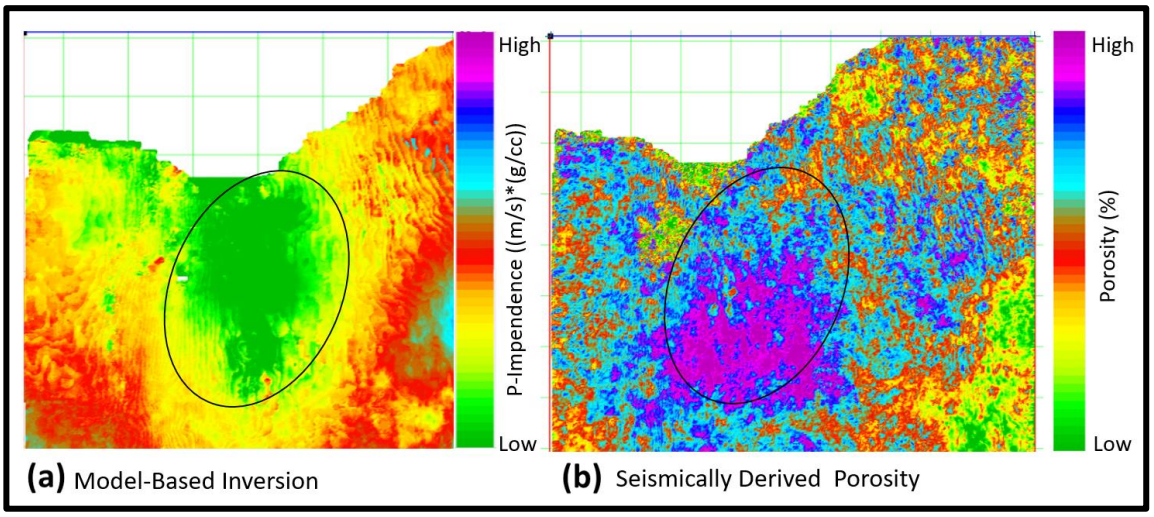

Figure 4.27. The oval shape highlights the low acoustic impedance area in Figure (a), closely corresponding to the high porosity in Figure (b).

The porosity model slices provided important information about the spatial distribution away from West Qurna/1 well control. The most distinctive zone and relatively homogenous among the Mishrif intervals in terms of porosity can be seen in the upper mB2 zone (porosity of more than 25 %) (Figure 4.28a). It is predominately an accumulation of rudist biostromes (limestone detrital) within grainstones and packstones. Although not all mB2 zones are characterized by homogenous porosity, significant porosity changes are highlighted in the lower mB2 zone and the whole mC zone (Figure 4.28b). These zones show variable porosity in some parts, mostly from moderate to high porosity. In general, high-porosity zones are highly linked to low acoustic impedance values. The porosity distribution maps generated from seismic inversion are vital in identifying new potential regions of good reservoir quality.

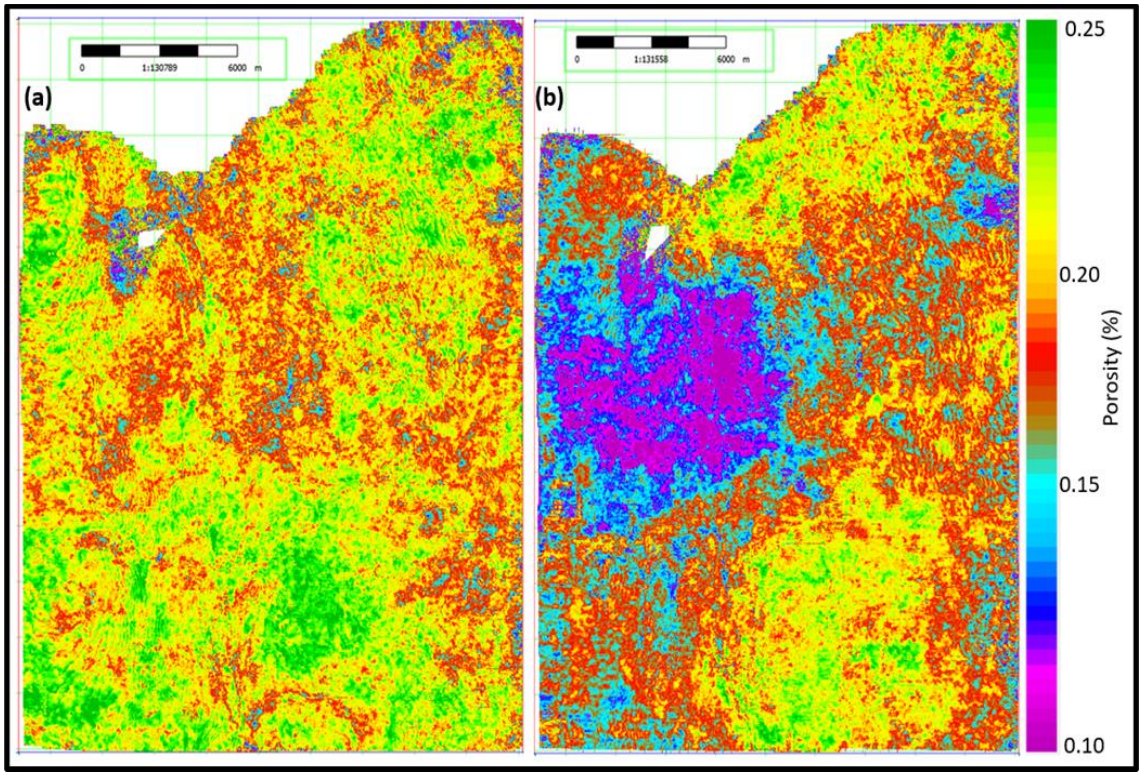

Figure 4.28. Seismically derived porosity model of Mishrif reservoir (a) porosity slice of upper mB2 zone (b) porosity slice of mC zone.

4.7 Summary and Conclusion

This chapter discusses the reservoir characterisation of the Mishrif reservoir from high-quality 3D seismic data acquired over the West Qurna/1 oilfield. In this work, linear regression algorithms were used based on 3D inverted acoustic impedance and rock physics analysis of the Mishrif reservoir. Core data analysis was used to determine the lateral and vertical distribution of Mishrif facies. Furthermore, the seismically derived porosity model is tested to determine whether it is consistent with current geological knowledge of the field. Our conclusions and insights gained from the present chapter are summarized below:

- An integrated workflow has provided a robust approach toward understanding the complexity of the depositional environments and classification of the Mishrif carbonate facies and their spatial distribution. A model-based inversion generated a more reliable estimation of the petrophysical properties due to its better resolution. The low acoustic impedance that correlates with high porosity areas can be seen clearly in all Mishrif channel distributions from the model-based inversion. The interpretation demonstrated promising results, with the model-based inversion, in terms of the detailed distribution of channel fairways and distinct definition seen on the lithological variation observed in mA zone displays. This is because the model-based inversion has the benefit of producing good results even with limited well control and poor quality seismic.

- A new application of the Mishrif porosity trends was proposed based on a seismically derived porosity model, well data, and core-based sequence stratigraphic, generally a good match between porosity extracted from seismic data and well-based porosity (Figure 4.23). An essential benefit of the work is that the acoustic impedance and porosity model slices highlighted a new understanding of Mishrif porosity systems through observations of a complex mosaic of carbonate tidal channels, high-energy coral mounds, and rudist shoals facies, which play a vital role on reservoir architecture, connectivity and ultimately on the dynamic performance of the field.

- An integrated multi-source interpretation, including geophysics, geology, and petrophysics, is necessary to achieve and provide an enhanced 3D understanding of the heterogeneity and quality of the Mishrif reservoir.

Chapter 5. Multi-Dimensional Approaches to Characterise the Mishrif Carbonate Tidal Channels[3]

This chapter begins with the sedimentary characteristics of the heterogeneous channelized zone of the Mishrif reservoir. This is followed by a section to identify channel geometries based on the expression of the seismic attributes. At the end of the chapter, seismic reservoir characterisation of the Mishrif carbonate tidal channels using a probabilistic neural network (PNN) algorithm through seismically derived porosity and facies classification will be introduced. Generally, an ideal approach to improving reservoir characterisation using multisource data should have the essential workflow elements established in the methodology section.

[3] This chapter contains material from "Al-Ali, A., Stephen, K. and Shams, A. (2019d). Characterization of Channelized Systems in a Carbonate Platform Setting: A Case Study on the Late Cretaceous Reservoir from the Supergiant Oilfield, Iraq. *SPE Reservoir Characterisation and Simulation Conference and Exhibition,* held in Abu Dhabi, UAE, 17-19 September 2019".

5.1 Introduction

Characterisation and prediction of channelized systems are essential for exploring hydrocarbons and obtaining a reliable estimation of reservoir production. Identification of tidal channel fairways is critical for predicting the behavior of areas at higher risk of water breakthrough (thief zones) or otherwise significantly impacting the development and monitoring of reservoir performance. Characterizing the spatial distribution of heterogeneity is challenging in inter-well regions without high-resolution seismic data and well-log data or core samples. To the researcher's knowledge, this is the first time that neural network algorithms have been applied to the Mishrif channelized reservoir in the West Qurna/1 seismic data. This includes facies classification and determining the nonlinear relationship between reservoir properties and seismic attributes for the seismic reservoir characterisation.

5.2 Methodology

Reservoir characterisation is based on various exploration and production (E&P) data gathered through geoscience studies and should provide the reservoir's detailed geological architecture and petrophysical properties. Following the methodology outlined in Chapter 4, channel characterisation should be subjected to a multi-dimensional workflow that demonstrates a variety of multisource data to determine the geometry of the channel fairways. In this chapter, the following research questions will be addressed:

• Could we use the proposed workflow to infer the seismic reservoir characterisation of such complex tidal channels?
• We aim to investigate the heterogeneity of complex channelized reservoirs and their petrophysical properties.
• Multiple approaches were created to account for the inherent uncertainty in the channel characterisation; how can an inter-well connection be determined using the integrated data?

To quantify the influence of tidal channels on the reservoir model and fluid flow, seismic data, well logs, and core data have been adopted to describe the depositional environmental setting and predict the reservoir properties. Modern analogue and outcrops

will be defined to establish a common platform for understanding seismic interpretation and petrographic analysis. This chapter introduces a new step to creating an integrated understanding of reservoir connectivity by delineating and characterizing the Mishrif heterogeneous carbonate channels (Figure 5.1).

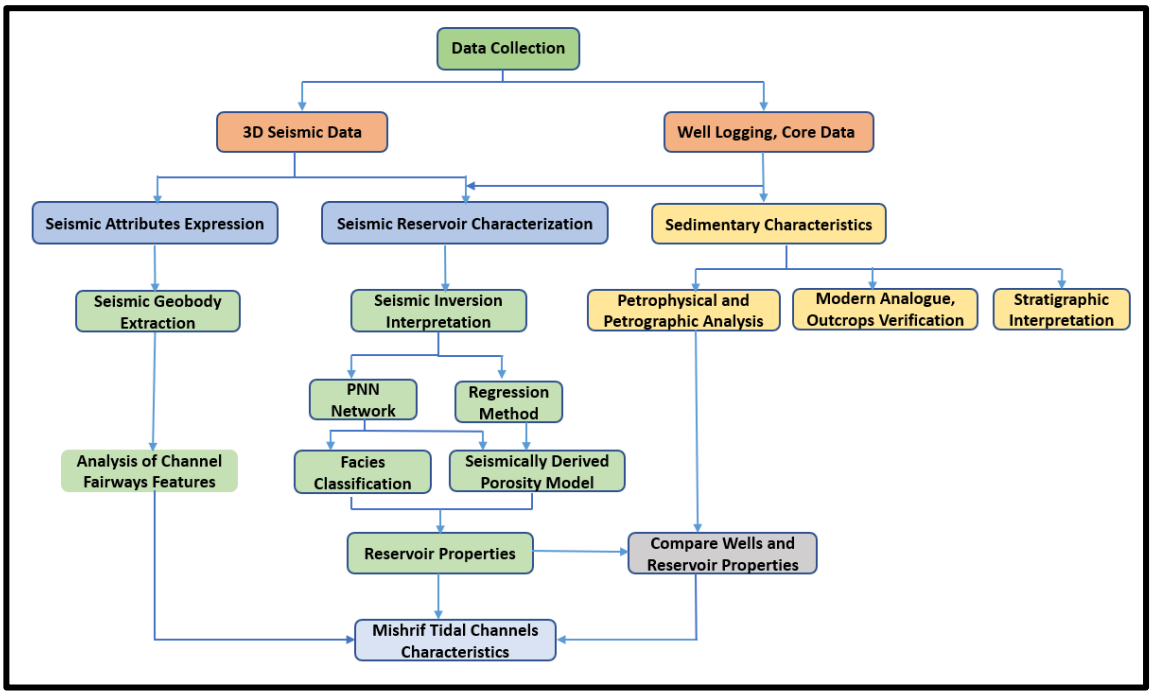

Figure 5.1. An overview of the multi-dimensional workflow developed during this project to characterise Mishrif carbonate tidal channels reservoir characteristics.

5.3 Sedimentary Characteristics of Mishrif Tidal Channels

Multisource data will ultimately lead to enhanced characterisation and spatial distribution of the Mishrif channel geometries and improve reservoir performance prediction, enabling alternative interpretation and limiting the bias in the reservoir characterisation. The input dataset consisted of well-log data, core analysis sections, modern analogue, and outcrops. Three steps are conducted and validated carefully under the control of the Mishrif sequence stratigraphic. The first step is to detect the channel bodies through available wells that pass through the channel fairways using petrophysical and petrographic analysis. The subsequent two steps analyse and compare modern analogue and outcrop with Mishrif tidal channels. The detailed description of the depositional environments of the carbonate channel systems is compared with modern analogue in the Bahama tidal flat. Mishrif tidal channels are compared with channel geometries observed

at the top of the Natih Formation in Wadi Mi'Aidin (SE of the Jabal Akhdar, Northern Oman) for outcrop data.

5.3.1 Sequence Stratigraphic of the Mishrif Channel Fairways

The sequence stratigraphy is established based on the sedimentary background, geology, and paleogeography. The detailed depiction of the sequence-stratigraphy in Figure 5.2 highlights the strong correlation between sequence stratigraphy, depositional facies, and reservoir quality. Figure 5.3 shows the depositional environment for the Mishrif reservoir. It highlights updip to downdip changes in the sedimentology, depositional texture, and the corresponding impact on pore type distribution. The highest reservoir quality facies were deposited in high-energy grainstone shoals and sub-tidal channels in updip environments. High-energy facies are related to the best developed in the middle to the upper portion of shallowing-upward depositional sequences (highstand systems tracts) (see sections 2.1.6 and 2.1.7 in Chapter 2 for more details).

As mentioned previously, tidal channels are widely developed in a restricted environment associated partly to the erosive but mainly in the depositional systems which formed during phases of flooding of the inner platform (Grélaud *et al.*, 2010). These channels occur in the Mishrif mB1 zone causing substantial heterogeneity of the facies and petrophysical properties. The depositional texture of the Mishrif mB1 zone is mainly grainstone and packstone with low-energy muddy lagoonal facies filled by high-porosity grainstones identified on many outcrops. This zone has sweet spots and good-quality facies, particularly subtidal shoals and grainstone channels within platform carbonate. High-flow zones within the mB1 lagoonal system are confined to tidal channels and shoals, showing rapid lateral changes in facies and reservoir quality.

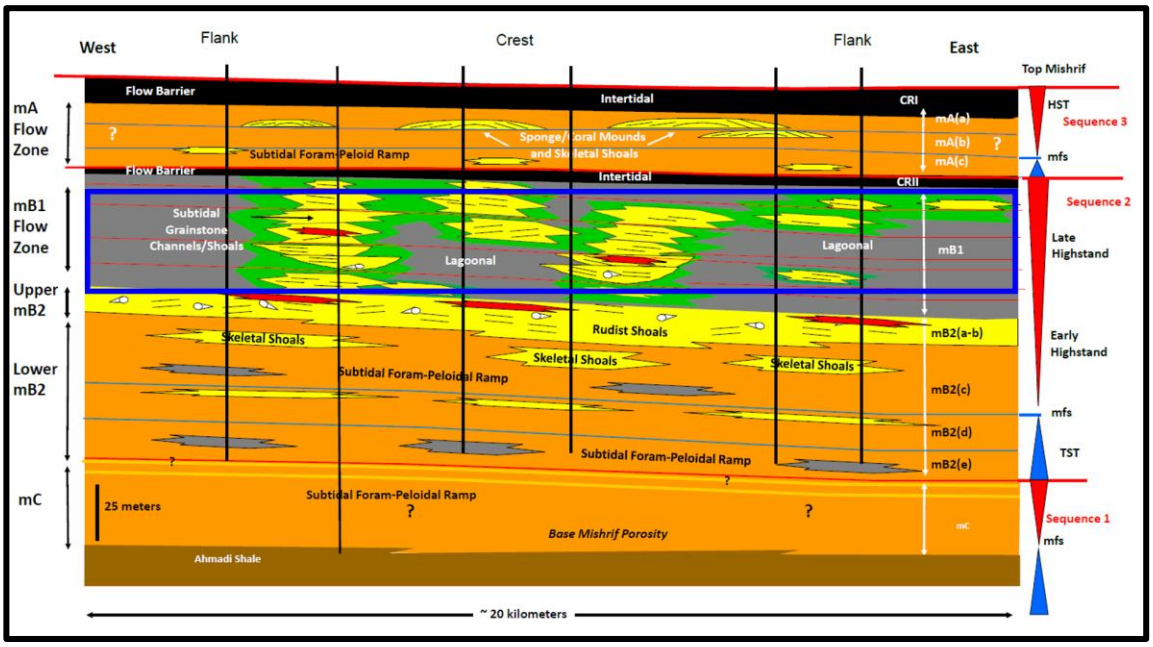

Figure 5.2. Mishrif stratigraphic model based on the core data, including the mB1 zone (blue rectangle) showing the variation of mB1 facies between the west flank, crest, and east flank (Basra Oil Company, 2013).

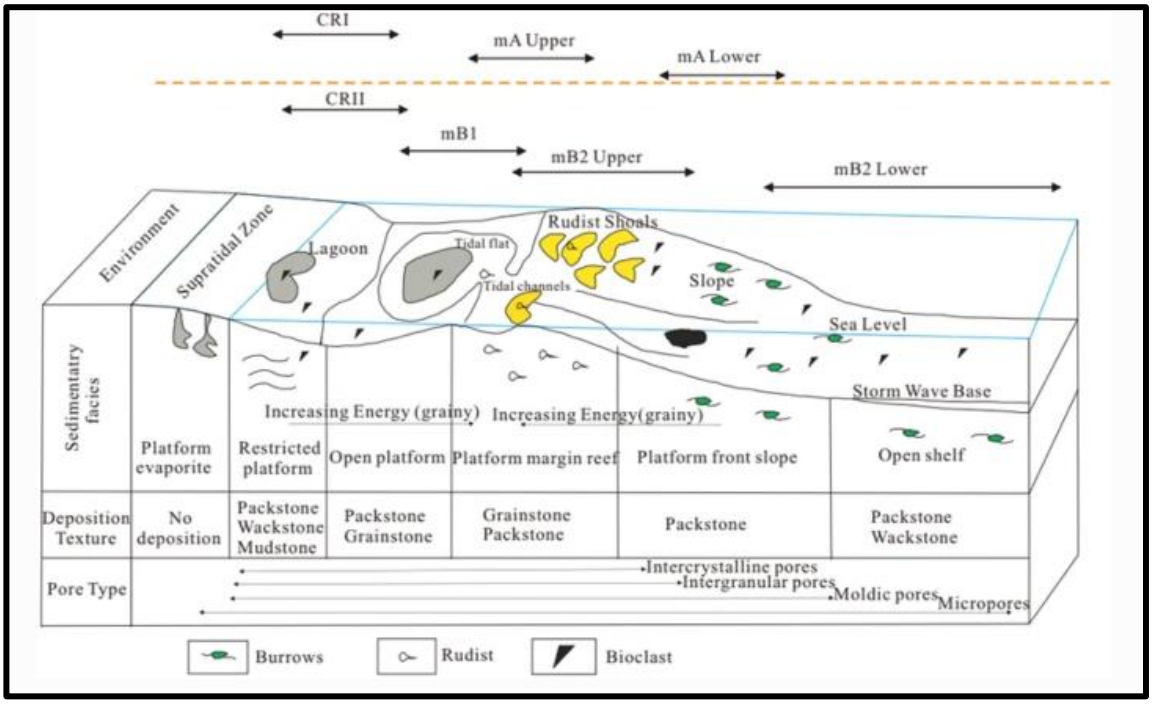

Figure 5.3. Schematic depositional model of the Mishrif Formation showing the depositional sub-environments of the Mishrif reservoir, including mB1 tidal channels (Basra Oil Company, 2013).

5.3.2 Petrographic and Petrophysical Characteristics

The sedimentary facies of Mishrif tidal channels are determined by core observation, using the petrophysical data, and outcrop analogues. The core analysis represents the basis of the sedimentary facies studies (Figure 5.4). Based on the depositional environment, mB1 zone exhibits a considerable variation in porosity and permeability (e.g. Miraglia *et al.*, 2015).

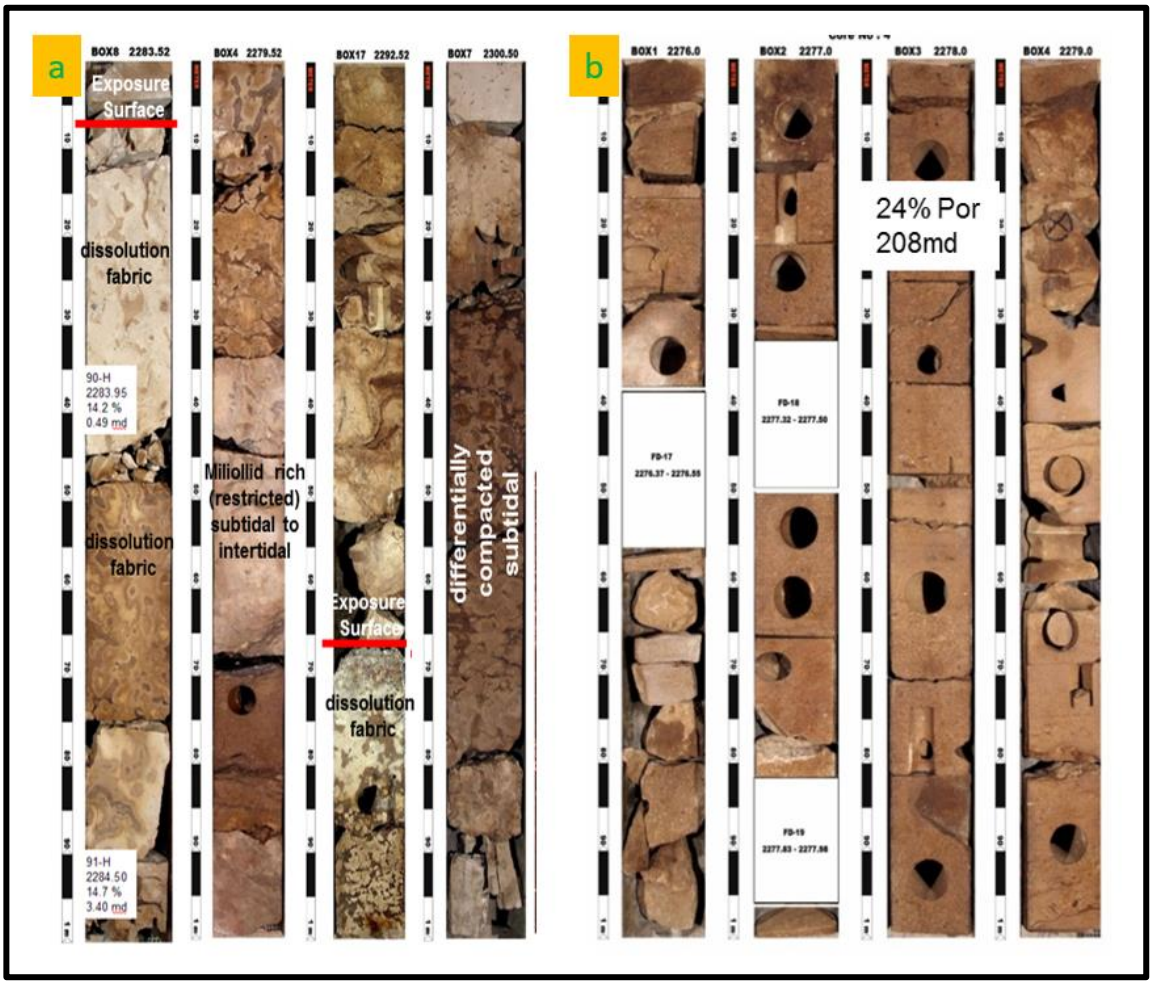

Figure 5.4. Core images of Mishrif mB1 zone of WQ1_A20. a) Intertidal and lagoonal mud-dominated facies (low reservoir quality). b) Tidal channel facies (high reservoir quality) (Basra Oil Company, 2013).

Accordingly, the Mishrif mB1 zone consists of restricted lagoonal facies (milliolids) and subtidal grainstone channels or shoal facies deposited in the inner ramp domain with a maximum thickness of about 50 m, as observed from the petrographic images of the thin sections at WQ1_A20 well. The first group forms discontinuous barriers and baffles to flow; this type has many bioturbated structures and apparent diagenetic differences

(Figure 5.4a). Wackestone dominates these lagoonal facies, interspersed with thin layers of micrite limestone and a minor quantity of packstone and local exposure surfaces (Figure 5.5a). Therefore, it mainly shows the reservoir's low-quality facies with porosity value (6.3 %) and permeability (0.075 md).

The second group of the mB1 zone facies displays sweet spots and good quality facies representing subtidal grainstone channels or shoals despotsited in the inner carbonate ramp domain (Figure 5.4b). Rudstone, bioclastic grainstone, and packstone are the most common facies found in tidal channels. It has mixed skeletal grainstone content with vuggy, interparticle, and connected moldic pore types (porosity: 24.0 %, permeability: 208 md) (Figure 5.5b). The grainstone is highly sorted, with obvious bidirectional cross-bedding, similar to the tidal channel sediment of the Mishrif Formation in the Halfaya oilfield and the Sarvak Formation in the Azadegan oilfield, Southwest Iran (Wenju *et al.*, 2020; Liu *et al.*, 2020). Tidal channel facies could be separated into grain-dominated tidal channel sediment and mud-dominated tidal channel sediment based on grain ratio.

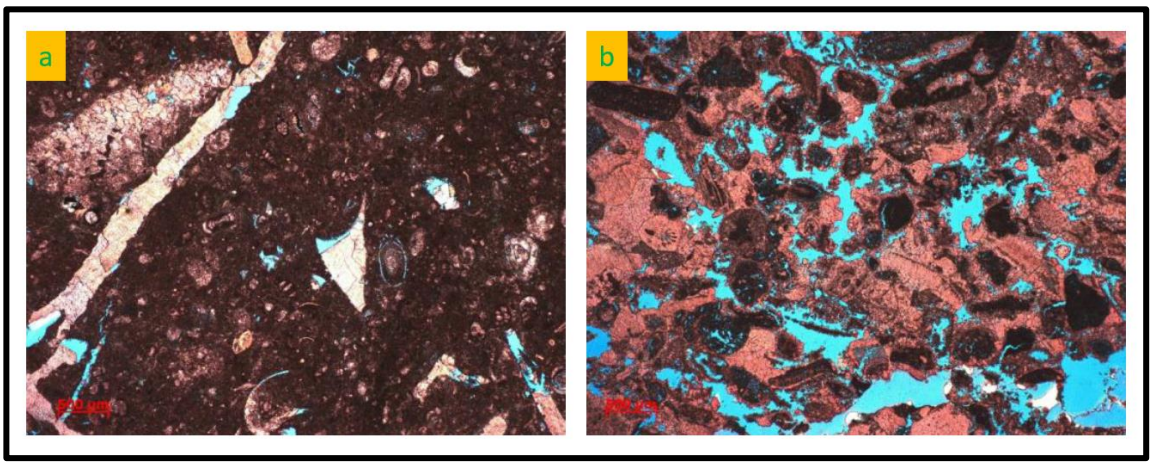

Figure 5.5. Thin section micrographs of Mishrif mB1 zone of WQ1_A20, a) Bioturbated packstone to wackestone facies with moldic and fracture pores, grain types: milliolid foraminifera and gastropods at the depth 2300.30 m, b) Rudstone to grainstone channel facies with moldic and intraparticle pores, the grain types: rudists and milliolid foraminifera at the depth 2278.10m.

A cross plot of permeability versus porosity colour-coded by mB1 zone facies has shown the distribution and the scatter of channel facies and lagoonal facies (Figure 5.6). Well data indicate that the tidal channel shows a bell curve with high porosity values and a gradual increase of gamma values downward for lagoonal facies (low porosity and high gamma-ray) (Figure 5.7).

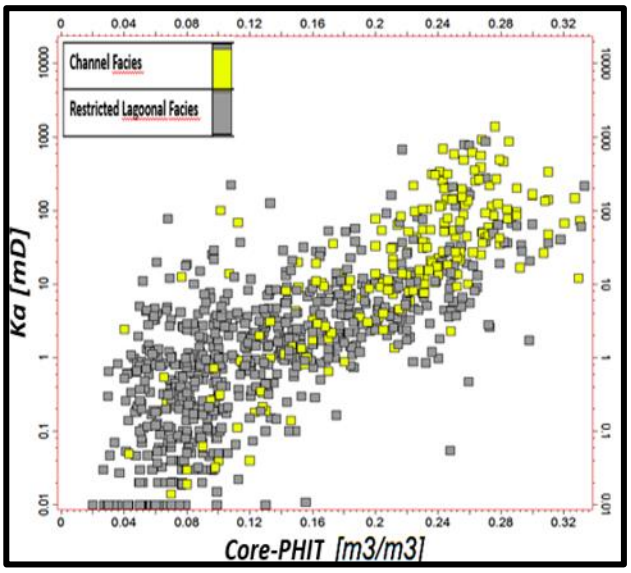

Figure 5.6. Cross plot of permeability versus porosity colour-coded by mB1 zone facies, lagoonal mud-dominated facies, and grainstone channel facies.

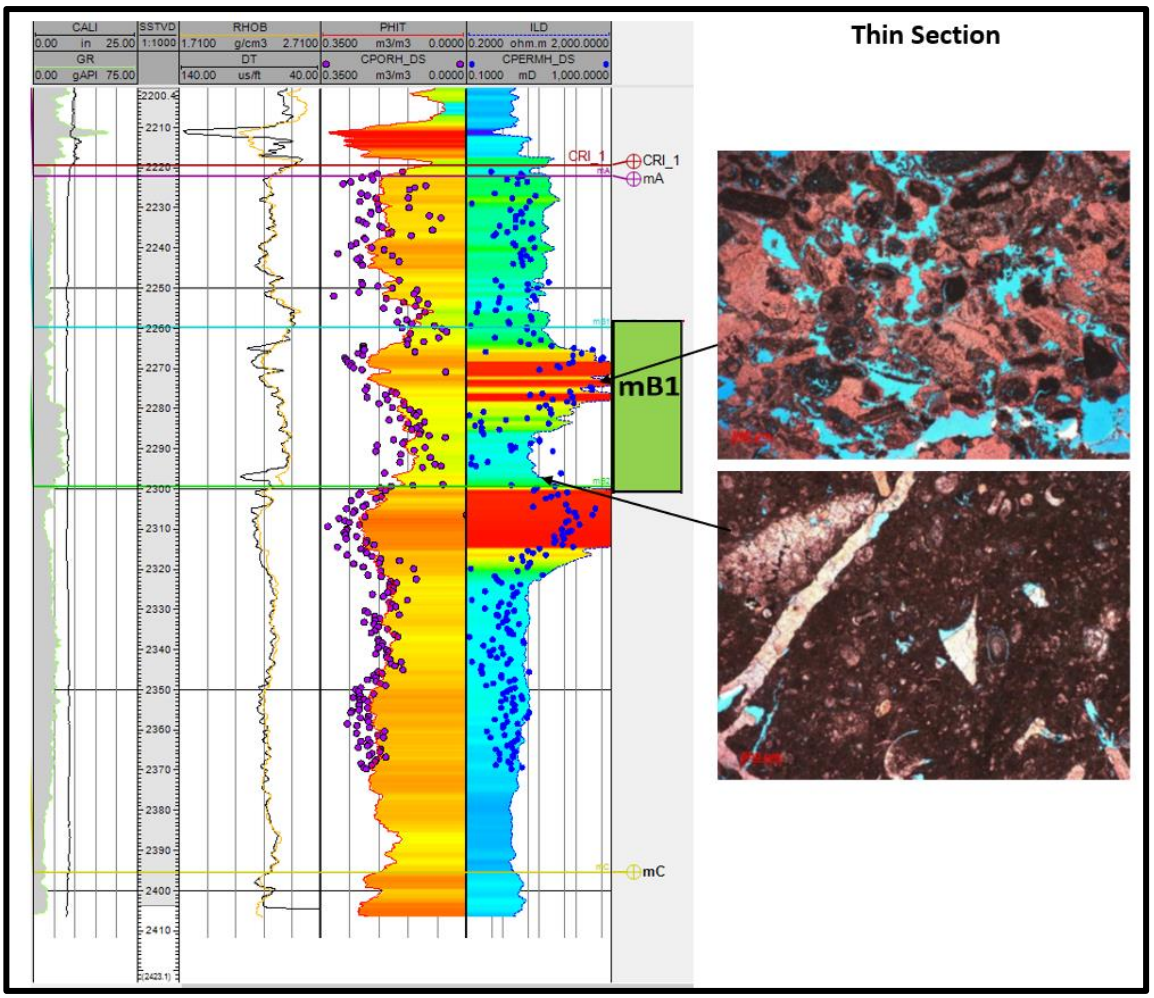

Figure 5.7. Comprehensive interpretation of cored well (WQ1_A20), Mishrif mB1 zone facies contained channel facies (skeletal peloidal grainstone/packstone mainly, low GR, high porosity) and lagoonal facies (wackestone and packstone, high GR, overall low porosity).

5.3.3 Modern Analogue of Carbonate Tidal Channels

Chapter Three refered to modern tidal channel environments from the coastal carbonate system in Abu Dhabi, United Arab Emirates. It gave further information on the lateral extent of the tidal channels and their petrophysical properties (see Chapter 3 for all details). The second one here, the Bahamas, Straits of Florida, helps deepen understanding of the internal geometry of channel fairways. It is critical to refer to reservoir analogues of comparable depositional environments to ensure the realistic distribution of the Mishrif channel fairways. Understanding how these analogues are characterized would aid in determining reservoir characteristics of the Mishrif tidal channel fairways based on seismic data and well data.

Carbonate tidal channels are widely noted in the Caribbean region, especially in the Straits of Florida. The Bahamas is one of the best examples of the modern carbonate tidal flat system. The carbonate platforms of the Bahamas are frequently utilized as a modern analogue to interpret ancient carbonate deposits. Great Bahama Bank is the biggest isolated platform in the Bahamas. It is a magnificent structure of around 600 km in length (northwest-southeast) and 350 km in breadth (east-west) (Eberli *et al.*, 2004). Aerial photographs of Bahamas modern carbonate illustrating tidal channels similar to those imaged from the seismic data of the Mishrif mB1 zone (Figure 5.8a).

In the petroleum domain, where only the channel depth (or sand body thickness) is known with data from wells, length and width are valuable parameters among the quantified geometries described in this study. Figure 5.8b shows a horizon slice of Mishrif-mB1 zone channels over the study area, which generates from acoustic impedance volume; more details will be later, in section 5.5. It can be seen that there are variable channel fairways in the shapes and patterns, which are similar to the Bahamas tidal channels on Andros Island. The form of the Mishrif tidal channel is identical to that of the river channel. It features a concave shape on the profile, and on the plane, it has a "meandering fairways" shape with multi-phase migration characteristics. Comparing the geometrical data between these two tidal channelized systems shows that these Mishrif channel fairways can extend up to 12 km in length, 1-2 km in width, and a depth of about 30 m. In the case of the modern Bahamas coast, Andros Island has individual tidal bars ranging from 12-50 km in length, 0.5-1.5 km in width, and 3-9 m in thickness. Tidal channels

between these bars are 1-3 km in width and 2-7 m deep and constrained by sea-level rise, (Kindler *et al.*, 2011).

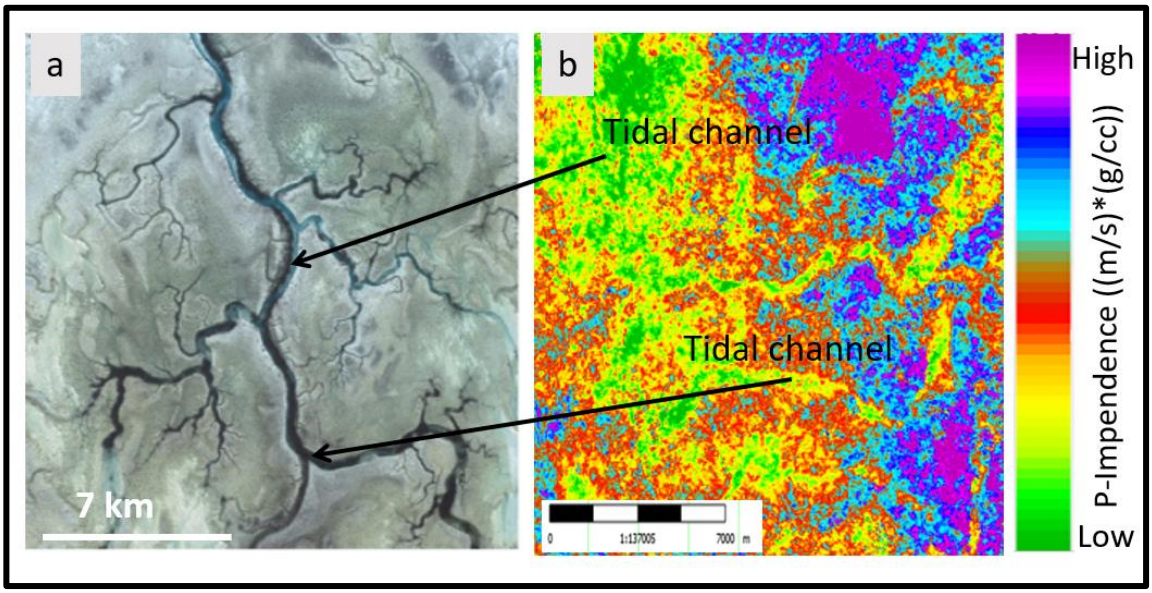

Figure 5.8. (a) Aerial photograph of the tidal channels in the Andros Island, Bahamas Bank, (Google satellite earth map), compared to (b) Time slice of Mishrif mB1 channel fairways from acoustic impedance volume to show the very good similarity between them.

5.3.4 Carbonate Channelized Outcrops

The Oman Mountains include a variety of outcrops that can be utilized as carbonate field analogues in the region. Many observations of tidal channels can be compared to those of the Mishrif Formation. Tidal channels can be observed at the outcrop scale located in Wadi Mi'Aidin (Northern Oman). Also, Similar tidal channels are found at the same stratigraphic level in Wadi Mi'Aidin on Wadi Khamah, Wadi Sumayt, and Wadi Tanuf sections (Grélaud *et al.*, 2010).

This series of channelized fairways is restricted to a small region, about 2-3 km in width, 1-4 m in-depth, and directed east-west (Figures 5.9). A complicated set of channelized entities, mostly fine–coarse grainstone with rudist fragments, other bivalves, corals, and echinoids, make up the channel fill. The filling of these channels includes a complex type of channelized bodies, mostly grainstone and rudist fragments.

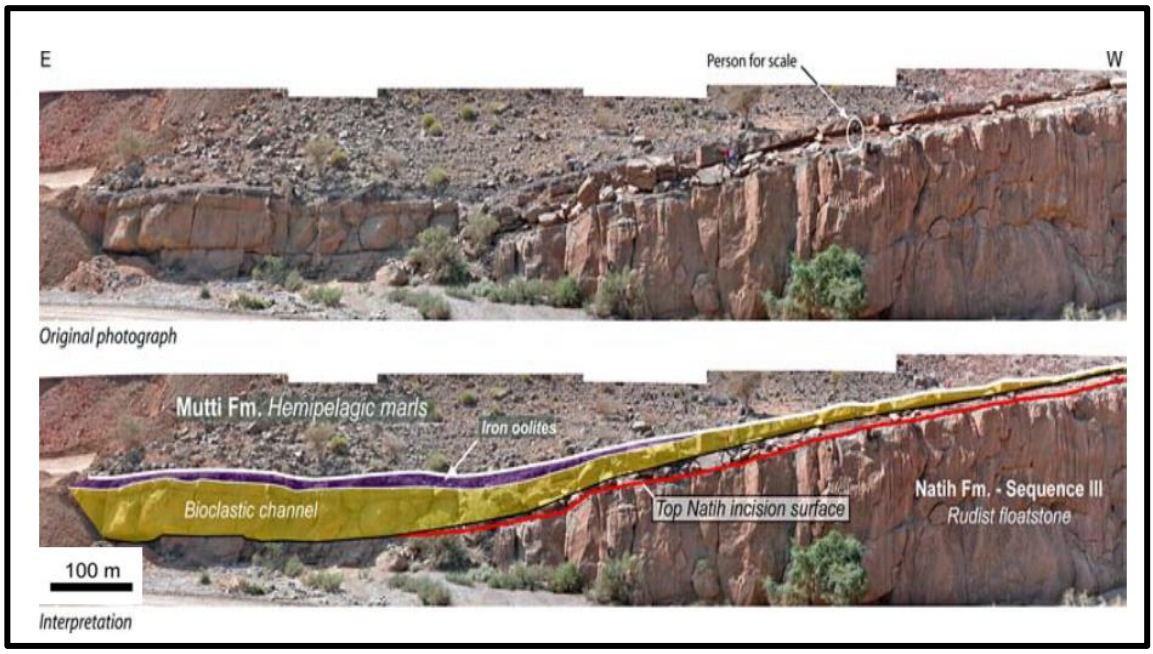

Figure 5.9. The outcrop scale of bioclastic channel geometries (yellow colour) observed at the top of the Natih Formation in Wadi Mi'Aidin (Northern Oman) shows an external geometry similar to that of the Mishrif tidal channel fairways (Grélaud *et al.*, 2010).

5.4 Seismic Attribute Expression: Identification of Channel Geometries

5.4.1 Combination of Surface Attributes

The RMS surface and acoustic impedance surface attributes were created for the target zone (Mishrif mB1 channelized zone) to recognize the features that could be identified. RMS amplitude is one of the most valuable surface attributes for characterisation, and it showed the margins and lateral extensions of the fairway geometries (Figure 5.10a). Similarly, the acoustic impedance surface identified the channel fairways, which are well defined (Figure 5.10b) (more details about acoustic impedance will be provided in the subsequent sections). Therefore, these slices were combined to analyse the planar distribution and lateral stacking of channel fairway geometries.

The fairway has a width of up to 1 km and a length of 10-12 km. In the mB1 channel zone, there are two-channel fairways established in the middle of the field. We may infer that the surface attribute extractions did not describe the channel expansion well especially for thin channels which are nearly invisible in default seismic data or surface attributes. A frequency spectral decomposition tool that provides a more detailed thorough description of the geometry and image geologic discontinuities.

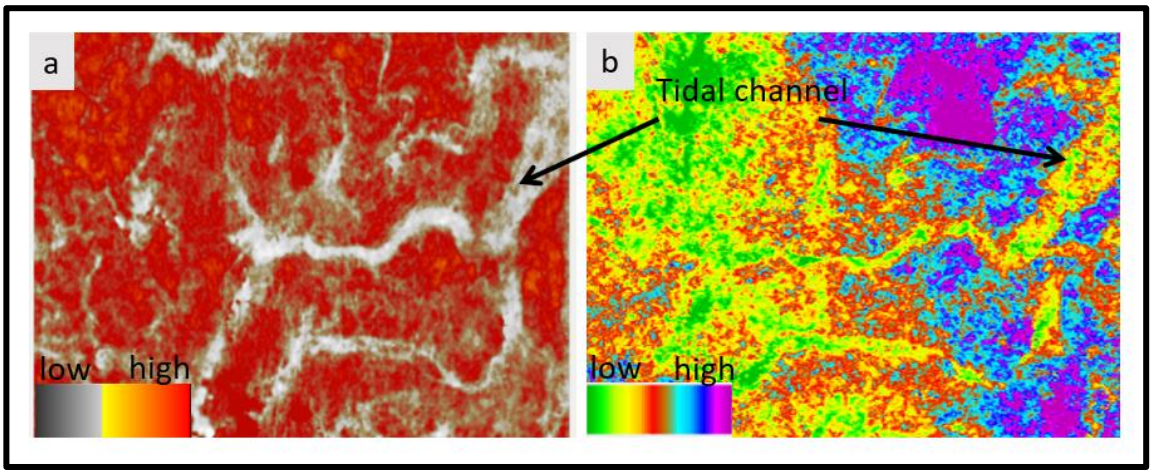

Figure 5.10. Comparison of the surface attributes (a) RMS amplitude surface attributes of the target zone (Mishrif mB1). (b) Acoustic impedance surface attribute for the Mishrif mB1 zone.

For the comparison, similar tidal channels have been observed on seismic attribute maps on the same Mishrif reservoir, H field, south of Iraq (Cantrell *et al.*, 2020). This demonstrated that several significant channels spanned the field that developed at the top of the underlying sequence during the ensuing transgression (Figure 5.11a). It would have been filled with sediment deposited at different depths compared to locations outside these channels (Cantrell *et al.*, 2020). Another analogue is the upper part of the Natih Formation in central Oman, which may be more than 1 km wide and reach lengths of over 30 km (Figure 5.11b) (Droste, 2010).

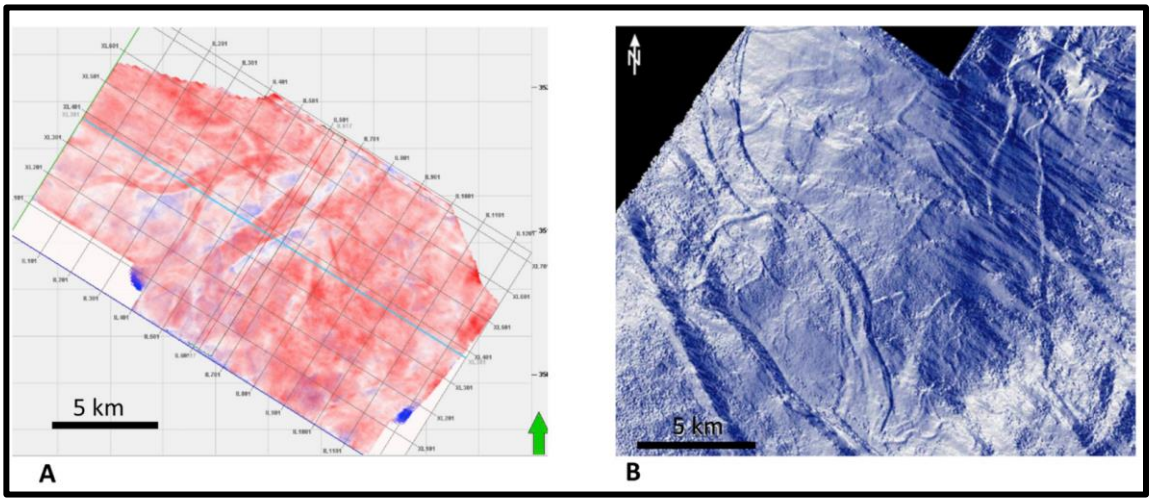

Figure 5.11. (a) Seismic image of interpreted channels of Mishrif formation, H field, south of Iraq (Cantrell *et al.*, 2020), (b) Channel incision into the top of Natih Formation imaged on an azimuth map of the top Natih seismic reflector, central Oman, modified from Droste, (2010).

5.4.2 Frequency Spectral Decomposition Techniques

Spectral decomposition is applied as a new approach in seismic imaging that provides seismic interpreters with reservoir information and is utilized for imaging and mapping geological discontinuities and temporal bed thickness from 3D seismic data. Using Petrel Software, the workflow is employed to split the seismic volume into its constituent frequencies based on the dissected seismic signal (Figure 5.12). The frequency and phase components that are obtained after spectrally dividing the data are the frequency components, where the former is a direct indicator of the relative seismic amplitude within a frequency range. To extract the geobodies of the tidal channel fairways in the Mishrif mB1 zone, we use both techniques of the generalized spectral decomposition, Geobody RGB (Red, Green, Blue) Blending and Mixer RGB Blending, to compare the results and reduce the uncertainties associated with the seismic data and considering the high heterogeneity of the Mishrif reservoir.

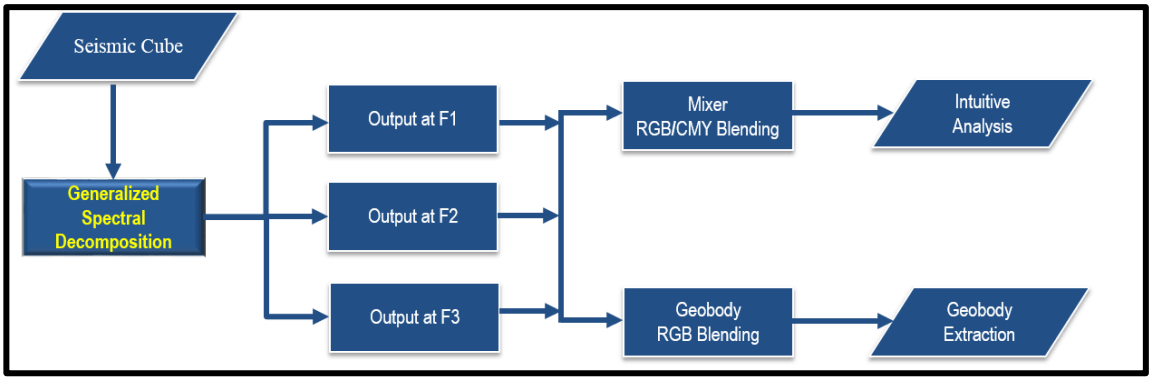

Figure 5.12. Generalized spectral decomposition qualitative RGB blending workflow for both techniques (Mixer and Geobody) using three frequency intervals (F1, F2, F3).

The three frequency intervals from the West Qurna/1 seismic dataset are 8 Hz (the lowest frequency value in the seismic dataset), 20 Hz (the predominant frequency value), and 28 Hz (the highest frequency value) (Figure 5.13). mB1 tidal channel zone amplitude reflects a low-frequency range and high-frequency outside channels depending on the seismic amplitude of these three volumes; however, the 8 Hz frequency section of the studied zone did not show any response for the channel features, and most of the area low-frequency (5.14).

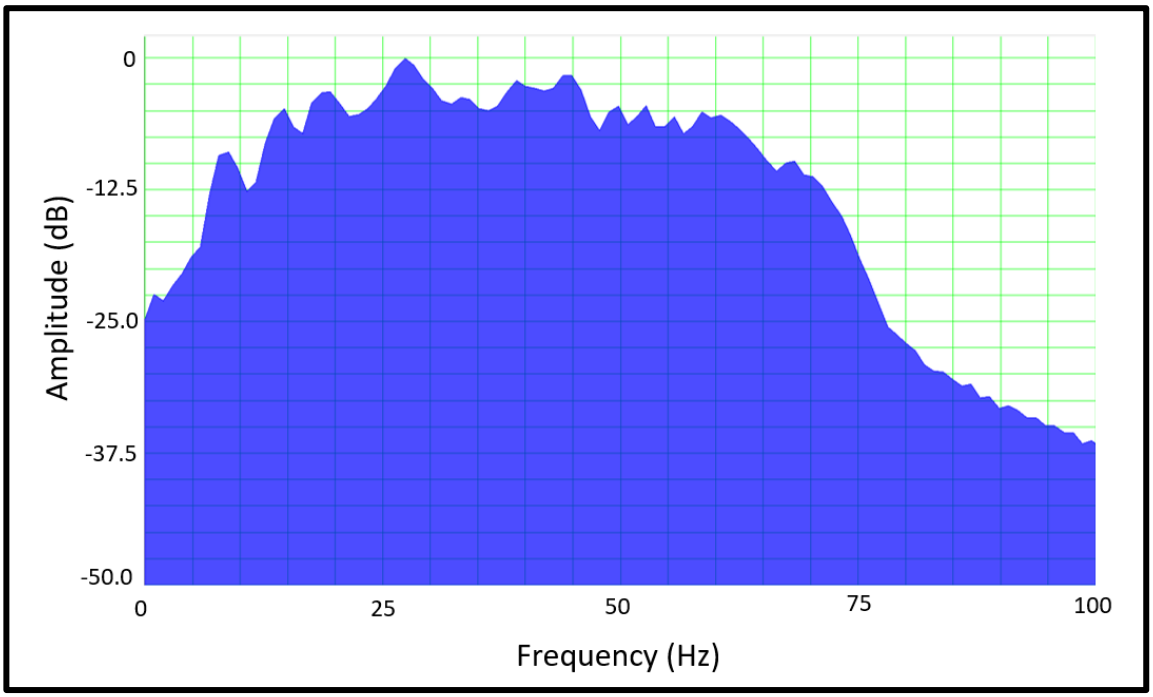

Figure 5.13. West Qurna/1 seismic frequency spectrum within the reservoir interval to extract three frequency intervals (F1, F2, F3).

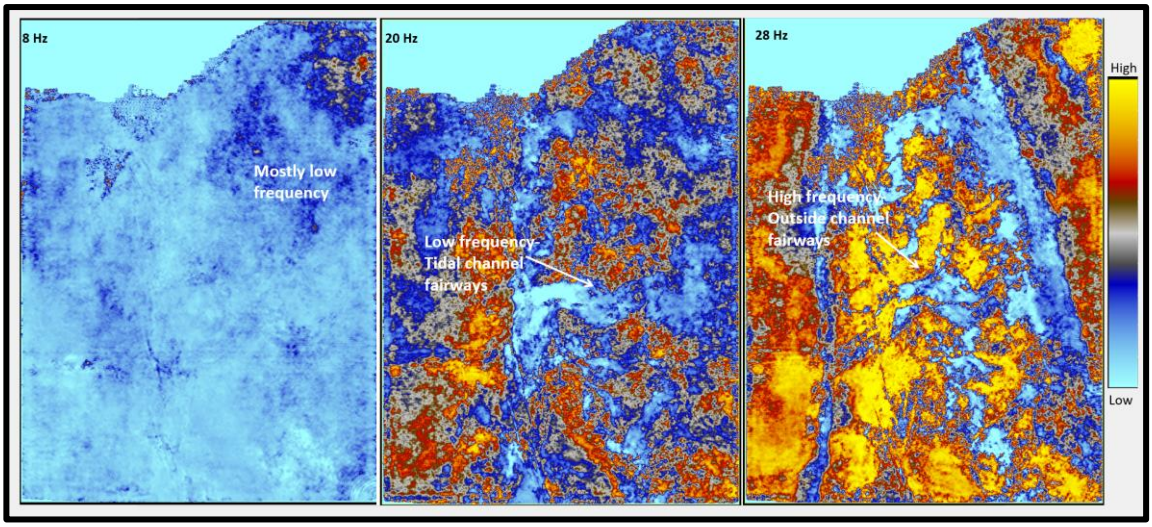

Figure 5.14. The amplitude variation of the Mishrif mB1 zone on different extracted frequencies indicates the connection of the tidal channel fairways and outside channels.

Following determining the frequency intervals (given in Appendix Figure A.2), each successive dataset is represented by a different colour for visual analysis for both techniques by the spectral decomposition displays (Figure 5.15). The 20 Hz frequency volume successfully defined the geometry of mB1 tidal channels, and the 28 Hz frequency volume also indicates a part of the channel fairways in less visualization. These two frequencies helped target the area of the channel that is the thickest and of the highest

quality, shown on display and permitted observing distinct frequencies of subsurface seismic interference. However, the lower frequency volume (8 Hz) failed to detect the channel fairways fully.

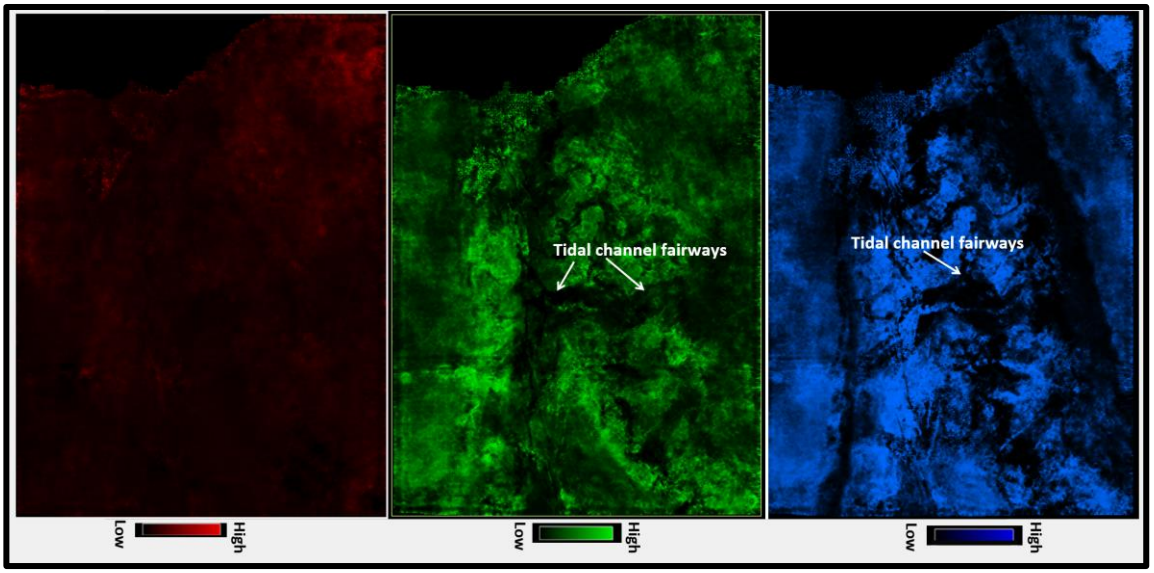

Figure 5.15. Three frequency volumes are Red, Green, and Blue. The frequency ranges are 8 Hz in Red colour, 20 Hz in Green colour, and 28 Hz in Blue colour.

In the final step, spectral decomposition recombines these individual volumes with these frequencies into one colour blended frequency volume. The results from these two tools appear very similar regarding channel delineation and geomorphology (Figure 5.16). Spectral decomposition over the Middle mB1 zone shows the sizeable tidal channel and is better defined at the field's eastern flank. This channel fairway is separated into two parts and has a discontinuity towards the western flank with a lack of definition due to the effect of fault movement between the eastern and western flanks. Spectral decomposition reveals more details, subtle geological features with a distinct border on the tidal channel fairways, and qualitative indications of reservoir quality. The spectrum decomposition approach, used on its own or combined with other seismic attributes, benefits the channel fairway delineation and geobody extraction of the Mishrif reservoir channels. The results show that using the spectrum decomposition approach yields reliable outcomes.

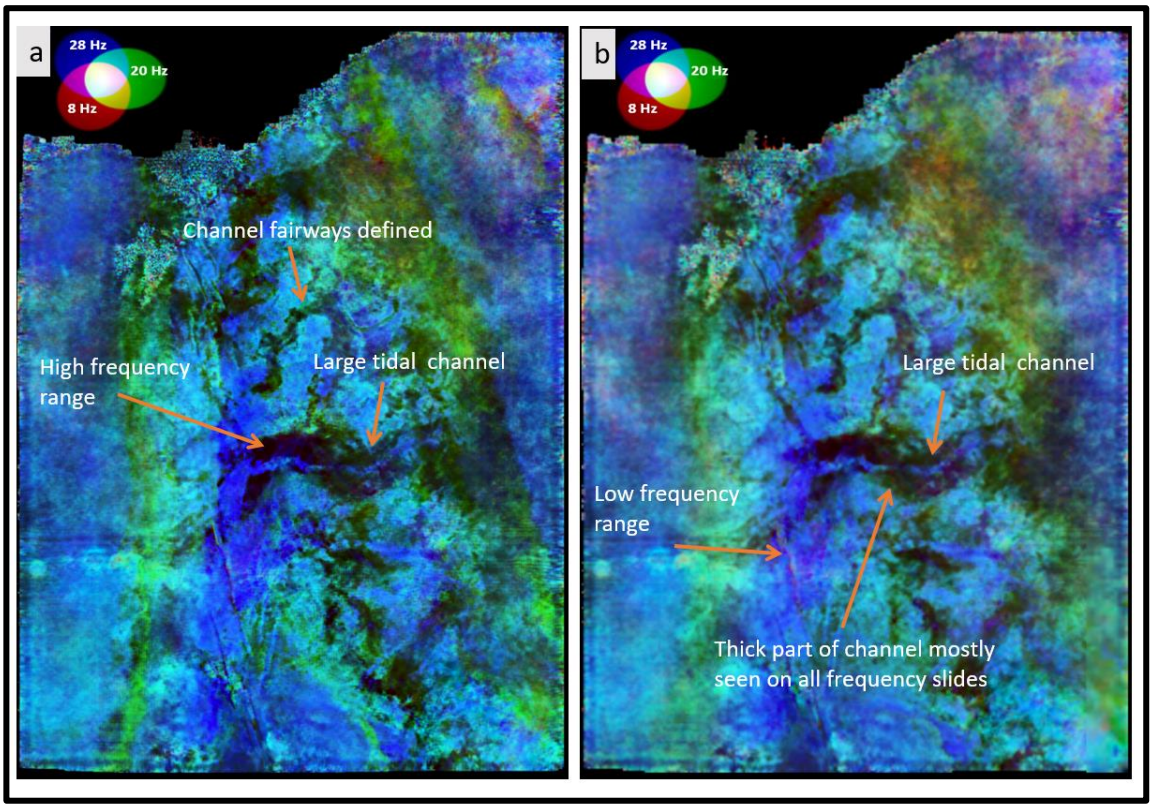

Figure 5.16. Spectral decomposition maps for the mB1 zone using (a) Mixer RGB blending and (b) Geobody RGB blending, both tools indicated bright and large tidal channels on the field's eastern flank (the middle channel with dark bule colour).

5.5 Seismic Reservoir Characterisation: Mishrif Tidal Channel Fairways

After identifying channel geometries using surface attributes and frequency spectral decomposition techniques, seismic data is analysed using another method. The lateral extension of individual channels will be characterized by a combination of acoustic impedance volume and seismically-derived porosity model in order to uncover additional characteristics in vertical profiles. The properties could be extracted from any seismic volume after it has been constrained vertically and laterally. Also, we have been using the PNN algorithm to detect new observations of the seismically-derived porosity of the channel fairways and compare the results with the linear regression tool described in the previous chapter.

5.5.1 Interpretation of Seismic Inversion Results

The seismic characterisation starts with the seismic amplitude analysis to identify mB1 zone features. The Mishrif mB1 carbonate tidal channel is well defined on the seismic

volume and interpreted and mapped. The channel of the arbitrary line (N to S trend) demonstrates a medium to strong amplitude in the seismic section, with a concave feature at the top and the bottom (Figure 5.17a). Due to the vertical resolution, it is impossible to precisely detect the channel's inner phases using an amplitude profile. As a result, a high-resolution inversion based on seismic waveform similarity was used to expose additional vertical information and estimate reservoir attributes. Further recognition with acoustic impedance (AI) volume, explained previously in Chapter 4, the outer shape and inner phases are interpreted more clearly with low acoustic impedance values surrounded by restricted lagoonal facies. This reflects that channel development is constrained and formed during the inner platform's flooding phases (Grélaud *et al.*, 2010) (Figure 5.17b).

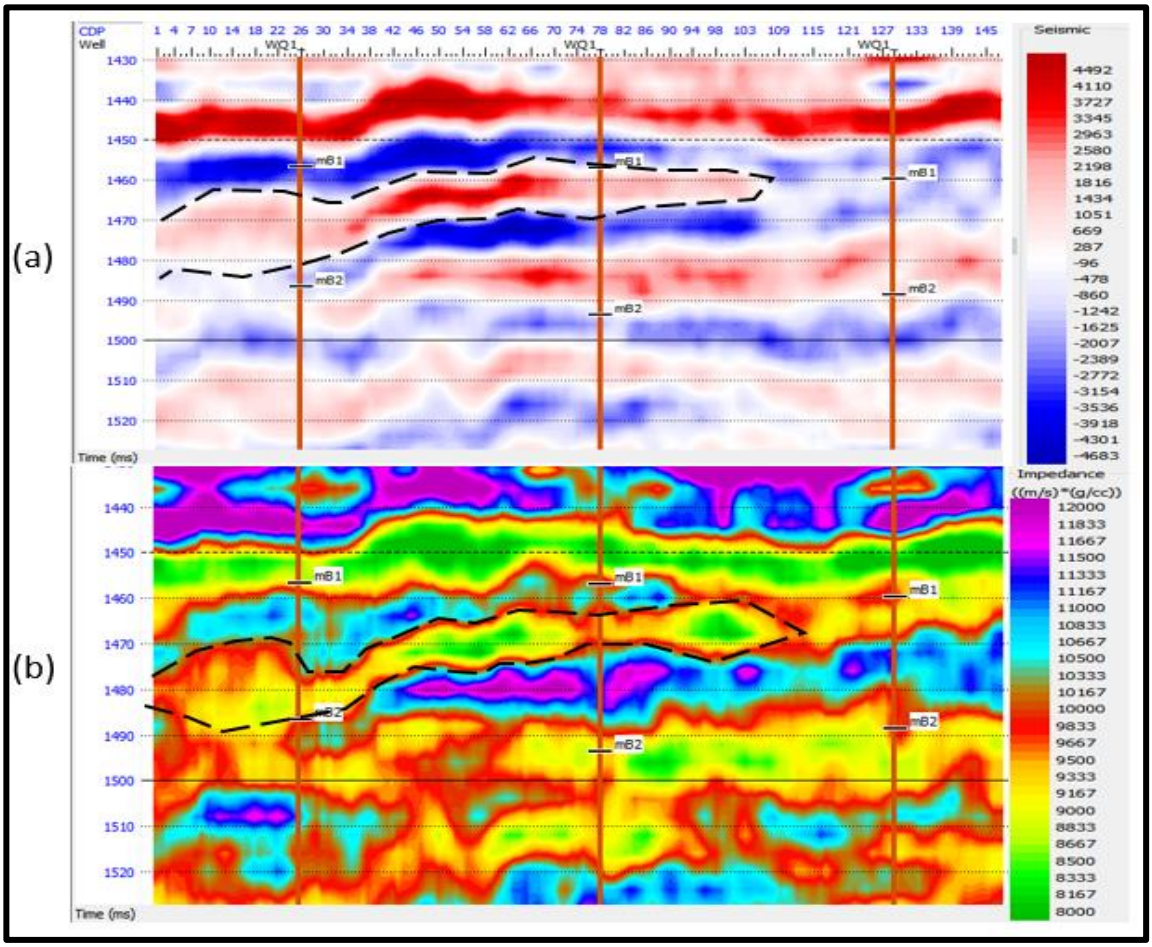

Figure 5.17. Channel distribution of mB1 zone in the dashed black line. (a) The seismic amplitude's arbitrary line (N to S trend) shows the channel character. (b) Profile of the channel zone highlights lower acoustic impendence areas in channel fairways and higher values outside channels.

In Chapter 4, we have discussed and compared the results of model-based and linear programming sparse spike (LPSS) inversions. There are some similarities between these

two algorithms' results and their interpretation; both methods were described in Chapter 2 (section 2.2.4) and Chapter 4 (section 4.4). However, there are many noticeable differences between the two methods. Figure 5.18 compares acoustic properties for each inversion in the Mishrif mB1 zone. The results indicated that model-based inversion (Figure 5.18a) shows more distinct connectivity of the channel fairways than the LPSS results (Figure 5.18b). The difference is that the reservoir's contrast is poorer for the LPSS method than for the model-based method. In the latter case, the observations of the acoustic properties of Mishrif channel fairways can be seen in different distribution bodies of the channel fairways (low acoustic impedance).

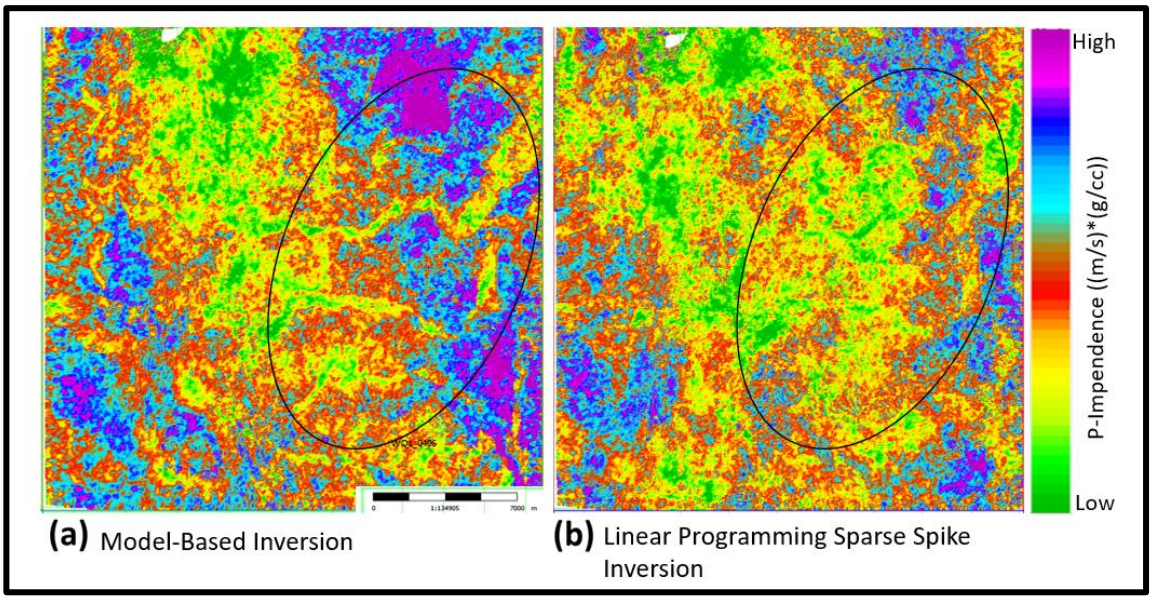

Figure 5.18. Comparison of acoustic impedance results using a) Model-Based Inversion and b) LPSS Inversion, the oval shape height of the distribution of the Mishrif mB1 channel fairways zone.

5.5.2 Capturing Channel Geometries Based on Seismically Derived Porosity

As explained in Chapter 4, the seismically derived porosity model and core analysis data show that the Mishrif-mB1 zone consists of restricted lagoonal facies (milliolids), meandering tidal channels, and elongated features related to the channelized system. This zone is one of the inner carbonate platform's most diverse and complex depositional systems. Therefore, many carbonate tidal channel features were observed in the porosity slices and reflected high porosity regions (porosity range: 17- 25%) (Figure 5.19). These Mishrif grainstone channels could be classified into the north, southwest, and east field. However, lagoonal facies outside these channel bodies is attributed to cementation

associated with exposure surfaces and characterized by high acoustic impedance anomalies with low quality of porosity distribution (porosity range: 6-14%).

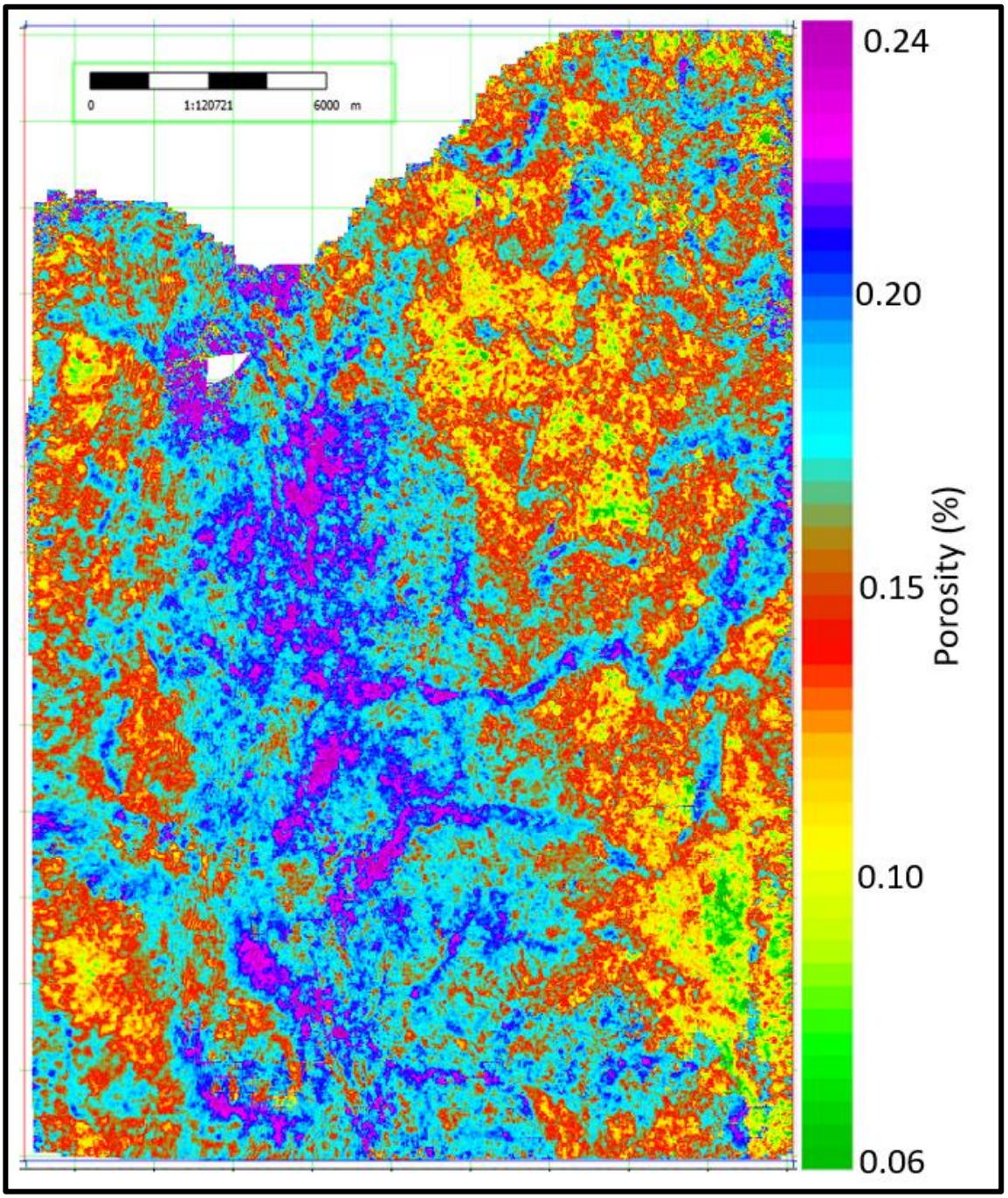

Figure 5.19. Seismically-derived porosity model showing spatial porosity distribution in mB1 zone. A large tidal channel with high porosity in the eastern flank (the centre right).

Several parameters, including wavelet, signal-to-noise ratio, and low frequency, are used in the inversion of seismic data, which are assigned a priori status and significantly affect inversion outcomes (Thore, 2015).

A combination has been made between the linear mode (linear regression) and nonlinear (neural network) to provide two sets of realizations of the seismically derived porosity, in other words, two approaches of seismically derived porosity to identify channel bodies and characterize the properties of the inter-well region. The steps of the first approach were explained previously with its parameters in Chapter 4 (description of this approach in section 4.6.1).

In the second approach, a neural network is trained nonlinearly using the chosen seismic attributes as inputs (Hampson et al., 2001) to derive the porosity model. The PNN seems the preferred network because of its straightforward mathematical design (more details in Chapter 2, section 2.2.13). Additionally, this method is chosen because PNNs are powerful and can infer intricate, nonlinear correlations without prior knowledge of the model (Iturrarán-Viveros and Parra, 2014). The PNN was trained to look for a nonlinear relationship between the parameters (seismic attributes) and the observed porosity at the wells to generate a 3D porosity model. Hundreds of seismic properties that can be produced by combining fundamental seismic attributes, such as seismic amplitude and frequency, are available as predictor variables. Primarily, we need to use groups of attributes (multi-attributes) taken simultaneously as the parameter of this method to distinguish subtle elements on the target property, which none of the individuals could predict by themselves. The phrase "multiattribute seismic analysis" refers to all geostatistical techniques that use several attributes to forecast a specific earthly physical feature (Hampson *et al.,* 2001).

One of the uncertainties here is that EMERGE Software will be choosing which attributes to employ and how to prioritize them. These attributes will be chosen for their capacity to define the target properties and accurately forecast the porosity distribution. To estimate the reliability of the derived multiattribute transform, every attribute has a weighting of the training errors and validation errors. Hence, these optimal attributes were selected based on the correlation and prediction errors, with the lowest validation errors. Adding additional attributes will increase the validation error, determining when to stop adding attributes to the input set (Hampson *et al.,* 2001).

PNN is applied to the high-resolution West Qurna/1 seismic dataset to delineate the complex mosaic of Mishrif carbonate tidal channels. In the case study, we used six post-stacked seismic attributes and the observed porosity at the 18 wells as the main parameters and obtained new known geologic features of the channel fairways in a different method. The six seismic attributes are absolute amplitude, acoustic impedance, integration of the data trace, average frequency, amplitude-weighted frequency, and dominant frequency (Table 1). The amplitude of the seismic volume measured these attributes. Previously, we observed the main fairways based on the linear regression approach, particularly in the eastern flank and the field's middle (Figure 5.20a). However, there are some differences and similarities between curvilinear geological features in the other regions of the mB1 channelized zone. A combination of these resulted in channel fairways characterisation, which was remarkably consistent with the geological scenarios. Using a probabilistic neural network (PNN) provided a more confident delineation of four distinct high-porosity channelized features in the field's upper and lower parts of the eastern flank (Figure 5.20b).

Multi-Attribute List: Multi Attribute List 2

	Target	Final Attribute	Training Error	Validation Error
1	Porosity	Integrated Absolute Amplitude	0.095314	0.097275
2	Porosity	1 / (inverted_Zp)	0.090397	0.092156
3	Porosity	Integrate	0.087984	0.089701
4	Porosity	Average Frequency	0.086896	0.088891
5	Porosity	Amplitude Weighted Frequency	0.085878	0.088055
6	Porosity	Dominant Frequency	0.085411	0.088254

Table.1 Multi-attributes list used for predicting porosity using PNN, with corresponding training and validation errors.

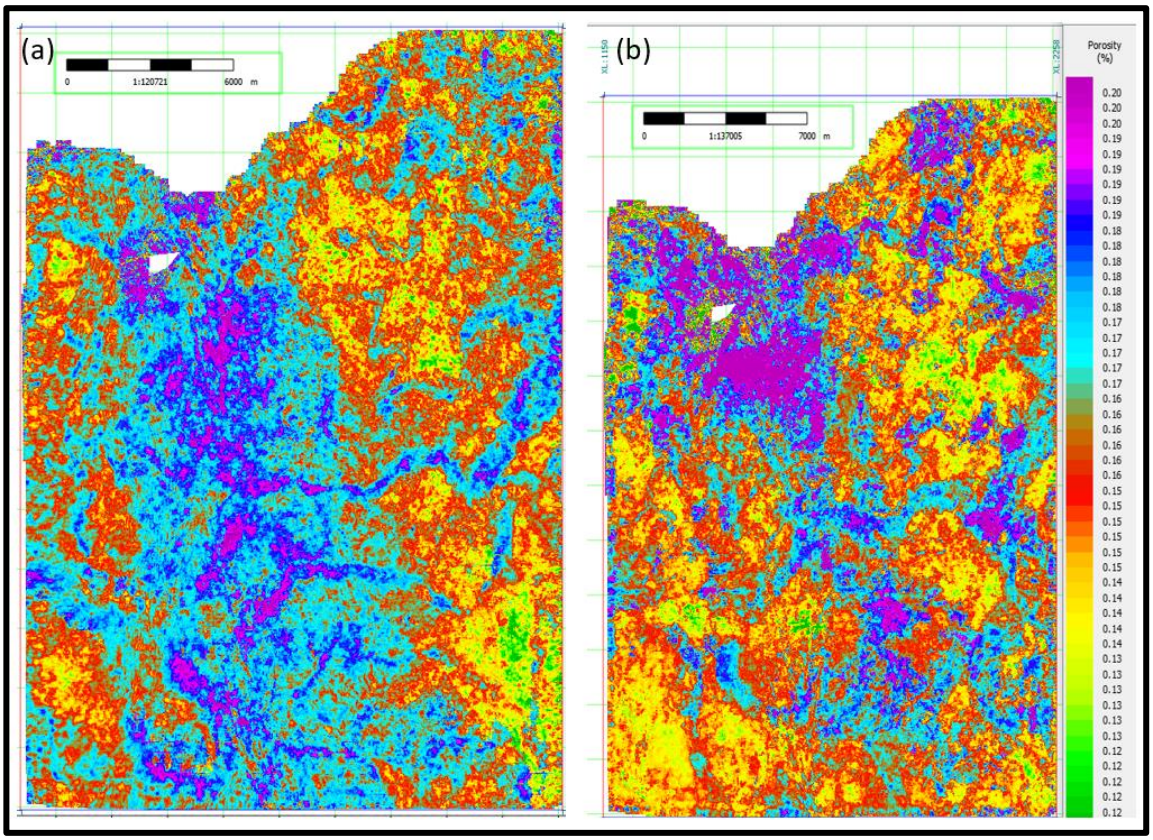

Figure 5.20. Porosity map of Mishrif tidal channels from different algorithms. a) Linear regression method and b) probabilistic neural network (PNN).

For the discussion, a seismically-derived porosity model was compared with AI volume in the mB1 zone (Figures 5.21a and b). By slicing through the porosity model, we saw high porosity values in carbonate tidal channel facies with low acoustic impedance, thus reflecting a good reservoir quality, including grainstone tidal channels or the accumulation of coral mound facies. Additionally, these results were confirmed by the spectral decomposition interpretation (as explained in the previous section).

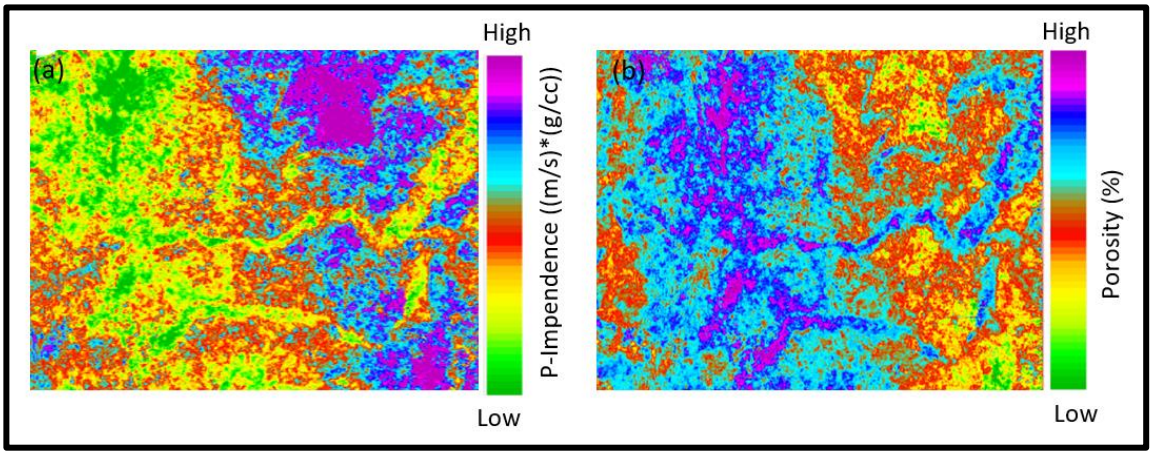

Figure 5.21. Mishrif carbonate tidal channel characterisation (mB1 zone), these channel fairways exhibit low acoustic impedance and high porosity. (a) Acoustic impedance inversion volume. (b) Seismically-derived porosity model.

5.5.3 Facies Classification Framework of Mishrif Channel Fairways

Mishrif channelized system is mainly observed in the mB1 zone we have studied in this chapter. The method of this work is explained by the steps in Figure 5.22, which demonstrates the approach of seismic facies classification. A multi-step approach was implemented by an integrated multi-attributes list obtained from a high-resolution 3-D seismic volume with well log data (facies logs based on porosity logs) to recognize and classify carbonate tidal channel facies and their distribution as output (target) data. For this classification, a probabilistic neural network (PNN) was used to predict channel facies within the Mishrif reservoir (the same method was used to predict the porosity model in the previous section). The proposed framework consists of two steps:

- Pre-processing
- Generation of seismic lithology maps

The primary step of the workflow is generating a facies distribution with available geological information. Based on step 2 (PNN training method), the probabilistic neural network will employ to characterize channelized facies distribution in the mB1 zone.

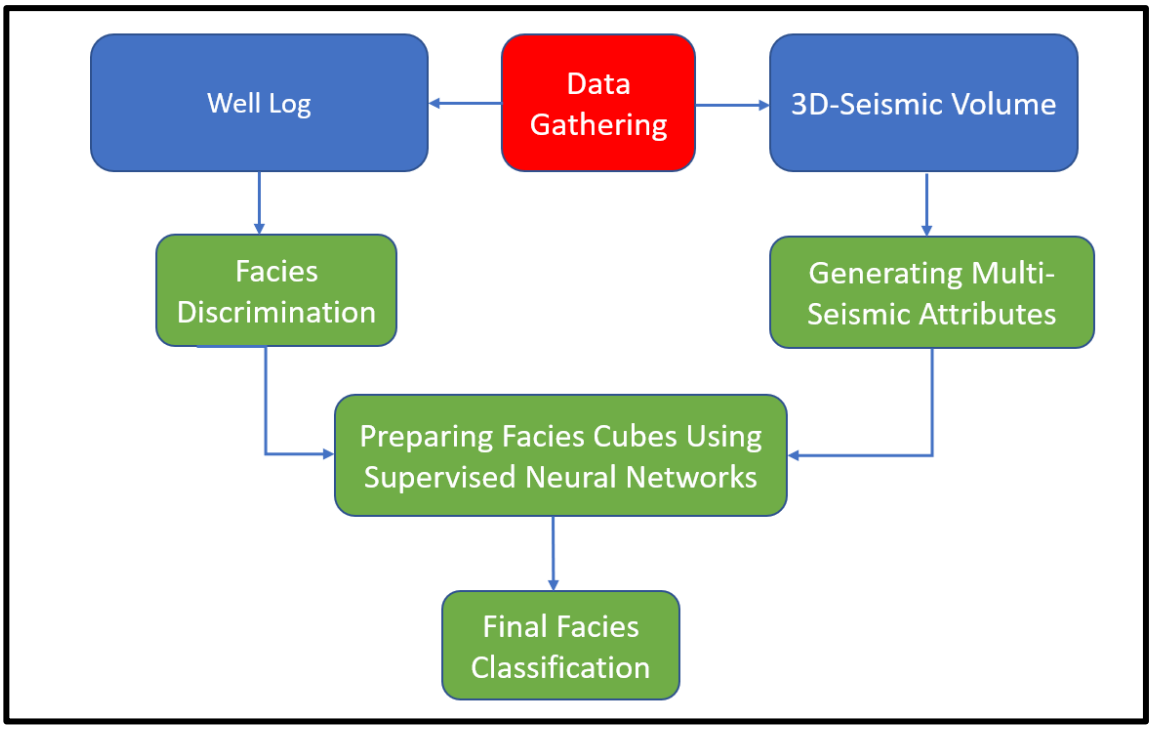

Figure 5.22. Seismic facies generation workflow based on probabilistic neural network (PNN) to reach the final facies classification of the carbonate tidal channels.

5.5.3.1 Pre-processing

After interpreting Mishrif tidal channel fairways from seismic data, facies discrimination was carried out at well locations with core and well data, especially on those inside the channelized system, representing a good indicator of tidal channels. Different petrophysical properties of the mB1 zone were observed in the well log data. The well log indicated a high gamma-ray, low porosity (8 %), and based on core data, a low permeability (0.4 mD) of the so-called restricted lagoonal facies. Channel facies showed high porosity and low gamma-ray (high-quality facies). Indeed, several wells show mainly sweet spots and good-quality facies in some regions of this zone, particularly grainstone channels or shoal facies (Figure 5.23).

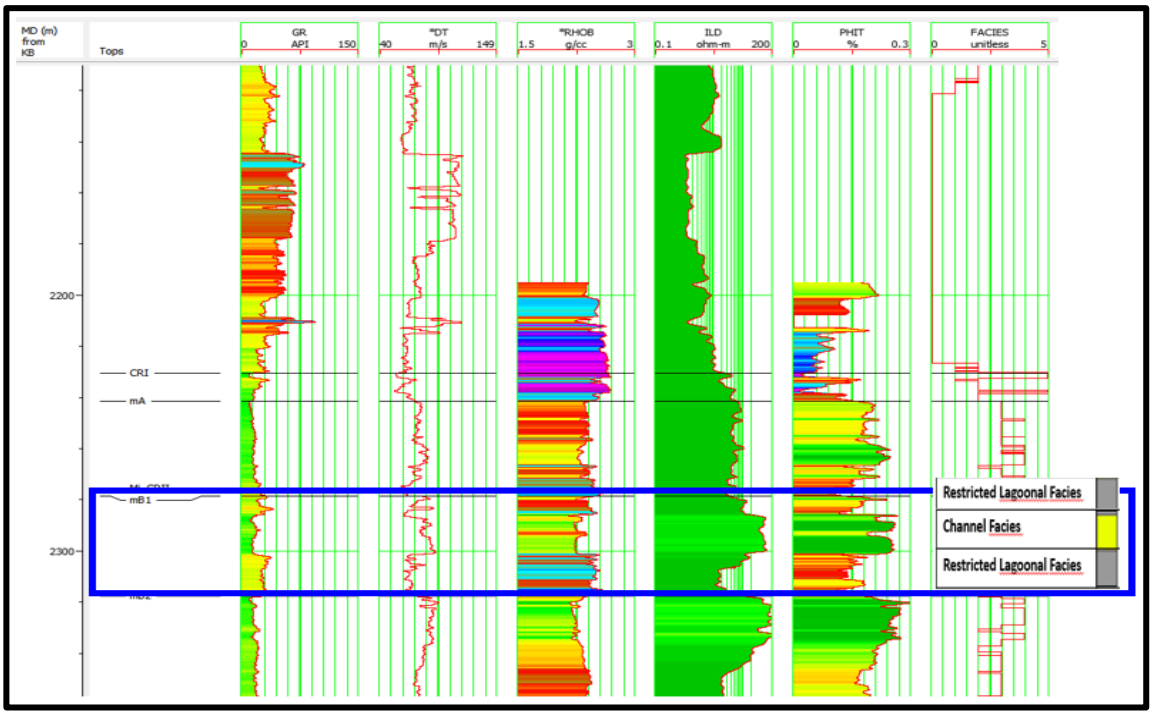

Figure 5.23. A comprehensive well-log display shows different facies in the mB1 Mishrif tidal channels zone (WQ1_B81).

5.5.3.2 Generation of Seismic Lithology Maps

Lithofacies classification was based on well data and several internal attributes created based on the correlation and errors used for the neural network. PNN was applied to the high-resolution West Qurna seismic dataset to classify channel fairway facies. The final product was a 3D facies volume of most likely classes. Combined with analysing petrophysical features of channel facies, two types were identified from 3D facies volume. As mentioned in the depositional sequence, we interpreted these two facies as channel facies surrounded by restricted lagoonal-filled mud facies (Figure 5.24). The final

lithofacies map was consistent with existing core data (well-controlled) and delineates the facies distribution of the mB1 channel zone. The outcomes of the seismic lithology demonstrated that the probabilistic neural network approach produced findings similar to those acquired from seismic inversion results and seismically porosity derived.

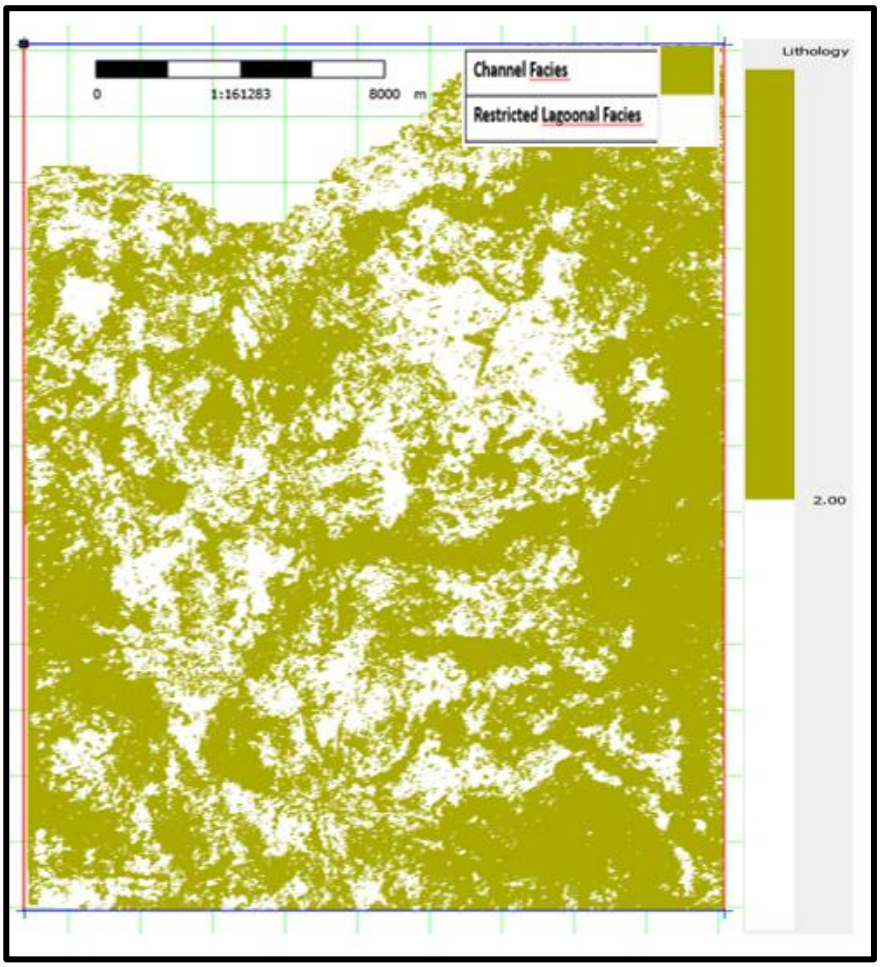

Figure 5.24. The horizon of mB1 channellized facies is based on a probabilistic neural network (PNN), the facies are defined (channels and restricted lagoonal facies).

5.6 Summary and Conclusion

In this chapter, petrophysical analysis is integrated with seismic data to determine the distribution of channel bodies and their petrophysical properties. The probabilistic neural network (PNN) and linear regression method were undertaken to detect an additional channel distribution. Also, this work demonstrates that artificial neural network algorithms can classify heterogeneous channelized systems. In addition to the fairway distribution, causal insights were derived from the available datasets. From this chapter, we can conclude the following points:

- The resulting 3-D Mishrif channel characterisation corresponds to the sequence stratigraphic analysis and the depositional environments described previously in the literature review. Advanced well data analysis and core thin sections provided a good understanding of Mishrif channelized facies. Compared with modern channels, it was highly valuable in acquiring information about channel fairways detected in the study area. The outcrop date provided knowledge of the types of channelized systems that are usually deposited in geological settings similar to the study area and helped stratigraphic correlations and, therefore, the prediction of the reservoir heterogeneity.

- The RMS surface and acoustic impedance attributes have been applied to the seismic volume, and they were valuable in delineating and giving information about the channel geometries. However, frequency spectral decomposition with colour blending provided a better geo-body extraction of the Mishrif mB1 zone and different depositional environments within channels than the seismic attribute surfaces.

- Acoustic impedance volume and the seismically-derived porosity model have helped define the main trends of different channel fairways. To derive a porosity model, the PNN algorithm was trained to determine the optimal nonlinear connection between the actual porosity log and seismic attributes. The PNN results, combined with the linear regression approach, provide a means of geologically realistic channel distribution and improve the subsurface physical property.

- The PNN logarithm has been successfully employed to classify and predict seismic lithology. Results show that the Mishrif mB1 zone is clustered into two different heterogeneity-quality lithofacies (channels and restricted lagoon facies).

- An incorporating interpretation of geology, geophysics, and petrophysics is significant in providing an enhanced understanding of complex carbonate tidal channels. An improved 3D channelized facies classification is crucial for raising the confidence for sweet oil spots, along with a water injection plan.

Chapter 6. Constraining the Porosity Model of the Mishrif Channelized Fairways Using 3D Seismic Data

In the processes of reservoir characterisation and interpretation, seismic attributes are being employed increasingly. They have been shown to be very helpful in improving the quality of the reservoir characteristic distribution in the areas between wells and those without wells in the property models. This chapter is organized as follows. First, we give an introductory overview, and the chapter methodology. Then, we describe the results, including seismic inversion, a framework for building a 3D model, and probabilistic algorithms used for the spatial distribution modelling porosity of the Mishrif mB1 tidal channel zone. Then, we use the seismic data to constrain the petrophysical property model. Finally, we evaluate and discuss the comparison between two porosity models for the Mishrif mB1 tidal channel zone with different data sampling, to assess the impact of the seismic data on the property modelling.

6.1 Introduction

In Chapter 4, we found seismic inversion was related to porosity through a negative correlation. Here, we can improve porosity modelling under using a different understanding of the second variable used as second input data with primary input data. Additionally, in the previous chapter, we demonstrated how to apply multi-dimensional approaches to describe all features of the Mishrif tidal channels as well as its contribution to improving reservoir characterisation. The scope of this chapter is to investigate and identify the spatial distribution of porosity in the mB1 channelized zone. Secondly, we aim to evaluate how the chosen seismic inversion affects the 3D property model and controls the porosity distribution (e.g., Budkina *et al.*, 2014). The contribution of the work is that such a workflow has incorporated high-resolution seismic data into the property model in the Mishrif reservoir. Enhancing the porosity models with seismic data will assist in a better comprehension of the behavior of the channelized carbonate reservoir throughout the exploitation of the field.

6.2 Methodology, Data

When seismic inversion is conditioned in the property modelling, the model's accuracy will be improved (Yong *et al.*, 2014). Therefore, seismic data can be fully utilized to model performance and add value to the field development and production outcome. In this chapter, we used seismic data in the property modelling of the Mishrif channelized reservoir in the West Qurna/1 oilfield to better understand the channelized system, porosity distribution and observe the contribution of the secondary variable. Based on the data available, as described previously in Chapter 3 (which includes a 3D seismic dataset, and conventional logs from 105 wells) a 3D property model of the Mishrif mB1 zone was built using Petrel software. The workflow (Figure 6.1) is divided into four discrete parts (e.g., post-stack seismic inversion, structural modelling, property modelling and constrained property modelling, and comparison of two models). The Mishrif mB1 zone model was designed through these steps for property modelling:

a) The workflow started with quality control of the database using commercial reservoir modelling software (Petrel® Schlumberger, 2011).

b) The post-stack seismic inversion was the first step in the workflow, as described in Chapter 4 using GeoSoftware (Hampson Russell Suite see section 4.4; for more details).

c) The grid was built to represent the structural framework by combining seismic interpretation, structural analysis, and stratigraphic correlation, and the geometry definition to establish the area of interest. The model was constructed with zones and layers based on the stratigraphic data.

d) Before incorporating seismic data into the porosity model, it is essential to understand the relationship between the primary and secondary variables and decide whether the secondary input could be used for the conditioning modelling (Schlumberger, 2011). The correlation coefficient will be estimated between primary and secondary at the upscaled well data (see Figure 6.16). Conducting a crosspost analysis and computing the correlation can help identify valuable secondary attributes or rule those out that show little or no correlation (Schlumberger, 2011). Paying attention to the magnitude of the correlation coefficient is important. Hence, a strong negative correlation may also be advantageous since the relationship need not have a positive correlation to be beneficial (Ma and Zhang 2019).

e) Various averaging techniques (arithmetic, geometric and harmonic) are available for scaling up well log data to describe the spatial continuity of the porosity data. Arithmetic averaging is usually applied to properties such as porosity, saturation, and net/gross since there are additive variables; hence it is the most common of porosity upscaling. It is an average approach to grid cells to establish their spatial distribution based on the sum of a collection of numbers divided by the count of numbers in the sample.

The porosity model is then stochastically distributed using Gaussian Random Function Simulation (GRFS) to generate the realizations without using the second variable (seismic inversion) (see Chapter 2, section 2.3.3 for more details). Stochastic simulation's major objective is to represent the heterogeneities of physical characteristics (Ma and Zhang 2019). Deterministic approaches are frequently not a preferred option when the heterogeneity of spatial properties is high; therefore, their model will decrease the heterogeneity. Keeping a property's heterogeneity in its model and reducing smoothing are two of stochastic simulation's key goals. In contrast to interpolation, which only considers the mean value, geostatistical simulation approaches maintain the variation in

the data. The probability distribution function describes the data distribution pattern, and the variogram describes the structural characteristic of a geological body. For estimating reservoir parameters far from known sites (well observations), Gaussian Simulation encompasses a variety of comparable techniques (Ringrose and Bentley, 2016).

Sequential Gaussian Simulation is one of the most stochastic simulation techniques used in the spatial domain based on kriging for the reservoir characterisation of the petrophysical properties. The SGS method is a conditional simulation that operates in the multi-gaussian random function mode and adheres to a sequential premise (GhojehBeyglou, 2021). In contrast to estimating techniques like regression and kriging, the method can preserve the supplied data's distributions, trends, and variograms. The probabilistic distribution function and the variogram are the two primary categories of input parameters for this technique. The probability distribution function describes the data distribution pattern, and the structural characteristic of a geological body is described by the variogram (Yong *et al.,* 2014). The work of the SGS method is carried out cell by cell sequentially, using a randomly chosen path that passes through every cell in the model and gives each cell a value for the simulation. Local highs and lows are produced between data points that honour the variogram during the simulation. The software uses a random number to determine the locations of these highs and lows. As a result, several realizations must be created to understand the ambiguity. For the approach to work, the reservoir property needs to have a Gaussian distribution, otherwise it will conduct a rank transform, turning the data into a standardized normal distribution. One benefit of Sequential Gaussian Simulation is the simplicity with which the input data may be respected because the input samples are employed as conditioning data in the approach (Ma and Zhang 2019) (see more details in Chapter 2, section 2.3.3).

The second method, Gaussian Random Function Simulation (GRFS), is a mathematical approach that considers changeable probabilistic and structural features in space for characterizing heterogeneous reservoirs and is based on statistics of geologic body parameters. GRFS is a conditional simulation based on parallel kriging, serving as its estimate foundation and unconditional simulation. Parallel kriging offers very accurate estimates and may be used with a variety of kriging extensions and other gaussian approaches. With high-quality model outputs, the parallel approach speeds up the kriging process's execution time (GhojehBeyglou, 2021). The second part of GRFS is an unconditional simulation built on the fast Fourier transform (FFT). The Fourier integral

approach is useful for creating random function realizations in multidimensional sections. The input statistical parameters' means, variance, and variogram can be reproduced more accurately via spectral simulation, since simulations are carried out in the frequency domain (Daly *et al.*, 2010). Also, another characteristic of the GRFS method is the reproduction of the variogram better than the SGS method because the standard search for the variogram correlation tends to find highly correlated neighbours along with the vertical wells.

Due to the usage of FFT, GRFS is quicker than SGS. SGS was first applied locally by extending the common practice of kriging to a nearby community. The SGS method has the disadvantage that large-range continuities might not be recreated. On the other hand, using a big neighborhood has the theoretical issue of implicitly assuming global stationarity and the practical issue of processing expense (Ma and Zhang 2019). Also, using collocated co-kriging with GRFS is fast and generally better than the equivalent option with SGS because the option for immediate modification of the correlation between primary and secondary has been implemented. Also, there is no systematic bias in the degree of variability of the simulated variables as in SGS. As a result, input recovery will be improved; primary and secondary variables' correlation will also increase. Consequently, the GRFS has more advantages and is more robust than SGS for honoring statistical input parameters, such as mean, variance, and variogram. It is faster to run and supports the collocated co-kriging.

The second stage of the modelling process incorporated secondary information into the porosity model using the collcoated co-kriging approach in the GRFS and SGS . It aims to predict an unknown property using the primary variable's values combined with another variable (secondary), which is ubiquitous and cross-correlated with the primary variable. The advantage of this method is that it is simple and fast due to the good permanence of using a data form, such as resampled seismic attributes (high density), to predict porosity at the well position (low density). It uses a correlation coefficient of the modelled secondary variable (Schlumberger, 2011) (see Chapter 2, section 2.3.4 for more details). The primary (porosity well log data) and the secondary variable (seismic inversion volume) are assigned parameters to the generated 3D-constrained property model. Based on the analysis of the strong negative correlation between the two variables, acoustic impedance (AI) volume is incorporated into the 3D porosity model to guide the porosity value in the condition of horizontal and vertical impedance constraints. The co-

simulation with secondary variables usually presumes that the second variable is available in a collocated form at the exact cell location or position as the cell is about to be simulated (Schlumberger, 2011). Finally, the constrained model is established (see Chapter 2, section 2.3.5 for more details).

f) These models were ultimately subjected to comparison and other validation procedures.

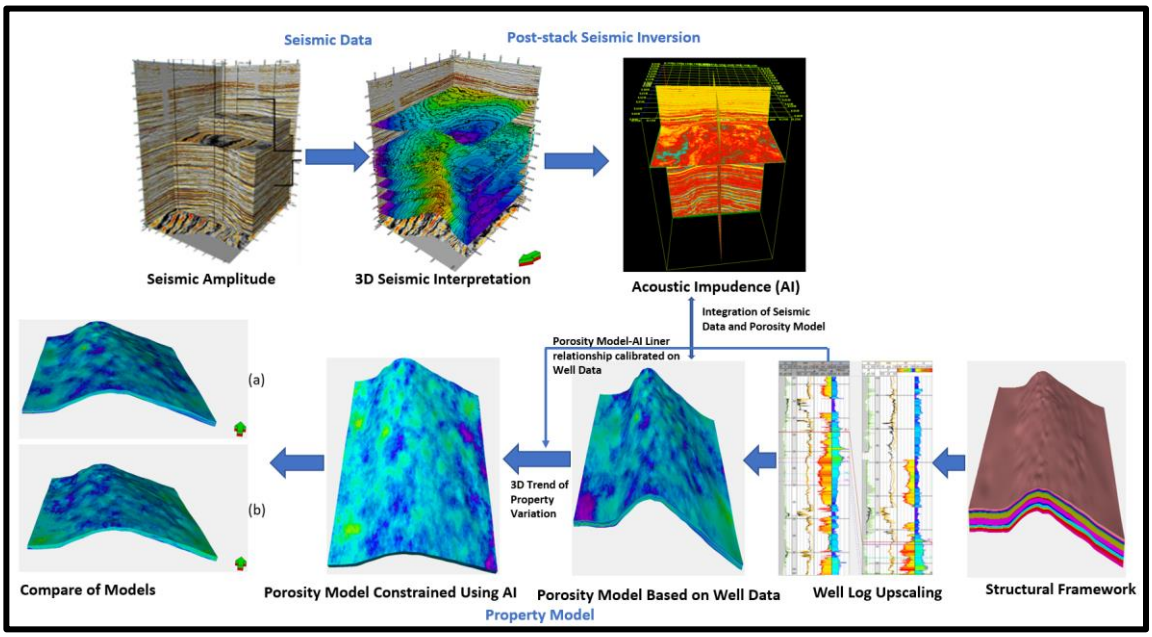

Figure 6.1. Schematic overview showing the modelling workflow for generating different porosity models for the Mishrif mB1 tidal channelized zone started from seismic amplitude, seismic inversion, and ending with building two different porosity models.

6.3 Seismic Inversion

Seismic attributes are increasingly being employed in reservoir characterisation and 3D property modelling. The seismic inversion is more useful than seismic amplitude in the delineation of the reservoir properties. The conversion used a model-based technique focused on the Mishrif mB1channlized zone. We will use acoustic impedance (AI) volume (Figure 6.2) as a secondary variable to constrain the 3D porosity model.

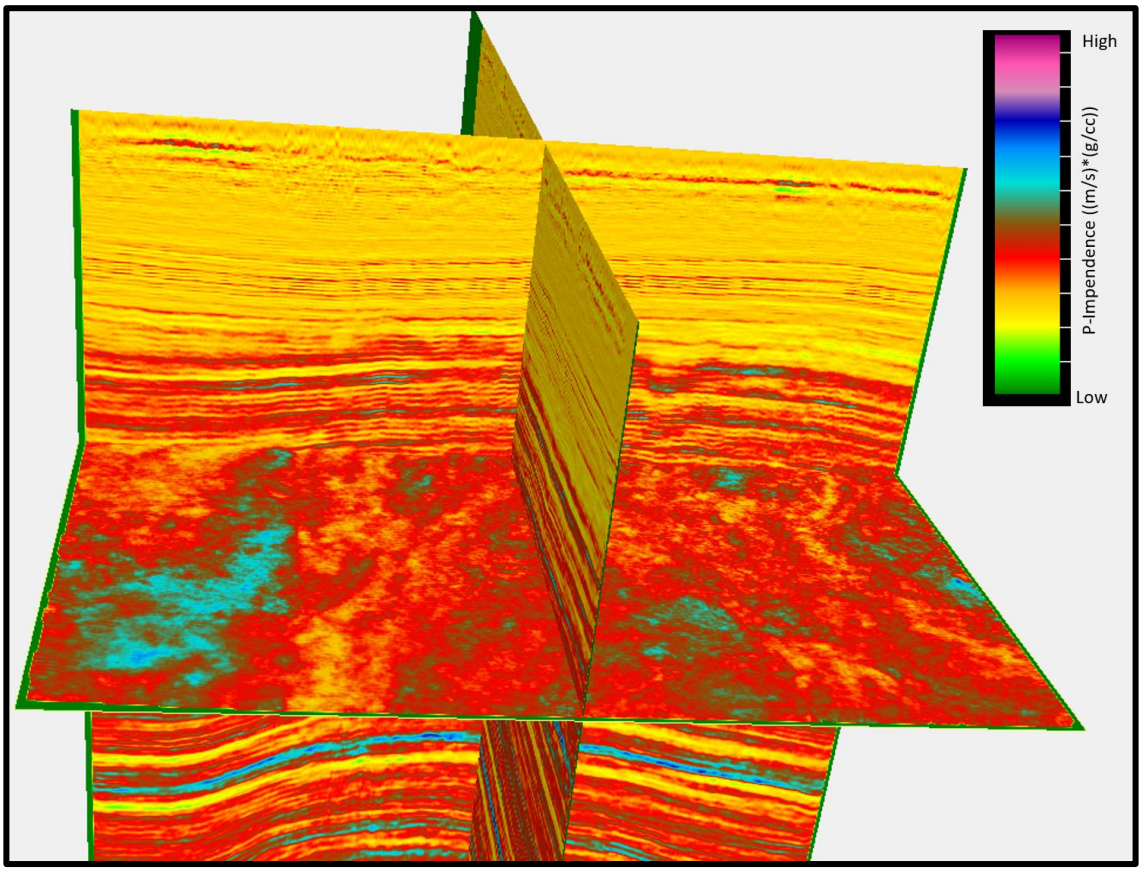

Figure 6.2. The acoustic impedance volume was used as a secondary variable to constrain the 3D porosity model (yellow and red colours indicate low acoustic impedance, while purple colour indicates high acoustic impedance).

6.4 Analysing the Relationship Between Primary and Secondary Variables

Following the step of seismic inversion generation outlined in the previous section, several evaluation and validation steps should be applied to the property model. Analysing the correlation between the primary and secondary variables is important while using collocated co-kriging. Determining how strong the secondary variable's impact should be on the results, 1 or -1 means 100 % correlation, while zero means no correlation; hence a smaller weight has a minor impact, and a more significant weight has a big impact (Ma and Zhang 2019). The key difference is that the primary data only contain a small number of sample points (such as a small number of upscaled well logs), but the secondary data are present in all grid cells (such as a resampled seismic attribute, more details are given in section 6.7 of rescaling seismic inversion into the 3D porosity model.

Averaging was undertaken to match the difference between the well log and seismic inversion resolution and to better compare the two datasets. Thus, the averaging of the upscaled porosity logs and acoustic impedance (AI) property were plotted to calculate the correlation coefficient by the best linear regression. The averaging was carried out to get a better comparison of the two datasets. The seismic inversion is a large scale, and the log scale is a small scale in resolution. The averaging over the mB1 zone was a way to have them with the same resolution. The calibration's AI with porosity has a negative correlation coefficient of -0.70 in the Mishrif-mB1 channelized zone based on 20 wells distributed between and outside the channel fairways (Figure 6.3). This negative correlation was also confirmed in Chapter 4 (see Figure 4.5) based on rock physics analysis between porosity and P-Impedance from the well data of the reservoir. Hence, the acoustic impedance (AI) volume will be used as a secondary variable to constrain the porosity model using a correlation coefficient.

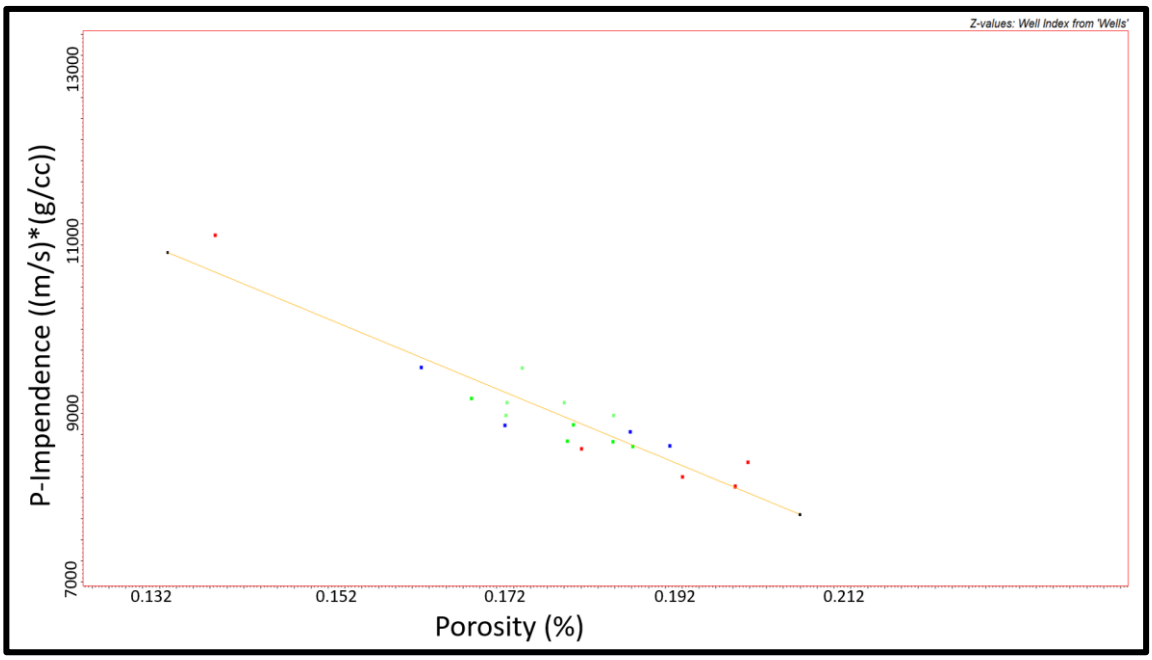

Figure 6.3. Cross-plot for the upscaled porosity well log and the acoustic impedance (AI) property calibration showing a negative correlation coefficient of -0.70 of the mB1 channelized zone (the colour data points indicate the wells that used in correlation).

6.5 Structural Modelling

6.5.1 Mishrif Top Horizons

As stated in chapter 3, a structural model was created based on interpreting the seismic horizons, formation tops, and interpreted faults. Five Mishrif horizons from top to bottom zones (CRI, mA, mB1, mB2, mC) were interpreted using seismic well-ties. At first, horizon interpretation was made in the time domain and then transferred into the depth domain using the velocity model in the Petrel project to generate top surfaces that were used as the input when building the 3D structural model (Figure 6.4).

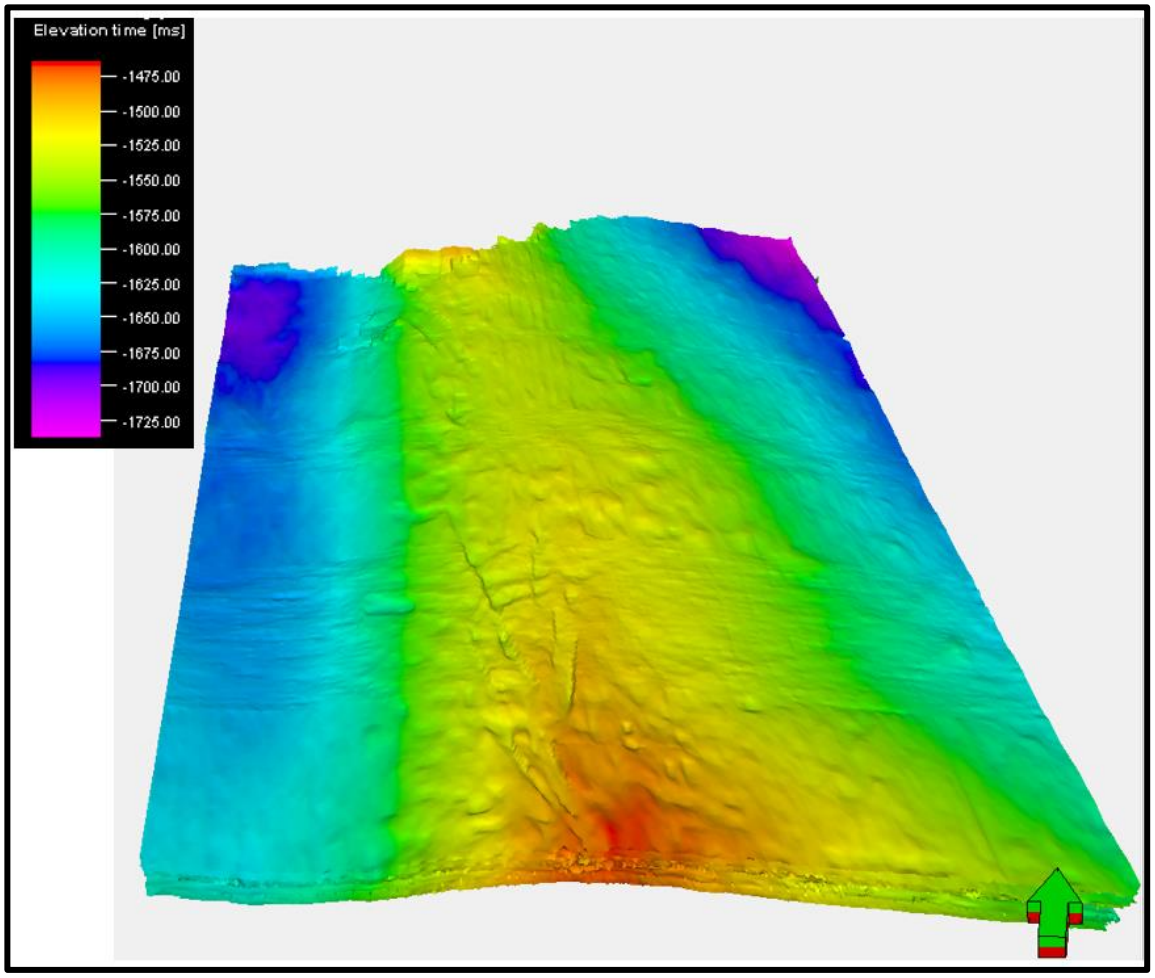

Figure 6.4. Mishrif horizons are based on seismic interpretation from top to bottom, including the mB1 channelized zone.

The middle sector of the field was selected for the modelling due to the main channel fairway location in this sector. Also, it has a good distribution of wells. The grid resolution

was designed for a 3D property model of the mB1 channelized zone to allow reasonable computation for the modelling procedure. Initially, there were 537 x 317 x 84 cells in x, y, and z directions, respectively, with each cell having an aerial dimension of 50 x 50 metres (Figure 6.5). We should build the model with the exact dimensions that are covered by the acoustic impedance (AI) boundary; the new grid size becomes 382 x 317 x 84.

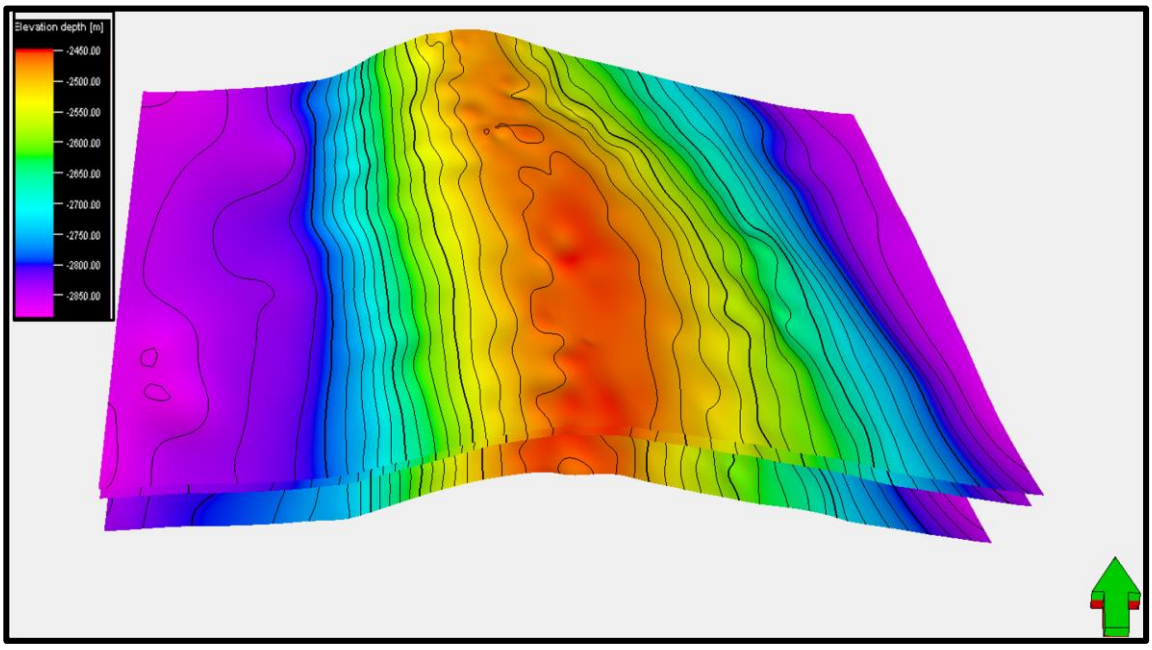

Figure 6.5. 3D Mishrif static model (Top structures of the CRI, mB1, Ahmadi Zones). The colour represents depth.

6.5.2 Fault Modelling

A reservoir model typically depicts faults as single, planar structures. However, they are intricate, three-dimensional structures that include fractures and deformation bands in damage zones. West Qurna/1 3D seismic data with high resolution reveal a wealth of information on the architecture and structural settings. The fault system of the West Qurna/1 oilfield was explained previously in Chapter 3 for the Mishrif reservoir and other reservoirs. The Mishrif reservoir has a complicated structure and comprising a variety of steep fault zones that vertically split and established a general pattern trending northwest and northeast direction. The presence of any possible compartments was determined using a fault throw analysis to estimate the throw displacement of each fault in the model. The faulting pattern analysis reveals extensional and en-echelon faults, which are wrench

faults. Most of these faults are extended through the Mishrif zones from the top CRI to the Ahmadi Formation. Figure 6.6 shows the fault network through Mishrif mB1 channelized zone, and fault displacement is expanded from 8 meters to 40 meters.

Additionally, regional trends of the faults in the data were investigated by West Qurna/1 seismic data (see section 3.6.5 in Chapter 3 for fault array and seismic attribute analysis). As an illustration, Figure 6.7 shows fault segments through the Mishrif mB1 channelized zone. The compartments comprised 51 fault segments defined from north to south according to the orientation of the bifurcating faults. Any fault with a throw displacement of more than 10 meters was highlighted as a possible segment. Based on the fault model, it can conclude that fault juxtaposition appears to provide clear communication and transmissibility between Mishrif zones and potentially act as a thief zone of water injection energy, diverting additional injection energy away from the main depleted zones.

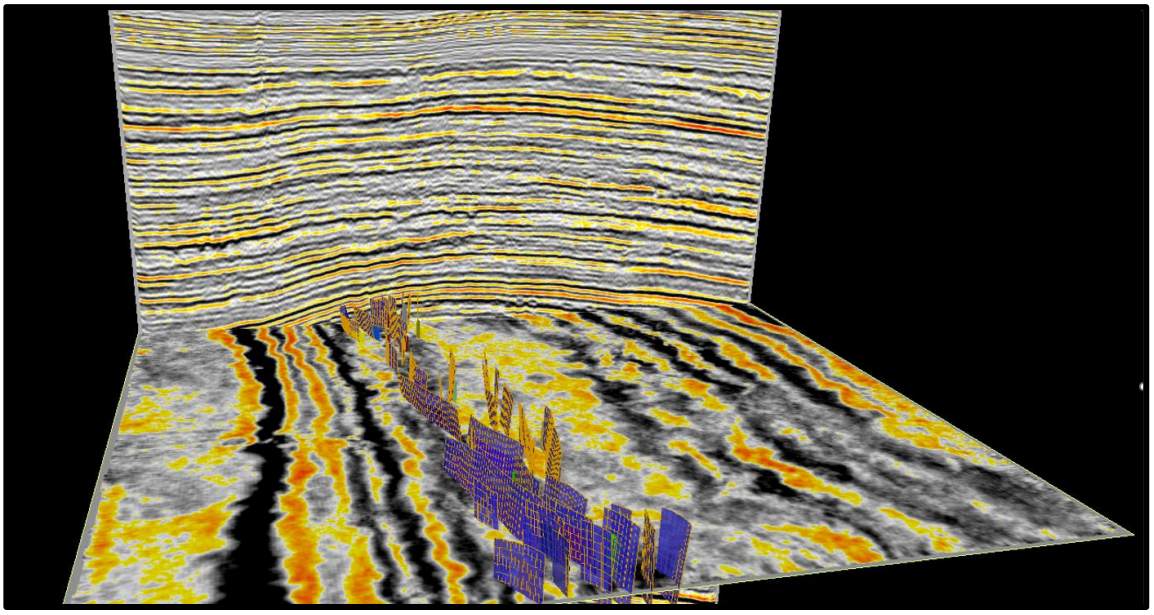

Figure 6.6. Seismic depth slice through mB1 channelized zone illustrates extensional and en-echelon faults, the 51 faults identified from the seismic cube and located in the model.

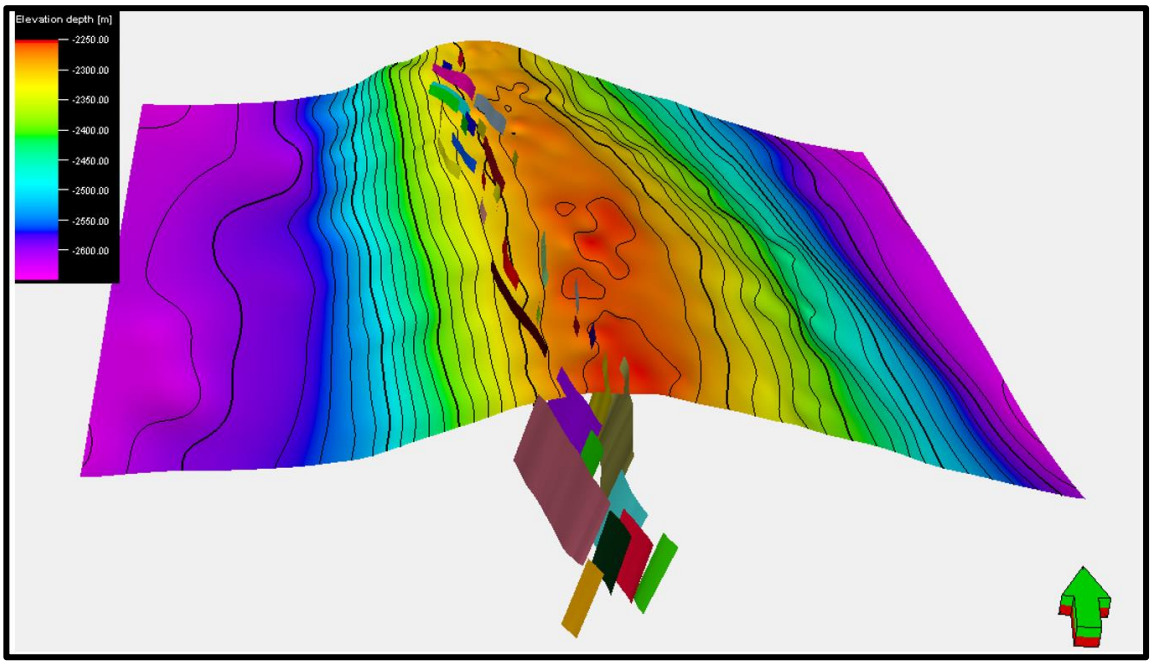

Figure 6.7. An illustration of the Mishrif faulted network model through the Mishrif mB1 channelized zone. The colour represents depth.

6.5.3 Reservoir Zonation

The Mishrif reservoir zonation was created based on core and well log data, and it was divided into 15 zones (Mishrif mB1 channelized zone being one of these zones); the zoning was built according to the rock properties (porosity, permeability, and lithology). Based on the stratigraphic correlation of the reservoir and the well-top markers (Figure 6.8), an isochore map for each zone was produced, hence creating similar zone characteristics while keeping a sufficient thickness for each zone (Figure 6.9). The zonation process in the model was carried out under quality checks by inspecting all of the horizontal well trajectories since most wells are vertical and have been drilled to depths of more than 2000 meters. Several of these wells were drilled in different zones.

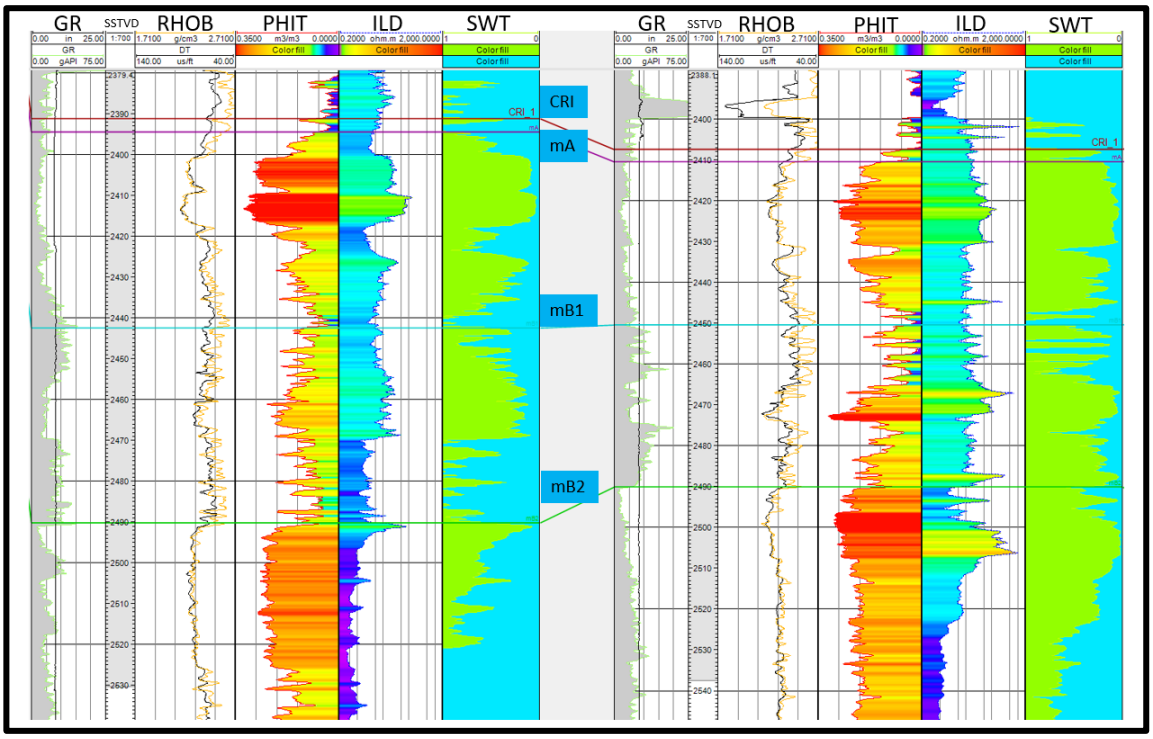

Figure 6.8. An example of the well correlation throughout the Mishrif reservoir. The first track represents the gamma-ray log. The second track is depth. On the third track are density and sonic logs. The fourth track is porosity log (neutron and density logs). The induction log is displayed on the fifth track. The last track represents the water saturation calculation.

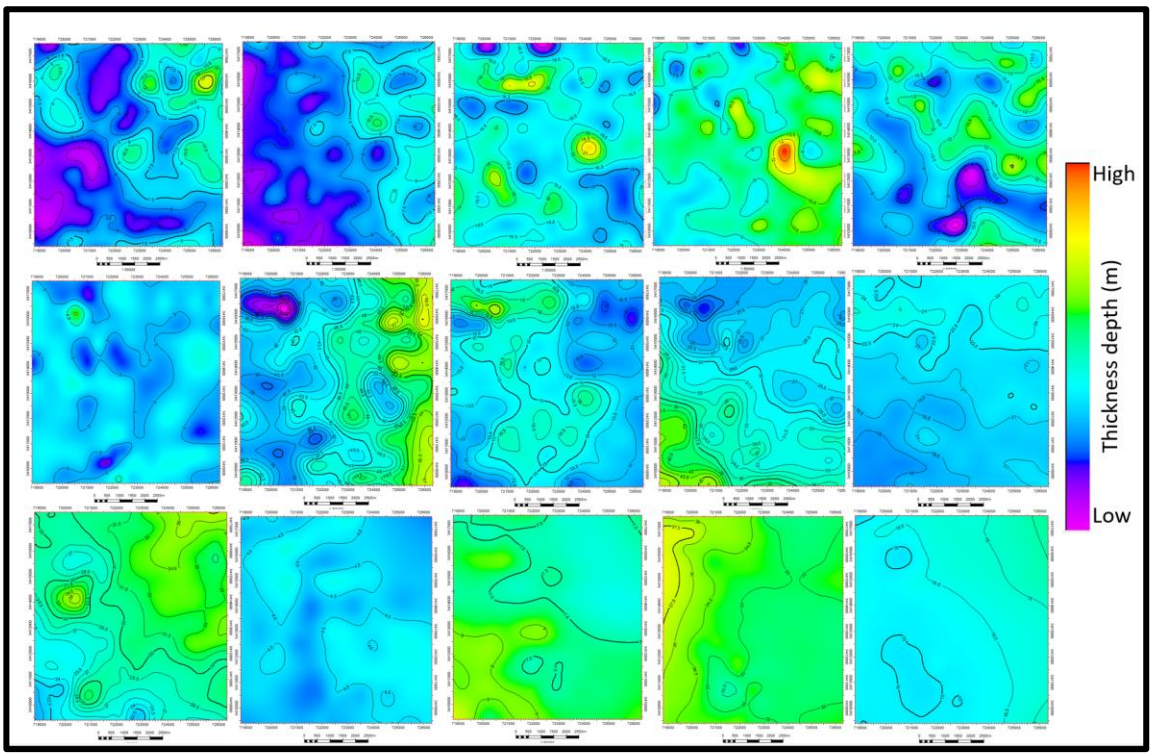

Figure 6.9. Isochore maps were generated, 15 primary subzones of the Mishrif reservoir were built using these maps. The colour indicates the thickness.

6.5.4 Layering

In terms of the geological structure, the study area is a north-south trending anticline, steep on the western flank and gentler on the eastern flank (Wang *et al.*, 2019). Depending on the number of layers chosen, the Mishrif reservoir will be subdivided into layers of similar thickness. Table 1 shows the layering of each zone. In order to match a log tool's vertical resolution as closely as feasible, the layering schemes' grid resolution was created. Eighty-four layers make up the final layering. The mB1 channelized zone was divided into 70 layers based on the bed thickness seen in the core and variations in porosity (Figure 6.10). Therefore, due to the geological heterogeneity, the vertical resolution varies across the mB1 channelized zone and can be as low as one meter.

Name	Color	Calculate	Zone division		
CRI_N_Iso		Yes	Proportional	Number of layers:	1
CRI_1_N_Iso		Yes	Proportional	Number of layers:	1
mA_N_Iso		Yes	Proportional	Number of layers:	1
Mi_mA_1_N_Isc		Yes	Proportional	Number of layers:	1
Mi_mA_2_N_Isc		Yes	Proportional	Number of layers:	1
Mi_CRII_N_Iso		Yes	Proportional	Number of layers:	1
mB1_N_Iso		Yes	Proportional	Number of layers:	70
mB2_N_Iso		Yes	Proportional	Number of layers:	1
Mi_mB2_2_N_Is		Yes	Proportional	Number of layers:	1
Mi_mB2_3_N_Is		Yes	Proportional	Number of layers:	1
Mi_mB2_4_N_Is		Yes	Proportional	Number of layers:	1
mC_N_Iso		Yes	Proportional	Number of layers:	1
Mi_mC_1_N_Isc		Yes	Proportional	Number of layers:	1
Mi_mC_2_N_Isc		Yes	Proportional	Number of layers:	1
Mi_mC_3_N_Isc		Yes	Proportional	Number of layers:	1

Table 1. Detailed the layering scheme in the Mishrif reservoir modelling, including the mB1 channelized zone.

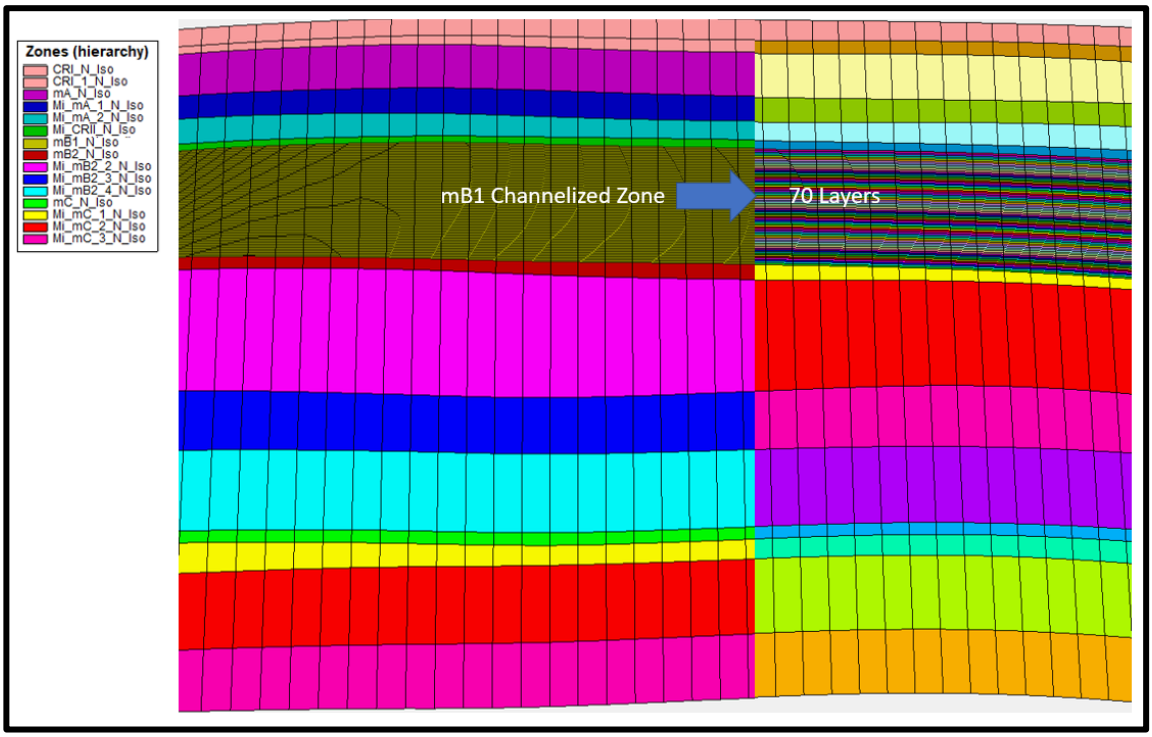

Figure 6.10. Illustration of the zonation and layering scheme for Mishrif reservoir modelling, mB1 channelized zone divided into 70 layers, with the majority of others intervals represented by a single layer in the model.

6.6 Porosity Modelling

The neutron and density logs were combined to determine the total porosity. Initially, these logs were scaled up into the 3D grid using arithmetic averaging (Figure 6.11). As mentioned in the method section, arithmetic averaging was used to scale up these logs into the 3D grid to describe the spatial continuity of the porosity data (Ma and Zhang, 2019). The average layer thickness is 70 cm and the average data points is seven per layer. The upscaling is very important to predict large-scale pore space behavior and spatial distribution when incorporating upscaled descriptions of that structure. The porosity model was constructed using the porosity log from the 105 wells. This approach was founded on the idea that we have a reasonably good distribution of the well control on the porosity. Hence for forecasting the porosity, there will be no problem; only in the inter-well regions could there be a concern.

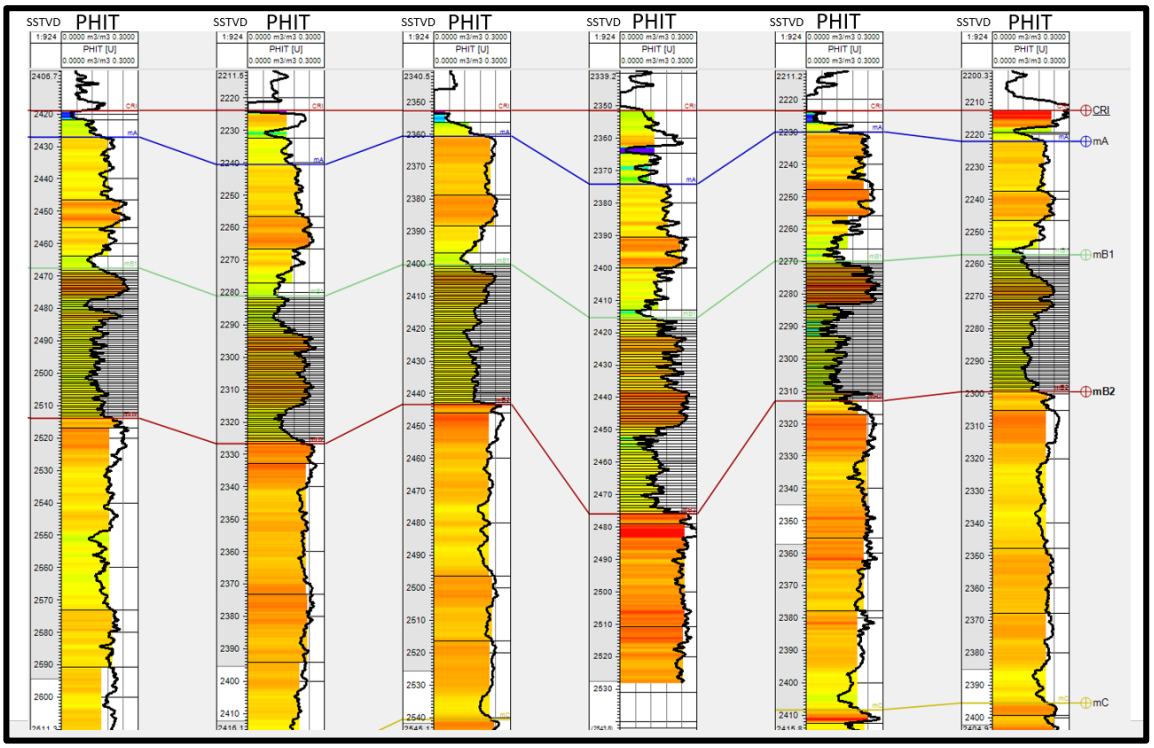

Figure 6.11. Example of upscaled porosity logs. The upscaled values are shown by the background colour, while the black curve depicts the porosity logs.

Commercial software programs such as Petrel offer several methods for the statistical upscaling of reservoir properties. The upscaled porosity data are carefully considered at the mB1 channelized zone to understand spatial variation and data distribution. Quality check is applied for matching the porosity model values: a) matching the porosity model values to the upscaled well log; b) matching the porosity model values to the original porosity log data. It can be seen that there was only a small variation in the pore volume when validated in the mB1 channelized zone (Figure 6.12).

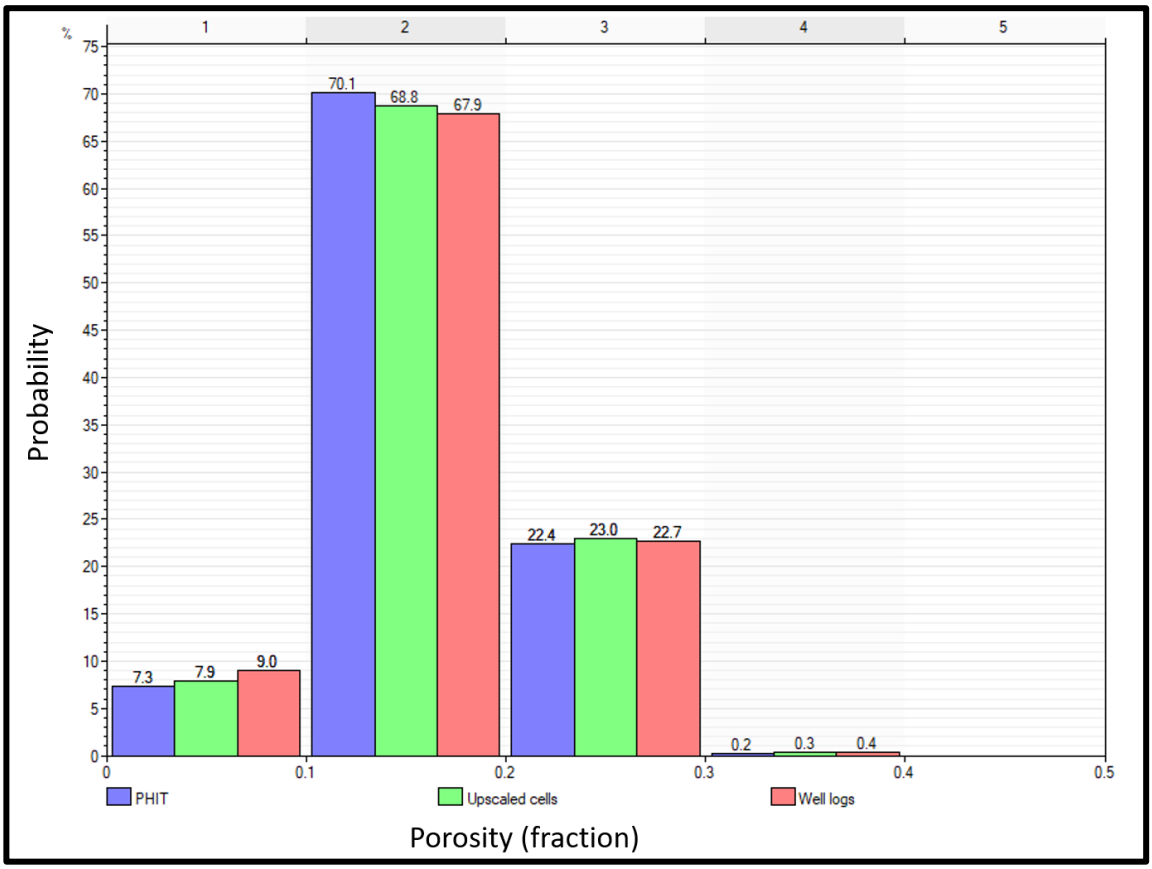

Figure 6.12. Histogram of the porosity model distribution in the mB1 channelized zone by matching the distribution to the original well logs and the upscaled.

Following that, we can define the variogram parameters involved in building the porosity model. The spatial variation of petrophysical characteristics is described using the variogram statistical approach. The approach presupposes that the correlation between closely spaced samples is more probable than between samples farther apart (Ringrose and Bentley, 2016). The variogram represents the spatial variation or the level of discontinuity of the geospatial property. An indicator variogram is an expression of the size of lithofacies bodies. Ideally, the variogram should be estimated from the geologic conceptual model, which describes the Mihrif reservoir as being deposited in a shallow-marine carbonate rock consisting of fine-grained carbonate, or from analog and modern data. Another technique is using seismic attributes as a proxy for horizontal variograms and finding ranges in major and minor directions. The reservoir distribution in the lateral direction can be partially reflected by seismic inversion, according to the association between AI inversion and porosity (Liu *et al.*, 2019). Hence, under the control of geological knowledge and the lateral prediction of the reservoir by seismic data (seismic

inversion), the following variogram parameters are established, which makes the model more reasonable and reliable:

- The horizontal major and minor direction variogram ranges were set to 1300 m and 1000 m, respectively.
- The vertical range was estimated to be 20 m.

After confirming the validity of the variogram parameters, we have selected Gaussian Random Function Simulation (GRFS) due to the applicability of this method using two or more variables, mainly if the primary variable is undersampled in the inter-well regions (Ma and Zhang, 2019). In contrast, the secondary variable(s) have more data available, such as 3D seismic inversion, and have a more thorough and broad coverage than the primary reservoir parameters (such as porosity and permeability), which often offer limited data (Ma and Zhang 2019). This method differs substantially from the Sequential Gaussian Simulation (SGS). It is typically faster than SGS and has a fast collocated co-simulation option to investigate the impact of the secondary variable on the porosity model, which is adopted to improve the consistency between the model and geological knowledge (Liu *et al.,* 2019).

Due to its parallel computing design, the GRFS algorithm can replicate distributions more precisely and quickly than SGS (Daly *et al.,* 2010). Several realizations were produced using Gaussian Random Function Simulation for three intervals (upper, middle, lower) of the mB1 channelized zone, and the resulting porosity model was created using the porosity from the well data (more details in section 6.8). It is important to mention that the density-neutron logs, calibrated and confirmed using core data, were used to generate the porosity log model in each realization.

The uncertainty in the highly heterogeneous Mishrif reservoir arises from the spatial distribution of porosity and permeability ambiguity between the wells. Therefore, a blind test was used for quality assurance and confirmation of all results to remove bias from the well selection procedure. The blind test was repeated on 12 wells not used for porosity modelling with a good distribution, as shown in the distribution map (Figure 6.13).
A comparison between the actual porosity log and the blind test model as shown in Figure 6.14. This comparison is between the blind porosity model (the background colour) and the actual porosity log (the black line) at the exact location of the six different wells. These wells indicate a reasonable consistency with a different acceptable range to predict

the porosity between the wells. The advantage of this test is that it allows us to reduce the model's uncertainty and eliminate bias in the selection process of the well.

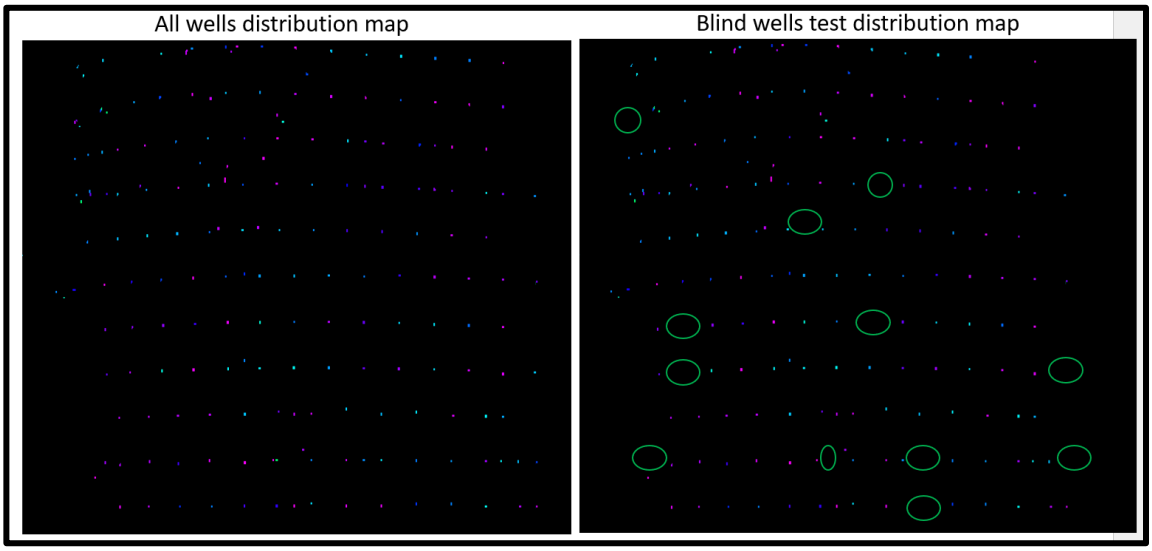

Figure 6.13. The distribution map of the location of all wells used in the original porosity model (left) and the distribution map of the blind wells (the green circles represent the location of these wells) used in the blind well test (right).

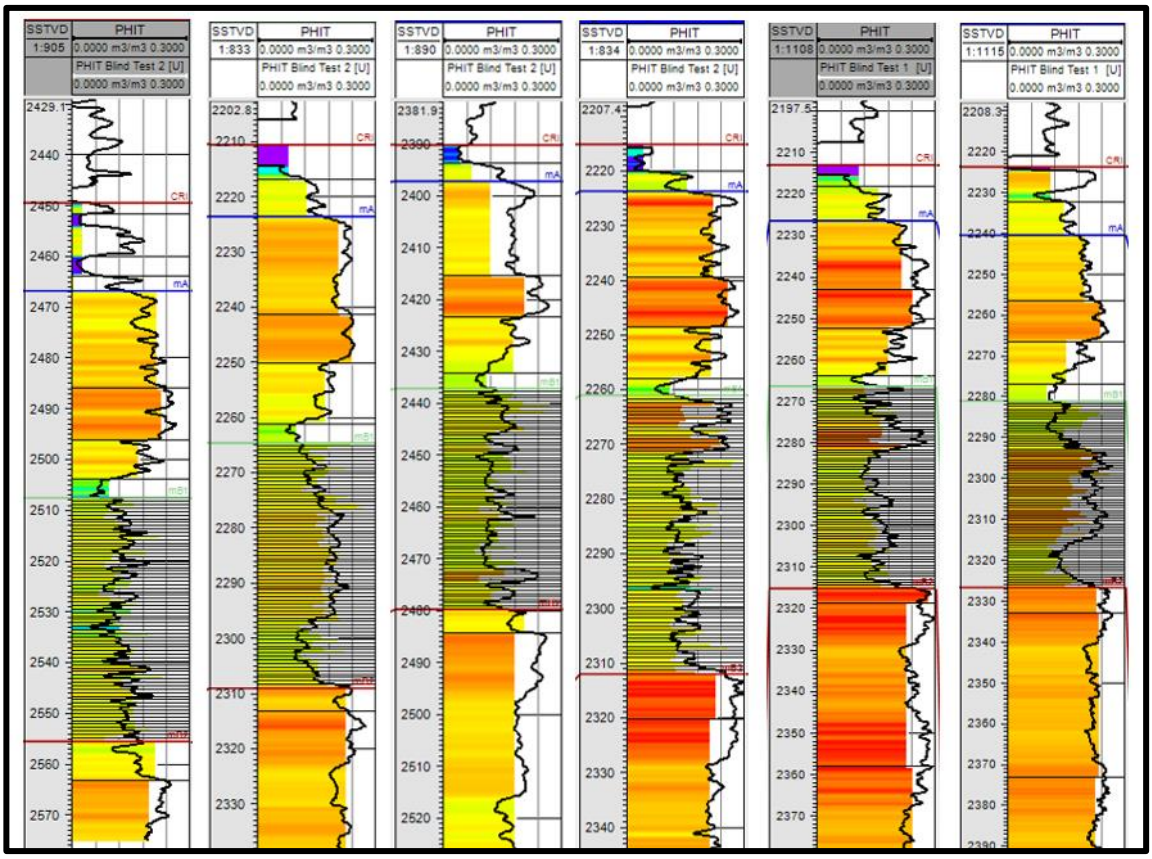

Figure 6.14. The comparison between the blind porosity model (the background colour) and the actual porosity log (the black line) for the six different wells.

6.7 Rescaling Seismic Inversion into 3D Model Framework

The geometric modelling process could generate the properties using a predefined system such as seismic resampling, cell volume, and zone index. Under the geometric modelling setting, we have chosen seismic resampling. Rescale was carried out for the acoustic impedance (AI) volume into a 3D property model framework. Initially, this process requires that the seismic volume is in the same domain as the 3D grid. In the dialog box in Petrel, we selected acoustic impedance volume. Then, the harmonic averaging method was selected when applying volume weighting, giving each cell a numerical value corresponding to the structural model framework. Another parameter was called the quality of the seismic resampling; the interpolation was chosen, and each property cell will be a weighted interpolation of the four seismic cells closest to the center of the grid cell. This approach is high-speed and suitable for resampling continuous value volumes and slightly lower-resolution grids (Schlumberger, 2011). The resulting acoustic impedance property of the mB1 channelized zone is shown in Figure 6.15 for the upper and lower intervals. This simulated property is then used as a secondary variable in each cell. To evaluate the results, the resampled AI is compared with the porosity well log (Figure 6.16). It is observed that there is a good correlation between well porosity and upscaled AI, mostly in thick grainstones with low AI values.

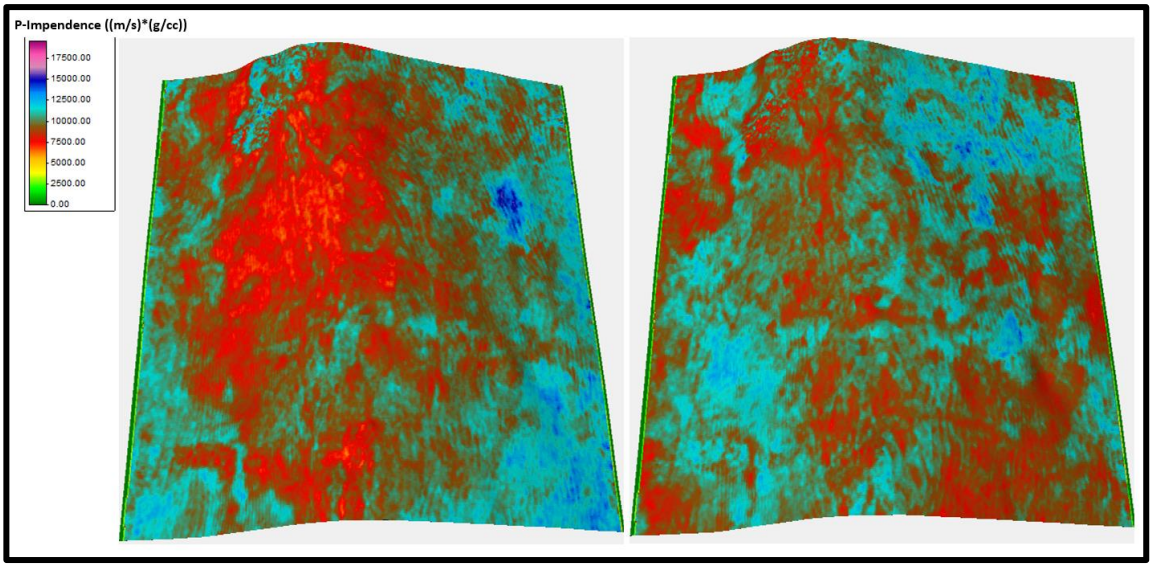

Figure 6.15. Acoustic impedance property of mB1 zone from the model after the seismic resampling, upper interval to the left, and lower interval to the right.

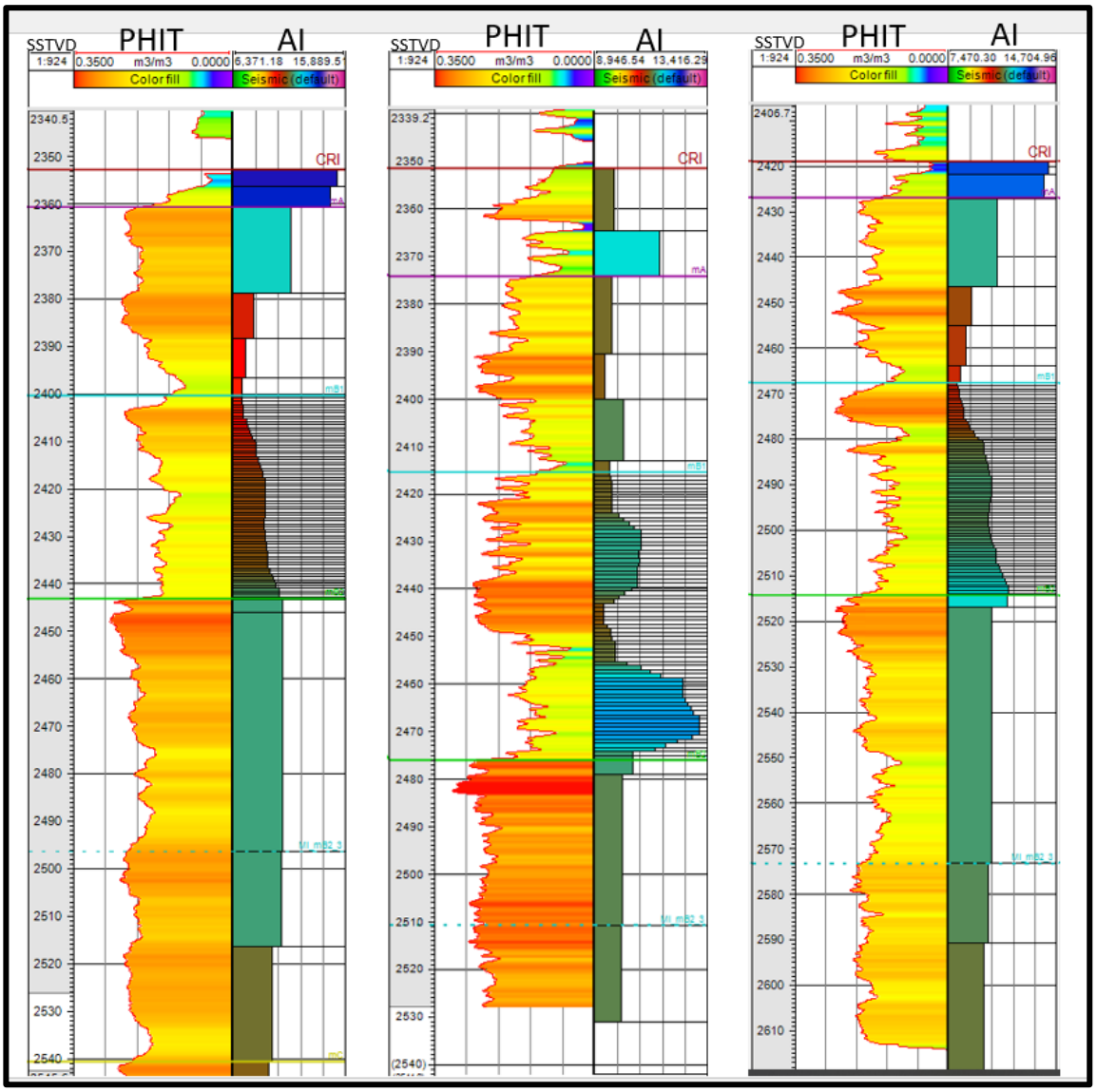

Figure 6.16. Comparison of rescaled acoustic impedance (AI) and porosity logs indicating that low acoustic impedance corresponded to the high porosity in the mB1 channelized zone (the shaded interval).

6.8 Integration of Seismic Data into 3D Property Modelling and Models Comparison

Due to their limited vertical resolution for earth models, seismic data only offer a dense lateral coverage. Additionally, the seismic resolution is greater than the thickness of the reservoir layers. Hence, the porosity model based on seismic data looks "smoothed," and small intervals of extremely low or extremely high porosity cannot be discerned. As a result, combining data at seismic and well log scales can result in the finest earth models.

Accordingly, the 3D acoustic impedance volume is employed as a trend using collocated co-kriging to constrain a porosity model.

6.8.1 Porosity Models Using Different Geostatistical Approaches

Understanding the key parameters, predicted value ranges and associated uncertainty should be the first step in developing a geological model (Albreiki, 2022). Thus, the stochastic simulation aims to measure uncertainty that arises in the Mishrif reservoir due to the spatial distribution of porosity and permeability. The porosity models were compared using Sequential Gaussian Simulation (SGS) and Gaussian Random Function Simulation (GRFS), creating multiple realizations to understand uncertainty.

Under the control of the seismic data, the porosity models are established. The porosity of the well log and acoustic impedance (AI) volume are used as input. As explained previously, the variogram parameters were established by seismic attribute as a proxy for the horizontal variogram. The porosity model was built using Sequential Gaussian Simulation (SGS) method with a secondary variable (AI) by the collocated co-kriging method.

The different porosity realizations are evaluated using another approach for the modelling with secondary data called Gaussian Random Function Simulation (GRFS) (see more details in the methodology section and Chapter 2, section 2.3.3). Also, this simulation method used a secondary variable (seismic inversion data) using collocated co-kriging. First, it must build a porosity model from well logs. Then, the input data (the secondary variable) is transformed using the coefficient correlation between the upscaled porosity and acoustic impedance (AI).

To compare the porosity distribution of the main channel fairways and hence reduce uncertainty, we have used these two simulation methods. From the resulting model produced by SGS, high porosity areas were missed especially in the eastern flank (Figure 6.17); however, there were high porosity areas that represented the grainstone channel fairways in the middle part. Although these porosity models were created using the same input data, the outer shapes of channel fairways (high porosity) are more obvious in the second average porosity map using GRFS (Figure 6.18). This comparison reveals that the degree of variation and the distribution in the porosity model varies significantly due to the chosen SGS or GRFS method.

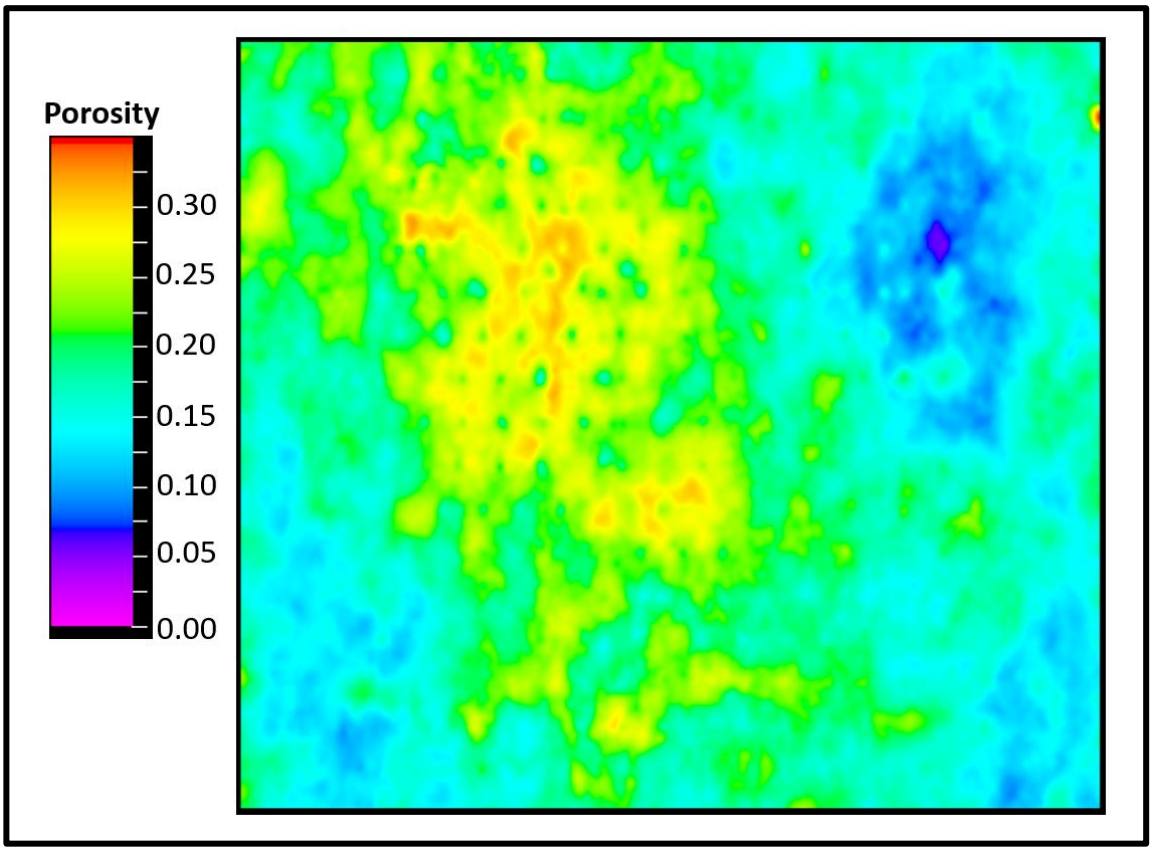

Figure 6.17. The average porosity map was constructed based on collocated co-kriging in the Sequential Gaussian Simulation (SGS) for the Mishrif mB1 channelized zone.

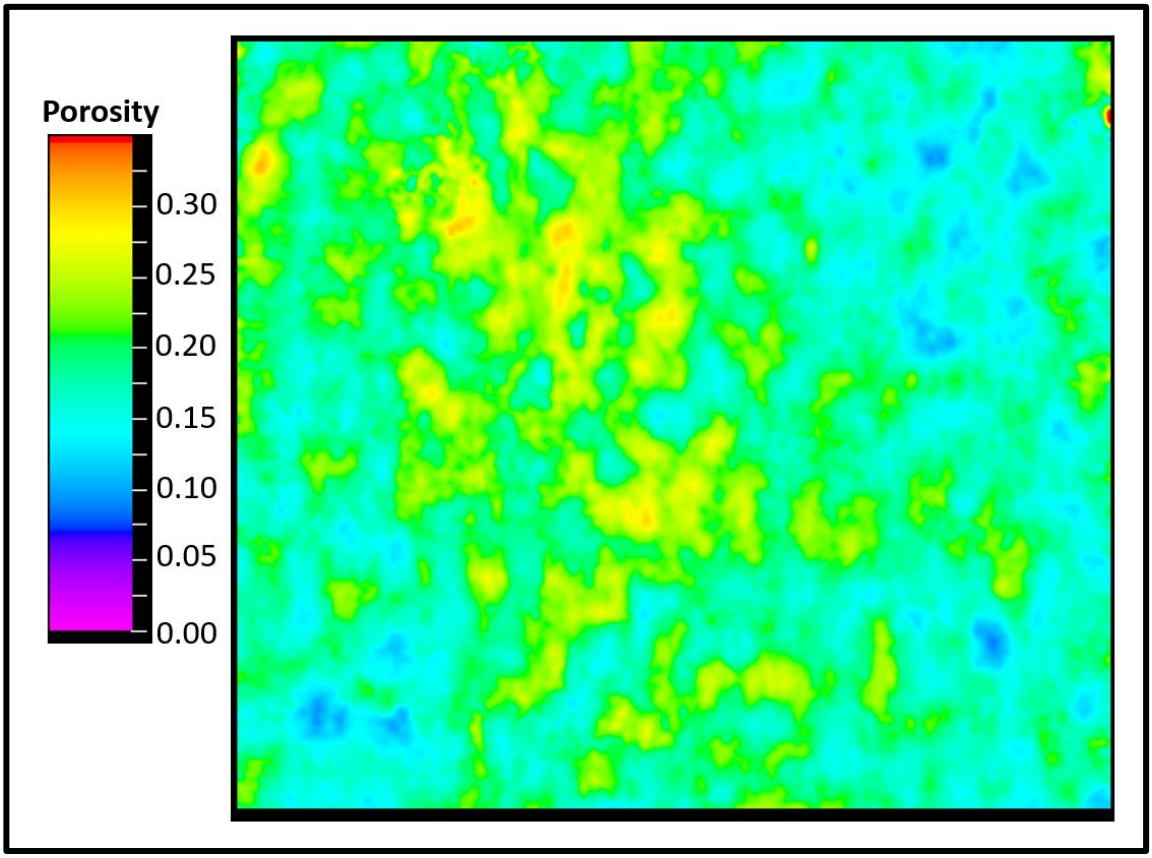

Figure 6.18. The average porosity map was constructed based on collocated co-kriging in the Gaussian Random Function Simulation (GRFS) for the Mishrif mB1 channelized zone.

The previous two figures provided an idea of the average porosity map; however, they cannot quantify the porosity distribution for individual layers in the mB1 zone. Figures 6.19 and 6.20 compare the porosity models for three intervals (upper, middle, lower) of the mB1 zone using SGS and GRFS algorithms (both models constrained by acoustic impedance volume), respectively. It can be seen that the difference is clear in the upper and middle intervals for good fairways and extraction of channel bodies and their properties with GRFS. Additionally, the outside regions of the tidal channels were better delineated in this method, which often comes upon lagoonal facies carbonates and lower reservoir quality. Thus, GRFS simulation shows highly reliable results for generating a more detailed model of the mB1 channelized zone.

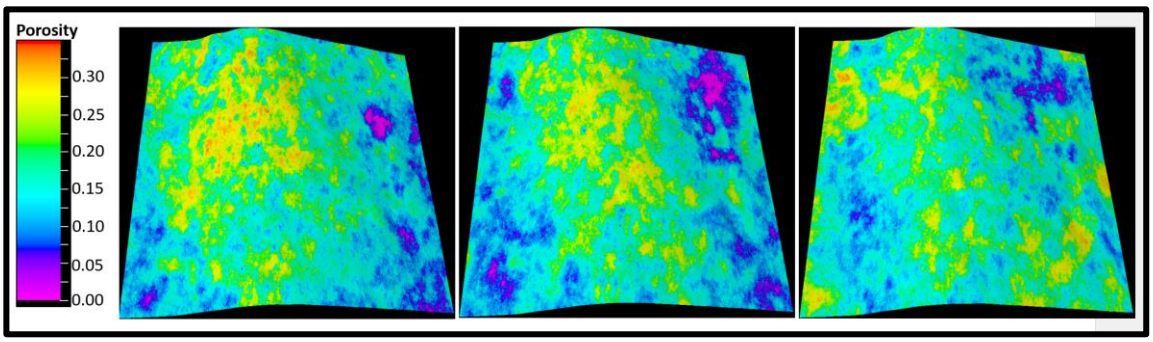

Figure 6.19. Porosity modelling for three intervals (upper, middle, lower) of mB1 channelized zone conditioned by seismic inversion data using collocated co-kriging in the Sequential Gaussian Simulation (SGS).

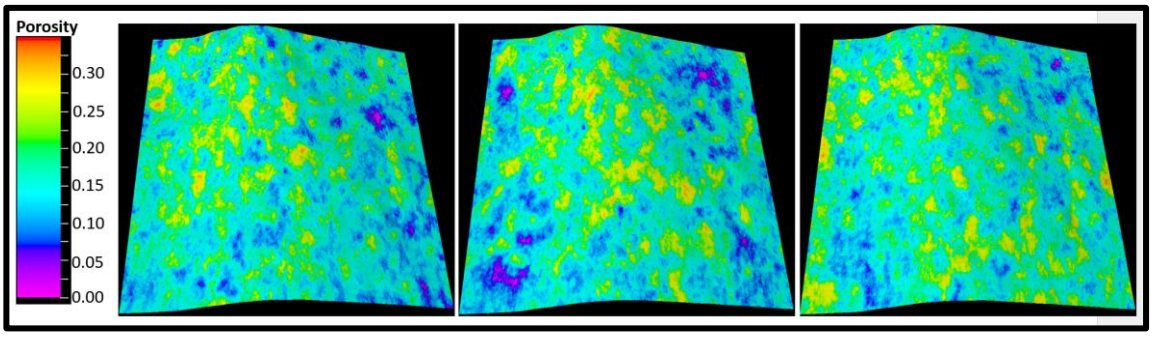

Figure 6.20. Porosity modelling for three intervals (upper, middle, lower) of mB1 channelized zone conditioned by seismic inversion data using collocated co-kriging in the Gaussian Random Function Simulation (GRFS).

Understanding the vertical distribution of the porosity, which affects the flow between the injection or production wells, it is necessary to capture and reduce uncertainties. The

GRFS approach of the porosity model for the mB1 channelized zone generated cross-sectional views aligned north to south.

The cross-section views for the Mishrif mB1 channelized zone for both cases of the GRFS model (with seismic data and without) are compared in the following figures. The initial quality assurance of the first-pass analysis results shows that the lateral trends and more remarkable parts of the porosity distribution are better depicted in the middle part with the porosity model constrained by seismic inversion (Figure 6.22) than the porosity model based only on well log data (Figure 6.21). Also, we can see that these highly porous areas match the seismic inversion results of the mB1 zone (Figure 6.23) more than the model based only on the wells. This can yield beneficial information in evaluating the inter-well channelized porosity.

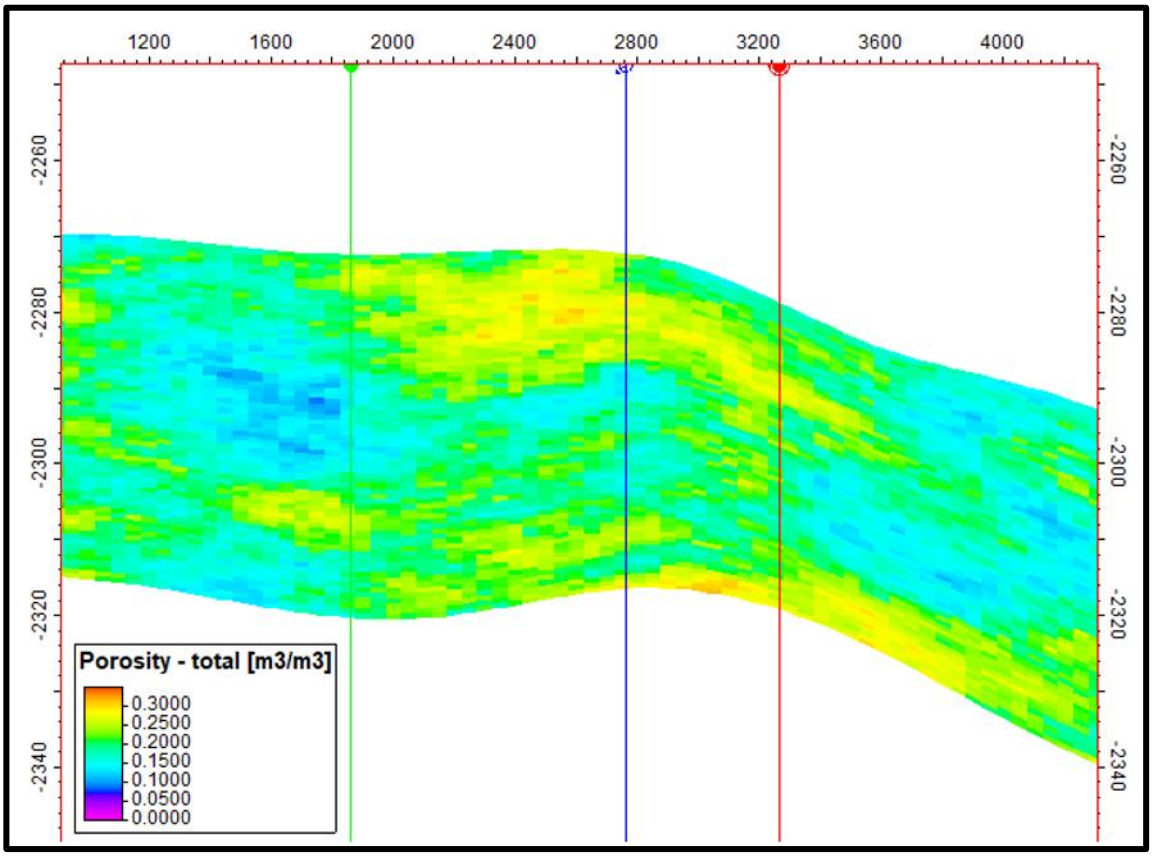

Figure 6.21. A cross-section view (north to south) of the porosity model for the mB1 channelized zone using the GRFS (without acoustic impedance (AI) volume).

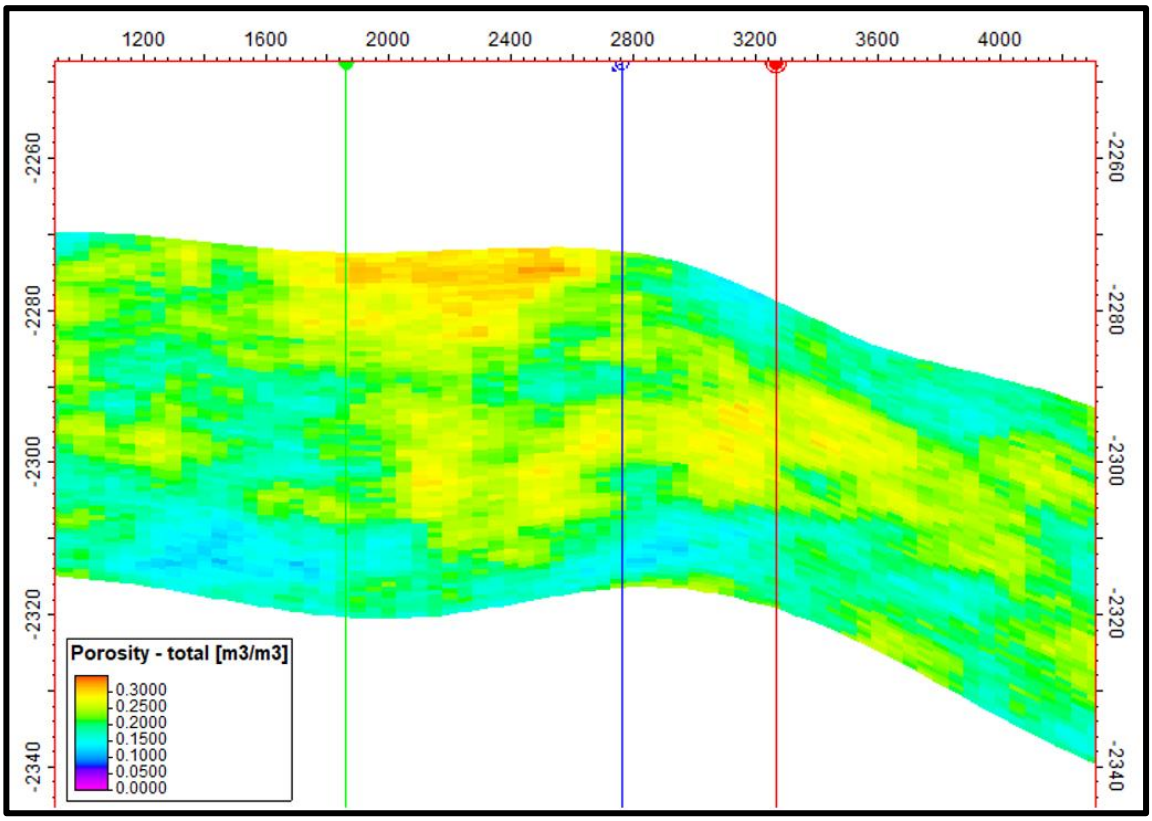

Figure 6.22. A cross-section view (north to south) of the porosity model for the mB1 channelized zone constrained using the GRFS with collocated co-kriging (acoustic impedance (AI) volume).

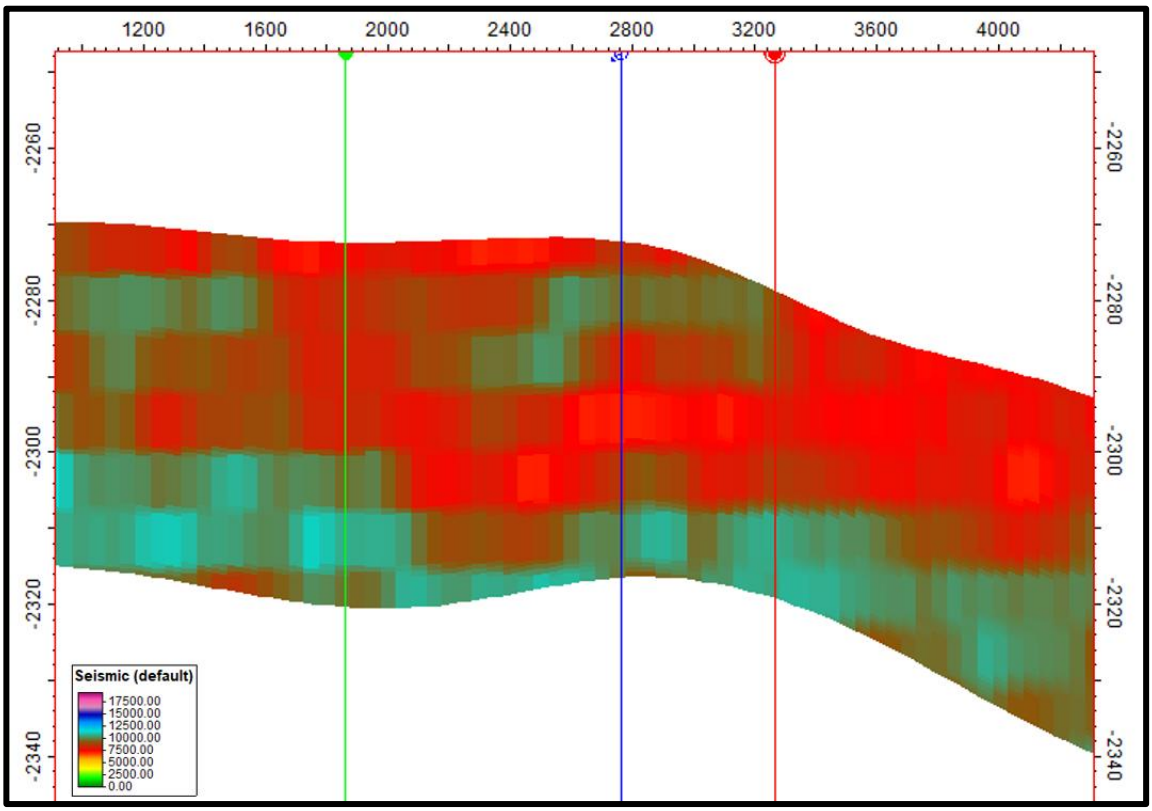

Figure 6.23. A cross-section view (north to south) of resampled acoustic impedance (AI) property for the mB1 channelized zone.

Additionally, cross-section views (aligned east to west) are created for the mB1 channelized zone using the GRFS method for both cases of the GRFS model (with seismic data and without) to capture uncertainties in the depth of mB1 channelized zone from another corner. In this part, the realization is shown that there is a clear difference between the model based on the wells and the constrained model by acoustic impedance (AI) volume. The result showed that the GRFS based on the wells (Figure 6.24) tried to smooth the model by neglecting the porosity distribution in some areas. In contrast, the GRFS constrained by seismic inversion (Figure 6.25) generated a more detailed porosity distribution and channel fairways as seen in the aligned north-to-south view. It can be seen that the more porous area in the distribution and some areas with less porosity now improved into medium (changing the colour from dark blue to light blue or more green and yellow), especially in the western and eastern sides. These areas with high porosity represent the grainstone channel fairways, and outside the channels are highlighted more with low porosity, which often comes upon lagoonal facies carbonates and lower reservoir quality. Also, this model is more reliable and closer to the seismic inversion results (Figure 6.26).

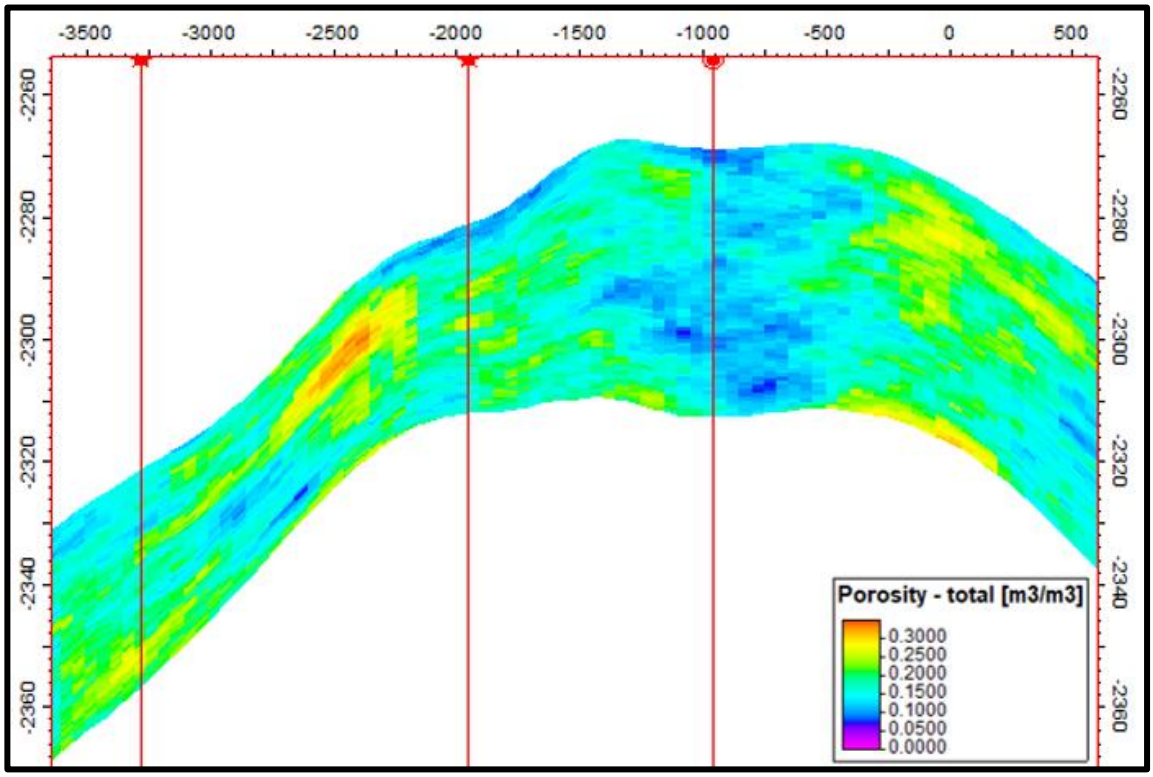

Figure 6.24. A cross-section view (east to west) of the porosity model for the mB1 channelized zone using the GRFS (without acoustic impedance (AI) volume).

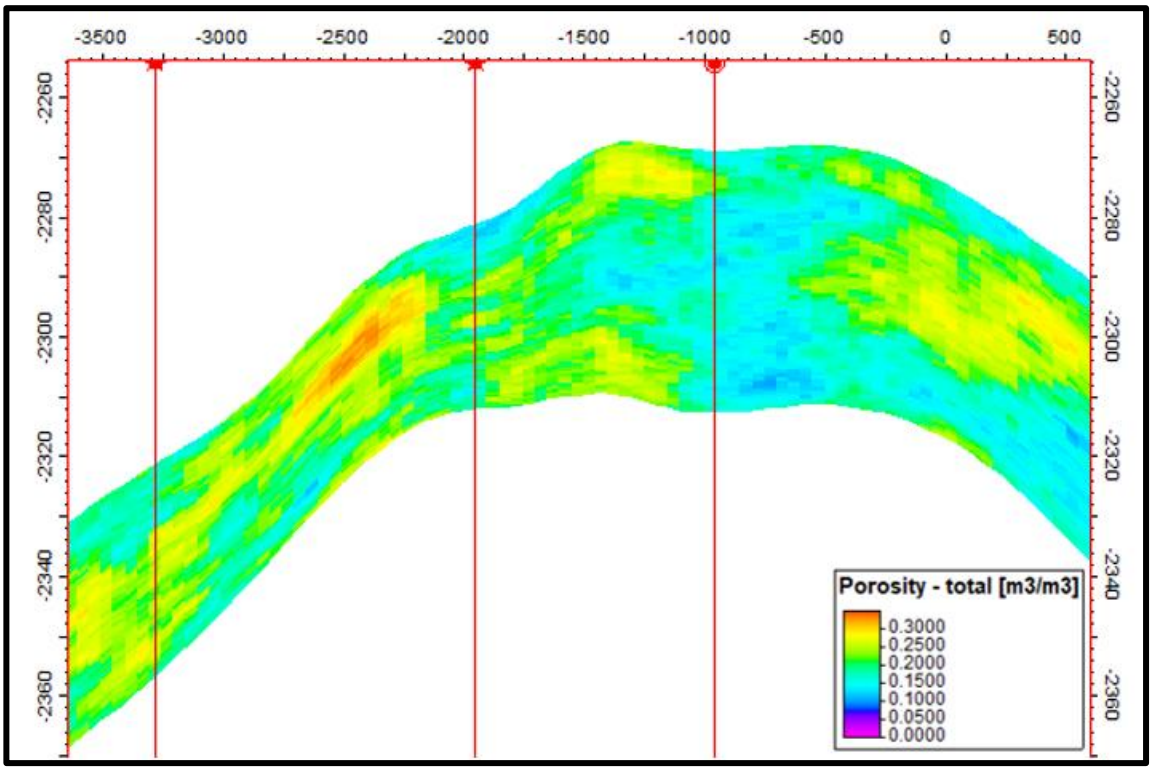

Figure 6.25. A cross-section view (east to west) of the porosity model for the mB1 channelized zone constrained using the GRFS with collocated co-kriging (acoustic impedance volume).

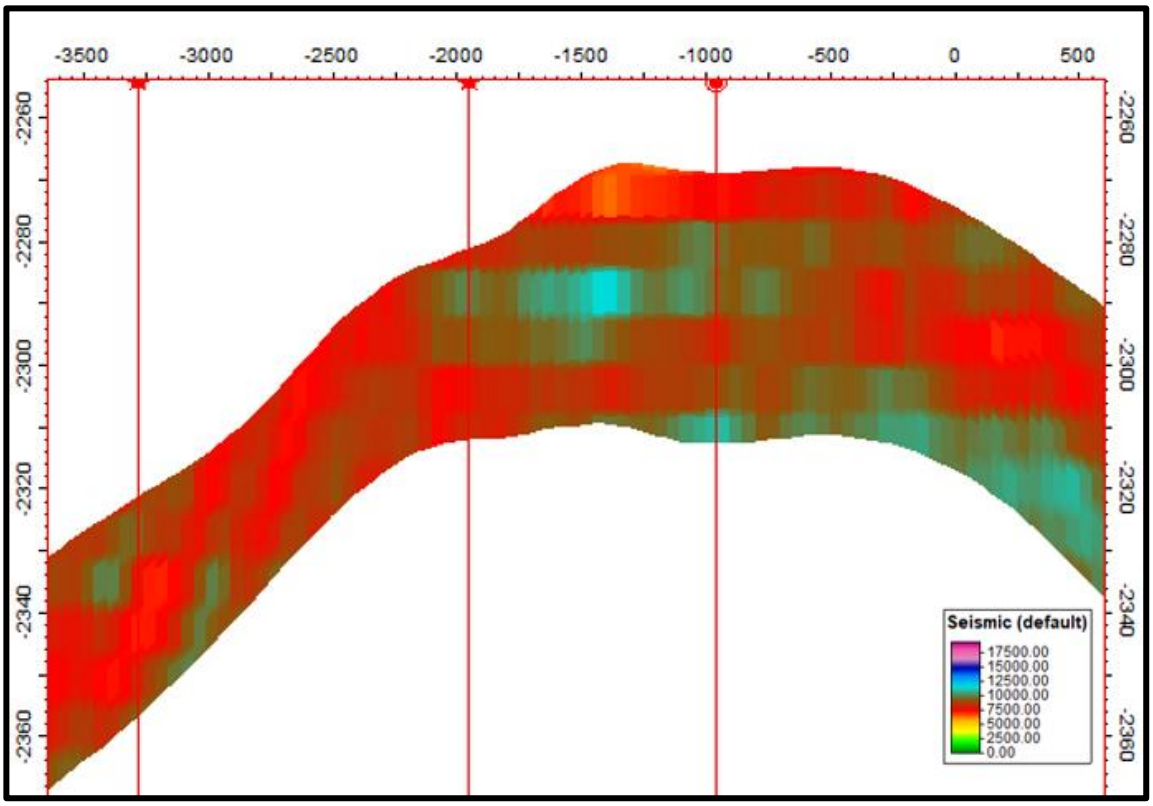

Figure 6.26. A cross-section view (east to west) of resampled acoustic impedance (AI) property for the mB1 channelized zone.

6.8.2 Porosity Models Using Different Reflection Coefficients (RC)

A variety of depositional and diagenetic processes can modify the petrophysical characteristics of carbonate rocks. This often makes carbonate reservoirs more geologically complex than their clastic equivalents, as was detailed in Chapter 2. As mentioned previously, the petrophysical features of the Mishrif reservoir are very complicated due to the numerous diagenetic overprints that might occur during different burial and uplift episodes throughout geological history. Thus, these processes played a vital role in creating the architecture of pore systems and storage space, making it challenging to estimate how the depositional facies will be distributed across the reservoir.

Therefore, to reduce the uncertainty and address this issue, we have tested different models using GRFS by altering the collocated co-kriging of the reflection coefficient (RC) for the upscaled porosity and resampled acoustic impedance (AI) during the stochastic stage of the modelling process. We have used the previous parameters and input the data used in the previous section, just changing the RC numbers. We also used smaller and higher values to compare RC (-0.70), which was repeated several times. Hence several porosity models have been generated (Figure 6.27). We increased the values of the RC (-0.90), the effect of the seismic inversion was slightly more pronounced in the connectivity of the porosity distribution of the mB1 channelized zone with high porosity value in the upper part and dark area (low porosity) become less. In contrast, reducing the RC to -0.50 can be seen in less distribution of the high porosity areas. The results show that a smaller correlation coefficient weight will have a minor impact on the porosity model, and a more significant weight will have a big impact.

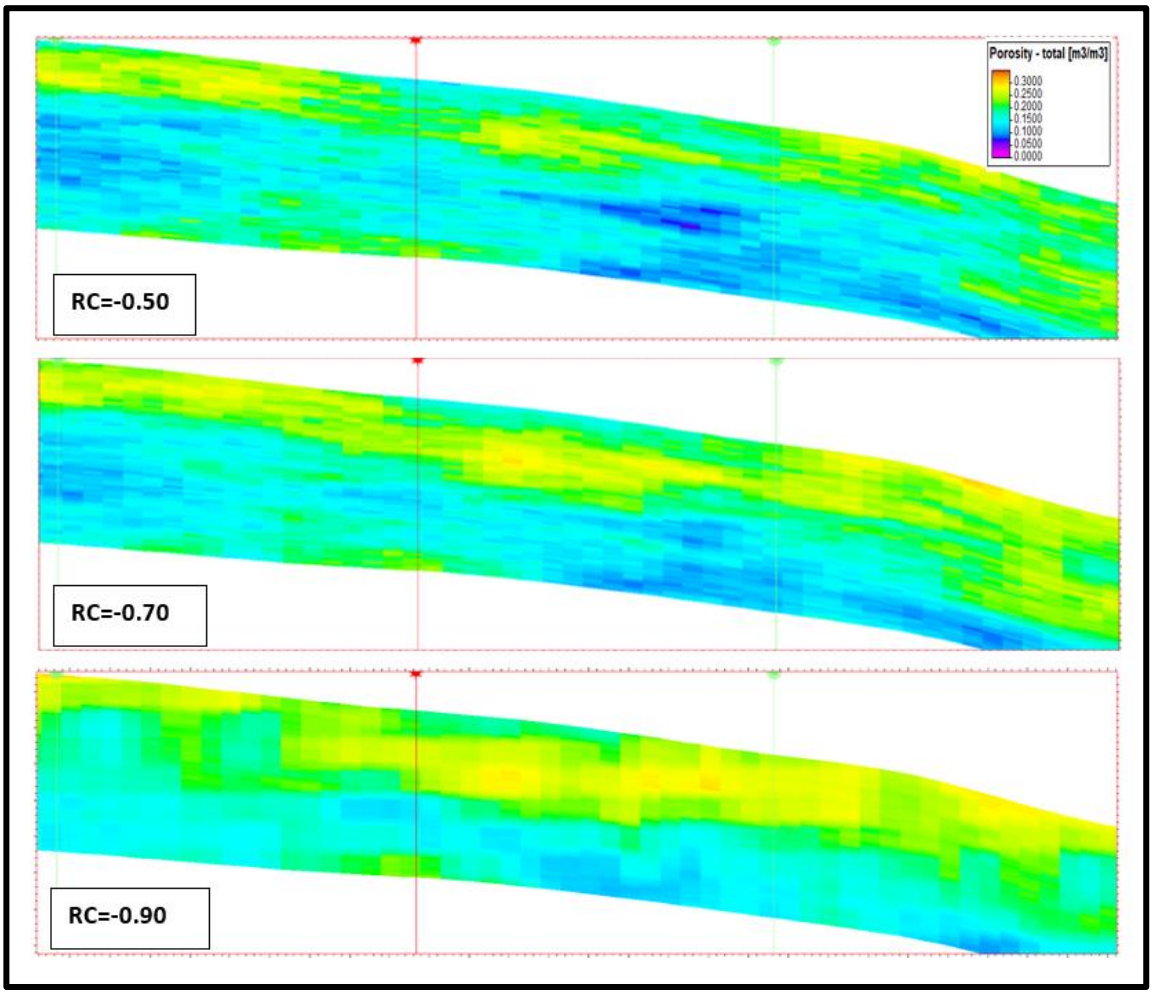

Figure 6.27. Comparison of the resulting porosity models (secondary conditioning data) using GRFS with collocated co-kriging for the three reflection coefficient values (RC= -0.50, -0.70, -0.90).

6.9 Discussion

This study shows that the proposed hierarchical approaches allow us to introduce the Mishrif channelized reservoir characterisation from different levels (geological knowledge, seismic data, and 3D property modelling). By constraining the reservoir characterisation, particularly seismic inversion which is incorporated into the 3D property model, we could generate various geological cases and parameter combinations more effectively.

As was mentioned in Chapter 5, we used different multidimensional approaches to the characteristics of the Mishrif carbonate tidal channels. The results of multidimensional scales provided a better knowledge of the complex carbonate tidal channels that requires

integrating interpretation from geology, seismic, and petrophysics. However, based on seismic inversion, the channel maps presented some features of channel fairways. We need to understand the realism distribution inside the giant Mishrif reservoir by building a property model through a combination workflow of well log and acoustic impedance (AI) as a secondary variable.

Here in this chapter, we established a different approach from the previous chapter, constraining the porosity model by seismic inversion, which resampled into a 3D property model. An enhanced porosity model depicting tidal channel fairway morphological and internal depositional features was first evaluated and shown using the combined seismic-based approaches. First, we handled two porosity models by comparing the two simulation approaches using SGS and GRFS. Then, we compared two porosity models of the GRFS, the first based only on the well data and the second constrained by seismic attribute (seismic inversion). This constrained simulation using GRFS, collocated co-kriging shows highly reliable results for generating a well-detailed model of the channel fairways, while the model based on the wells is missing some distribution of the porosity. Using seismic data in the 3D property model proves the channels' delineation with high porosity distribution, whereas a model based on the wells distributes the high porosity randomly. Most notably, the impact of the seismic inversion trend will be less when a small weight of the correlation between the primary and secondary variables and significant when a considerable weight is used.

The conditioned model by seismic inversion demonstrates the value of the secondary variable and improved the prediction of true reservoir properties. This is understandable given that the acoustic impedance (AI) property- upscaled porosity relationship was created using a collocated co-kriging approach that respects the well data and that the primary variable (well log porosity) and secondary variable (seismic inversion) complement each other. By testing different models, we aimed to reduce the geological uncertainties and improve porosity model representation and the delineation of the channel fairways.

6.10 Summary and Conclusion

This chapter examined how the conditioning of a complex channelized reservoir model, using seismic data in the West Qurna/1 oilfield and arising from different stochastic methods, significantly impacts the 3D pore space distributions of the mB1 channelized fairways, and subsequent oil-in-place estimation. Resampled acoustic impedance (AI) property correlates fairly with upscaled porosity (correlation coefficient of -0.70) in the mB1 channelized zone and can be used as a 3D probability trend for the porosity models. Two different porosity maps using two different methods (SGS and GRFS algorithms) were derived to represent the average porosity for the mB1 channelized zone. Each map represents a different level of impact of seismic data. Then, a porosity map using the collocated co-kriging technique in the GRFS has been selected to compare three intervals (upper, middle, lower) of mB1 channelized zone conditioned by seismic inversion data with another porosity model not conditioned by seismic data based on GRFS.

We demonstrated that seismic data improved the porosity distribution and better emphasized the channel fairway geometries and outside tidal channel regions by generating a different insight from a constrained 3D property model. The collocated co-kriging technique showed the influence of seismic data in the final distribution with good well control. The value of constrained reservoir models allows for exploring the impact of the second variable on 3D property across complex channelized reservoirs with diverse lateral and vertical rock complexities. The constrained model that combines well log and seismic data as a trend proves to yield better results than the individual parameters alone. Additionally, the constrained porosity model by seismic data minimizes the randomness of the reservoir prediction and improves consistency between the model and geological knowledge in inter-well connectivity areas. The mapping of the channelized reservoir is significantly improved compared with conventional modelling approaches or the 3-D seismic attributes.

Chapter 7. Conclusions and Recommendations

7.1 Conclusions

The overall aim of the thesis was to perform carbonate reservoir characterisation using seismic data and well data. Using a case study from the mid-Cretaceous Mishrif reservoir in the West Qurna/1 oilfield, this thesis has proved that reservoir characterisation workflows can be successfully applied to giant channelized carbonate reservoirs to provide an accurate prediction of reservoir properties and quantify the impact of seismic inversion on the property model. The main conclusions from the results chapters can be summarized:

Chapter 4 describes the characteristics of the Mishrif reservoir based on the seismic from high-quality 3D seismic data acquired over the West Qurna/1 oilfield and well data. Combining several datasets is necessary for the characterisation of the Mishrif reservoir in order to pinpoint notable geological characteristics through the 3D seismic inversion and rock physics analysis. The reservoir's vertical and lateral heterogeneity will be adequately characterized by integrating seismic data and other data. It was noted that with model-based inversion over the linear programming sparse spike (LPSS) inversion, the interpretation shows encouraging findings regarding the precise distribution of channel fairways and clear delineation found on the lithological variance exhibited in mA zone displays. Reservoir characterisation of Mishrif facies was classified into three differentiated groups (high-AI facies, medium-AI facies, low-AI facies) based on acoustic impedance (AI) and core analysis data. 3D acoustic impedance within the study area was used for the facies discrimination to begin with in attaining the primary goal, which is to combine the 3-D seismic data and petrophysical well logs to understand better the spatial distribution of the key features of the reservoir. Furthermore, a seismically derived porosity model was the foundation for a new application of the Mishrif porosity trends. The porosity model typically shows a good match between well-based porosity and porosity derived from seismic data. The observations of a complex mosaic of carbonate tidal channels, high-energy corals, mounds, and rudist shoals facies emphasized a new understanding of Mishrif porosity systems.

Chapter 5 extended the research from Chapter 4 and used multi-dimensional approaches to the characteristics of Mishrif carbonate tidal channels. In order to improve the

geologically realistic channel characterisation, a multi-dimensional workflow should include a variety of multisource data to determine the geometry of the channel fairways. The results showed that the 3-D Mishrif channel characterisation matches the prior literature review descriptions of the depositional settings and sequence stratigraphic analysis. Thin core sections and comprehensive well data analysis helped to understand the sedimentary characteristics of the heterogeneous channelized zone of the Mishrif reservoir. Furthermore, applying the RMS surface attribute and acoustic impedance volume helped define and provide details about the channel geometry. However, frequency spectrum decomposition with colour mixing provides a better geo-body extraction of the Mishrif mB1 zone. Additionally, we have used the seismic inversion from the previous chapter to seismically derived properties such as porosity and facies using a probabilistic neural network (PNN) to determine the distribution of channel bodies and their petrophysical properties. The application of the facies classification workflow improved to identify that the Mishrif mB1 zone is clustered into two different heterogeneity-quality lithofacies (channels and restricted lagoon facies).

Finally, Chapter 6 applied the knowledge from the previous two chapters to assess the degree to which the selected seismic inversion influences the 3D porosity model and regulates the porosity distribution. This chapter highlights the most important aspect of integrating seismic inversion into the porosity model. We have discussed two different porosity models using two different methods, SGS and GRFS algorithms, using the collocated co-kriging, which allowed a broader range of uncertainties to be explored, and each map represents a different level of impact of seismic data. For the Mishrif mB1 zone, resampled acoustic impedance property as a secondary variable using the GRFS algorithm enhanced the porosity distribution and better emphasized the channel fairway geometries and outside tidal channel areas than the SGS algorithm. However, we observed that increasing the seismic weighting increases confidence in the porosity model and matching acoustic impedance results. Furthermore, the porosity model conditioned by seismic data reduces the variability of reservoir prediction and enhances consistency between the model and geological knowledge in inter-well connection zones. Even with adequate well control, the collocated co-kriging approach demonstrated the impact of seismic data on the final distribution.

In summary, we can conclude that the proposed workflows improved the geologically realistic reservoir characterisation of the giant Mishrif reservoir.

7.2 Recommendations

This thesis has focused on an improved reservoir characterisation of the mid-Cretaceous Mishrif reservoir. In addition, it has considered constrained property modelling by seismic data in the channelized carbonate reservoirs. Considering the complexity of the channelized carbonate reservoir, there are remaining challenges, such as the low seismic resolution in deep areas, low recovery factor, sub-seismic scale, and channelized connectivity. It would be possible to investigate these matters and enhance the offered solutions with more work on the identified issues. There are various suggestions for future work based on the research carried out in this thesis:

- Chapter 4 presented the methodology followed to improve the reservoir characterisation with the non-availability of the pre-stack seismic volume. The latter was a fundamental limitation, so it would be interesting in the future to analyse and compare the pre-stack simultaneous inversion results generated with those from the post-stack seismic inversion, and this will enhance the inversion interpretation.

- Chapter 5 used post-stack seismic inversion for seismically derived properties. Seismically derived porosity and facies classification would be interesting to carry out by pre-stack seismic inversion too. This could make reservoir characteristics more predictable. Therefore, enhances characterizing and delineating of tidal channel fairways in the reservoir will be used for defining new well targets.

- Chapter 6 employed 3D seismic inversion to condition the property model of the mB1 channelized zone. To evaluate the reservoir connection, greater integration with more drill data or even well testing would be helpful. The results of this analysis would support earlier research findings and contribute new information for more accurate modelling of channelized features. Due to the data limitation, the current study carried out porosity modelling that was constrained by seismic inversion. Therefore, it is recommended that a high-resolution sector of the heterogeneous petrophysical properties (permeability, water saturation, relative permeability) could be modelled and simulated to add more geological realism in model realisations. In order to evaluate how the chosen secondary variable (seismic inversion or seismic attributes) affects the simulation model, a further study is suggested to build another constrained simulation model by seismic scenarios to compare with the first

simulation model. Another aspect worth examining would be performing a history match of the field production data; a detailed analysis could be conducted to understand how the influence of the seismic data on the reservoir performance, and how the production forecasts vary as a function of well-matched reservoir models with different constrained models. These investigations would strengthen the existing research findings and provide additional data for better modelling of the tidal channel characteristics.

Appendix

Wavelet Extraction Procedure:

Statistical approach was used to derive a statistical wavelet from the seismic trace itself (Figure A.1). This approach used autocorrelation based on the seismic data, and the phase is assumed to be known. The main drawback of this method was that it makes it difficult to precisely predict the proper phase spectrum.

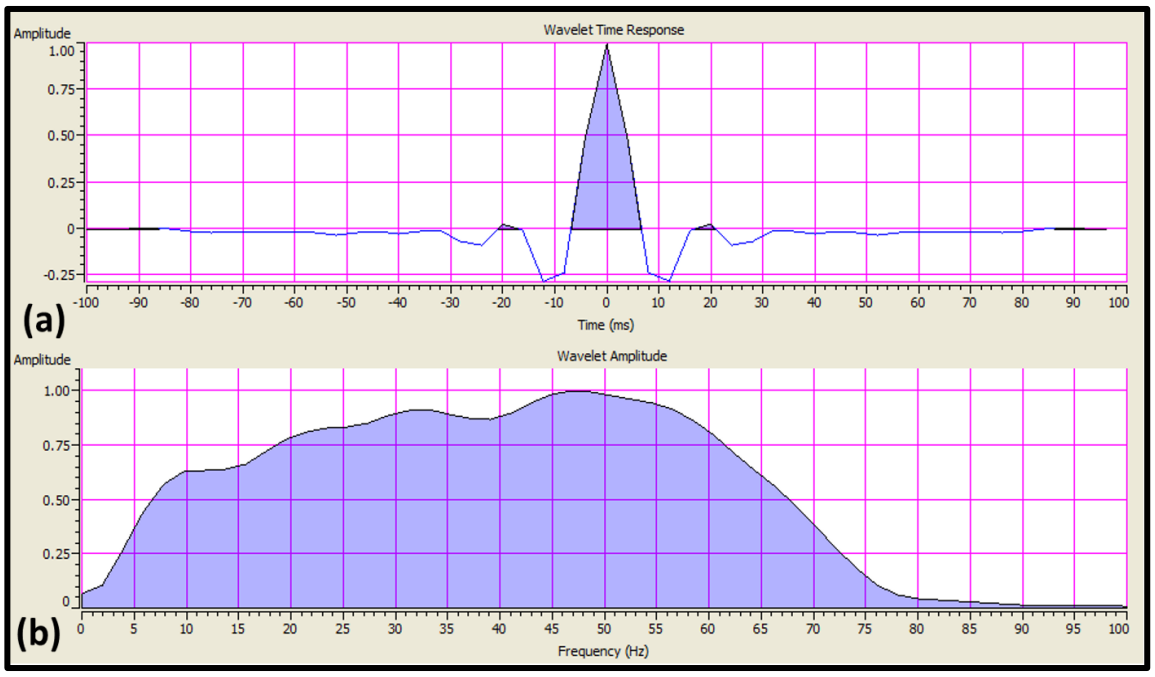

Figure A.1. Statistical wavelet extracted from reservoir window in the full-stack seismic volume (a) time and (b) frequency response.

Spectral decomposition recombines these individual volumes with these frequencies into one colour blended frequency volume (Figure A.2).

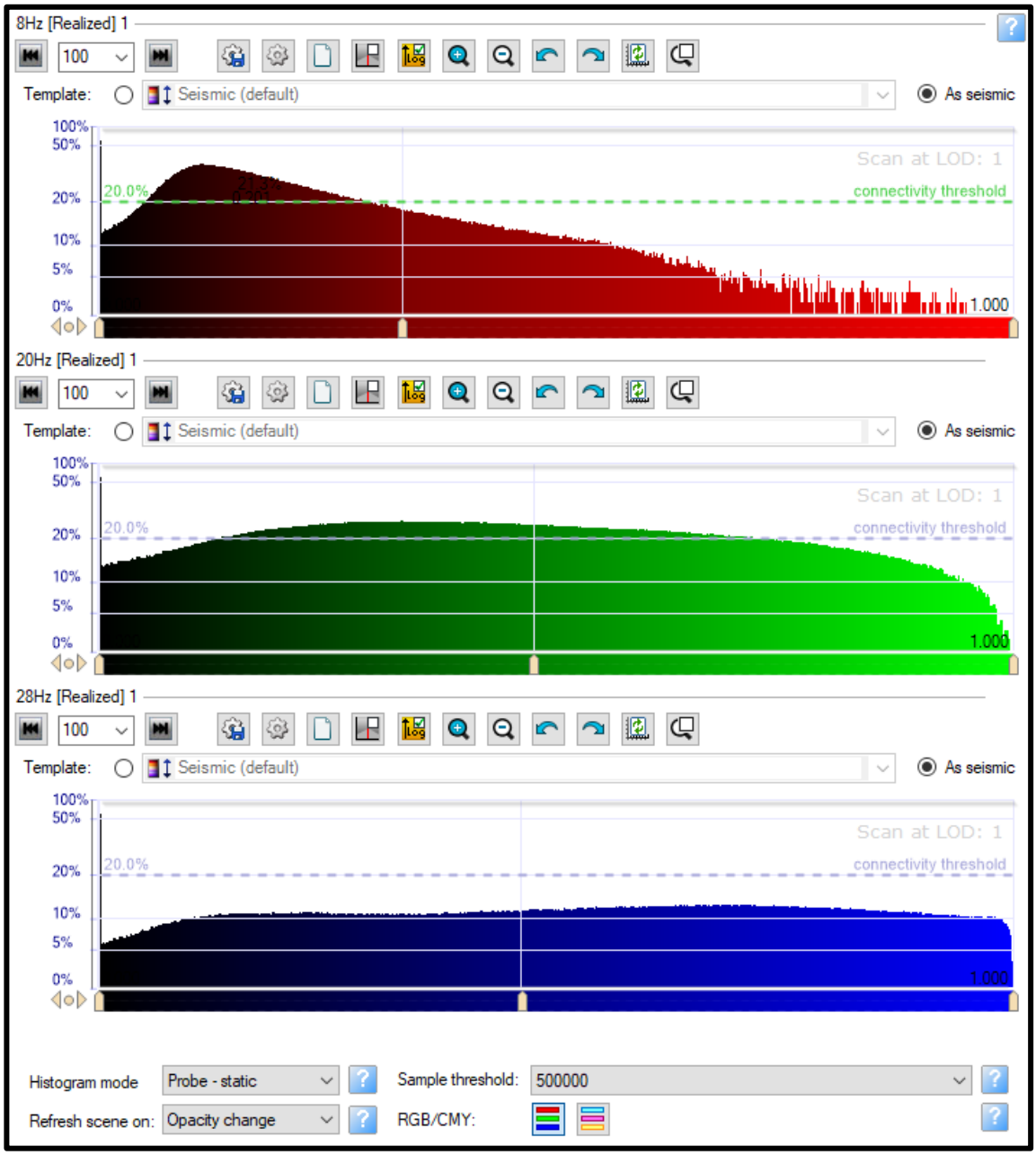

Figure A.2. The RGB (Red, Green, Blue) blending of the three spectrally decomposed volumes (8 Hz, 20 Hz, and 28 Hz) respectively.

References

Adams, A., Mackenzie, W. and Guilford, C., (1984). *Atlas of Sedimentary Rocks Under the Microscope*. Longman: Wiley.

Agar, S.M. and Geiger, S., (2015). Fundamental controls on fluid flow in carbonates: current workflows to emerging technologies. *Geological Society, London, Special Publications, 406*(1), pp.1-59.

Ahr, W. M. (2008). *Geology of carbonate reservoirs: the identification, description, and characterization of hydrocarbon reservoirs in carbonate rocks.* Wiley.

Ahr, W.M. Allan, D. Boyd, A. Bachman, H.N. Smithson, T. Clerke, E.A. Gzara, K.B.M. Hassall, J.K. Murty, C.R.K. Zubari, H. Ramamoorthy, R. (2005). Confronting the carbonate conundrum. *Oilfield Review, Spring,* pp.18-29.

Al-Ameri, T. Al-Khafaji, A. Zumberge, J. (2009). Petroleum system analysis of the Mishrif reservoir in the Ratawi, Zubair, North and South Rumaila oilfields, southern Iraq. *GeoArabia, Petrolink, Bahrain,* 14 (4), pp.91-108.

Al-Ali, A., Stephen, K. D. and Shams, A., (2019a). Improved Carbonate Reservoir Characterization: A Case Study from a Supergiant Field in Southern of Iraq. *SPE Middle East Oil & Gas Show and Conference,* held in Manama, Bahrain, 18-21 March 2019.

Al-Ali, A., Shams, A., and Stephen, K. D. (2019b). Identification of Fault Systems and Characterization of Structural Model: A Case Study from the Cretaceous Reservoir in the Giant Oil Field, Southern of Iraq. *SPE Europec featured at 81st EAGE Conference and Exhibition,* held in London, UK, 3-6 June 2019.

Al-Ali, A., Stephen, K. and Shams, A. (2019c). New Insights into the Spatial Distribution of Complex Carbonate Channels Using Geostatistical Approach: A Case Study. *Fourth Petroleum Geostatistics, Extended Abstract,* held in Florence, Italy, 2-6 September 2019.

Al-Ali, A., Stephen, K. and Shams, A. (2019d). Characterization of Channelized Systems in a Carbonate Platform Setting: A Case Study on the Late Cretaceous Reservoir from the

Supergiant Oilfield, Iraq. *SPE Reservoir Characterisation and Simulation Conference and Exhibition*, held in Abu Dhabi, UAE, 17-19 September 2019.

Al-Ali, A., Stephen, K. D. and Shams, A., (2020a). Toward Reservoir Characterization-Comparing Inversion Methods of a Heterogeneous Carbonate Reservoir in Supergiant Onshore Field. *International Petroleum Technology Conference*, held in Dhahran, Saudi Arabia, 13 – 15 January 2020.

Al-Ali, A., Stephen, K. D. and Shams, A., (2020b). Lithofacies Classification and Distribution for Heterogeneous Channelized System Based on Neural Network Process: Case Study from Middle East Carbonate Reservoir. *SPE Virtual Norway Subsurface Conference.* 2-3 November 2020.

Al-Siddiki, A.A., (1978). Subsurface geology of southeastern Iraq. In *10th Arab Petroleum Congress, Tripoli, Libya* (Vol. 47).

Albreiki, M.A.B., (2022). *An improved approach for quantifying the impact of geological uncertainty and modelling decisions on static and dynamic reservoir models-a case study from a giant fractured carbonate reservoir* (Doctoral dissertation, Heriot-Watt University).

Almasgari, A., Elsaadany, M. and Abdul Latiff, A., (2020). Application of seismic attributes to delineate the geological features of the Malay Basin. *Bulletin Of The Geological Society Of Malaysia,* 69, pp.97-110.

Alsharhan, A. and Kendall, C., (2003). Holocene coastal carbonates and evaporites of the southern Arabian Gulf and their ancient analogues. *Earth-Science Reviews*, 61(3-4), pp.191-243.

Aminzadeh, F. and Dasgupta, S., (2013). Fundamentals of Petroleum Geophysics. *Developments in Petroleum Science*, pp.37-92.

Aqrawi, A., Goff, J., Horbury, A. and Sadooni, F. (2010). *The petroleum geology of Iraq*. Beaconsfield (U.K.): Scientific Press. 424 pp.

Aqrawi, A.A.M., Thehni, G.A., Sherwani, G.H. and Kareem, B.M.A., (1998). Mid-Cretaceous rudist-bearing carbonates of the Mishrif Formation: An important reservoir sequence in the Mesopotamian Basin, Iraq. *Journal of petroleum Geology*, *21*(1), pp.57-82.

Armitage, P.J., Butcher, A.R., Churchill, J.M., Csoma, A.E., Hollis, C., Lander, R.H., Omma, J.E. and Worden, R.H., (2018). Reservoir Quality of Clastic and Carbonate Rocks: Analysis, Modelling and Prediction. Geological Society, London, Special Publications, 435, pp.85–105

Asheibi, A.M., (2018). *Seismic geomorphology and reservoir characterization of isolated tertiary reefs in the Eastern Sirt Basin, Libya* (Doctoral dissertation, Heriot-Watt University).

Avseth, P., Mukerji, T. and Mavko, G. (2010a). Rock physics interpretation of texture, lithology and compaction. *Quantitative Seismic Interpretation*, pp.48-110.

Avseth, P., Mukerji, T., Mavko, G. and Dvorkin, J. (2010b). Rock-physics diagnostics of depositional texture, diagenetic alterations, and reservoir heterogeneity in high-porosity siliciclastic sediments and rocks — A review of selected models and suggested workflows. *GEOPHYSICS*, 75(5), pp.75A31-75A47.

Awadeesian, A., Al-Jawed, S. and Saleh, A. (2014). Reservoir-scale sequence stratigraphy of Mishrif carbonates and implication to water injection strategy North Rumaila field case. *Arabian Journal of Geosciences*, 8(9), pp.7025-7040.

Azevedo, L., Amaro, C., Grana, D., Soares, A. and Guerreiro, L., (2017). Coupling Geostatistics and Rock Physics in Reservoir Modeling and Characterization. In *Abu Dhabi International Petroleum Exhibition & Conference*.

Babasafari, A., Ghosh, D., Salim, A., Ratnam, T., Sambo, C. and Rezaee, S., (2018). Petro-elastic modeling for enhancement of hydrocarbon prediction: Case study in southeast Asia. *SEG Technical Program Expanded Abstracts 2018*.

Bahar, A., Abdel-Aal, O., Ghani, A., Silva, F.P. and Kelkar, M., (2004). Seismic integration for better modeling of rock type based reservoir characterization: A field case example. In *Abu Dhabi International Conference and Exhibition*.

Barnes, A. (2001). Seismic Attributes in your Facies. *Canadian Society of Exploration Geophysicists Recorder*, pp.41-47.

Basra Oil Company, (2013). Core description and interpretation report Mishrif Formation, West Qurna Phase 1, internal report, Iraq.

Basra Oil Company, (2014). West Qurna 1 3D Seismic Project Acquisition, West Qurna Phase 1, internal report, Iraq.

Basra Oil Company, (2017). West Qurna 1 3D Seismic Project Acquisition, West Qurna Phase 1, internal report, Iraq.

Bentley, M. and Ringrose, P., (2018). Future directions in reservoir modelling: new tools and 'fit-for-purpose' workflows. In *Geological Society, London, petroleum geology conference series* (Vol. 8, No. 1, pp. 537-546). Geological Society of London

Berge, P. A., G. J. Fryer, and R. H. Wilkens, (1992). Velocity-porosity relationships in the upper oceanic crust: Theoretical considerations: *Journal of Geophysical Research*, 97, 15239–1525

Berryman, J. G., (1980). Long-wavelength propagation in composite elastic media. I. Spherical inclusions: *Journal of the Acoustical Society of America*, 68, 1809–1819.

Beydoun, Z.R., (1991). Middle East hydrocarbon reserves enhancement, 1975-1990. *Journal of Petroleum Geology*, *14*(Suppl. I), pp.II-IV.

Borgomano, J., Lanteaume, C., Léonide, P., Fournier, F., Montaggioni, L.F. and Masse, J.P., (2020). Quantitative carbonate sequence stratigraphy: Insights from stratigraphic forward models. *AAPG Bulletin*, *104*(5), pp.1115-1142.

Buday, T., and Jassim, S.Z., (1987). The Regional Geology of Iraq. Vol.2.Tectonism,

Magmatism and Metamorphism. In: M.J., Abbas and I.I., Kassab (Eds.). GEOSURV, Baghdad, 352pp.

Budkina, K., Philippe, K., Emang, M., Fetel, E. and Pigeaud, T., (2014). Conditioning of a carbonate reservoir model using seismic data in an offshore Upper Mishrif field in the Middle East. In *International Petroleum Technology Conference*. OnePetro.

Burchette, T. (2012). Carbonate rocks and petroleum reservoirs: a geological perspective from the industry. *Geological Society, London, Special Publications*, 370(1), pp.17-37.

Cantrell, D., Shah, R., Ou, J., Xu, C., Phillips, C., Li, X. and Hu, T., (2020). Depositional and diagenetic controls on reservoir quality: Example from the upper Cretaceous Mishrif Formation of Iraq. *Marine and Petroleum Geology*, 118, p.104415.

Castagna, J., Sun, S. and Siegfried, R., (2003). Instantaneous spectral analysis: Detection of low-frequency shadows associated with hydrocarbons. *The Leading Edge*, 22(2), pp.120-127.

Chopra, S. and Marfurt, K., (2007). *Seismic attributes for prospect identification and reservoir characterization*. Tulsa, Okla: Society of Exploration Geophysicists.

Chopra, S. and Marfurt, K., (2005). Seismic attributes — A historical perspective. *Geophysics*, 70(5), pp.3SO-28SO.

Chopra, A.K., Severson, C.D. and Carhart, S.R., (1990). Evaluation of geostatistical techniques for reservoir characterization. *In SPE Annual Technical Conference and Exhibition*.

Choquette, P. W. and Pray, L. C. (1970). Geologic nomenclature and classification of porosity in sedimentary carbonates: *AAPG Bulletin*, 54, pp.207–244.

Cox, D.R., Newton, A.M. and Huuse, M., (2020). An introduction to seismic reflection data: Acquisition, processing and interpretation. In *Regional Geology and Tectonics* (pp. 571-603). Elsevier.

Christian, L. (1997). Structural and Stratigraphic Study of Cretaceous Super-Giant Oil Fields of the Middle East. *GeoArabia*, 2(3).

Coburn, T.C., Yarus, J.M. and Chambers, R.L. eds., (2005). *Stochastic modeling and geostatistics: principles, methods, and case studies, vol. II, AAPG computer applications in geology 5* (Vol. 5). AAPG.

Daly, C., Quental, S. and Novak, D., (2010). A faster, more accurate Gaussian simulation. In *proceedings of the geocanada conference, calgary, AB, Canada* (pp. 10-14).

Davis, R. and Dalrymple, R., (2012). Principles of tidal sedimentology. Dordrecht: Springer.

de Macedo, I., da Silva, C., de Figueiredo, J. and Omoboya, B., (2017). Comparison between deterministic and statistical wavelet estimation methods through predictive deconvolution: Seismic to well tie example from the North Sea. *Journal of Applied Geophysics*, 136, pp.298-314.

de Matos, M., Osorio, P. and Johann, P. (2007). Unsupervised seismic facies analysis using wavelet transform and self-organizing maps. *GEOPHYSICS*, 72(1), pp.P9-P21.

de Periere, M.D., Durlet, C., Vennin, E., Caline, B., Boichard, R. and Meyer, A., (2017). Influence of a major exposure surface on the development of microporous micritic limestones-Example of the Upper Mishrif Formation (Cenomanian) of the Middle East. *Sedimentary Geology*, *353*, pp.96-113.

Dong, J.C. and Zhao, L.D., (2013). Tidal Channels in Carbonate Platform-Taking Azadegan Oilfiled as an Example. In *75th EAGE Conference & Exhibition incorporating SPE EUROPEC 2013* (pp. cp-348). European Association of Geoscientists & Engineers.

Droste, H., (2010). High-resolution seismic stratigraphy of the Shu'aiba and Natih formations in the Sultanate of Oman: implications for Cretaceous epeiric carbonate platform systems. *Geological Society, London, Special Publications*, 329(1), pp.145-162.

Dunham, R.J., (1962). Classification of carbonate rocks according to depositional textures. pp.108-121.

Eberli, G.P., Anselmetti, F.S., Betzler, C., Van Konijnenburg, J.-H., Bernoulli, D., (2004). Carbonate platform to basin transitions on seismic data and in outcrops: Great Bahama Bank and the Maiella Platform margin, Italy. In: Seismic Imaging of Carbonate Reservoirs and Systems*: AAPG Memoir.* vol. 81. pp. 207–250.

Ehrenberg, S., Aqrawi, A. and Nadeau, P. (2008). An overview of reservoir quality in producing Cretaceous strata of the Middle East. *Petroleum Geoscience*, 14(4), pp.307-318.

El-Behiry, M., Al Araby, M. and Ragab, R., (2020). Impact of phase rotation on reservoir characterization and implementation of seismic well tie technique for calibration offshore Nile Delta, Egypt. *The Leading Edge*, 39(5), pp.346-352.

Elhaj, M., Abdullatif, O., Abdulraheem, A., Hassan, A. and Sultan, A. (2019). Acoustic Properties of Carbonate: An Experimental and Modelling Study. In *SPE Middle East Oil and Gas Show and Conference*.

Finlayson, L., Aziz, A., Viator, D., Mardon, D., Abdullah, R. and Alali, F. (2012). Applications of New Wireline Technology in a Mature Middle-East Oil Field. *First EAGE Workshop on Iraq - Hydrocarbon Exploration and Field Development*.

Garland, J., Neilson, J., Laubach, S. and Whidden, K. (2012). Advances in carbonate exploration and reservoir analysis. *Geological Society, London, Special Publications*, 370(1), pp.1-15.

Gassmann, F. (1951). Elastic waves through a packing of spheres. *Society of Exploration Geophysicists.* Vol (16), pp.673–685.

Gavotti, P., Lawton, D., Margrave, G. and Isaac, H. (2013). Post stack inversion of broadband seismic data from Alberta, Canada. *SEG Technical Program Expanded Abstracts 2013*.

Ghafoori, M. R. Roostaeian, M. and Sajjadian, V. A. (2009). Secondary porosity: A key parameter controlling the hydrocarbon production in heterogeneous carbonate reservoirs (case study). *Petrophysics,* 50(1), pp.67–78.

GhojehBeyglou, M., (2021). Geostatistical modeling of porosity and evaluating the local and global distribution. *Journal of Petroleum Exploration and Production Technology*, *11*(12), pp.4227-4241.

Gomes, J.C., (2022). *AN OPEN ACCESS CARBONATE RESERVOIR MODEL* (Doctoral dissertation, Heriot-Watt University).

Grabowski Jr., G.W., (2014). Iraq. In: Marlow, L., Kendall, C., Yose, L. (Eds.), Petroleum Systems of the Tethyan Region: *American Association of Petroleum Geologists*, vol.106. pp. 379–467 Memoir.

Grana, D., Lang, X. and Wu, W. (2017). Statistical facies classification from multiple seismic attributes: comparison between Bayesian classification and expectation-maximization method and application in petrophysical inversion. *Geophysical Prospecting*, 65(2), pp.544-562.

Grana, D., Stright, L., Connolly, P., Gutierrez, M., Gonzalez, E., Florez, J., Amato del Monte, A. and Trainor-Guitton, W. (2016). Introduction to special section: Seismic facies classification and modeling. *Interpretation*, 4(3), p.SLi-SLi.

Grélaud, C., Razin, P. and Homewood, P. (2010). Channelized systems in an inner carbonate platform setting: differentiation between incisions and tidal channels (Natih Formation, Late Cretaceous, Oman). *Geological Society, London, Special Publications*, 329(1), pp.163-186.

Grélaud, C., Razin, P., Homewood, P. and Schwab, A., (2006). Development of Incisions on a Periodically Emergent Carbonate Platform (Natih Formation, Late Cretaceous, Oman). *Journal of Sedimentary Research,* 76(4), pp.647-669.

Hamilton, E. L., Bachman, R. T. (1982). Sound Velocity and Related Properties of Marine Sediments. *Journal of the Acoustical Society of America*. 72, pp. 1891-1904.

Hampson, D., Schuelke, J. and Quirein, J. (2001). Use of multiattribute transforms to predict log properties from seismic data. *GEOPHYSICS*, 66(1), pp.220-236.

Handford, C.R., Loucks, R.G., (1993). Carbonate depositional sequences and systems tracts-responses of carbonate platforms to relative sea-level changes. In: Loucks, R.G.,

Hardy, H.H., Beier, R.A. and Gaston, J.D., (2003). Frequency estimates of seismic traces. *Geophysics*, *68*(1), pp.370-380.

Hashemi, S., Javaherian, A., Ataee-pour, M., Tahmasebi, P. and Khoshdel, H. (2014). Channel characterization using multiple-point geostatistics, neural network, and modern analogy: A case study from a carbonate reservoir, southwest Iran. *Journal of Applied Geophysics, 111*, pp.47-58.

Hendry, J., Burgess, P., Hunt, D., Janson, X. and Zampetti, V., (2021). Seismic characterization of carbonate platforms and reservoirs: an introduction and review. *Geological Society, London, Special Publications*, *509*(1), pp.1-28.

Hollis, C., (2011). Diagenetic controls on reservoir properties of carbonate successions within the Albian-Turonian of the Arabian Plate, *Petroleum Geoscience*, Vol. 17, pp. 223-241.

Hosken, J., (1988). Ricker wavelets in their various guises. *First Break*, 6(1).

International Energy Agency (2021). World Energy Outlook 2021 - revised version October 2021. Available at: www.iea.org/weo (Accessed: 15 October 2022).

International Energy Agency (2022). World Energy Outlook 2021 - revised version July 2022. Available at: www.iea.org/weo (Accessed: 15 October 2022).

Iturrarán-Viveros, U. and Parra, J.O., (2014). Artificial neural networks applied to estimate permeability, porosity and intrinsic attenuation using seismic attributes and well-log data. *Journal of Applied Geophysics*, *107*, pp.45-54.

Jassim, S.Z. and Buday, T. (2006). Tectonic Framwork, *In;* Jassim, S.Z. and Goff, J.C.

(Eds), Geology of Iraq. Dolin, Prague and Moravian Museum, Brno, Czech Republic, pp.45-55.

Jassim, S. and Goff, J. (2007). *Geology of Iraq*. Brno: Dolin, Prague and Moravian Museum.

Javaux, C. and Chenot, D. (2014). Specific Workflow for Integrated and Multiscale Geoscience & Reservoir Evaluation Dedicated to Middle East Carbonate Reservoirs. *Abu Dhabi International Petroleum Exhibition and Conference*.

Johann, P., de Castro, D. and Barroso, A. (2001). Reservoir Geophysics: Seismic Pattern Recognition Applied to Ultra-Deepwater Oilfield in Campos Basin, Offshore Brazil. *SPE Latin American and Caribbean Petroleum Engineering Conference*.

John, A., Lake, L., Torres-Verdin, C. and Srinivasan, S. (2008). Seismic Facies Identification and Classification Using Simple Statistics. *SPE Reservoir Evaluation & Engineering*, 11(06), pp.984-990.

Karimpouli, S., Hassani, H., Nabi-Bidhendi, M., Khoshdel, H. and Malehmir, A. (2013). Application of probabilistic facies prediction and estimation of rock physics parameters in a carbonate reservoir from Iran. *Journal of Geophysics and Engineering*, 10(1), p.015008.

Kendall, C. G. S. C. Flood, P. (2011). *Classification of Carbonates*. Springer, Dordrecht.

Kindler, P., Godefroid, F., Curran, H.A., Dupraz, C.H., Mylroie, J.E., Strasses, A. and Verrecchia, E.P., (2011). Modern and quaternary carbonate environments. In *Proceedings of the ESPP Bahamas Workshop 2011*.

Konert, G., Afifi, A.M., Al-Hajri, S.A., Droste, H.J., (2001). Paleozoic stratigraphy and hydrocarbon habitat of the Arabian Plate. *GeoArabia* 6, 407–442

Koson, S., Chenrai, P. and Choowong, M., (2014). Seismic attributes and their applications in seismic geomorphology. *Bulletin of Earth Sciences of Thailand*, *6*(1), pp.1-9.

Kumar, M. and Han, D. (2005). Pore shape effect on elastic properties of carbonate rocks. *SEG Technical Program Expanded Abstracts 2005*.

Kuster, G. T., and M. N. Toksöz, (1974). Velocity and attenuation of seismic waves in two-phase media: Part I. Theoretical formulations: *Geophysics*, 39, 587–606.

Larue, D.K. and Hovadik, J., (2006). Connectivity of channelized reservoirs: a modelling approach. *Petroleum Geoscience*, *12*(4), pp.291-308.

Li, J., Zhang, X., Lu, B., Ahmed, R. and Zhang, Q., (2019). Static Geological Modelling with Knowledge Driven Methodology. *Energies*, *12*(19), p.3802.

Li, M. and Zhao, Y., (2014). Seismic Attribute Analysis. *Geophysical Exploration Technology*, pp.103-131.

Li, Q., (2001). Lp Sparse Spike Inversion. Strata Technique Document, Hampson-Russell Software Services Ltd.

Li, X., Qin, R., Ping, H., Wei, D. and Liu, X. (2018). Analysis and application of classification methods of complex carbonate reservoirs. *Journal of Geophysics and Engineering*, 15(3), pp.830-840.

Lindseth, R.O., (1979). Synthetic sonic logs-A process for stratigraphic interpretation: *Geophysics*, 44, 3-26.

Ling, H., Lun, Z., Jianxin, L., Ji, M.A., Ruilin, L.U.I., Shuqin, W.A.N.G. and Wenqi, Z.H.A.O., (2014). Complex relationship between porosity and permeability of carbonate reservoirs and its controlling factors: A case study of platform facies in Pre-Caspian Basin. *Petroleum Exploration and Development*, *41*(2), pp.225-234.

Liu, H., Shi, K., Liu, B., Song, X., Deng, L., Guo, R., Tian, Z., Li, Y., Deng, Y. and Wang, G., (2021). The characteristics and origins of thief zones in the Cretaceous limestone reservoirs of Central and southern Mesopotamian Basin. *Journal of Petroleum Science and Engineering*, 201, p.108395.

Liu, H., Tian, Z., Liu, B., Guo, R., Yang, D., Deng, Y., Yu, Y. and Shi, K., (2018). Pore types, origins and control on reservoir heterogeneity of carbonate rocks in Middle Cretaceous Mishrif Formation of the West Qurna oilfield, Iraq. *Journal of Petroleum Science and Engineering*, 171, pp.1338-1349.

Liu, J., Dai, X., Gan, L., Liu, L. and Lu, W. (2017). Supervised seismic facies analysis based on image segmentation. *GEOPHYSICS*, 83(2), pp. O25-O30.

Liu, Y. and Wang, Y. (2017). Seismic characterization of a carbonate reservoir in Tarim Basin. *GEOPHYSICS*, 82(5), pp. B177-B188.

Liu, Y.M., Dong, J.C. and Guo, R., (2019). Facies-Controlled Modeling Constrained by 2D Seismic and Pseudo Well for Carbonate. In *International Field Exploration and Development Conference* (pp. 1984-1994). Springer, Singapore.

Liu, Y.M., Dong, J.C., Wang, W.J. and Lin, T.F., (2020). Characteristics of Rimmed Shelf-type Carbonate Platform with Large Tidal Channel: A Case Study for a Oilfield, Middle East. In *International Field Exploration and Development Conference* (pp. 2391-2397). Springer, Singapore.

Liu, X., Xu, G., Zhao, L., Duan, T. and Wang, X., (2016). Seismic sedimentology characteristics of platform marginal shoal: A case from Mesopotamia Basin, Persian Basin. In *SEG Technical Program Expanded Abstracts 2016* (pp. 1829-1833). Society of Exploration Geophysicists.

Lu, X., Wang, Y., Tian, F., Li, X., Yang, D., Li, T., Lv, Y. and He, X., (2017). New insights into the carbonate karstic fault system and reservoir formation in the Southern Tahe area of the Tarim Basin. *Marine and Petroleum Geology*, *86*, pp.587-605.

Ma, Y.Z. and Zhang, X., (2019). *Quantitative geosciences: Data analytics, geostatistics, reservoir characterization and modeling*. Cham: Springer International Publishing.

Mahdi, T.A. and Aqrawi, A.A., (2018). Role of facies diversity and cyclicity on the reservoir quality of the mid-Cretaceous Mishrif Formation in the southern Mesopotamian Basin, Iraq. *Geological Society, London, Special Publications*, *435*(1), pp.85-105.

Mahdi, T.A. and Aqrawi, A.A.M., (2014). Sequence stratigraphic analysis of the mid-Cretaceous Mishrif formation, southern Mesopotamian Basin, Iraq. *Journal of petroleum geology*, *37*(3), pp.287-312.

Mahdi, T. Aqrawi, A. Horbury, A and Sherwani, G. (2013). Sedimentological characterization of the mid Cretaceous Mishrif reservoir in southern Mesopotamian Basin, Iraq. *GeoArabia (Manama),* 18(1), pp.139-174.

Mahgoub, M., Padmanabhan, E. and Abdullatif, O. (2017). Seismic inversion as a predictive tool for porosity and facies delineation in Paleocene fluvial/lacustrine reservoirs, Melut Basin, Sudan. *Marine and Petroleum Geology*, 86, pp.213-227.

Mahmood, S., Salazar, P., Zhao, X., Pointing, M. and Sayed, A. (2017). Waterflooding in Giant Carbonate Reservoir; Successes and Challenges. *Abu Dhabi International Petroleum Exhibition & Conference.*

Maliva, R. (2016). Aquifer Characterization Techniques. *Springer Hydrogeology.*

Marroquín, I. (2014). A knowledge-integration framework for interpreting seismic facies. *Interpretation,* 2(1), pp.SA1-SA9.

Marroquín, I., Brault, J. and Hart, B. (2009). A visual data-mining methodology for seismic facies analysis: Part 1-Testing and comparison with other unsupervised clustering methods. *GEOPHYSICS*, 74(1), pp.P1-P11.

Martínez, G., Hanson, G., Tariq, H., Toorn, J., Souza, J., Molen, M., Okprekyi, O., Dandapani, R. and Shah, Z., (2021). Well-to-seismic tie. *Applied Techniques to Integrated Oil and Gas Reservoir Characterization,* pp.249-271.

Maurya, S. and Singh, N. (2018). Application of LP and ML sparse spike inversion with probabilistic neural network to classify reservoir facies distribution - A case study from the Blackfoot field, Canada. *Journal of Applied Geophysics,* 159, pp.511 –521.

Melville, P.D. and Guruswamy, S., (2002). Integration of 3D seismic with a reservoir model for reservoir characterisation. In *Abu Dhabi International Petroleum Exhibition and Conference*.

Miraglia, S., Borromeo, O., Maragliulo, C., Rodrigues, J. and Sartorio, D. (2015). Architecture, Facies Distribution and Reservoir Properties of the Mishrif Formation (Zubair Field, Southern Iraq): An Example of Integration of Seismic Interpretation with Well Data. *Abu Dhabi International Petroleum Exhibition and Conference.*

Montaron, B. (2008). 'Carbonate Evolution,' Oil and Gas Middle East, (August), pp. 26–32. Available at: www.arabianbusiness.com/energy.

Moore, C.H. and Wade, W.J., (2013). Carbonate diagenesis: Introduction and tools. In *Developments in Sedimentology* (Vol. 67, pp. 67-89). Elsevier.

Naeem, M., El-Araby, H., Khalil, M., Jafri, M., and Khan, F. (2015). Integrated study of seismic and well data for porosity estimation using multi-attribute transforms: a case study of Boonsville Field, Fort Worth Basin, Texas, USA. *Arabian Journal of Geosciences*, 8(10), pp.8777-8793.

Ødegaard, E. and Avseth, P., (2003). Interpretation of Elastic Inversion Results Using Rock Physics Templates. *65th EAGE Conference & Exhibition*.

Oldenburg, D.W., Scheuer, T. and Levy, S. (1983). Recovery of the acoustic impedance from reflection seismograms: *Geophysics,* 48, p. 1318–1337.

Organization of the Petroleum Exporting Countries (2021). OPEC Annual Statistical Bulletin 2021, Organization of the Petroleum Exporting Countries. Available at: https://asb.opec.org/ASB_PDFDownload.php (Accessed: 15 October 2022).

Othman, A., Fathy, M. and Maher, A., (2016). Use of spectral decomposition technique for delineation of channels at Solar gas discovery, offshore West Nile Delta, Egypt. *Egyptian Journal of Petroleum*, 25(1), pp.45-51.

Othman, A.A., Fathy, M. and Negm, A., (2018). Identification of channel geometries applying seismic attributes and spectral decomposition techniques, Temsah Field, Offshore East Nile Delta, Egypt. *NRIAG Journal of Astronomy and Geophysics*, *7*(1), pp.52-61.

Ourabah, A., Grimshaw, M., Ernst, S. and Tough, K., (2015). Tackling Interbed Multiples with High Density Surveys, a Case Study Over the Rumaila Field. In *Abu Dhabi International Petroleum Exhibition and Conference*. OnePetro.

Partyka, G., Gridley, J. and Lopez, J., (1999). Interpretational applications of spectral decomposition in reservoir characterization. *The leading edge*, *18*(3), pp.353-360.

Perras, M.A. and Diederichs, M.S., (2011). The importance of classification for carbonates and mudrocks in engineering. In *Proceedings of the 2011 Pan-Am Canadian Geotechnical Conference* (Vol. 3, pp. 2668-2675). Canadian Geotechnical Society.

Posamentier, H.W., Jervey, M.T. and Vail, P.R., (1988). Eustatic controls on clastic deposition I—conceptual framework.

Pramanik, A., Singh, V., Vig, R., Srivastava, A. and Tiwary, D. (2004). Estimation of effective porosity using geostatistics and multiattribute transforms: A case study. *GEOPHYSICS*, 69(2), pp.352-372.

Pyrcz, M.J. and Deutsch, C.V., (2014). *Geostatistical reservoir modeling*. Oxford university press.

Ringrose, P. and Bentley, M., (2016). *Reservoir model design.* Berlin, Germany: Springer.

Ringrose, P. and Bentley, M. (2021). *Reservoir Model Design: A Practitioner's Guide*. Springer Nature.

Rossebø, Ø.H., Brevik, I., Ahmadi, G.R. and Adam, L., (2005). Modeling of acoustic properties in carbonate rocks. In *SEG Technical Program Expanded Abstracts 2005* (pp. 1505-1508). Society of Exploration Geophysicists.

Roy, A. and Marfurt, K.J., (2011). Cluster assisted 3D and 2D unsupervised seismic facies analysis, an example from the Barnett Shale formation in the Fort Worth Basin, Texas. *SEG Technical Program Expanded Abstracts 2011*, pp.1734-1738.

Russell, B.H., (2015). Visualizing inversion results with rock physics templates. *CREWES Research Report, 27*.

Russell, B.H., (2004). *The application of multivariate statistics and neural networks to the prediction of reservoir parameters using seismic attributes*. Ph.D. Dissertation, University of Calgary, Alberta.

Russell, B. and Hampson, D. (1991). A comparison of post-stack seismic inversion methods. *61st Annual International Meeting, SEG, Expanded Abstracts, 876–878.*

Russell, B., Hampson, D., Todorov, T. and Lines, L., (2002). Combining geostatistics and multi-attribute transforms: A channel sand case study, Blackfoot oilfield (Alberta). *Journal of Petroleum Geology, 25*(1), pp.97-117.

Sadooni, F. (2005). The nature and origin of Upper Cretaceous basin-margin rudist buildups of the Mesopotamian Basin, southern Iraq, with consideration of possible hydrocarbon stratigraphic entrapment. *Cretaceous Research*, 26(2), pp.213-224.

Saggaf, M., Toksöz, M. and Marhoon, M. (2003). Seismic facies classification and identification by competitive neural networks. *GEOPHYSICS*, 68(6), pp.1984-1999.

Sams, M., Begg, P. and Manapov, T. (2017). Seismic inversion of a carbonate buildup: A case study. *Interpretation*, 5(4), pp.T641-T652.

Schlumberger, (2011). Property Modeling Course, Schlumberger, (pp. 421-461).

Scholle, P. and Ulmer-Scholle, D., (2003). A Color Guide to the Petrography of Carbonate Rocks: Grains, textures, porosity, diagenesis: *AAPG Memoir* 77, pp. 474.

Scotese, C.R., (2001). Atlas of Earth History, vol. 1. Paleogeography: *PALEOMAP Project*, Arlington, Texas, pp. 52.

Sharland, P.R., Archer, R., Casey, D.M., Davies, R.B., Hall, S.H., Heward, A.P., Horbury, A.D., Simmons, M.D., (2001). Arabian Plate Sequence Stratigraphy, vol. 2. *GeoArabia, Special Publication,* pp. 371.

Sharland, P.R., D.M. Casey, R.B. Davies, M.D. Simmons and O.E. Sutcliffe, (2004). Arabian Plate sequence stratigraphy- revision to SP2. *GeoArabia 9*, pp.199–214.

Simm, R. and Bacon, M. (2014). Seismic Amplitude: *An Interpreter's Handbook*. Cambridge University Press.

Song, C., Liu, Z., Cai, H., Qian, F. and Hu, G. (2016). Pre-stack-texture-based reservoir characteristics and seismic facies analysis. *Applied Geophysics*, 13(1), pp.69-79.

Song, C., Liu, Z., Wang, Y., Li, X. and Hu, G. (2017). Multi-waveform classification for seismic facies analysis. *Computers & Geosciences*, 101, pp.1-9.

Stoneley, R. (1990). The Middle East basin: a summary overview. In: BROOKS, J. (ed.) *Classic Petroleum Provinces. Geological Society, London, Special Publication,* 50, pp.293-298.

Telford, W. M., Geldart, L. P., and Sheriff, R. E. (1990). *Applied Geophysics*, 2nd edition. Cambridge: Cambridge University Press.

Thore, P., (2015). Uncertainty in seismic inversion: What really matters?. *The Leading Edge*, *34*(9), pp.1000-1004.

Tucker, M. (1985). Shallow-marine carbonate facies and facies models. *Geological Society, London, Special Publications*, 18(1), pp.147-169.

Tucker, M.E. and Wright, V.P., (1990). *Carbonate sedimentology*. John Wiley & Sons.
van Gestel, J., (2015). 4D noise observations-Key to successful subsalt 4D: *85th Annual International Meeting*, SEG, Expanded Abstracts, 5363–5367.

Veeken, P. C., Priezzhev, I. I., Shmaryan, L. E., Shteyn, Y. I., Barkov, A. Y. and Ampilov, Y. P. (2009). Nonlinear multitrace genetic inversion applied on seismic data across the Shtokman field, offshore northern Russia, *Geophysics*, 74(6), pp. WCD49- WCD59.

Vogel, K. R., and Follows, E. J. (2016). Tectonic and Eustatic Control on Mishrif Regional Reservoir Distribution. *Abu Dhabi International Petroleum Exhibition & Conference.*

Wagner, C., Gonzalez, A., Agarwal, V., Koesoemadinata, A., Ng, D., Trares, S., Biles, N., and Fisher, K. (2012). Quantitative application of poststack acoustic impedance inversion to subsalt reservoir development. *The Leading Edge*, 31(5), pp.528-537.

Walls, J., Dvorkin, J. and Carr, M. (2004). Well Logs and Rock Physics in Seismic Reservoir Characterization. *Offshore Technology Conference*.

Wang, J., Guo, R., Zhao, L., Li, W., Zhou, W. and Duan, T. (2016). Geological features of grain bank reservoirs and the main controlling factors: A case study on Cretaceous Mishrif Formation, Halfaya Oilfield, Iraq. *Petroleum Exploration and Development*, 43(3), pp.404-415.

Wang, R., Wang, Z., Osumanu, A., Zhang, G., Li, B. and Lu, Y., (2019). Grid density overlapping hierarchical algorithm for clustering of carbonate reservoir rock types: A case from Mishrif Formation of West Qurna-1 oilfield, Iraq. *Journal of Petroleum Science and Engineering*, *182*, p.106209.

Williams, D.B. and Aqrawi, A.A.M., (2006). Utility of using acoustic impedance data in the stochastic modelling of a carbonate reservoir.

Wenju, S.U.N., Zhanfeng, Q.I.A.O., Guanming, S.H.A.O., Xiaowei, S.U.N., Jixian, G.A.O., Peng, C.A.O., ZHANG, J. and Wangang, C.H.E.N., (2020). Sedimentary and reservoir architectures of MB1-2 sub-member of Middle Cretaceous Mishrif Formation of Halfaya Oilfield in Iraq. *Petroleum Exploration and Development*, *47*(4), pp.762-772.

White, R. and Simm, R. (2003). 'Tutorial: Good practice in well ties,' *First Break*, 21(10).

Wong, L.J., (2020). *A tiered, integrated platform for maximising the value of noisy 4D seismic data acquired over a carbonate reservoir* (Doctoral dissertation, Heriot-Watt University).

Wu, H., Li, Z., Liu, N. and Zhang, B., (2022). Improved seismic well tie by integrating variable-size window resampling with well-tie net. *Journal of Petroleum Science and Engineering,* 208, p.109368.

Xinghe, Y., Shengli, L., Shu, Z., Jianyang, C.H.E.N. and Guowei, H.O.U., (2008). Constraining method of stochastic modeling for fluvial petroleum reservoir controlled by depositional facies using wells and seismic data. *Earth Science Frontiers, 15*(4), pp.33-41.

Xu, S. and Payne, M., (2009). Modeling elastic properties in carbonate rocks. *The Leading Edge,* 28(1), pp.66-74.

Ya, D., Rui, G., Zhongyuan, T., Wenhao, T., Yingjie, Y., Zhenyong, X., Cong, X., Xunchen, C. and Liang, C., (2016). Geologic features and genesis of the barriers and intercalations in carbonates: A case study of the Cretaceous Mishrif Formation, West Qurna oil field, Iraq. *Petroleum Exploration and Development, 43*(1), pp.149-157.

Yadav, L., Ghosh, D., Maurya, S. N. and Bhattacharya, A. N. (2004). Calibration of sonic logs for seismic applications in Upper Assam. *Conference & Exposition on Petroleum Geophysics. Hyderabad, India*. pp. 154-161.

Yanlin, S., Ailing, Z., You-bin, H. and Keyan, X., (2011). 3D geological modeling and its application under complex geological conditions. *Procedia Engineering, 12,* pp.41-46.

Yilmaz, Ö. (2001). *Seismic data analysis: Processing, inversion, and interpretation of seismic data.* Society of exploration geophysicists.

Yong, H.U., Xinghe, Y.U., Shengli, L.I., Gongyang, C., Yanli, Z.H.O.U. and Zhaopu, G.A.O., (2014). Improving the accuracy of geological model by using seismic forward and inverse techniques. *Petroleum Exploration and Development, 41*(2), pp.208-216.

Yose, L., Alqassab, H., Fullmer, S., Van Simaeys, S., Wawrzynski, A., Viator, D. and Stone, M. (2015). Impact of Reservoir Heterogeneity on Field Development and Reservoir Management of the Mishrif Reservoir, West Qurna I, Southern Iraq. *Third EAGE workshop on Iraq*.

Yose, L.A., A.S. Ruf, C.J. Strohmenger, J.S. Schuelke, A. Gombos, I. Al-Hosani, S. Al-Maskary, G. Bloch, Y. Al-Mehairi and I.G. Johnson (2006). Three-dimensional characterization of a heterogeneous carbonate reservoir, Lower Cretaceous, Abu Dhabi (United Arab Emirates). In P.M. Harris and L.J. Weber (Eds.), Giant Hydrocarbon Reservoirs of the World: From Rock to Reservoir Characterization and Modeling. *American Association of Petroleum Geologists Memoir 88/Society of Economic Paleontologists and Mineralogists Special Publication*, pp. 173-212.

Yose, L., Mitchell, J., Broomhall, R., Hasiuk, F. and Liu, C. (2012). Sequence Stratigraphy of the Mishrif Formation, West Qurna 1 Field, Iraq. *First EAGE Workshop on Iraq - Hydrocarbon Exploration and Field Development.*

Zachariassen, E., Meisingset, H., Otterlei, C., Andersen, T., Hatland, K., Hoye, T., Mangeroy, G. and Liestol, F., (2006). Method for conditioning the reservoir model on 3D and 4D elastic inversion data applied to a fluvial reservoir in the North Sea. In *SPE Europec/EAGE Annual Conference and Exhibition*.

Zare, A., Bagheri, M. and Ebadi, M., (2020). Reservoir facies and porosity modeling using seismic data and well logs by geostatistical simulation in an oil field. *Carbonates and Evaporites*, *35*(3), pp.1-10.

Zeng, H., Loucks, R., Janson, X., Wang, G., Xia, Y., Yuan, B. and Xu, L., (2011). Three-dimensional seismic geomorphology and analysis of the Ordovician paleokarst drainage system in the central Tabei Uplift, northern Tarim Basin, western China. *AAPG bulletin*, *95*(12), pp.2061-2083.

Zhan, X., Fullmer, S., Lu, C., Kaczmarek, S., Harris, C. and Martinez, A., (2012). Study Geophysical Response of Middle East Carbonate Reservoir using Computational Rock Physics Approach. *SEG Technical Program Expanded Abstracts 2012*.

Zhao, L., Nasser, M. and Han, D.H., (2013). Quantitative geophysical pore-type characterization and its geological implication in carbonate reservoirs. *Geophysical Prospecting*, *61*(4), pp.827-841.

Zhong, Y., Tan, X., Zhao, L., Guo, R., Li, F., Jin, Z., Chen, Y. and Xiao, D. (2018). Identification of facies-controlled eogenetic karstification in the Upper Cretaceous of the Halfaya oilfield and its impact on reservoir capacity. *Geological Journal*, pp.1-16.